

Advances

in Clinical and Experimental Medicine

MONTHLY ISSN 1899-5276 (PRINT) ISSN 2451-2680 (ONLINE)

www.advances.umw.edu.pl

2022, Vol. 31, No. 8 (August)

Impact Factor (IF) – 1.736
Ministry of Science and Higher Education – 70 pts
Index Copernicus (ICV) – 166.39 pts



WROCLAW
MEDICAL UNIVERSITY

Advances
in Clinical and Experimental
Medicine



Advances in Clinical and Experimental Medicine

ISSN 1899-5276 (PRINT)

ISSN 2451-2680 (ONLINE)

www.advances.umw.edu.pl

MONTHLY 2022
Vol. 31, No. 8
(August)

Advances in Clinical and Experimental Medicine (*Adv Clin Exp Med*) publishes high-quality original articles, research-in-progress, research letters and systematic reviews and meta-analyses of recognized scientists that deal with all clinical and experimental medicine.

Editorial Office

ul. Marcinkowskiego 2–6
50-368 Wrocław, Poland
Tel.: +48 71 784 12 05
E-mail: redakcja@umw.edu.pl

Publisher

Wrocław Medical University
Wybrzeże L. Pasteura 1
50-367 Wrocław, Poland

Online edition is the original version
of the journal

Editor-in-Chief

Prof. Donata Kurpas

Deputy Editor

Prof. Wojciech Kosmala

Managing Editor

Marek Misiak, MA

Statistical Editors

Wojciech Bombała, MSc
Katarzyna Giniewicz, MSc Eng.
Anna Kopszak, MSc
Dr. Krzysztof Kujawa

Manuscript editing

Marek Misiak, MA, Jolanta Krzyżak, MA

Scientific Committee

Prof. Sabine Bährer-Kohler
Prof. Antonio Cano
Prof. Breno Diniz
Prof. Erwan Donal
Prof. Chris Fox
Prof. Naomi Hachiya
Prof. Carol Holland
Prof. Markku Kurkinen
Prof. Christos Lionis

Prof. Raimundo Mateos
Prof. Zbigniew W. Ras
Prof. Jerzy W. Rozenblit
Prof. Silvina Santana
Prof. James Sharman
Prof. Jamil Shibli
Prof. Michal Toborek
Prof. László Vécsei
Prof. Cristiana Vitale

Section Editors

Anesthesiology

Prof. Marzena Zielińska

Basic Sciences

Prof. Iwona Bil-Lula
Prof. Bartosz Kempisty
Dr. Anna Lebedeva
Dr. Mateusz Olbromski
Dr. Maciej Sobczyński

Clinical Anatomy, Legal Medicine, Innovative Technologies

Prof. Rafael Boscolo-Berto

Dentistry

Prof. Marzena Dominiak
Prof. Tomasz Gedrange
Prof. Jamil Shibli

Dermatology

Prof. Jacek Szepietowski

Emergency Medicine, Innovative Technologies

Prof. Jacek Smereka

Gynecology and Obstetrics

Prof. Olimpia Sipak-Szmigiel

Histology and Embryology

Prof. Marzena Podhorska-Okołów

Internal Medicine

Angiology

Dr. Angelika Chachaj

Cardiology

Prof. Wojciech Kosmala
Dr. Daniel Morris

Endocrinology

Prof. Marek Bolanowski

Gastroenterology

Assoc. Prof. Katarzyna Neubauer

Hematology

Prof. Andrzej Deptała

Prof. Dariusz Wołowicz

Nephrology and Transplantology

Assoc. Prof. Dorota Kamińska

Assoc. Prof. Krzysztof Letachowicz

Pulmonology

Prof. Anna Brzecka

Microbiology

Prof. Marzenna Bartoszewicz

Assoc. Prof. Adam Junka

Molecular Biology

Dr. Monika Bielecka

Prof. Jolanta Saczko

Neurology

Assoc. Prof. Magdalena Koszewicz

Assoc. Prof. Anna Pokryszko-Dragan

Dr. Masaru Tanaka

Neuroscience

Dr. Simone Battaglia

Oncology

Prof. Andrzej Deptała

Dr. Marcin Jędryka

Gynecological Oncology

Dr. Marcin Jędryka

Ophthalmology

Dr. Agnieszka Rafalska

Orthopedics

Prof. Paweł Reichert

Otolaryngology

Assoc. Prof. Tomasz Zatoński

Pediatrics

Pediatrics, Metabolic Pediatrics, Clinical Genetics, Neonatology, Rare Disorders

Prof. Robert Śmigiel

Pediatric Nephrology

Prof. Katarzyna Kiliś-Pstrusińska

Pediatric Oncology and Hematology

Assoc. Prof. Marek Ussowicz

Pharmaceutical Sciences

Assoc. Prof. Marta Kepińska

Prof. Adam Matkowski

Pharmacoeconomics, Rheumatology

Dr. Sylwia Szafraniec-Buryło

Psychiatry

Prof. Jerzy Leszek

Public Health

Prof. Monika Sawhney

Prof. Izabella Uchmanowicz

Qualitative Studies, Quality of Care

Prof. Ludmiła Marcinowicz

Radiology

Prof. Marek Sząsiadek

Rehabilitation

Prof. Jakub Taradaj

Surgery

Assoc. Prof. Mariusz Chabowski

Prof. Renata Taboła

Telemedicine, Geriatrics, Multimorbidity

Assoc. Prof. Maria Magdalena

Bujnowska-Fedak

Editorial Policy

Advances in Clinical and Experimental Medicine (Adv Clin Exp Med) is an independent multidisciplinary forum for exchange of scientific and clinical information, publishing original research and news encompassing all aspects of medicine, including molecular biology, biochemistry, genetics, biotechnology and other areas. During the review process, the Editorial Board conforms to the "Uniform Requirements for Manuscripts Submitted to Biomedical Journals: Writing and Editing for Biomedical Publication" approved by the International Committee of Medical Journal Editors (www.ICMJE.org). The journal publishes (in English only) original papers and reviews. Short works considered original, novel and significant are given priority. Experimental studies must include a statement that the experimental protocol and informed consent procedure were in compliance with the Helsinki Convention and were approved by an ethics committee.

For all subscription-related queries please contact our Editorial Office:

redakcja@umw.edu.pl

For more information visit the journal's website:

www.advances.umw.edu.pl

Pursuant to the ordinance No. 134/XV R/2017 of the Rector of Wrocław Medical University (as of December 28, 2017) from January 1, 2018 authors are required to pay a fee amounting to 700 euros for each manuscript accepted for publication in the journal Advances in Clinical and Experimental Medicine.

Indexed in: MEDLINE, Science Citation Index Expanded, Journal Citation Reports/Science Edition, Scopus, EMBASE/Excerpta Medica, Ulrich's™ International Periodicals Directory, Index Copernicus

Typographic design: Piotr Gil, Monika Kołęda

DTP: Wydawnictwo UMW

Cover: Monika Kołęda

Printing and binding: Drukarnia I-BIS

Contents

Editorials

- 821 Piril Hepsomali, Christle Coxon
Inflammation and diet: Focus on mental and cognitive health

Meta-analysis

- 827 Xiuli Nie, Jie Zhou, Jingyu Zeng, Jing Sun, Weiwei Chen, Jurong Niu
Does PET scan have any role in the diagnosis of perineural spread associated with the head and neck tumors?

Original papers

- 837 Junwu Yang, Maolin Chu, Yuzhuo Qi, Haifeng Zhang, Tan Yuan, Li Zhou, Wei Cao, Chunying Zhang
Correlation between age and curative effects of selective dorsal neurectomy for primary premature ejaculation
- 847 Lixiu Chen, Ying Cheng, Liang Zhou, Lei Zhang, Xueyan Deng
Quantitative shear wave elastography compared to standard ultrasound (qualitative B-mode grayscale sonography and quantitative power Doppler) for evaluation of achillotendinopathy in treatment-naïve individuals: A cross-sectional study
- 855 Mabel Aoun, Reine-Marie Kahwaji, Ghassan Sleilat, Celine Boueri, Jenny Hawi, Christelle Bou Khalil, Valerie Hage
Factors predictive of anti-spike antibody titers after COVID-19 vaccination in hemodialysis patients
- 863 Paweł Rogalski, Marta Zaborowska, Maria Mazur, Żaneta Jankowska, Alicja Piszczyk, Edyta Mermer, Andrzej Dąbrowski, Jarosław Daniluk
Gastrointestinal hemorrhage as an acute-on-chronic liver failure trigger in cirrhotic patients
- 873 Bożena Karolko, Adam Serafin, Monika Przewłocka-Kosmala
Impact of moderately reduced renal function on the diagnostic and prognostic value of galectin-3 in patients with exertional dyspnea
- 881 Wei Kou, Haibin Huang, Shuangwu Dai, Xinmei Tan, Qi Chen, Renwei Huang, Hequn Zou
***mGluR5* promotes the progression of multiple myeloma in vitro via Ras–MAPK signaling pathway**
- 889 Jing Wan, Juan Lv, Chun Wang, Li Zhang
***RPS27* selectively regulates the expression and alternative splicing of inflammatory and immune response genes in thyroid cancer cells**
- 903 Chunmou Li, Chuchu Feng, Yantao Chen, Pingping Wu, Peng Li, Xilin Xiong, Xiaomin Peng, Zhixuan Wang, Yang Li
Arsenic trioxide induces the differentiation of retinoic acid-resistant neuroblastoma cells via upregulation of *HoxC9*

Reviews

- 913 Radosław Andrzej Konieczny, Wiktor Kuliczkowski
Trimethylamine N-oxide in cardiovascular disease

Inflammation and diet: Focus on mental and cognitive health

Piril Hepsomali^{A–F}, Christle Coxon^{A–F}

School of Psychology, University of Roehampton, London, United Kingdom

A – research concept and design; B – collection and/or assembly of data; C – data analysis and interpretation;
D – writing the article; E – critical revision of the article; F – final approval of the article

Advances in Clinical and Experimental Medicine, ISSN 1899–5276 (print), ISSN 2451–2680 (online)

Adv Clin Exp Med. 2022;31(8):821–825

Address for correspondence

Piril Hepsomali
E-mail: P.Hepsomali@roehampton.ac.uk

Funding sources

None declared

Conflict of interest

None declared

Received on June 24, 2022

Reviewed on July 21, 2022

Accepted on July 25, 2022

Published online on August 11, 2022

Abstract

It has been well established that chronic low-grade inflammation is implicated in both physical and mental noncommunicable diseases. Diet, a leading risk factor for non-communicable diseases, has been repeatedly shown to be related to inflammation, as well as various health outcomes, including mental and cognitive health. In the current editorial paper, we briefly summarize the current state of evidence and discuss the potential mediating role of inflammation between diet and mental/cognitive health. We also outline our perspective on challenges and future research directions in the domain of inflammation and diet, with a specific focus on mental and cognitive health.

Key words: inflammation, diet, nutrition, mental health, cognitive health

Cite as

Hepsomali P, Coxon C. Inflammation and diet: Focus on mental and cognitive health. *Adv Clin Exp Med.* 2022;31(8):821–825. doi:10.17219/acem/152350

DOI

10.17219/acem/152350

Copyright

Copyright by Author(s)

This is an article distributed under the terms of the Creative Commons Attribution 3.0 Unported (CC BY 3.0) (<https://creativecommons.org/licenses/by/3.0/>)

Systemic chronic inflammation, diet and health

Chronic low-grade inflammation is implicated in the etiology of various noncommunicable diseases, including diabetes,¹ obesity,² cancer,³ and cardiovascular diseases,⁴ and even increased mortality.^{5,6} Additionally, inflammation is also implicated in numerous mental disorders. For instance, meta-analytic and systematic reviews that focused on observational evidence have shown that a range of blood and cerebrospinal fluid pro-inflammatory markers such as interleukin-6 (IL-6), interleukin-8 (IL-8), tumor necrosis factor alpha (TNF- α), and C-reactive protein (CRP) were increased in a range of mental illnesses including depression, anxiety, schizophrenia, and bipolar disorder.^{7–11} Large cohort studies have also shown elevated CRP levels and white blood cell counts in depressive and anxiety disorders.^{12–16}

In terms of cognitive health, evidence from cross-sectional and prospective studies indicate that peripheral inflammatory markers, such as IL-6 and CRP, are associated with the global cognitive decline,^{17–20} and a decline in specific cognitive domains, particularly short-term memory,^{21–23} processing speed,²⁴ verbal fluency, and executive function.^{25–27} For neurodegenerative conditions, meta-analyses of prospective studies have reported that higher levels of CRP and IL-6 are associated with a higher risk of all-cause dementia.^{28–30} While inflammation was not associated with an increased risk of Alzheimer's disease (AD), evidence from cross-sectional studies indicates that peripheral markers of inflammation such as CRP, IL-1 β , IL-6, and IL-8 are significantly higher in AD patients compared to controls.^{31–33} Elevated peripheral inflammatory markers such as monocyte chemoattractant protein-1 (MCP-1), IL-6 and IL-8 have been reported in mild cognitive impairment,³³ but this finding is not consistent,^{31,34} and it may be that systemic inflammation is similar to that of healthy individuals and occurs at a later stage in the progression of AD.³⁵ Additionally, due to kynurenine pathway enzymes directly influencing inflammation and the immune system, kynurenic acid was shown to be lower in individuals with neurodegenerative conditions.^{36,37}

The aforementioned adverse physical, mental and cognitive health outcomes are also known to be associated with poor diet quality.^{38–40} Diet, a leading risk factor for noncommunicable diseases, affects disease risk via modulation of various mechanisms including, but not limited to, oxidative stress, plasticity, microbiota–gut–brain axis, and, most importantly, inflammatory responses.^{41,42} Negative associations between adherence to a Mediterranean style diet (MED) and food groups that are abundant in these diets, such as fruits, vegetables, oily and non-oily fish, and inflammatory markers such as platelet and leukocyte counts, neutrophil to lymphocyte ratios (NLRs), and CRP^{43–47} levels have been observed. Intervention studies

have also shown a similar pattern of results. For instance, results from meta-analyses of randomized controlled trials (RCTs) have provided evidence that a MED decreases inflammation, specifically CRP, IL-6 and IL-1 β .^{48,49}

Based on the evidence discussed above, inflammation may mediate the association between anti-inflammatory diets, such as the MED, and health outcomes. In fact, a recent cross-sectional study found a role for various inflammatory biomarkers in the relationship between diet and sleep quality,⁴⁵ though the role of inflammation on the relationship between diet and mental and cognitive health has not yet been examined. However, there is a considerable amount of cross-sectional evidence showing that the adherence to a MED or healthy dietary patterns, including higher intakes of fruit, vegetables, fish, and wholegrains, were associated with a reduced risk of depression (but not anxiety), age-related cognitive decline, pathological neurodegeneration, and better general mental well-being.^{50–55} Additionally, the consumption of various nutrients (B vitamins, vitamin D, polyphenols, n-3 fatty acids, fiber) and certain food groups (fish/seafood, vegetables, fruits) were also shown to be associated with better mental and cognitive outcomes.^{51,54,56–61} Similarly, based on recent reviews, a low number of heterogeneous dietary intervention studies have shown beneficial effects of the MED on symptoms of depression (but not anxiety) and cognitive decline.^{62–64} Though, to the best of our knowledge, none of these studies have tested the extent to which these benefits are due to changes in inflammation.

Challenges and future directions


The research briefly presented above, unfortunately, is not free from challenges. First and foremost, many of the studies are observational, and either cross-sectional or prospective in design, which limits our ability to infer a causal relationship between diet, inflammation, and physical, cognitive and mental health. Secondly, although various RCTs have been conducted in this area, they recruited small numbers of participants, and the heterogeneity of research methodology cannot be underestimated. Specifically, there is considerable variation in assessment of mental and cognitive health and dietary outcomes, and not all of the studies utilized consistent, validated and sensitive measures. Of specific importance, dietary intake measures are known to rely on the ability of participants to recall and report, and are prone to under-reporting.⁶⁵ Furthermore, the definition of a specific dietary pattern differs across distinct geographical and cultural contexts.⁴⁸ Third, the majority of the evidence in the area relies mainly on clinical samples and specific disorders (such as depression); however, research in sub-clinical samples and across a variety of psychopathological conditions is warranted. Fourth, most of the studies examined only a small subset of single measurements

of inflammation biomarkers, and time of the blood draw was not taken into consideration. Indeed, while single measurements of various inflammatory biomarkers have been shown to predict a range of health outcomes,^{12,66} it is also important to note that intraindividual variability in inflammatory biomarkers has been observed before,⁶⁷ and some biomarkers show circadian rhythms.⁶⁸ Fifth, one of the biggest challenges to the field is conducting interdisciplinary research to address the interactions between peripheral and brain alterations. Therefore, future research studies would benefit from combining multiple techniques and linking inflammation to the structure, function and connectivity of the brain, as well as to other biomarkers, such as neurometabolites, amyloid, tau, and α -synuclein, that are known to be sensitive to mental and cognitive health alterations. Moreover, there is no current consensus regarding the best diet that has anti-inflammatory potential, and, to the best of our knowledge, no trials have compared the efficacy of dietary interventions on mental and cognitive health outcomes to pharmacological and/or other nonpharmacological interventions. Finally, it is important to note that interpopulation differences in dietary patterns may result in markedly different inflammatory potential, as energy, nutrient intake and density differ greatly across populations.⁶⁹

Based on the challenges and limitations discussed above, we invite researchers to conduct longitudinal studies that aim to clarify the temporal relationships between mental/cognitive health, inflammation and nutritional domains, in order to ascertain whether immune dysregulation is a precursor or the result of mental and cognitive health outcomes, or if it is a bidirectional pathway. We would also like to encourage researchers to conduct large RCTs: 1) by using consistent, validated, sensitive (and ideally objective) diet, mental and cognitive health measures; 2) in clinical and subclinical samples, across various psychopathological conditions; 3) by using wide range of inflammation biomarkers (measured at multiple time points to control for intraindividual variations); and 4) ideally by also utilising brain imaging and cerebrospinal fluid biomarkers, to identify the best anti-inflammatory diets, test the efficacy of these on mental and cognitive health outcomes, and test the efficacy of these in comparison to pharmacological and other nonpharmacological interventions. These interventions should, of course, control for various participant (such as sex,⁷⁰ severity of health issues, body mass index (BMI), smoking, exercise, medical comorbidities,⁷¹ genetic heterogeneity, etc.) and sample (collection/processing/storage practices, time of the sample collection, etc.) characteristics. Filling the knowledge gaps discussed in this editorial will not only advance theoretical frameworks that characterize interactions between the gut and the brain, but also move fundamental research towards translational applications that could be used for disorders where inflammation is implicated.

ORCID iDs

Piril Hepsomali  <https://orcid.org/0000-0001-5812-1081>

Christle Coxon  <https://orcid.org/0000-0002-9168-9071>

References

1. Tsalamandris S, Antonopoulos AS, Oikonomou E, et al. The role of inflammation in diabetes: Current concepts and future perspectives. *Eur Cardiol*. 2019;14(1):50–59. doi:10.15420/ecr.2018.33.1
2. Ellulu MS, Patimah I, Khaza'ai H, Rahmat A, Abed Y. Obesity and inflammation: The linking mechanism and the complications. *Arch Med Sci*. 2017;13(4):851–863. doi:10.5114/aoms.2016.58928
3. Greten FR, Grivennikov SI. Inflammation and cancer: Triggers, mechanisms, and consequences. *Immunity*. 2019;51(1):27–41. doi:10.1016/j.immuni.2019.06.025
4. Golia E, Limongelli G, Natale F, et al. Inflammation and cardiovascular disease: From pathogenesis to therapeutic target. *Curr Atheroscler Rep*. 2014;16(9):435. doi:10.1007/s11883-014-0435-z
5. Proctor MJ, McMillan DC, Horgan PG, Fletcher CD, Talwar D, Morrison DS. Systemic inflammation predicts all-cause mortality: A Glasgow inflammation outcome study. *PLoS One*. 2015;10(3):e0116206. doi:10.1371/journal.pone.0116206
6. Bonaccio M, Di Castelnuovo A, Pounis G, et al. A score of low-grade inflammation and risk of mortality: Prospective findings from the Moli-sani study. *Haematologica*. 2016;101(11):1434–1441. doi:10.3324/haematol.2016.144055
7. Goldsmith DR, Rapaport MH, Miller BJ. A meta-analysis of blood cytokine network alterations in psychiatric patients: Comparisons between schizophrenia, bipolar disorder and depression. *Mol Psychiatry*. 2016;21(12):1696–1709. doi:10.1038/mp.2016.3
8. Wang AK, Miller BJ. Meta-analysis of cerebrospinal fluid cytokine and tryptophan catabolite alterations in psychiatric patients: Comparisons between schizophrenia, bipolar disorder, and depression. *Schizophr Bull*. 2018;44(1):75–83. doi:10.1093/schbul/sbx035
9. Fond G, Lançon C, Auquier P, Boyer L. C-reactive protein as a peripheral biomarker in schizophrenia: An updated systematic review. *Front Psychiatry*. 2018;9:392. doi:10.3389/fpsy.2018.00392
10. Costello H, Gould RL, Abrol E, Howard R. Systematic review and meta-analysis of the association between peripheral inflammatory cytokines and generalised anxiety disorder. *BMJ Open*. 2019;9(7):e027925. doi:10.1136/bmjopen-2018-027925
11. Yuan N, Chen Y, Xia Y, Dai J, Liu C. Inflammation-related biomarkers in major psychiatric disorders: A cross-disorder assessment of reproducibility and specificity in 43 meta-analyses. *Transl Psychiatry*. 2019;9(1):233. doi:10.1038/s41398-019-0570-y
12. Wium-Andersen MK, Ørsted DD, Nielsen SF, Nordestgaard BG. Elevated C-reactive protein levels, psychological distress, and depression in 73 131 individuals. *JAMA Psychiatry*. 2013;70(2):176–184. doi:10.1001/2013.jamapsychiatry.102
13. Kennedy E, Niedzwiedz CL. The association of anxiety and stress-related disorders with C-reactive protein (CRP) within UK Biobank. *Brain Behav Immun Health*. 2021;19:100410. doi:10.1016/j.bbih.2021.100410
14. Meyer D, Chrusciel T, Salas J, Scherrer J. The relationship between white blood cell counts and mental health conditions in adults. *Psychoneuroendocrinology*. 2021;131:105500. doi:10.1016/j.psyneuen.2021.105500
15. Ye Z, Kappelmann N, Moser S, et al. Role of inflammation in depression and anxiety: Tests for disorder specificity, linearity and potential causality of association in the UK Biobank. *EClinicalMedicine*. 2021;38:100992. doi:10.1016/j.eclinm.2021.100992
16. Horsdal HT, Köhler-Forsberg O, Benros ME, Gasse C. C-reactive protein and white blood cell levels in schizophrenia, bipolar disorders and depression – associations with mortality and psychiatric outcomes: A population-based study. *Eur Psychiatr*. 2017;44:164–172. doi:10.1016/j.eurpsy.2017.04.012
17. Bradburn S, Sarginson J, Murgatroyd CA. Association of peripheral interleukin-6 with global cognitive decline in non-demented adults: A meta-analysis of prospective studies. *Front Aging Neurosci*. 2018;9:438. doi:10.3389/fnagi.2017.00438
18. West NA, Kullo IJ, Morris MC, Mosley TH. Sex-specific associations of inflammation markers with cognitive decline. *Exp Gerontol*. 2020;138:110986. doi:10.1016/j.exger.2020.110986

19. Yang J, Fan C, Pan L, et al. C-reactive protein plays a marginal role in cognitive decline: A systematic review and meta-analysis. *Int J Geriatr Psychiatry*. 2015;30(2):156–165. doi:10.1002/gps.4236
20. Sartori AC, Vance DE, Slater LZ, Crowe M. The impact of inflammation on cognitive function in older adults: Implications for health-care practice and research. *J Neurosci Nurs*. 2012;44(4):206–217. doi:10.1097/JNN.0b013e3182527690
21. Marsland AL, Gianaros PJ, Kuan DCH, Sheu LK, Krajina K, Manuck SB. Brain morphology links systemic inflammation to cognitive function in midlife adults. *Brain Behav Immun*. 2015;48:195–204. doi:10.1016/j.bbi.2015.03.015
22. Arce Rentería M, Gillett SR, McClure LA, et al. C-reactive protein and risk of cognitive decline: The REGARDs study. *PLoS One*. 2020; 15(12):e0244612. doi:10.1371/journal.pone.0244612
23. Noble JM, Manly JJ, Schupf N, Tang MX, Mayeux R, Luchsinger JA. Association of C-reactive protein with cognitive impairment. *Arch Neurol*. 2010;67(1):87–92. doi:10.1001/archneurol.2009.308
24. Lin T, Liu GA, Perez E, et al. Systemic inflammation mediates age-related cognitive deficits. *Front Aging Neurosci*. 2018;10:236. doi:10.3389/fnagi.2018.00236
25. Vintimilla R, Hall J, Johnson L, O'Bryant S. The relationship of CRP and cognition in cognitively normal older Mexican Americans: A cross-sectional study of the HABLE cohort. *Medicine (Baltimore)*. 2019; 98(19):e15605. doi:10.1097/MD.00000000000015605
26. Schram MT, Euser SM, De Craen AJM, et al. Systemic markers of inflammation and cognitive decline in old age. *J Am Geriatr Soc*. 2007; 55(5):708–716. doi:10.1111/j.1532-5415.2007.01159.x
27. Kipinoinen T, Toppala S, Viitanen M, Rinne JO, Jula A, Ekblad LL. Chronic low-grade inflammation predicts greater decline in verbal fluency and word-list learning on 10 years' follow-up. *Alzheimers Dement*. 2021;17(S10). doi:10.1002/alz.055447
28. Darweesh SKL, Wolters FJ, Ikram MA, Wolf F, Bos D, Hofman A. Inflammatory markers and the risk of dementia and Alzheimer's disease: A meta-analysis. *Alzheimers Dement*. 2018;14(11):1450–1459. doi:10.1016/j.jalz.2018.02.014
29. Koyama A, O'Brien J, Weuve J, Blacker D, Metti AL, Yaffe K. The role of peripheral inflammatory markers in dementia and Alzheimer's disease: A meta-analysis. *J Gerontol A Biol Sci Med Sci*. 2013;68(4):433–440. doi:10.1093/gerona/gls187
30. Metti AL, Cauley JA. How predictive of dementia are peripheral inflammatory markers in the elderly? *Neurodegener Dis Manag*. 2012; 2(6):609–622. doi:10.2217/nmt.12.68
31. Su C, Zhao K, Xia H, Xu Y. Peripheral inflammatory biomarkers in Alzheimer's disease and mild cognitive impairment: A systematic review and meta-analysis. *Psychogeriatrics*. 2019;19(4):300–309. doi:10.1111/psyg.12403
32. Park JC, Han SH, Mook-Jung I. Peripheral inflammatory biomarkers in Alzheimer's disease: A brief review. *BMB Rep*. 2020;53(1):10–19. doi:10.5483/BMBRep.2020.53.1.309
33. Shen XN, Niu LD, Wang YJ, et al. Inflammatory markers in Alzheimer's disease and mild cognitive impairment: A meta-analysis and systematic review of 170 studies. *J Neurol Neurosurg Psychiatry*. 2019; 90(5):590–598. doi:10.1136/jnnp-2018-319148
34. Saleem M, Herrmann N, Swardfager W, Eisen R, Lanctôt KL. Inflammatory markers in mild cognitive impairment: A meta-analysis. *J Alzheimers Dis*. 2015;47(3):669–679. doi:10.3233/JAD-150042
35. Dursun E, Gezen-Ak D, Hanağası H, et al. The interleukin 1 alpha, interleukin 1 beta, interleukin 6 and alpha-2-macroglobulin serum levels in patients with early or late onset Alzheimer's disease, mild cognitive impairment or Parkinson's disease. *J Neuroimmunol*. 2015;283:50–57. doi:10.1016/j.jneuroim.2015.04.014
36. Török N, Tanaka M, Vécsei L. Searching for peripheral biomarkers in neurodegenerative diseases: The tryptophan-kynurenine metabolic pathway. *Int J Mol Sci*. 2020;21(24):9338. doi:10.3390/ijms21249338
37. Tanaka M, Vécsei L. Monitoring the kynurenine system: Concentrations, ratios or what else? *Adv Clin Exp Med*. 2021;30(8):775–778. doi:10.17219/acem/139572
38. Ley SH, Pan A, Li Y, et al. Changes in overall diet quality and subsequent type 2 diabetes risk: Three U.S. prospective cohorts. *Diabetes Care*. 2016;39(11):2011–2018. doi:10.2337/dc16-0574
39. Neelakantan N, Koh WP, Yuan JM, van Dam RM. Diet-quality indexes are associated with a lower risk of cardiovascular, respiratory, and all-cause mortality among Chinese adults. *J Nutr*. 2018;148(8): 1323–1332. doi:10.1093/jn/nxy094
40. Wolongevic DM, Zhu L, Pencina MJ, et al. Diet quality and obesity in women: The Framingham Nutrition Studies. *Br J Nutr*. 2010;103(8): 1223–1229. doi:10.1017/S0007114509992893
41. Marx W, Moseley G, Berk M, Jacka F. Nutritional psychiatry: The present state of the evidence. *Proc Nutr Soc*. 2017;76(4):427–436. doi:10.1017/S0029665117002026
42. Marx W, Lane M, Hockey M, et al. Diet and depression: Exploring the biological mechanisms of action. *Mol Psychiatry*. 2021;26(1): 134–150. doi:10.1038/s41380-020-00925-x
43. Bonaccio M, Di Castelnuovo A, De Curtis A, et al. Adherence to the Mediterranean diet is associated with lower platelet and leukocyte counts: Results from the Moli-sani study. *Blood*. 2014;123(19): 3037–3044. doi:10.1182/blood-2013-12-541672
44. Rodríguez-Rodríguez E, López-Sobaler AM, Ortega RM, Delgado-Losada ML, López-Parra AM, Aparicio A. Association between neutrophil-to-lymphocyte ratio with abdominal obesity and healthy eating index in a representative older Spanish population. *Nutrients*. 2020;12(3):855. doi:10.3390/nu12030855
45. Hepsomali P, Groeger JA. Examining the role of systemic chronic inflammation in diet and sleep relationship. *J Psychopharmacol*. 2022;2022:0269881122111292. doi:10.1177/02698811221112932
46. Wu PY, Chen KM, Tsai WC. The Mediterranean dietary pattern and inflammation in older adults: A systematic review and meta-analysis. *Adv Nutr*. 2021;12(2):363–373. doi:10.1093/advances/nmaa116
47. Whalen KA, McCullough ML, Flanders WD, Hartman TJ, Judd S, Bostick RM. Paleolithic and Mediterranean diet pattern scores are inversely associated with biomarkers of inflammation and oxidative balance in adults. *J Nutr*. 2016;146(6):1217–1226. doi:10.3945/jn.115.224048
48. Schwingshackl L, Hoffmann G. Mediterranean dietary pattern, inflammation and endothelial function: A systematic review and meta-analysis of intervention trials. *Nutr Metab Cardiovasc Dis*. 2014; 24(9):929–939. doi:10.1016/j.numecd.2014.03.003
49. Koelman L, Egea Rodrigues C, Aleksandrova K. Effects of dietary patterns on biomarkers of inflammation and immune responses: A systematic review and meta-analysis of randomized controlled trials. *Adv Nutr*. 2022;13(1):101–115. doi:10.1093/advances/nmab086
50. Angeloni C, Businaro R, Vauzour D. The role of diet in preventing and reducing cognitive decline. *Curr Opin Psychiatry*. 2020;33(4):432–438. doi:10.1097/YCO.0000000000000605
51. Scarmeas N, Anastasiou CA, Yannakoulia M. Nutrition and prevention of cognitive impairment. *Lancet Neurol*. 2018;17(11):1006–1015. doi:10.1016/S1474-4422(18)30338-7
52. Lai JS, Hiles S, Bisquera A, Hure AJ, McEvoy M, Attia J. A systematic review and meta-analysis of dietary patterns and depression in community-dwelling adults. *Am J Clin Nutr*. 2014;99(1):181–197. doi:10.3945/ajcn.113.069880
53. Psaltopoulou T, Sergentanis TN, Panagiotakos DB, Sergentanis IN, Kosti S, Scarmeas N. Mediterranean diet, stroke, cognitive impairment, and depression: A meta-analysis. *Ann Neurol*. 2013;74(4):580–591. doi:10.1002/ana.23944
54. Hepsomali P, Groeger JA. Diet, sleep, and mental health: Insights from the UK biobank study. *Nutrients*. 2021;13(8):2573. doi:10.3390/nu13082573
55. van den Brink AC, Brouwer-Brolsma EM, Berendsen AAM, van de Rest O. The Mediterranean, Dietary Approaches to Stop Hypertension (DASH), and Mediterranean-DASH Intervention for Neurodegenerative Delay (MIND) diets are associated with less cognitive decline and a lower risk of Alzheimer's disease: A review. *Adv Nutr*. 2019;10(6):1040–1065. doi:10.1093/advances/nmz054
56. Li F, Liu X, Zhang D. Fish consumption and risk of depression: A meta-analysis. *J Epidemiol Community Health*. 2016;70(3):299–304. doi:10.1136/jech-2015-206278
57. Liu X, Yan Y, Li F, Zhang D. Fruit and vegetable consumption and the risk of depression: A meta-analysis. *Nutrition*. 2016;32(3):296–302. doi:10.1016/j.nut.2015.09.009
58. El Ansari W, Adetunji H, Oskrochi R. Food and mental health: Relationship between food and perceived stress and depressive symptoms among University students in the United Kingdom. *Cent Eur J Public Health*. 2014;22(2):90–97. doi:10.21101/cejph.a3941

59. Miki T, Eguchi M, Kurotani K, et al. Dietary fiber intake and depressive symptoms in Japanese employees: The Furukawa Nutrition and Health Study. *Nutrition*. 2016;32(5):584–589. doi:10.1016/j.nut.2015.11.014
60. Hepsomali P, Groeger JA. Diet and general cognitive ability in the UK Biobank dataset. *Sci Rep*. 2021;11(1):11786. doi:10.1038/s41598-021-91259-3
61. Hepsomali P, Greyling A, Scholey A, Vauzour D. Acute effects of polyphenols on human attentional processes: A systematic review and meta-analysis. *Front Neurosci*. 2021;15:678769. doi:10.3389/fnins.2021.678769
62. Firth J, Marx W, Dash S, et al. The effects of dietary improvement on symptoms of depression and anxiety: A meta-analysis of randomized controlled trials. *Psychosom Med*. 2019;81(3):265–280. doi:10.1097/PSY.0000000000000673
63. Chen X, Maguire B, Brodaty H, O'Leary F. Dietary patterns and cognitive health in older adults: A systematic review. *J Alzheimers Dis*. 2019;67(2):583–619. doi:10.3233/JAD-180468
64. Opie RS, O'Neil A, Itsiopoulos C, Jacka FN. The impact of whole-of-diet interventions on depression and anxiety: A systematic review of randomised controlled trials. *Public Health Nutr*. 2015;18(11):2074–2093. doi:10.1017/S1368980014002614
65. Shim JS, Oh K, Kim HC. Dietary assessment methods in epidemiologic studies. *Epidemiol Health*. 2014:e2014009. doi:10.4178/epih/e2014009
66. Ruggiero C, Metter EJ, Cherubini A, et al. White blood cell count and mortality in the Baltimore longitudinal study of aging. *J Am Coll Cardiol*. 2007;49(18):1841–1850. doi:10.1016/j.jacc.2007.01.076
67. deGoma EM, French B, Dunbar RL, Allison MA, Mohler ER, Budoff MJ. Intraindividual variability of C-reactive protein: The multi-ethnic study of atherosclerosis. *Atherosclerosis*. 2012;224(1):274–279. doi:10.1016/j.atherosclerosis.2012.07.017
68. Lange T, Luebbert F, Grasshoff H, Besedovsky L. The contribution of sleep to the neuroendocrine regulation of rhythms in human leukocyte traffic. *Semin Immunopathol*. 2022;44(2):239–254. doi:10.1007/s00281-021-00904-6
69. Shivappa N, Wirth MD, Hurley TG, Hébert JR. Association between the dietary inflammatory index (DII) and telomere length and C-reactive protein from the National Health and Nutrition Examination Survey-1999-2002. *Mol Nutr Food Res*. 2017;61(4):1600630. doi:10.1002/mnfr.201600630
70. Grzymisławska M, Puch E, Zawada A, Grzymisłowski M. Do nutritional behaviors depend on biological sex and cultural gender? *Adv Clin Exp Med*. 2020;29(1):165–172. doi:10.17219/acem/111817
71. Carrera-González M del P, Cantón-Habas V, Rich-Ruiz M. Aging, depression and dementia: The inflammatory process. *Adv Clin Exp Med*. 2022;31(5):469–473. doi:10.17219/acem/149897

Does PET scan have any role in the diagnosis of perineural spread associated with the head and neck tumors?

Xiuli Nie^{1,A}, Jie Zhou^{2,A}, Jingyu Zeng^{3,B}, Jing Sun^{1,C}, Weiwei Chen^{1,C,E}, Jurong Niu^{4,D,F}

¹ Department of Radiology, Jinan Central Hospital, Shandong First Medical University, Jinan, China

² Department of Otolaryngology, Chongqing Qianjiang National Hospital, China

³ Department of Ward 16, 908th Hospital of Joint Support Force (Yingtian Barracks), China

⁴ Department of Radiology, Shengli Oilfield Central Hospital, Dongying, China

A – research concept and design; B – collection and/or assembly of data; C – data analysis and interpretation;

D – writing the article; E – critical revision of the article; F – final approval of the article

Advances in Clinical and Experimental Medicine, ISSN 1899–5276 (print), ISSN 2451–2680 (online)

Adv Clin Exp Med. 2022;31(8):827–835

Address for correspondence

Jurong Niu

E-mail: niujunrong990127@sina.com

Funding sources

None declared

Conflict of interest

None declared

Received on November 8, 2021

Reviewed on January 30, 2022

Accepted on March 14, 2022

Published online on April 25, 2022

Cite as

Nie X, Zhou J, Zeng J, Sun J, Chen W, Niu J. Does PET scan have any role in the diagnosis of perineural spread associated with the head and neck tumors? *Adv Clin Exp Med.*

2022;31(8):827–835. doi:10.17219/acem/147359

DOI

10.17219/acem/147359

Copyright

Copyright by Author(s)

This is an article distributed under the terms of the Creative Commons Attribution 3.0 Unported (CC BY 3.0) (<https://creativecommons.org/licenses/by/3.0/>)

Abstract

Background. Perineural spread of head and neck tumors is linked to a worse chance of survival as well as a higher risk of local recurrence and metastasis. Particle emission tomography/computed tomography (PET/CT) using 2-[fluorine-18]fluoro-2-deoxy-d-glucose (FDG) is part of the work-up and follow-up of many afflicted patients, and radiologists play an essential role in the assessment and management of head and neck cancer.

Objectives. The purpose of the current study was to investigate the diagnostic performance of ¹⁸F-FDG PET in detecting perineural spread among patients with head and neck tumors through a meta-analysis.

Materials and methods. Relevant articles were searched using appropriate keywords from PubMed, MEDLINE and PubMed Central (PMC) databases. Retrospective and prospective studies were included as per the predefined PICOS criteria. Demographic summary and event data for diagnostic accuracy of ¹⁸F-FDG PET were determined, and odds ratio (OR), sensitivity, specificity, likelihood ratios, and predictive values were calculated using RevMan software. The bias risk was analyzed with Egger's and Begg's tests using MedCalc software.

Results. Fourteen clinical trials performed between 2000 and 2021, with 977 head and neck cancer patients with perineural spread, were included according to the inclusion criteria. Included studies used ¹⁸F-FDG PET imaging of tumors and reported its high sensitivity. In the current study, we obtained the pooled OR = 3.088 (95% confidence interval (95% CI): [1.486; 6.419]), pooled sensitivity of 91.7%, pooled specificity of 92.35%, positive predictive value (PPV) of 92.27%, negative predictive value (NPV) of 91.13%, positive likelihood ratio of 7.45, negative likelihood ratio of 0.28, disease prevalence of 95.8%, and accuracy of 91.5%. Data was heterogeneous, with Q value of 33.8%, degrees of freedom (df) value of 13, I² value of 61.5% (31.23–78.5), and p-value = 0.0013. The risk of publication bias was low, with a p = 0.7490 (Egger's test) and p = 0.7843 (Begg's test).

Conclusions. The present meta-analysis highly recommends ¹⁸F-FDG PET as an effective imaging method for patients with head and neck tumors with perineural spread.

Key words: MRI, head and neck tumors, perineural spread, perineural invasion, FDG PET scan

Background

The concept of ‘head and neck cancer’ refers to a diverse class of cancers that affect the oral cavity, pharynx, larynx, nasal cavity, paranasal sinuses, and salivary glands. Head and neck cancer has several histologic subtypes due to the large array of structures and cell types.¹

Head and neck tumors can spread through several processes, including direct extension, hematogenous dissemination and lymphatic dissemination. Furthermore, a phenomenon known as perineural spread allows some cancers to exploit peripheral nerves as a direct conduit for tumor development, away from the initial location. Perineural spread is important in clinical practice because it indicates a poor prognosis, even asymptomatic. Furthermore, it is frequently overlooked during surgery and can develop without hematogenous or lymphatic metastases.²

In the literature, the words ‘perineural invasion’ and ‘perineural spread’ are frequently used interchangeably; thus, it is vital to distinguish between them.

Perineural spread can affect any cranial nerve and its branches. However, the trigeminal nerve (cranial nerve V) and the facial nerve (cranial nerve VII) are the most afflicted, owing to their extensive innervation of the head and neck tissues. In addition, the perineural spread is more likely in tumors that are located in the midface, in men, in larger tumors, in recurrence after therapy, and in tumors with poor histologic distinction.³

Perineural invasion is a histologic diagnosis that is difficult to establish with macroscopic imaging modalities. However, the perineural spread spreads tumor cells along a nerve and such infiltration may be seen with imaging tools. Therefore, the radiologist must determine whether a tumor that is directly next to a nerve is considered a perineural spread or not.

The perineural spread has an adverse impact on the treatment outcome with a poor prognosis. The long-term survival is jeopardized. Previous studies have reported that unrecognized perineural tumor invasion leads to treatment failure. Henceforth, it is necessary to detect and accurately diagnose such spread.^{4,5}

Imaging is widely known to have an essential role in diagnosis and treatment of head and neck cancers. The frequently used imaging methods for detecting perineural spread are magnetic resonance imaging (MRI), computed tomography (CT) and positron emission tomography (PET) scan, among others. Among these, the use of ¹⁸F-FDG PET (PET with 2-[fluorine-18]fluoro-2-deoxy-d-glucose (FDG)) is highly recommended in various studies due to its high sensitivity for detecting perineural spread and recurrent metastatic tumors.^{6–20} For example, Schroeder et al. reported that MRI and ¹⁸F-FDG PET have identical detection rates of recurrent metastatic tumors.¹⁶ Similarly, Lee et al. reported that the application of ¹⁸F-FDG PET in clinical diagnosis could enhance the tumor detection rate in head and neck cancers.²⁰

In contrast to these studies, Hanna et al. concluded that MRI has higher sensitivity and specificity for perineural

spread and malignant tumor detection.²¹ These contrasting reports limited the use of ¹⁸F-FDG PET as an effective diagnostic tool. Therefore, the current meta-analysis aimed to statistically analyze the available literature related to ¹⁸F-FDG PET and predict its diagnostic accuracy.

Objective

This study aims to investigate the diagnostic performance of ¹⁸F-FDG PET in determining perineural spread in patients with head and neck tumors.

Materials and methods

We followed the Preferred Reporting Items for Systematic Reviews and Meta-Analyses (PRISMA) normative recommendations in this study with the PROSPERO registration No. CRD42021244688. All procedures performed in the study were in accordance with the institutional and/or national research standards set by the Ethics Committee of the Shandong University (Jinan, China), and with the 1964 Helsinki Declaration and its later amendments, or comparable ethical standards.

Search strategy

This meta-analysis is based on an extensive search conducted in databases of MEDLINE (through PubMed), Cinahl (through EBSCO), Scopus, and Web of Sciences. The following keywords were used for searching the relevant studies: [¹⁸F-FDG PET], [perineural spread], [head and neck cancer], [CT scan], and [MRI]. All the included articles were selected as per the predefined PICOS criteria and PRISMA guidelines, and studies were selected randomly, irrespective of the language, publication status or type of study (prospective, retrospective, clinical trial). Demographic summary of the patients and event data of the included studies are summarized in Table 1.^{6–19} Two authors (XN and JZ) scanned the relevant sources for related studies separately. Mainly, the full-texts articles of the sources were collected, and abstracts were used to obtain sufficient information for the meta-analysis. Obsolete references were excluded, and valuable studies were included as per the inclusion criteria. Then, event data with useful variables were collected by 2 researchers (ZJ and JS) independently.

Inclusion and exclusion criteria

The studies included in the meta-analysis reported the use of ¹⁸F-FDG PET as an effective imaging method for diagnosing patients with head and neck tumors with perineural spread, and were published between 2000 and 2021. Only the full-text data were included in the current study, while studies with insufficient data, studies reporting the use

Table 1. Demographic summary of the studies

| Study and year | Total samples studied | Type of study | Age of patients [years] | Duration | Gender (M/F) | Instrument detail |
|--|-----------------------|---------------|-------------------------|---------------------|--------------|---|
| Ng et al. 2005 ⁶ | 151 | prospective | 26–82 | 2 weeks | 121 M/3 F | PET system (ECAT EXACT HR; Siemens/CTI, Knoxville, USA) |
| Schöder et al. 2006 ⁷ | 142 | prospective | 37–84 | 2 years 2 months | 21 M/10 F | Integrated PET/CT scanner: Biograph (Siemens) or Discovery LS (GE Healthcare, Milwaukee, USA) |
| Kim et al. 2007 ⁸ | 64 | retrospective | 60 | 1 year | 267 M/82 F | Biograph Sensation16 scanner (Siemens/CTI) |
| Gu et al. 2010 ⁹ | 46 | retrospective | 39–89 | 2 weeks | 39 M/7 F | Discovery STE Whole Body PET/CT System (GE Healthcare) |
| El-Khodary et al. 2011 ¹⁰ | 38 | retrospective | 58 | 3 years 2 months | 51 M/12 F | Discovery STE 16 (GE Healthcare) |
| Pereira et al. 2012 ¹¹ | 49 | retrospective | 36–81 | 4 years | 44 M/5 F | Siemens Biograph Integrated PET/CT scanner (Siemens/CTI) |
| Karapolat and Kumanlioğlu 2012 ¹² | 20 | retrospective | 20–76 | 3 years 2 months | 19 M/1 F | Siemens HI-REZ Biograph 6 (Siemens/CTI) |
| Gódnéy et al. 2016 ¹³ | 38 | retrospective | 24–78 | 4 years | 24 M/14 F | 3T wide-bore MR scanner (General Electric Discovery 750w; GE Healthcare) |
| Ceylan et al. 2018 ¹⁴ | 22 | retrospective | 18–89 | 1 year 10 months | 49 M/16 F | Siemens Biograph 16 TruePoint PET/CT scanner (Siemens/CTI) |
| Sherif et al. 2018 ¹⁵ | 50 | retrospective | 17–74 | 1 year | 34 M/16 F | PET/CT scanner (Gemini TF; Philips, Andover, USA) with multislice-16 scanner |
| Schroeder et al. 2020 ¹⁶ | 25 | retrospective | 49–79 | 4 years | 17 M/8 F | Integrated PET/CT system (Biograph mCT 128 True V; Siemens/CTI) |
| Park et al. 2020 ¹⁷ | 134 | retrospective | 47–83 | 9 months | 48 M/25 F | PET/MRI system (Biograph mMR; Siemens Healthcare, Erlangen, Germany) |
| Sarma et al. 2021 ¹⁸ | 63 | retrospective | 32–83 | 8 years | 55 M/8 F | General Electric Discovery PET 8 slice CT scanner (GE Healthcare) |
| Linz et al. 2021 ¹⁹ | 135 | prospective | 23–88 | 2 years 6 months | 74 M/61 F | PET/CT scanner (Siemens Biograph mCT 64; Siemens Healthcare) |

M – male; F – female; PET/CT – particle emission tomography/computed tomography.

of other imaging methods, and all studies published before 2000 were excluded, as shown in Fig. 1.

Evaluation of the analytical standard and source of heterogeneity

Two reviewers (XN and JZ) separately evaluated the methodological validity of the included studies and calculated the heterogeneity in the included experiments. At the same time, one author (WC) was responsible for resolving disagreements between authors (XN and JZ). In order to investigate the heterogeneity, Cochran's Q statistic and I² index in the random bivariate model were calculated with the help of RevMan software v. 5 (The Cochrane Collaboration, The Nordic Cochrane Center, Copenhagen, Denmark). The investigated heterogeneity sources were the use of full-text publication compared to abstracts, prospective compared to retrospective studies, different numbers of patients with diverse types of head and neck cancers, and different imaging instruments.

Statistical analyses

The DerSimonian–Laird technique calculated the diagnostic odds ratio (OR) for statistical analysis. A 2 × 2 table was

made using the event data, and meta-analysis was performed using RevMan and MedCalc v. 20.100 (MedCalc Software, Ostend, Belgium) software. Pooled diagnostic OR with 95% confidence intervals (95% CIs), respective forest plot, heterogeneity of studies (in terms of Q value, degrees of freedom (df) value, I² value, and p-value), pooled sensitivity, specificity, likelihood ratios, predictive values, disease prevalence, accuracy, and receiver operating characteristic (ROC) analysis were performed with the help of MedCalc software. In addition, Deeks' funnel plot for publication bias, Youden plot to assess investigation error, and hierarchical summary receiver operating characteristic (HSROC) curve were created using MedCalc software, while forest plot of sensitivity and specificity was plotted using RevMan software.

Results

Literature search results

We found a total of 1246 studies in different databases, and excluded 227 studies after reading their titles and abstracts; as a result, 1019 records were screened. Further, due to invalid references and duplicity, we excluded 784 studies and included only 235 studies for the final

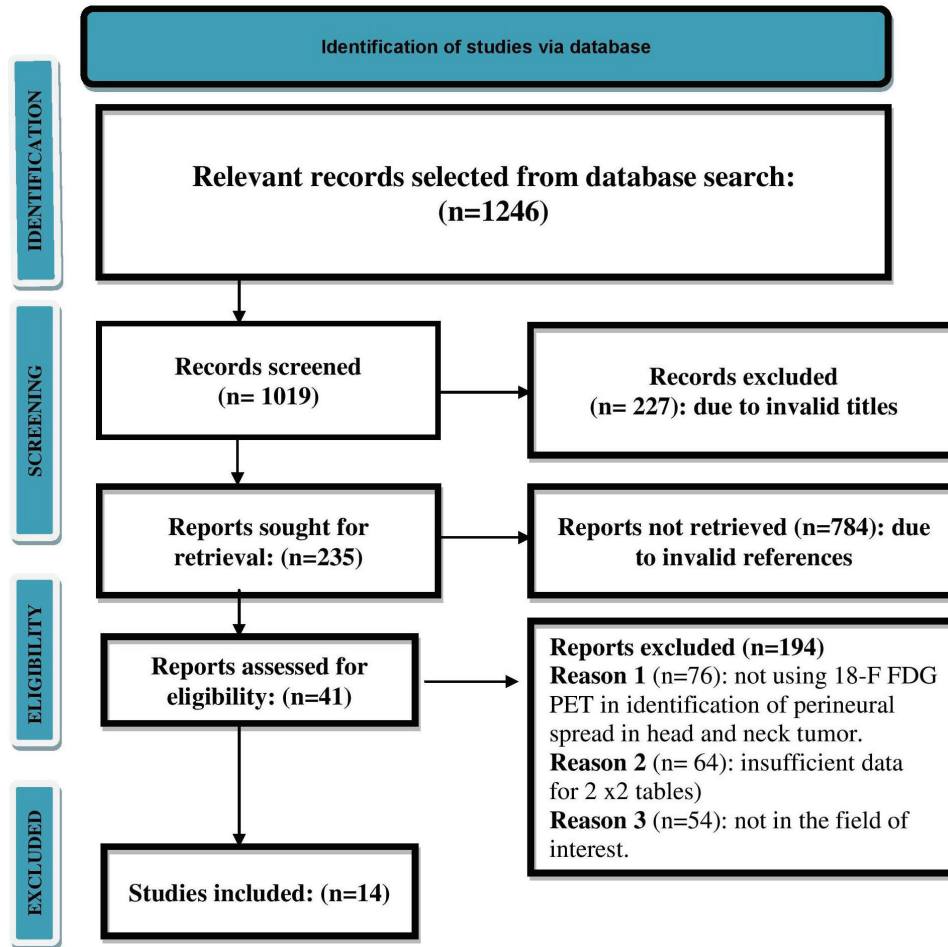


Fig. 1. Preferred Reporting Items for Systematic Reviews and Meta-Analyses (PRISMA) flow diagram of the study group

screening. Out of these 235 studies, 194 studies were excluded based on the inclusion criteria, and eligibility of the remaining 41 studies was assessed further. The critical reasons for omission were inadequate evidence and inappropriate comparison criteria to create 2 × 2 tables for review. Finally, 14 studies from 2000–2021 which fulfilled the inclusion criteria, i.e., ¹⁸F-FDG-PET for detection of perineural spread in head and neck tumor patients, were subject to meta-analysis, as shown in Fig. 1. Those 14 studies included a total of 977 head and neck tumor patients of different age groups, chosen randomly and scanned with ¹⁸F-FDG PET and CT or MRI. The demographic details of the studies included in this meta-analysis are shown in Table 1 – the author of the study, publishing year, duration of the study, type of study, total sample size, age of patients, gender of patients, and type of instrument used. In addition, event data of these studies (including the number of total samples studied, a true positive result, true negative result, false negative result, and false positive results) were collected.

Meta-analysis results

The risk of bias for included studies was assessed as shown in Table 2, and publication bias was measured with the help of Egger’s test, Begg’s test and Deeks’ funnel

plot. The current meta-analysis has a low risk of publication bias, as apparent from the funnel plot (Fig. 2), since p-values of both tests are greater than 0.05 (p-value of Egger’s test = 0.7490 and p-value of Begg’s test = 0.7843).

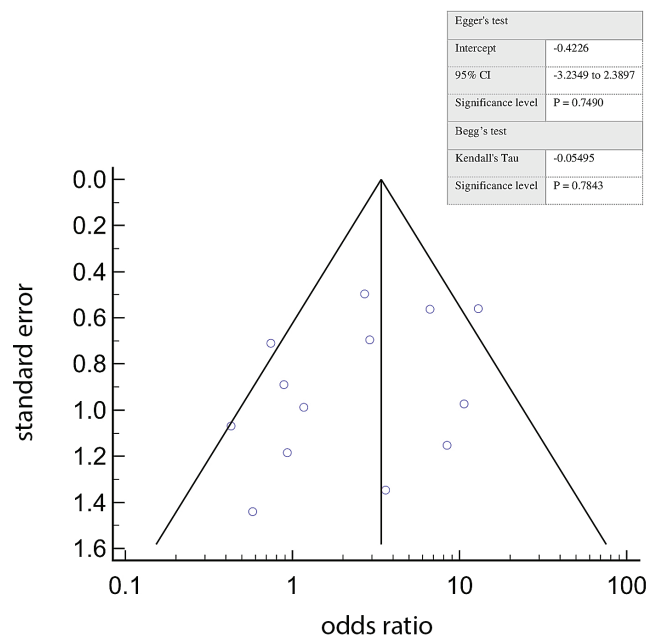


Fig. 2. Funnel plot for publication bias

95% CI – 95% confidence interval.

Table 2. Risk assessment for included studies

| Variable | Ng et al. 2005 ⁶ | Schöder et al. 2006 ⁷ | Kim et al. 2007 ⁸ | Gu et al. 2010 ⁹ | El-Khodary et al. 2011 ¹⁰ | Pereira et al. 2012 ¹¹ | Karapolat and Kumanlioglu 2012 ¹² | Gódný et al. 2016 ¹³ | Ceylan et al. 2018 ¹⁴ | Sherif et al. 2018 ¹⁵ | Schroeder et al. 2020 ¹⁶ | Park et al. 2020 ¹⁷ | Sarma et al. 2021 ¹⁸ | Linz et al. 2021 ¹⁹ |
|--|-----------------------------|----------------------------------|------------------------------|-----------------------------|--------------------------------------|-----------------------------------|--|---------------------------------|----------------------------------|----------------------------------|-------------------------------------|--------------------------------|---------------------------------|--------------------------------|
| Type of study | P | P | R | R | R | R | R | R | R | R | R | R | R | P |
| Was a consecutive or random sample of patients enrolled? | Y | Y | Y | Y | Y | Y | Y | Y | Y | Y | Y | Y | Y | Y |
| Did the study avoid inappropriate exclusions? | Y | Y | Y | Y | Y | Y | Y | Y | Y | Y | Y | Y | Y | Y |
| Were all patients included in the analysis? | N | N | N | N | N | N | N | N | N | N | N | N | N | N |
| Was the target population having patients of different age groups and included both genders? | Y | Y | Y | Y | Y | Y | Y | Y | Y | Y | Y | Y | Y | Y |
| Were study participants sampled in an appropriate way? | Y | Y | Y | Y | Y | Y | Y | Y | Y | Y | Y | Y | Y | Y |
| Were the study subjects and the setting described in detail? | Y | Y | Y | Y | Y | Y | Y | Y | Y | Y | Y | Y | Y | Y |
| Were valid methods used for the identification of the condition? | Y | Y | Y | Y | Y | Y | Y | Y | Y | Y | Y | Y | Y | Y |
| Was the condition measured in a standard, reliable way for all participants? | Y | Y | Y | Y | Y | Y | Y | Y | Y | Y | Y | Y | Y | Y |
| Was there appropriate statistical analysis conducted? | Y | Y | Y | Y | Y | Y | Y | Y | Y | Y | Y | Y | Y | Y |

P – prospective; R – retrospective; Y – yes; N – no.

The OR of the included studies was calculated using MedCalc software, and the respective forest plot was created (Fig. 3). We obtained the pooled OR value of 3.088

with 95% CI of [1.486; 6.419]. Data used for this analysis were heterogeneous, and we achieved the Q value of 33.8%, df value of 13, I² value of 61.5% (31.23–78.5),

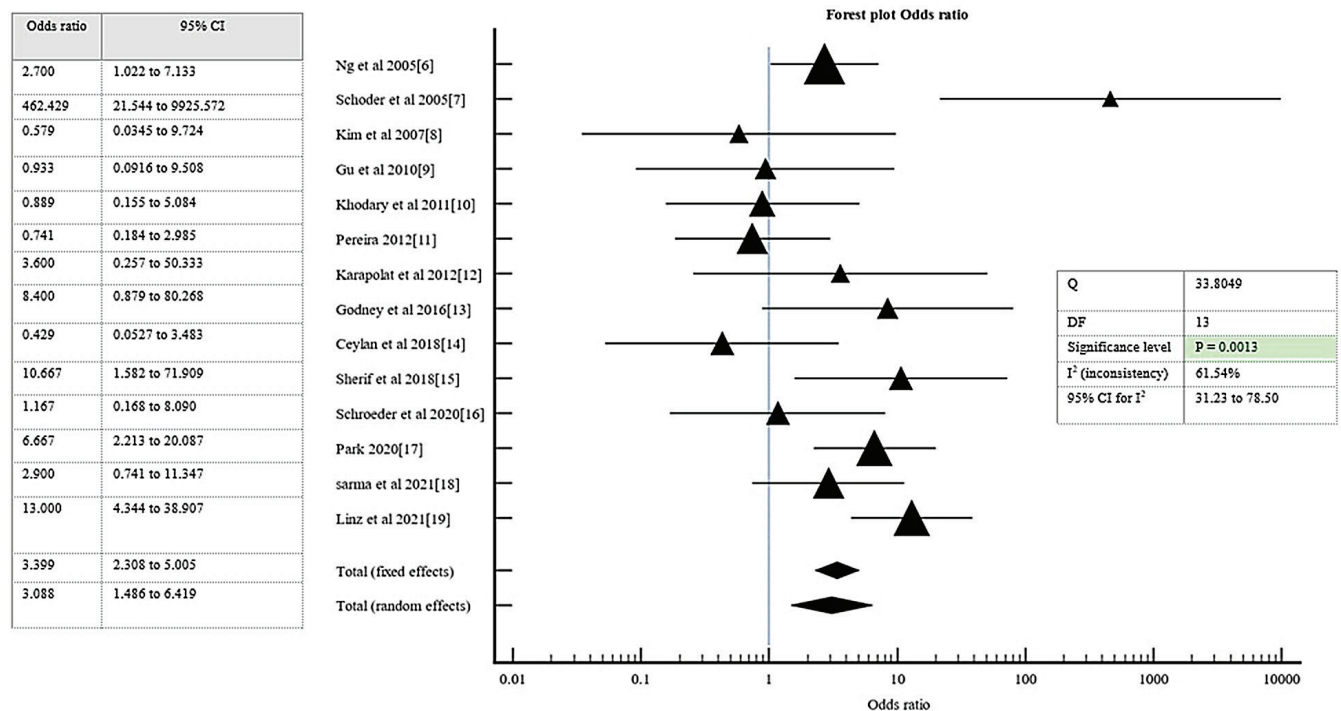


Fig. 3. Forest plot for diagnostic odds ratio

95% CI – 95% confidence interval; df – degrees of freedom.

Forest Plot

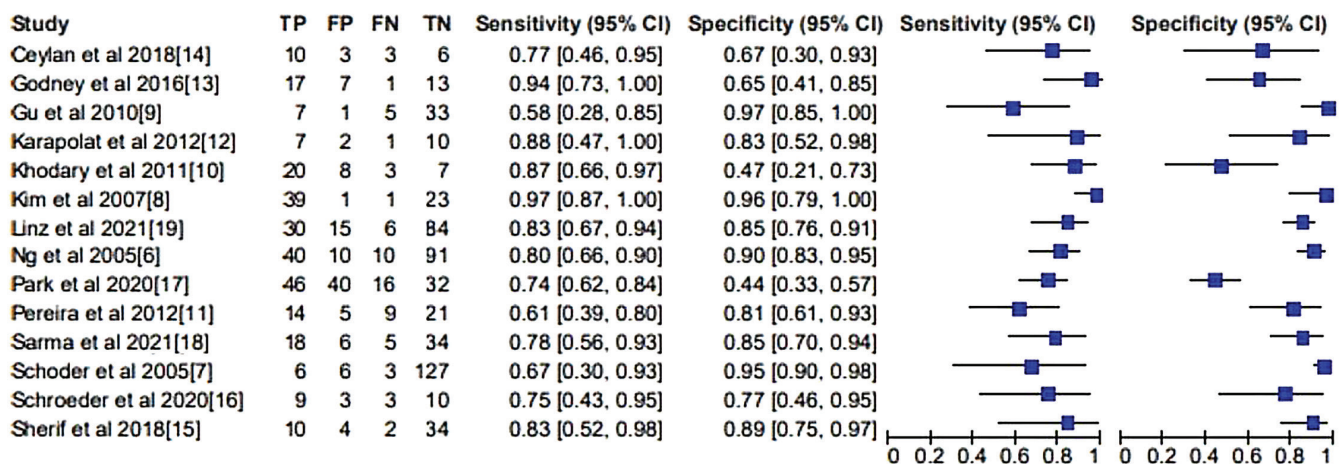


Fig. 4. Forest plot for sensitivity and specificity

95% CI – 95% confidence interval; TP – true positive; FP – false positive; FN – false negative; TN – true negative.

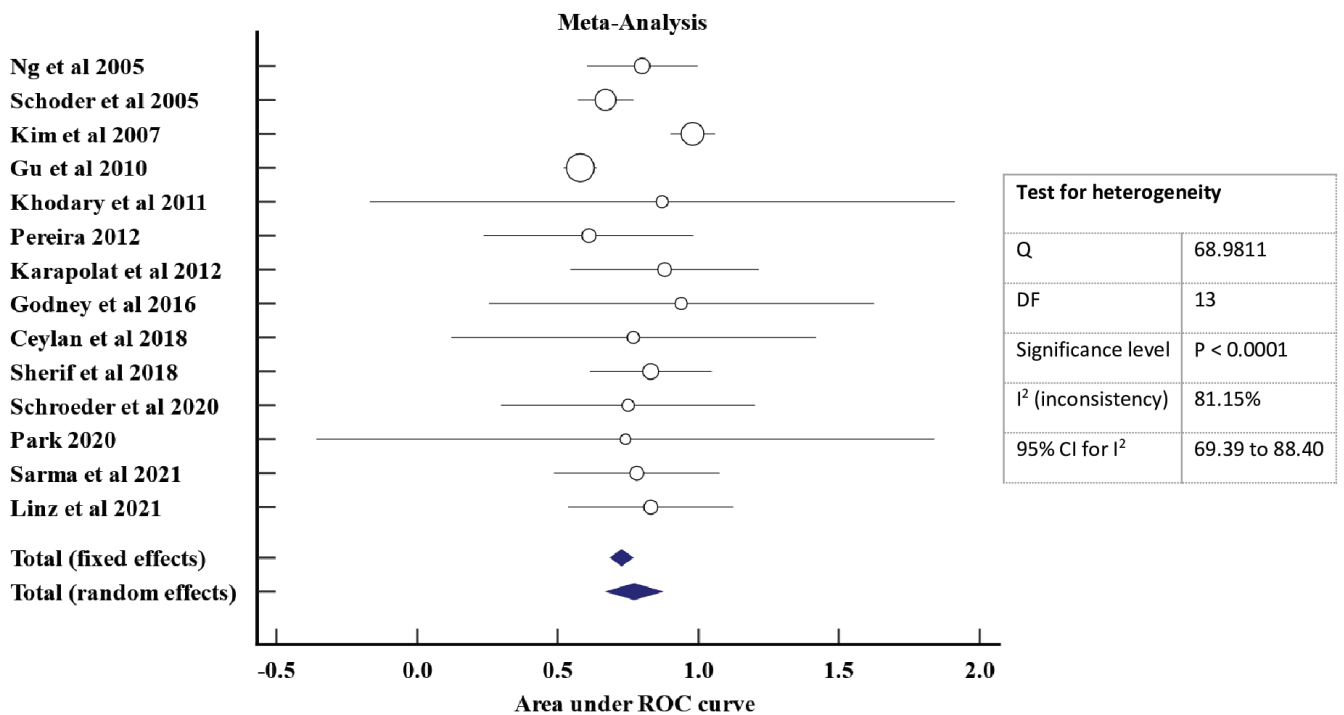


Fig. 5. Forest plot area under receiver operating characteristic (ROC) curve (area under the curve (AUC)

95% CI – 95% confidence interval; df – degrees of freedom.

and p-value of 0.0013. We obtained the pooled sensitivity of 91.7%, pooled specificity of 92.35%, positive predictive value (PPV) of 92.27%, negative predictive value (NPV) of 91.13%, the positive likelihood ratio of 7.45, negative likelihood ratio of 0.28, disease prevalence of 95.8%, and accuracy of 91.5%, as reported in Table 3. All of these results are statistically significant. The forest plot of sensitivity and specificity was designed using RevMan software, as shown in Fig. 4.

The ROC analysis was performed using MedCalc software, a forest plot was designed as shown in Fig. 5 and heterogeneity was assessed. The included data were

heterogeneous, as we obtained the Q value of 68.9%, df value of 13, I² consistency of 81.15% with 95% CI of [69.39; 88.40], and significance level (p-value) of 0.0001. In order to assess the study errors, the Youden curve was plotted between PPV and NPV (Fig. 6), and we found that the included studies have minimum investigations error. The HSROC curve was also plotted between the sensitivity and specificity of included studies (Fig. 7). All these curves and results are statistically significant and reflect the high sensitivity and specificity of ¹⁸F-FDG PET, as an effective imaging method for detecting perineural spread in patients of head and neck tumors.

Table 3. Statistical summary of the included studies: 95% CI – 95% confidence interval.

| Study ID | Sensitivity [%] [95% CI] | Specificity [%] [95% CI] | PLR [95% CI] | NLR [95% CI] | Disease prevalence [%] [95% CI] | PPV [95% CI] | NPV [95% CI] | Accuracy [%] [95% CI] |
|---|-----------------------------|-----------------------------|-------------------------|----------------------|------------------------------------|-------------------------|-------------------------|--------------------------|
| Ng et al. 2005 ⁶ | 80 [66.28; 89.97] | 90.09 [82.54; 95.15] | 8.08 [4.41; 14.79] | 0.22 [0.13; 0.39] | 33.11 [25.68; 41.23] | 80 [68.61; 87.98] | 90.10 [83.89; 94.08] | 86.75 [80.29; 91.72] |
| Schöder et al. 2006 ⁷ | 66.7 [29.93; 92.51] | 95.48 [90.44; 98.33] | 14.77 [5.96; 36.65] | 0.34 [0.14; 0.88] | 6.34 [2.94; 11.69] | 50 [28.74; 71.26] | 97.69 [94.38; 99.07] | 93.66 [88.31; 97.06] |
| Kim et al. 2007 ⁸ | 97.5 [86.84; 99.94] | 95.83 [78.88; 99.89] | 23.4 [3.43; 159.51] | 0.02 [0.00; 0.18] | 62.50 [49.51; 74.30] | 97.5 [85.12; 99.63] | 95.83 [76.82; 99.38] | 96.87 [89.16; 99.62] |
| Gu et al. 2010 ⁹ | 58.3 [27.67; 84.83] | 97.05 [84.67; 99.93] | 19.83 [2.71; 144.99] | 0.42 [0.22; 0.84] | 26.09 [14.27; 41.13] | 87.5 [77.12; 92.82] | 86.84 [77.12; 92.82] | 86.95 [73.74; 95.06] |
| El-Khodary et al. 2011 ¹⁰ | 86.9 [66.41; 97.22] | 46.66 [21.27; 73.41] | 1.63 [0.99; 2.69] | 0.27 [0.09; 0.91] | 60.53 [43.39; 75.96] | 71.43 [60.28; 80.46] | 70.00 [41.62; 88.42] | 71.05 [54.10; 84.58] |
| Pereira et al. 2012 ¹¹ | 60.86 [38.54; 80.29] | 80.76 [60.65; 93.45] | 3.16 [1.35; 7.43] | 0.48 [0.28; 0.83] | 46.94 [32.53; 61.73] | 73.68 [54.4; 86.79] | 70.00 [57.55; 80.07] | 71.42 [56.74; 83.42] |
| Karapolat and Kumanlioğlu et al. 2012 ¹² | 87.5 [47.35; 99.68] | 83.33 [51.59; 97.91] | 5.25 [1.44; 19.11] | 0.15 [0.02; 0.95] | 40.00 [19.12; 63.95] | 77.78 [49.02; 92.72] | 90.91 [61.11; 98.45] | 85 [62.11; 96.79] |
| Gödény et al. 2016 ¹³ | 94.44 [72.71; 99.86] | 65 [40.78; 84.61] | 2.69 [1.47; 4.95] | 0.08 [0.01; 0.59] | 47.37 [30.98; 64.18] | 70.83 [56.95; 81.68] | 92.86 [65.32; 98.90] | 78.94 [62.68; 90.45] |
| Ceylan et al. 2018 ¹⁴ | 76.92 [46.19; 94.96] | 66.66 [29.93; 92.51] | 2.30 [0.87; 6.09] | 0.34 [0.12; 1.03] | 59.09 [36.35; 79.29] | 76.92 [55.80; 89.80] | 66.67 [40.09; 85.67] | 72.7 [49.78; 89.27] |
| Sherif et al. 2018 ¹⁵ | 83.33 [51.59; 97.91] | 89.47 [75.20; 97.06] | 7.91 [3.03; 20.69] | 0.18 [0.05; 0.66] | 24.00 [13.06; 38.17] | 71.43 [48.88; 86.73] | 94.44 [82.68; 98.37] | 88 [75.69; 95.47] |
| Schroeder et al. 2020 ¹⁶ | 75 [42.81; 94.51] | 76.92 [46.19; 94.96] | 3.25 [1.14; 9.24] | 0.32 [0.12; 0.91] | 48.00 [27.80; 68.69] | 75 [51.34; 89.51] | 76.92 [54.48; 90.28] | 76 [54.87; 90.64] |
| Park et al. 2020 ¹⁷ | 74.19 [61.50; 84.47] | 44.44 [32.72; 56.64] | 1.33 [1.04; 1.72] | 0.58 [0.35; 0.95] | 46.27 [37.62; 55.08] | 53.49 [47.16; 59.71] | 66.67 [54.94; 76.64] | 58.2 [49.38; 66.67] |
| Sarma et al. 2021 ¹⁸ | 78.26 [56.30; 92.54] | 85 [70.16; 94.29] | 5.21 [2.42; 11.25] | 0.25 [0.12; 0.56] | 36.51 [24.73; 49.60] | 75 [58.18; 86.61] | 87.18 [75.60; 93.72] | 82.53 [70.90; 90.95] |
| Linz et al. 2021 ¹⁹ | 83.33 [67.19; 93.63] | 84.84 [76.24; 91.26] | 5.5 [3.37; 8.96] | 0.19 [0.09; 0.41] | 26.67 [19.43; 34.96] | 66.67 [55.10; 76.52] | 93.33 [87.03; 96.69] | 84.44 [77.21; 90.11] |

PLR – positive likelihood ratio; NLR – negative likelihood ratio; PPV – positive predictive value; NPV – negative predictive value.

Discussion

Head and neck tumors are different types of oral cavity malignancies, including pharynx, larynx, nasal cavity, paranasal sinuses, and salivary glands. They can spread through several processes, including direct extension, hematogenous dissemination, perineural spread, and others. Perineural spread is the most dangerous of the above, as it allows metastasis of tumors through peripheral nerves, so its early detection is crucial to the patient's well-being and survival. The perineural spread can be seen with imaging tools.

The preferred methods for detecting perineural spread among head and neck tumors are MRI, CT, PET scan, among others. However, because of the high sensitivity and specificity of ¹⁸F-FDG PET for cellular change and tumors, its use is highly recommended in various studies due to its high sensitivity in detecting perineural spread and recurrent metastatic tumors.^{6–20} For example, Linz et al. reported the sensitivity of ¹⁸F-FDG PET as 78.6% and specificity as 83.1%.¹⁹ Similarly, Sherif et al. reported a high sensitivity of 83.33% and specificity of 89.47%.¹⁵ Pyatigorskaya et al. reported a sensitivity of 90% and specificity of 98%.²²

Similar to the studies mentioned above, we achieved a high sensitivity of 91.7% and high specificity of 92.35%.

Apart from high sensitivity of ¹⁸F-FDG PET, various studies reported its high accuracy; for example, in the study conducted by Tantiwongkosi, PET scanning has been deemed an accurate method and crucial initial step in identification and treatment planning of head and neck tumor.²³ Furthermore, Ng et al. reported its high accuracy of 98.4%, while Sherif et al. reported its accuracy of 88%.^{6,15} Similarly, we obtained the accuracy of 91.5%. Based on these statistically significant results and high sensitivity, specificity and high diagnostic accuracy, this meta-analysis highly recommends using ¹⁸F-FDG PET in predicting the perineural spread and in an accurate diagnosis of head and neck tumors.

Limitations

The limitation of the present study is the variability of PET instruments used and tests performed by different radiographers, which influences the risk of false negative results. Many studies reported comparable diagnosis of PNS with MRI, however, its comparability with PET scan

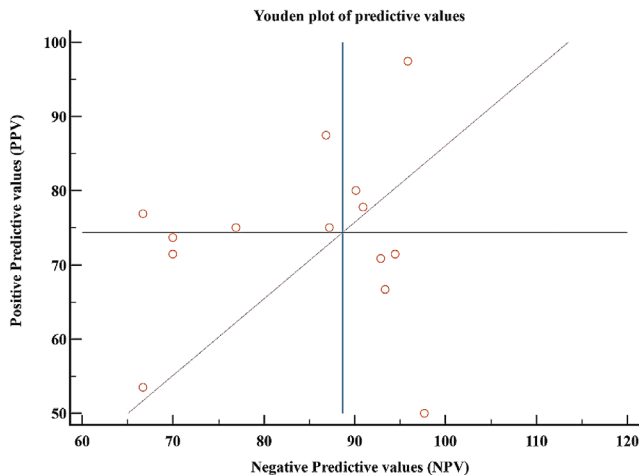


Fig. 6. Youden plot for predictive values

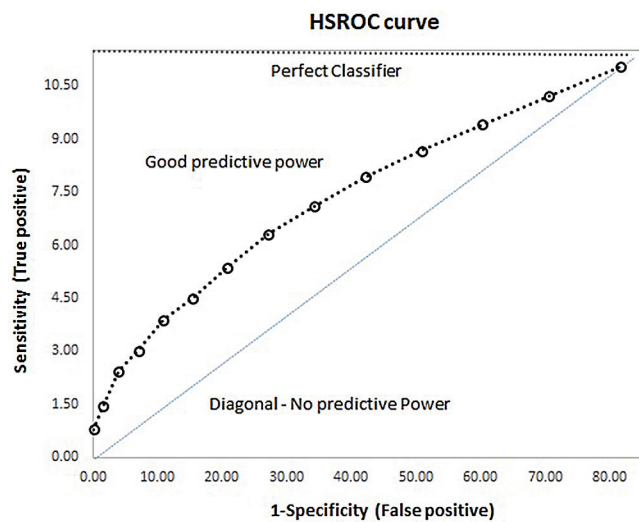


Fig. 7. Hierarchical summary receiver operating characteristic (HSROC) curve

in the diagnosis of PNS was not mentioned in the contemporary literature, so assessing the diagnostic comparability of MRI with PET scan accurately might affect the homogeneity of the data of the included studies. Data from other relevant studies showing the diagnostic accuracy of ^{18}F -FDG PET compared to other diagnostic imaging methods could also be included to support the role PET scan in the diagnosis of PNS. In order to reduce the variability among the data, detailed data on the patient's case history, physical examination and pathological tests could be included to further boost the diagnostic accuracy rate of ^{18}F -FDG PET in predicting perineural spread in head and neck tumors.

Conclusions

Magnetic resonance imaging is the gold standard for assessing perineural spread among head and neck tumors; still, ^{18}F -FDG PET is preferred chiefly as an effective imaging method due to its high sensitivity toward cellular change,

perineural spread and early tumor detection rate. Furthermore, it is highly recommended since early detection can prevent metastasis and increase the chances of survival. In the current study, we analyzed the available related literature, and based on our statistically significant results, we highly recommend the use of ^{18}F -FDG PET to detect perineural spread among patients with head and neck tumors.

ORCID iDs

Jurong Niu <https://orcid.org/0000-0003-4825-0992>
 Xiuli Nie <https://orcid.org/0000-0002-6563-355X>
 Lei Zhou <https://orcid.org/0000-0003-0531-4247>
 Jingyu Zeng <https://orcid.org/0000-0002-0182-5894>
 Jing Sun <https://orcid.org/0000-0002-1729-9374>
 Weiwei Chen <https://orcid.org/0000-0002-0842-7020>

References

1. Uraizee I, Cipriani NA, Ginat DT. Adenoid cystic carcinoma of the oral cavity: Radiology–pathology correlation. *Head and Neck Pathol.* 2018; 12(4):562–566. doi:10.1007/s12105-017-0849-3
2. Baulch J, Gandhi M, Sommerville J, Panizza B. 3T MRI evaluation of large nerve perineural spread of head and neck cancers: 3T MRI evaluation of PNS. *J Med Imaging Radiat Oncol.* 2015;59(5):578–585. doi:10.1111/1754-9485.12338
3. Wensing BM, Vogel WV, Marres HAM, et al. FDG-PET in the clinically negative neck in oral squamous cell carcinoma. *Laryngoscope.* 2006;116(5):809–813. doi:10.1097/01.mlg.0000209151.78362.d0
4. Derclé L, Hartl D, Rozenblum-Beddok L, et al. Diagnostic and prognostic value of ^{18}F -FDG PET, CT, and MRI in perineural spread of head and neck malignancies. *Eur Radiol.* 2018;28(4):1761–1770. doi:10.1007/s00330-017-5063-x
5. Haerle SK, Schmid DT, Ahmad N, Hany TF, Stoeckli SJ. The value of ^{18}F -FDG PET/CT for the detection of distant metastases in high-risk patients with head and neck squamous cell carcinoma. *Oral Oncol.* 2011;47(7):653–659. doi:10.1016/j.oraloncology.2011.05.011
6. Ng SH, Yen TC, Liao CT, et al. ^{18}F -FDG PET and CT/MRI in oral cavity squamous cell carcinoma: A prospective study of 124 patients with histologic correlation. *J Nucl Med.* 2005;46(7):1136–1143. PMID:16000282.
7. Schöder H, Carlson DL, Kraus DH, et al. ^{18}F -FDG PET/CT for detecting nodal metastases in patients with oral cancer staged N0 by clinical examination and CT/MRI. *J Nucl Med.* 2006;47(5):755–762. PMID:16644744.
8. Kim SY, Roh JL, Yeo NK, et al. Combined ^{18}F -fluorodeoxyglucose-positron emission tomography and computed tomography as a primary screening method for detecting second primary cancers and distant metastases in patients with head and neck cancer. *Ann Oncol.* 2007;18(10):1698–1703. doi:10.1093/annonc/mdm270
9. Gu DH, Yoon DY, Park CH, et al. CT, MR, (^{18}F -FDG PET/CT, and their combined use for the assessment of mandibular invasion by squamous cell carcinomas of the oral cavity. *Acta Radiol.* 2010;51(10):1111–1119. doi:10.3109/02841851.2010.520027
10. El-Khodary M, Tabashy R, Omar W, Mousa A, Mostafa A. The role of PET/CT in the management of head and neck squamous cell carcinoma. *Egypt J Radiol Nucl Med.* 2011;42(2):157–167. doi:10.1016/j.ejrnm.2011.05.006
11. Pereira G, Silva JC, Monteiro E. Positron emission tomography in the detection of occult primary head and neck carcinoma: A retrospective study. *Head Neck Oncol.* 2012;4(1):34. doi:10.1186/1758-3284-4-34
12. Karapolat I, Kumanlioğlu K. Impact of FDG-PET/CT for the detection of unknown primary tumours in patients with cervical lymph node metastases. *Mol Imaging Radionucl Ther.* 2012;21(2):63–68. doi:10.4274/Mirt.344
13. Gődény M, Lengyel Z, Polony G, et al. Impact of 3T multiparametric MRI and FDG-PET-CT in the evaluation of occult primary cancer with cervical node metastasis. *Cancer Imaging.* 2016;16(1):38. doi:10.1186/s40644-016-0097-x
14. Ceylan Y, Ömür Ö, Hatipoğlu F. Contribution of ^{18}F -FDG PET/CT to staging of head and neck malignancies. *Mol Imaging Radionucl Ther.* 2018;27(1):19–24. doi:10.4274/mirt.51423

15. Sherif MF, Dawoud MM, Nagy HA, Ghannam AA. Diagnostic accuracy of 18-F FDG-PET/CT in evaluation of malignant neuronal involvement in neurologically manifested cancer patients. *Egypt J Radiol Nucl Med.* 2018;49(2):453–460. doi:10.1016/j.ejnm.2018.03.002
16. Schroeder C, Lee JH, Tetzner U, Seidel S, Kim SY. Comparison of diffusion-weighted MR imaging and 18F fluorodeoxyglucose PET/CT in detection of residual or recurrent tumors and delineation of their local spread after (chemo) radiotherapy for head and neck squamous cell carcinoma. *Eur J Radiol.* 2020;130:109157. doi:10.1016/j.ejrad.2020.109157
17. Park J, Pak K, Yun TJ, et al. Diagnostic accuracy and confidence of [18F] FDG PET/MRI in comparison with PET or MRI alone in head and neck cancer. *Sci Rep.* 2020;10(1):9490. doi:10.1038/s41598-020-66506-8
18. Sarma M, Padma S, Sundaram PS. Diagnostic performance of 18F-FDG PET-CT in patients presenting with secondary neck nodes from an unknown primary. *Iran J Nucl Med.* 29(1):15–22. https://irjnm.tums.ac.ir/article_39903.html. Accessed December 12, 2021.
19. Linz C, Brands RC, Herterich T, et al. Accuracy of 18-F fluorodeoxyglucose positron emission tomographic/computed tomographic imaging in primary staging of squamous cell carcinoma of the oral cavity. *JAMA Netw Open.* 2021;4(4):e217083. doi:10.1001/jamanet-workopen.2021.7083
20. Lee H, Lazor JW, Assadsangabi R, Shah J. An imager's guide to perineural tumor spread in head and neck cancers: Radiologic footprints on 18F-FDG PET, with CT and MRI correlates. *J Nucl Med.* 2019;60(3):304–311. doi:10.2967/jnumed.118.214312
21. Hanna E, Vural E, Prokopakis E, Carrau R, Snyderman C, Weissman J. The sensitivity and specificity of high-resolution imaging in evaluating perineural spread of adenoid cystic carcinoma to the skull base. *Arch Otolaryngol Head Neck Surg.* 2007;133(6):541. doi:10.1001/archotol.133.6.541
22. Pyatigorskaya N, De Laroche R, Bera G, et al. Are gadolinium-enhanced MR sequences needed in simultaneous 18F-FDG-PET/MRI for tumor delineation in head and neck cancer? *AJNR Am J Neuroradiol.* 2020;41(10):1888–1896. doi:10.3174/ajnr.A6764
23. Tantiwongkosi B. Role of (18)F-FDG PET/CT in pre and post treatment evaluation in head and neck carcinoma. *World J Radiol.* 2014;6(5):177. doi:10.4329/wjr.v6.i5.177

Correlation between age and curative effects of selective dorsal neurectomy for primary premature ejaculation

*Junwu Yang^{B-F}, *Maolin Chu^{E,F}, Yuzhuo Qi^{B,F}, Haifeng Zhang^{E,F},
Tan Yuan^{E,F}, Li Zhou^{E,F}, Wei Cao^{E,F}, Chunying Zhang^{A,E,F}

2nd Department of Urology, Second Affiliated Hospital of Harbin Medical University, China

A – research concept and design; B – collection and/or assembly of data; C – data analysis and interpretation;
D – writing the article; E – critical revision of the article; F – final approval of the article

Advances in Clinical and Experimental Medicine, ISSN 1899–5276 (print), ISSN 2451–2680 (online)

Adv Clin Exp Med. 2022;31(8):837–845

Address for correspondence

Chunying Zhang
E-mail: cyzhanghlj@qq.com

Funding sources

None declared

Conflict of interest

None declared

*Junwu Yang and Maolin Chu contributed equally to this manuscript.

Received on January 2, 2022

Reviewed on February 24, 2022

Accepted on March 16, 2022

Published online on April 19, 2022

Abstract

Background. The use of selective dorsal neurectomy (SDN) as a surgical treatment of premature ejaculation (PE) has increased for many years in Asian countries.

Objectives. To investigate the correlation between age and curative effects of SDN in primary premature ejaculation (PPE) in mainland China.

Materials and methods. From September 2016 to September 2020, 65 patients with PPE treated with SDN were selected for study. All of the patients were followed up from 12 to 56 (30.07 ±13.48) months. They were divided into 3 groups according to age: group A (22–30 years, n = 23), group B (31–37 years, n = 20) and group C (38–45 years, n = 22). The 5-item version of the International Index of Erectile Function (IIEF-5) and Premature Ejaculation Diagnostic Tool (PEDT) results, erectile rigidity grade, intravaginal ejaculation latency time (IELT), ejaculation control abilities (ECA) scores, and sexual intercourse satisfaction (SIS) scores were assessed in the 3 groups before and after operation to evaluate the clinical efficacy of surgery.

Results. Fifty-nine patients were finally followed up. The IIEF-5 scores and erectile rigidity grade of group A was significantly higher than that of groups B and C, both before and after surgery. The change of PEDT scores in group A was significantly higher than in groups B and C; the difference was statistically significant ($p < 0.05$). The IELT, ECA and SIS scores in group A were significantly higher than in groups B and C ($p < 0.05$). Operational efficiency ratio in groups B and C (65%, 70%) was significantly lower than in group A (95.24%).

Conclusions. The SDN as a treatment of PPE in different age groups allowed to achieve certain results. The highest surgical efficiency (95.24%) was observed in the 22–30 years age group and the lowest (65%) in the 38–45 years age group. Therefore, we believe that the best time for surgery is between 22 and 30 years of age.

Key words: curative effect, age, primary premature ejaculation, selective dorsal neurectomy

Cite as

Yang J, Chu M, Qi Y, et al. Correlation between age and curative effects of selective dorsal neurectomy for primary premature ejaculation. *Adv Clin Exp Med.* 2022;31(8):837–845. doi:10.17219/acem/147426

DOI

10.17219/acem/147426

Copyright

Copyright by Author(s)

This is an article distributed under the terms of the Creative Commons Attribution 3.0 Unported (CC BY 3.0) (<https://creativecommons.org/licenses/by/3.0/>)

Background

Premature ejaculation (PE) is among the most common sexual disorders in adult males, affecting approx. 8–30% of adult males worldwide.¹ It is generally accepted that PE is divided into primary premature ejaculation (PPE) and acquired premature ejaculation (APE).² According to the International Society for Sexual Medicine (ISSM) definition, PE has the following characteristics: 1) ejaculation that always or nearly always occurs before or within 1 min of vaginal penetration (primary PE), or a clinically significant and bothersome reduction in latency time, often to about 3 min or less (acquired PE); 2) the inability to delay ejaculation in all or nearly all vaginal penetrations; 3) negative personal consequences, such as distress, bother, frustration, and/or the avoidance of sexual intimacy.³ Premature ejaculation treatment methods include psychological, behavioral, medication,^{4–6} surgical and Chinese medicine treatment, among others.⁷ The above-mentioned therapies can be used alone or in combination, and the relevant literature reports specific clinical curative effects. However, there are still problems such as high recurrence rate, side effects and uncertain long-term efficacy.^{8,9} In the course of our clinical work, we found that an increasing number of patients with PPE still cannot be treated with conservative therapies, and some patients even voluntarily give up nonsurgical therapies and seek surgical treatment. A representative surgical procedure for PE is selective dorsal neurectomy (SDN), and the clinical application of SDN has opened up new avenues for the treatment of PPE. Although ISSM guidelines disregard surgical treatment of PE arguing that SDN may lead to permanent loss of sexual function, no literature supports its view.¹⁰ On the contrary, over the years, in Asian countries, an increasing number of studies have found significant curative effects of the procedure. Still, varying levels of efficiency in different studies may be related to the inclusion criteria of surgical cases, selection of surgical modalities and standards of efficacy assessment. Also, in our regular follow-up, we found that the improvement in intravaginal ejaculatory latency time (IELT), ejaculation control abilities (ECA) score and sexual intercourse satisfaction (SIS) score was more pronounced in younger patients (22–30 years) after the procedure. We conducted a controlled study to investigate the correlation between SDN curative effects and age. This study encompassed 65 patients with PPE treated with SDN in our hospital from September 2016 to September 2020, in order to compare the postoperative efficacy of SDN in PPE patients of different ages, and investigate the correlation between age and curative effects of SDN.

The study followed the ethical principles for clinical research based on the Declaration of Helsinki. Patients in the study agreed and volunteered to participate in the study, and all patients received informed consent and the confidentiality of their personal data was has been

ensured. The Ethics Committee of our hospital – an independent body composed of medical and nonmedical staff – approved the study (approval No. KY2021-340).

Objectives

To investigate the correlation between age and curative effects of SDN in PPE in mainland China.

Materials and methods

General information

Sixty-five patients were included in this study and divided into 3 groups according to age: 23 in group A (22–30 years); 20 in group B (31–37 years); and 22 in group C (38–45 years). All patients had normal erectile function (IIEF-5 \geq 22) and varying degrees of symptoms of premature ejaculation (PEDT \geq 11). The development of external genitalia was normal, and there were no abnormalities in the testes, epididymis and spermatic cord examination. The measurement of blood glucose, blood pressure and thyroid hormone (T3 and T4) tests were not abnormal.

Selection criteria

The inclusion criteria were as follows: 1) good psychological state; 2) normal erectile hardness during sexual intercourse; 3) sensitive penile glans; 4) quality of sex life seriously affecting the relationship between couples; 5) strong desire for surgery; 6) voluntary abandonment of nonsurgical treatments. Based on Clinical Characteristics Consistent with Primary Premature Ejaculation,¹¹ patients who had a regular sexual partner and had regular sex for at least 6 months and met the above criteria were enrolled in this study.

The exclusion criteria were as follows: 1) patients younger than 22 and older than 45 years; 2) patients with poor psychological status; 3) patients with concomitant prostatitis; 4) patients with hyperthyroidism; 5) patients addicted to drugs; 6) patients with insertion disorders; 7) patients with APE, etc.

Surgical method

Following proper anesthesia, the surgeon made a circular incision at 0.6–0.8 cm from the coronal sulcus (circumcision first if the foreskin is redundant; if circumcision has been done, the cut ran along the original incision; Fig. 1A). Then, the surgeon cut the skin and subcutaneous tissue layer by layer, and separated the penile fascia tissue at a distance of about 0.8–1.5 cm from the coronal sulcus. After separating about 3–4 layers of penile fascial tissue, the dorsal penile nerve could be seen above the anatomical level

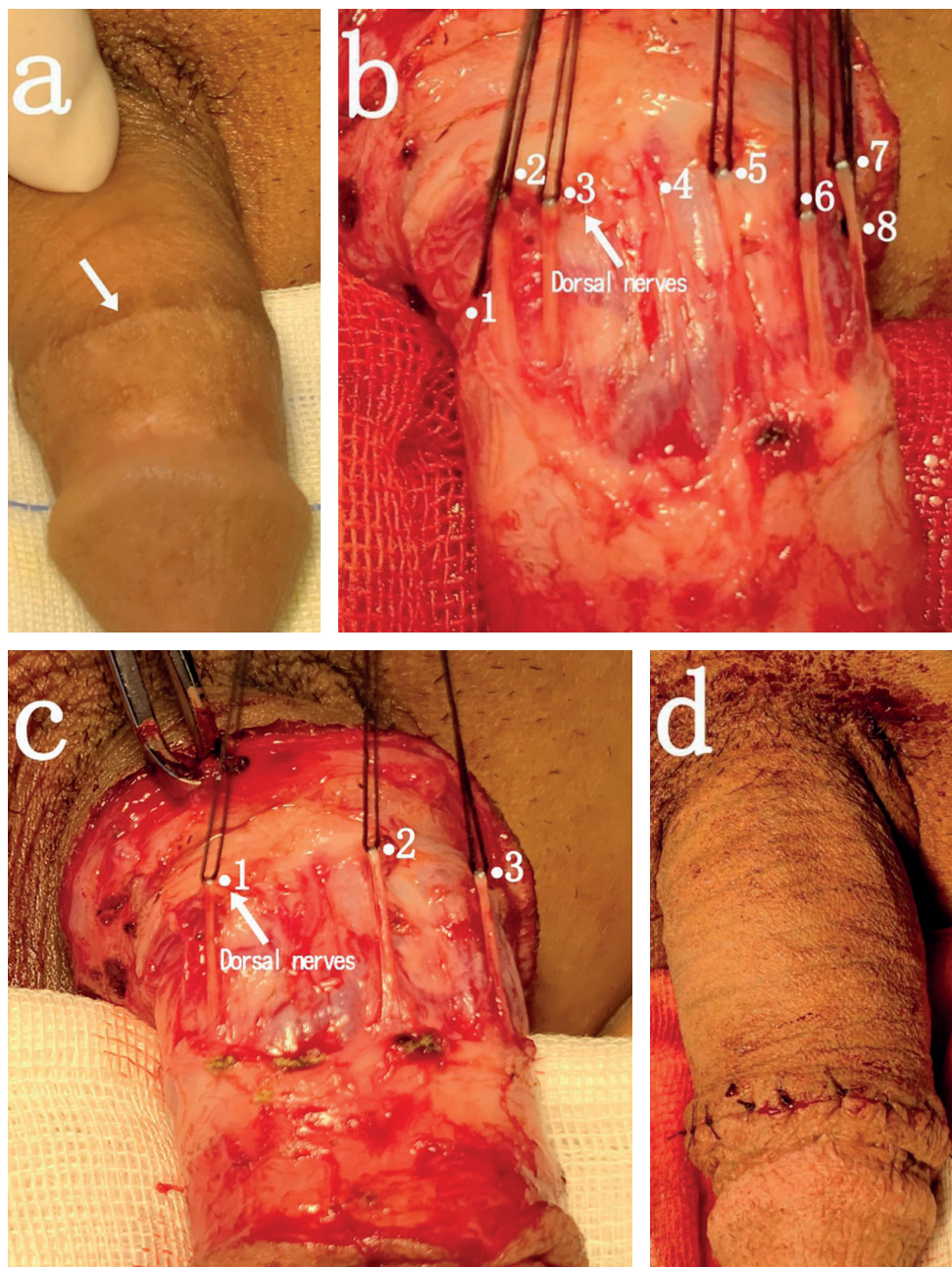


Fig. 1. A. Incision of the skin; B. Exposed dorsal nerves; C. Preserved dorsal nerves; D. Closed incision

of the deep dorsal penile vein and dorsal penile artery. It is yellowish, elastic and rich in trophoblastic vessels, with about 0.2–1.5 mm transverse diameter. Centering on the 12 o'clock in the middle of the dorsal side of the penis, the surgeon used fine tip forceps and microscopic mosquito-type separator forceps to reveal the dorsal penile nerve by separating both sides, reached the urethral corpus cavernosum ventrally to the penis, and used silk thread to gently lift and mark the separated dorsal penile nerve (Fig. 1B). Depending on the patient's specific condition, one nerve at each of the 3, 9 and 12 o'clock of the penile head was preserved. In principle, approx. 3–4 dorsal penile nerves were preserved, and the rest of the dorsal penile nerves were severed and a length of 3–4 cm was removed (Fig. 1C). If the retained dorsal penile nerve was >1.5 mm in transverse diameter, the surgeon continued

to separate dorsal penile nerves distally until approaching the head of the penis, and then the operative area was sutured in 2 layers (Fig. 1D). We performed the indwelling of the catheter at the end of the procedure.

Observation items and method

Observation items

The following measurement tools were used: 5-item version of the International Index of Erectile Function (IIEF-5) score, erectile hardness grade, Premature Ejaculation Diagnostic Tool (PEDT) score, IELT, ECA score, and SIS scores for patients and partners. The efficiency of surgery and the incidence of adverse reactions were also recorded.

Survey data

The patients resumed normal sexual life 1 month after surgery.¹² All patients were requested to measure and record IELT (in seconds) for each sexual intercourse with a stopwatch, for 4 occurrences of sexual intercourse over 2 weeks. The geometric mean IELT calculated for each patient.¹³ The following items were calculated from the data and statistics prepared by the physicians: ECA scores (PEDT 1, 2, 3 items), SIS scores of patients (IIEF6, 7 and 8 items), SIS scores of partners (IIEF 10, 13, 14 items), and the occurrence of postoperative adverse effects.

Evaluation of the curative effect

According to the expert consensus on SDN in China, patients in whom surgery was judged to be effective had the following characteristics: 1) IELT \geq 2 min after surgery; 2) increased ejaculatory control; 3) improved sexual satisfaction of patients and spouses. These 3 items are essential indicators for assessing the treatment effect of PE after surgery, and meeting any of them is considered adequate.¹⁴

Statistical analyses

The IBM SPSS v. 26.0 (IBM Corp., Armonk, USA) and GraphPad Prism v. 8.3.0 (GraphPad Software, San Diego, USA) software were used for statistical analysis and graphical plotting. All the data were analyzed with the Shapiro–Wilk test for normal distribution (Table 1). The variables not distributed normally (age, duration of PE, number of DN, follow-up time, IELT, ECA, SIS, IIEF-5, and PEDT) were described using median and quartiles (M (Q1, Q3)), the comparison between groups (IELT, ECA, SIS, IIEF-5, and PEDT) was performed with the Kruskal–Wallis test and the intra-group comparisons (IELT, ECA, SIS, IIEF-5, and PEDT) was performed with the Friedman's test. Numeric data (marital status) were expressed as n (%); the erectile hardness grade of the penis was compared using nonparametric rank-sum test; the exact Fisher's test was used for comparison between groups, for efficiency

of surgery and incidence of adverse reactions; the Cochran–Armitage χ^2 test¹⁵ was used to determine the relationship between age and efficiency of surgery. A value of $p < 0.05$ was considered statistically significant.

Results

Clinical data

Two patients in the group A and 1 patient in group C refused to be followed up, while 1 patient in group C was lost to follow-up due to a change of personal information; the remaining 61 patients completed the follow-up (Table 2). There was no statistically significant difference regarding the IIEF-5 score between the 3 groups before and after surgery; we observed a statistically significant difference between groups A and C and groups A and B ($p < 0.05$), and no statistically significant difference between groups B and C (Fig. 2). No statistically significant difference regarding PEDT between the 3 groups before and after surgery was observed; a statistically significant difference between groups A and C and groups B and C ($p < 0.05$) could be seen, while no statistically significant difference between groups A and B (Fig. 3) was visible. There was no statistically significant difference regarding erectile rigidity grade between the 3 groups before and after surgery. Before the surgery, the difference between groups A and B ($Z = -1.763$, $p = 0.078$) was not statistically significant, while the difference between groups A and C ($Z = -2.949$, $p = 0.003$) was statistically significant, and the difference between groups B and C ($Z = -1.255$, $p = 0.209$) was not statistically significant (Fig. 4). After the surgery, the difference between groups A and B ($Z = -2.063$, $p = 0.039$) was statistically significant, the difference between groups A and C ($Z = -2.654$, $p = 0.008$) was statistically significant, and the difference between groups B and C ($Z = -0.628$, $p = 0.53$) was not statistically significant (Fig. 5).

There were statistically significant differences in IELT, ECA scores, SIS scores of patients, and SIS scores of partners for intragroup comparisons before and after surgery

Table 1. The p-values of Shapiro–Wilk test for variables between the study groups

| Variable | p-value | | | | | |
|------------------|---------|--------|--------|--------|--------|--------|
| | pre-A | pre-B | pre-C | post-A | post-B | post-C |
| IELT | 0.056 | 0.067 | 0.131 | 0.012* | 0.195 | 0.086 |
| ECA | 0.009* | 0.018* | 0.024* | 0.003* | 0.086 | 0.192 |
| SIS | 0.000* | 0.006* | 0.003* | 0.182 | 0.705 | 0.015* |
| SIS ^Δ | 0.005* | 0.002* | 0.000* | 0.327 | 0.372 | 0.011* |
| IIEF-5 | 0.000* | 0.019* | 0.001* | 0.000* | 0.000* | 0.012* |
| PEDT | 0.010* | 0.086 | 0.011* | 0.000* | 0.002* | 0.111 |

IELT – intravaginal ejaculatory latency time; ECA – ejaculation control abilities; SIS – sexual intercourse satisfaction; ^Δ – partners; IIEF-5 – 5-item version of the International Index of Erectile Function; PEDT – Premature Ejaculation Diagnostic Tool; post- – post-operation; pre- – pre-operation; * – statistically significant. Kruskal–Wallis test and Friedman's test were used.

Table 2. Baseline characteristics

| Variable | Group A (n = 21) | Group B (n = 20) | Group C (n = 20) | p-value |
|------------------------|----------------------|----------------------|----------------------|----------|
| Age [years] | 27.00 (23.50, 28.00) | 32.00 (30.00, 33.75) | 38.50 (38.00, 40.75) | p < 0.05 |
| Duration of PE [years] | 5.00 (3.50, 7.00) | 10.00 (10.00, 13.50) | 15.00 (11.50, 18.00) | p < 0.05 |
| Marital status, n (%) | | | | |
| Married | 13 (61.90) | 15 (75.00) | 14 (70.00) | p < 0.05 |
| Single | 8 (38.10) | 5 (25.00) | 6 (30.00) | p < 0.05 |
| Number of DN | | | | |
| Total | 9.00 (9.00, 10.00) | 9.50 (9.00, 11.00) | 9.50 (9.00, 11.00) | p < 0.05 |
| Resected | 5.00 (5.00, 6.00) | 5.50 (5.00, 7.00) | 5.50 (5.00, 7.00) | p < 0.05 |
| Follow-up [months] | 33.00 (24.50, 42.00) | 24.00 (13.00, 38.25) | 26.00 (24.00, 42.00) | p < 0.05 |

PE – premature ejaculation; DN – dorsal nerves. Values are expressed as number, median and quartiles (M (Q1, Q3)) and percentages. For variables not distributed normally, non-parametric tests were used.

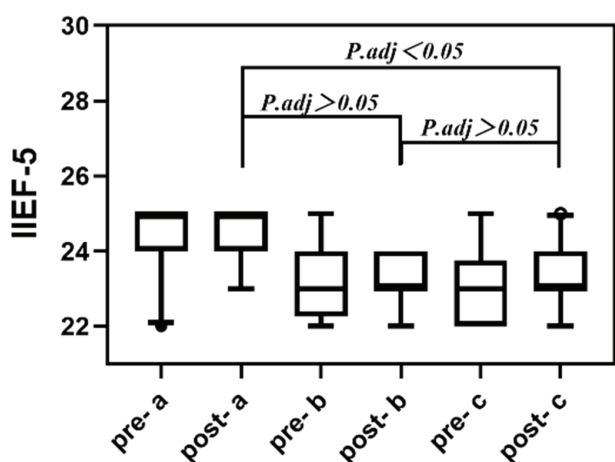


Fig. 2. Presentation of 5-item version of the International Index of Erectile Function (IIEF-5) results alteration before and after operation. Values are presented as median and quartiles (M (Q1, Q3)). Boxplots show the minimum value, 1st quartile (Q1), median, 3rd quartile (Q3), and maximum value. The M (Q1, Q3) of postoperative IIEF-5 in groups A, B and C were 25.00 (25.00, 25.00), 23.00 (22.25, 24.00) and 23.00 (22.00, 22.75), respectively; p.adj < 0.05 for post-a compared to post-b and post-c pre- – pre-operation; post- – post-operation; p.adj – p-value corrected with Bonferroni’s correction.

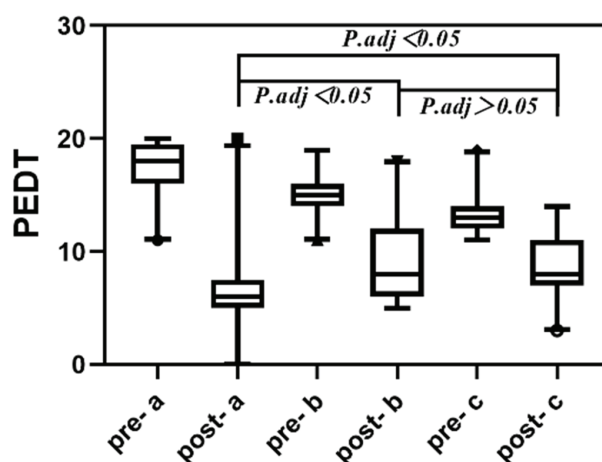


Fig. 3. Presentation of Premature Ejaculation Diagnostic Tool (PEDT) results alteration before and after operation. Values are presented as median and quartiles (M (Q1, Q3)). Boxplots show the minimum value, 1st quartile (Q1), median, 3rd quartile (Q3), and maximum value. The M (Q1, Q3) of postoperative PEDT in groups A, B and C were 6.00 (5.00, 7.50), 8.00 (6.00, 12.00) and 8.00 (7.00, 11.00), respectively; p.adj < 0.05 for post-a compared to post-c pre- – pre-operation; post- – post-operation; p.adj – p-value corrected with Bonferroni’s correction.

in the 3 groups (p < 0.05). Before the surgery, there were no statistically significant differences in IELT, ECA scores, SIS scores of patients, and SIS scores of partners between the 3 groups (p > 0.05). After the surgery, there were statistically significant differences between groups A and C and A and B in IELT and ECA scores (p < 0.05). While we observed statistically significant differences between groups A and C in SIS scores of patients and SIS scores of partners (p < 0.05), the remaining groups showed no statistically significant differences between them regarding these scores (Table 3).

Clinical efficacy

The results of postoperative efficacy assessment were as follows: (n = 21): 20 cases of valid and 1 case of invalid; group B (n = 20): 14 cases of good and 6 instances of invalid;

group C (n = 20): 13 cases of valid and 7 instances of invalid. The effective rate of patients in group A (95.24%) was significantly higher than those in groups B and C (70% and 65%, respectively); the difference was statistically significant (p < 0.05) and the gradual decrease in curative effect rate with age was also statistically significant (Fig. 5).

Adverse reactions

In group A, 1 case of local pain and 1 case of tethered edema was observed, while in group B, 2 cases of local pain, 2 cases of tethered edema and 1 case of subcutaneous hard nodes were recorded. As for group C, 1 case of tethered edema and 1 case of poor appearance occurred, with no statistically significant difference (p > 0.05). None of the patients in the 3 groups had any complications such as abnormal penile erection or erectile dysfunction.

Table 3. Comparison of IELT, ECA score, SIS score for patients, and SIS score for partners in groups A, B and C before and after the operation

| Subjects | M (Q _L , Q _U) | | | H | p-value |
|------------------|--------------------------------------|----------------------|----------------------|-------|--------------------|
| | group A | group B | group C | | |
| IELT | | | | | |
| Pre- | 0.80 (0.45, 1.40) | 0.75 (0.40, 1.18) | 1.10 (0.40, 1.18) | 0.48 | 0.79 |
| Post- | 5.10 (4.45, 6.00) | 4.00 (2.00, 5.15) | 2.85 (1.83, 3.58) | 14.62 | 0* |
| ECA | | | | | |
| Pre- | 11.00 (10.00, 12.00) | 11.00 (10.00, 11.75) | 10.00 (10.00, 11.00) | 0.58 | 0.75 |
| Post- | 4.00 (3.00, 6.00) | 7.00 (4.25, 10.00) | 7.00 (6.00, 9.75) | 14.41 | 0 ^{&} |
| SIS | | | | | |
| Pre- | 2.00 (1.00, 3.00) | 2.00 (1.00, 3.00) | 2.00 (1.25, 3.00) | 0.19 | 0.91 |
| Post- | 8.00 (6.50, 10.00) | 6.50 (3.25, 8.00) | 5.00 (3.00, 6.00) | 10.66 | 0 ^μ |
| SIS ^Δ | | | | | |
| Pre- | 2.00 (1.50, 3.00) | 2.00 (2.00, 3.00) | 1.50 (1.00, 3.00) | 0.93 | 0.63 |
| Post- | 9.00 (7.00, 10.50) | 7.00 (4.00, 8.75) | 5.00 (2.50, 5.75) | 12.19 | 0 ^γ |

M (Q_L, Q_U) – median (lower quartile, upper quartile); pre- – pre-operation; post- – post-operation; IELT – intravaginal ejaculation latency time; ECA – ejaculation control abilities; SIS – sexual intercourse satisfaction; ^Δ – partners.

*Kruskal–Wallis test results are as follows: H = 14.62, p < 0.001. According to the test standard α = 0.05, if null hypothesis (H₀) is rejected, IELT differences can be considered statistically significant in groups A, B and C after operation.

[&] – Kruskal–Wallis test results are as follows: H = 14.62, p < 0.001. According to the test standard α = 0.05, if H₀ is rejected, ECA score differences can be considered statistically significant in groups A, B and C after operation.

^μ – Kruskal–Wallis test results are as follows: H = 14.62, p < 0.001. According to the test standard α = 0.05, if H₀ is rejected, SIS score (patients) differences can be considered statistically significant in groups A, B and C after operation.

^γ – Kruskal–Wallis test results are as follows: H = 14.62, p < 0.001. According to the test standard α = 0.05, if H₀ is rejected, SIS score (partners) differences can be considered statistically significant in groups A, B and C after operation.

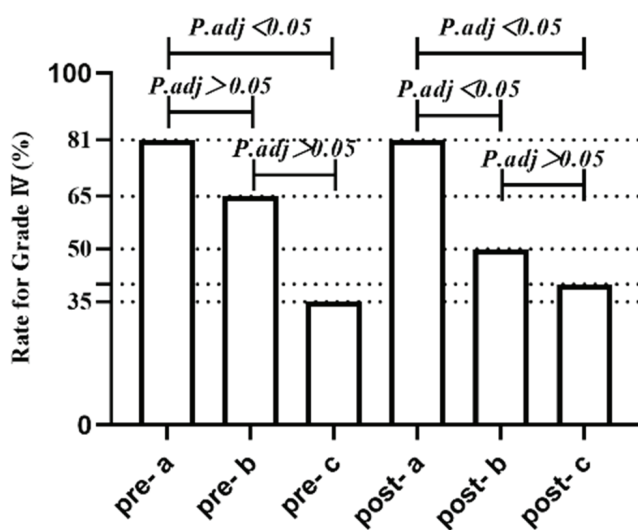


Fig. 4. Presentation of rigidity grade alteration before and after operation. The preoperative rate for grade IV in groups A, B and C were 81%, 65% and 35%, respectively. The postoperative rate for grade IV in groups A, B and C were 81%, 50% and 40%, respectively; p.adj < 0.05 for pre-a compared to pre-c; p.adj < 0.05 for post-a compared to post-b and post-c.

p.adj – p-value corrected with Bonferroni's correction; pre- – pre-operation; post- – post-operation,

Discussion

The causes and mechanisms of PE are not fully understood. It is currently believed that PPE is a sexual dysfunction caused by psychological,¹⁶ behavioral and neurobiological factors. The neurobiological causes include

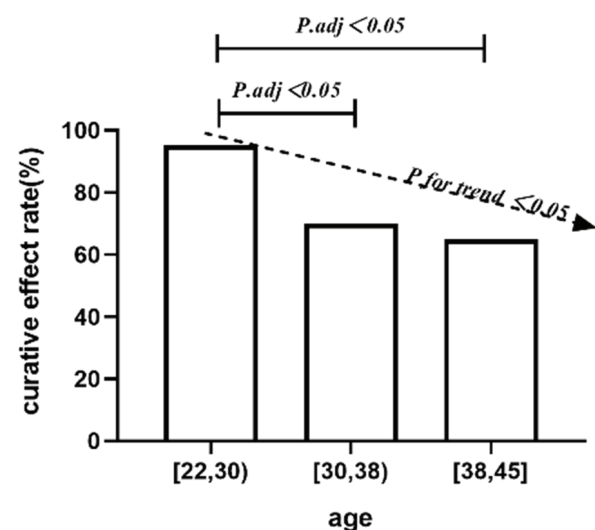


Fig. 5. Presentation of curative effect rate alteration after the operation. The curative effect rate in groups A, B and C was 95.24%, 70% and 65%, respectively. The p-value for trend indicates that the gradual decrease in curative effect rate with age was statistically significant; p.adj < 0.05 for post-a compared to post-b and post-c

p.adj – p-value corrected with Bonferroni's correction; pre- – pre-operation; post- – post-operation.

penile sensory hypersensitivity,^{17–19} ejaculatory reflex hyperactivity, enhanced sexual arousal, possible endocrine diseases, genetic susceptibility, and central 5-HT receptor dysfunction.^{20,21} Factors such as penile sensory hypersensitivity or increased penile sensory nerve excitability play an essential role in PPE.²² Zhang et al.

found that patients with PPE have more dorsal penile nerves compared to normal subjects, which may be one of the reasons for their penile sensory hypersensitivity or increased penile sensory excitability.²³ Rosen et al. suggested that the cause of PE may be closely related to a decrease in penile sensory threshold and increased neural excitability.²⁴ However, the current view is that penile head hypersensitivity and ejaculatory reflex hyperactivity are the leading causes of PE. The main idea of clinical surgery for PPE includes selectively removing the dorsal penile nerve endings, which can reduce nerve impulse transmission, thus reducing the sensitivity of the penile head and prolonging the ejaculatory latency.¹⁴ Some studies have shown that SDN is effective in delaying ejaculation and does not affect erectile function. Zhang et al. found that at a 6-month follow-up the efficacy rate in 128 patients was 87.5%, with satisfactory clinical outcomes and no severe complications such as erectile dysfunction.²⁵ Zhang et al. conducted a randomized controlled clinical study on 78 patients with a 2-year postoperative follow-up, and the patients showed significant improvement in IELT and ejaculatory control compared with the preoperative period, as well as no complications such as erectile and ejaculatory dysfunction.²⁶ In a nationwide study of 286 patients with PE treated with SDN in Korea, Yang et al. found that 96.6% of the patients felt that the symptoms of PE had subsided and only 0.4% of the patients had erectile dysfunction.²⁷ Zhou et al. treated 78 cases of PPE with microscopic SDN. They showed significant improvement in IELT and patient and partner SIS scores at 3-month postoperative follow-up compared with the pre-treatment period, as well as no complications such as penile head numbness, abnormal penile erection and erectile dysfunction (ED).²⁸

Liu et al. found that patients in the surgical treatment group presented significant improvements in IELT and ejaculatory control compared with the sham-operated group at 6-month follow-up. There were no severe complications such as ED.²⁹ Genov et al. reported a patient with PPE in whom the conservative treatment had failed, who underwent microscopic SDN and who were followed up for 12 months after surgery – and found a 6-fold increase in IELT compared to preoperative measurements. The patient was free of symptoms of PE at the last follow-up, with no severe complications.³⁰ Alyaev and Akhvediani observed that the efficiency of the surgical group was 88% higher than that of the sham-operated group (10.2%), and no erectile dysfunction occurred after surgery.³¹ It is important to note that pharmacological treatment as the first-line treatment for PE is still widely accepted worldwide, and SDN is not mainstream treatment for PE, but a complementary rather than a substitute for non-surgical treatment.

This study showed that most patients treated with SDN showed significant improvement compared with

those before treatment. However, the curative effects of some patients have not yet reached the clinical ideal. According to the efficacy assessment criteria, the curative effect in group A was significantly higher than in groups B and C. There was a correlation between curative effect and age. According to the IIEF-5 score and nocturnal penile tumescence test (NPT), the erectile function and erectile hardness in patients in the group A were significantly better than in the other 2 groups before and after surgery. In addition, the PEDT scores of patients in group A were significantly higher than in groups B and C before surgery.

In contrast, the PEDT scores of patients in group A were substantially lower than in groups B and C after surgery. The patients in group A had a better erectile function and erectile rigidity, and more significant improvement in PEDT scores before and after surgery. At the same time, it has been pointed out that there is a tendency for the values of each point of the penile biosensor threshold test to increase gradually with age in patients with PPE, and the sensitivity of the penile head was reduced to varying degrees.^{32,33} It can be seen that PPE treatment with SDN should be performed as early as possible – optimally at the age of 22–30. It may be due to the patients' higher penile sensitivity and better erectile function that the degree of postoperative improvement is relatively more apparent and the efficacy tends to be better. Postoperative complications were also analyzed, and the incidence of local pain, tethered edema, subcutaneous sclerosis, or poor appearance of penile foreskin in the 3 groups was not statistically significant. No complications such as abnormal penile erection or erectile dysfunction occurred in any patient, indicating that increasing age does not affect treatment safety. Thus, it can be seen that the efficacy of SDN in the treatment of PPE is remarkable, with few adverse effects. Moreover, the effectiveness of patients is closely related to their age, and the clinic should clarify the diagnosis early.

Limitations



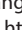
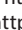


There are several limitations to this study. First, the minimum age to be enrolled in the study was 22, since the legal age of marriage for men in China is 22, but in fact, most of the patients presented PE symptoms before they reached such age. At the same time, the number of patients over 45 years attending our clinic is low. In the future, we can further expand the age span in the study group in order to study the relationship between efficacy and age. Second, there is no uniform standard for the assessment of ejaculatory control, and the 3 questions we used (PEDT items 1, 2 and 3) for review may cause some inaccuracies. Third, the number of cases included in this study is limited, and the results of multicenter studies are lacking; further expansion

of the sample size is needed in the future to reduce errors. Fourth, there is no unified surgical efficacy assessment standard. The Chinese guidelines for diagnosing and treating PE and the expert consensus criteria may be appropriate only for the Asian population. Future multi-geographic and multi-institutional studies are needed to clarify them further. Fifth, our patients did not have complications such as glans numbness, probably due to the appropriate number of dorsal penile nerves preserved during the procedure. Still, we did not determine how many dorsal nerves should be selectively resected in each patient to achieve optimal IELT prolongation.

Conclusions

The SDN as surgical treatment of PPE in different age groups has achieved certain results. The highest surgical efficiency (95.24%) was achieved in the 22–30 age group and the lowest (65%) in the 38–45 age group. Therefore, we believe that the best time for a such surgery is between 22 and 30 years of age.

ORCID iDs

Junwu Yang  <https://orcid.org/0000-0002-7792-1380>
 Maolin Chu  <https://orcid.org/0000-0002-6285-7777>
 Yuzhuo Qi  <https://orcid.org/0000-0002-0106-8539>
 Haifeng Zhang  <https://orcid.org/0000-0003-0698-594X>
 Tan Yuan  <https://orcid.org/0000-0003-4721-5810>
 Li Zhou  <https://orcid.org/0000-0002-3081-7009>
 Wei Cao  <https://orcid.org/0000-0002-2755-7023>
 Chunying Zhang  <https://orcid.org/0000-0003-0924-0943>

References

- Laumann EO, Paik A, Rosen RC. Sexual dysfunction in the United States: Prevalence and predictors. *JAMA*. 1999;281(6):537–544. doi:10.1001/jama.281.6.537
- McMahon CG, Althof SE, Waldinger MD, et al. An evidence-based definition of lifelong premature ejaculation: Report of the International Society for Sexual Medicine (ISSM) Ad Hoc Committee for the Definition of Premature Ejaculation. *J Sex Med*. 2008;5(7):1590–1606. doi:10.1111/j.1743-6109.2008.00901.x
- Serefoglu EC, McMahon CG, Waldinger MD, et al. An evidence-based unified definition of lifelong and acquired premature ejaculation: Report of the Second International Society for Sexual Medicine Ad Hoc Committee for the Definition of Premature Ejaculation. *J Sex Med*. 2014;11(6):1423–1441. doi:10.1111/jsm.12524
- Qin Z, Wang Y, Zhu J, et al. Safety and efficacy characteristics of oral drugs in patients with premature ejaculation: A Bayesian network meta-analysis of randomized controlled trials. *Int J Impot Res*. 2019; 31(5):356–368. doi:10.1038/s41443-019-0146-7
- Rowland DL, Dabbs CR, Medina MC. Sex differences in attributions to positive and negative sexual scenarios in men and women with and without sexual problems: Reconsidering stereotypes. *Arch Sex Behav*. 2019;48(3):855–866. doi:10.1007/s10508-018-1270-z
- Zhang D, Cheng Y, Wu K, Ma Q, Jiang J, Yan Z. Paroxetine in the treatment of premature ejaculation: A systematic review and meta-analysis. *BMC Urol*. 2019;19(1):2. doi:10.1186/s12894-018-0431-7
- Guo J, Wang F, Zhou Q, et al. Safety and efficacy of traditional Chinese medicine, Qiaoshao formula, combined with dapoxetine in the treatment of premature ejaculation: An open-label, real-life, retrospective multicentre study in Chinese men. *Andrologia*. 2021;53(1):e13915. doi:10.1111/and.13915
- Burton TD, Liday C. The comparison of combination SSRI and PDE-5 inhibitor therapy to SSRI monotherapy in men with premature ejaculation. *Ann Pharmacother*. 2011;45(7–8):1000–1004. doi:10.1345/aph.1Q008
- Moheeb A, Eardley I. Medical therapy for premature ejaculation. *Ther Adv Urol*. 2011;3(5):211–222. doi:10.1177/1756287211424172
- Althof SE, Abdo CH, Dean J, et al. International Society for Sexual Medicine's guidelines for the diagnosis and treatment of premature ejaculation. *J Sex Med*. 2010;7(9):2947–2969. doi:10.1111/j.1743-6109.2010.01975.x
- Salonia A, Bettocchi C, Boeri L, et al. European Association of Urology Guidelines on Sexual and Reproductive Health – 2021 Update: Male sexual dysfunction. *Eur Urol*. 2021;80(3):333–357. doi:10.1016/j.eururo.2021.06.007
- Basal S, Goktas S, Ergin A, et al. A novel treatment modality in patients with premature ejaculation resistant to conventional methods: The neuromodulation of dorsal penile nerves by pulsed radiofrequency. *J Androl*. 2010;31(2):126–130. doi:10.2164/jandrol.108.007344
- Waldinger MD, Zwinderman AH, Olivier B, Schweitzer DH. Geometric mean IELT and premature ejaculation: Appropriate statistics to avoid overestimation of treatment efficacy. *J Sex Med*. 2008;5(2):492–499. doi:10.1111/j.1743-6109.2007.00696.x
- Journal of Chinese Medicine Information Society MB. Guidelines for the multidisciplinary treatment of premature ejaculation with Chinese and Western medicine (2021 edition) [in Chinese]. *Zhonghua Nan Ke Xue*. 2021;35(3):66–72. <https://kns.cnki.net/kcms/detail/detail.aspx?dbcode=CJFD&dbname=CJFDLAST2021&filename=NXXX202103014&uniplatform=NZKPT&v=JeWkic7V1RNWuQxDVOD7YmH1yIjgz640nOYXezxS89wPPnoCGQZ2yrDNjbyQjT4J>. Accessed December 15, 2021.
- Armitage P. Tests for linear trends in proportions and frequencies. *Biometrics*. 1955;11(3):375–386. doi:10.2307/3001775
- Kempeneers P, Andrienne R, Cuddy M, Blairy S. Sexual cognitions, trait anxiety, sexual anxiety, and distress in men with different subtypes of premature ejaculation and in their partners. *J Sex Marital Ther*. 2018;44(4):319–332. doi:10.1080/0092623X.2017.1405299
- Wiggins A, Farrell MR, Tsambarlis P, Levine LA. The penile sensitivity ratio: A novel application of biothesiometry to assess changes in penile sensitivity. *J Sex Med*. 2019;16(3):447–451. doi:10.1016/j.jsxm.2019.01.002
- Chen X, Wang FX, Hu C, Yang NQ, Dai JC. Penile sensory thresholds in subtypes of premature ejaculation: Implications of comorbid erectile dysfunction. *Asian J Androl*. 2018;20(4):330–335. doi:10.4103/aja.aja_62_17
- Guo L, Liu Y, Wang X, et al. Significance of penile hypersensitivity in premature ejaculation. *Sci Rep*. 2017;7(1):10441. doi:10.1038/s41598-017-09155-8
- Khan HL, Bhatti S, Abbas S, et al. Serotonin transporter (5-HTTLPR) genotypes and trinucleotide repeats of androgen receptor exert a combinatorial effect on hormonal milieu in patients with lifelong premature ejaculation. *Andrology*. 2018;6(6):916–926. doi:10.1111/andr.12518
- Roaiha MF, Elkhayat YI, Rashed LA, GamalEl Din SF, El Guindi AM, Abd El Salam MA. Study of the prevalence of 5-HT2C receptor gene polymorphisms in Egyptian patients with lifelong premature ejaculation. *Andrologia*. 2018;50(2). doi:10.1111/and.12855
- Xin ZC, Chung WS, Choi YD, Seong DH, Choi YJ, Choi HK. Penile sensitivity in patients with primary premature ejaculation. *J Urol*. 1996;156(3):979–981. PMID:8709378.
- Zhang CY, Li XH, Yuan T, Zhang HF, Liu JH, Ye ZQ. Regional anatomy of the dorsal penile nerve and its clinical significance [in Chinese]. *Zhonghua Nan Ke Xue*. 2009;15(2):130–133. PMID:19323372.
- Rosen RC, McMahon CG, Niederberger C, Broderick GA, Jamieson C, Gagnon DD. Correlates to the clinical diagnosis of premature ejaculation: Results from a large observational study of men and their partners. *J Urol*. 2007;177(3):1059–1064, discussion 1064. doi:10.1016/j.juro.2006.10.044
- Zhang CY, Zhang HF, Guo J, Li Q, Guo TJ, Shao KQ. 128 cases of primary premature ejaculation treated by modified dorsal penile neurectomy [in Chinese]. *Zhonghua Nan Ke Xue*. 2005;10:789–791. https://kns.cnki.net/kcms/detail/detail.aspx?dbcode=CJFD&dbname=CJFD2005&filename=NKXB200510019&uniplatform=NZKPT&v=6tcaQH-19md2WJGwhEYmHR1luW-ptK9C19_17604mc-GuVOirJyLo2oLcyTfVqct. Accessed December 15, 2021.

26. Zhang GX, Yu LP, Bai WJ, Wang XF. Selective resection of dorsal nerves of penis for premature ejaculation. *Int J Androl*. 2012;35(6):873–879. doi:10.1111/j.1365-2605.2012.01296.x
27. Yang DY, Ko K, Lee WK, et al. Urologist's practice patterns including surgical treatment in the management of premature ejaculation: A Korean nationwide survey. *World J Mens Health*. 2013;31(3):226–231. doi:10.5534/wjmh.2013.31.3.226
28. Zhou XJ, Zhang ZG, Hao L, Zhang WD, Dong BZ, Han CH. Elective microscopic resection of dorsal penile nerves for primary premature ejaculation: A clinical observation [in Chinese]. *Zhonghua Nan Ke Xue*. 2013;19(11):1003–1006. PMID:24341095.
29. Liu Q, Li S, Zhang Y, et al. Anatomic basis and clinical effect of selective dorsal neurectomy for patients with lifelong premature ejaculation: A randomized controlled trial. *J Sex Med*. 2019;16(4):522–530. doi:10.1016/j.jeucr.2019.100937
30. Genov PP, Kolev NH, Dunev VR. Premature ejaculation: Operative management after failure of conservative treatment. *Urol Case Rep*. 2019;26:100937. doi:10.1016/j.jeucr.2019.100937
31. Alyaev YG, Akhvediani ND. Comparing efficacy of selective penile denervation and circumcision for primary premature ejaculation [in Russian]. *Urologiia*. 2016;(1 Suppl 1):60–64. PMID:28247749.
32. Peng L, Chen N, Qi R. Analysis of penile nerve detection in 486 cases with premature ejaculation [in Chinese]. *Chinese Journal of Human Sexuality*. 2015;24(12):22–25. <https://kns.cnki.net/kcms/detail/detail.aspx?dbcode=CJFD&dbname=CJFDLAST2016&filename=XKXZ201512009&uniplatform=NZKPT&v=6BmsYd4bFyPR9ofKlAXsDCMMXcdOkP6115wZUjAVMq45Zx2qVxgV4h7rwATGXPA5>. Accessed December 15, 2021.
33. Yu HL, Chen YZ, Bo LW. Influence of age, height, weight and body mass index on the glans sensitivity of patients with premature ejaculation [in Chinese]. *Chinese Journal of Human Sexuality*. 2019;28(8):21–24. <https://kns.cnki.net/kcms/detail/detail.aspx?dbcode=CJFD&dbname=CJFDLAST2019&filename=XKXZ201908008&uniplatform=NZKPT&v=VdnXd7cpsPliAnt9unZFP4qjmyrqbXWdStR7VxFAaQ8fndZYjSyQW6AOnpG8mLU>. Accessed December 15, 2021.

Quantitative shear wave elastography compared to standard ultrasound (qualitative B-mode grayscale sonography and quantitative power Doppler) for evaluation of achillotendinopathy in treatment-naïve individuals: A cross-sectional study

Lixiu Chen^{1,B,E,F}, Ying Cheng^{1,B,E,F}, Liang Zhou^{1,A,C,E,F}, Lei Zhang^{1,B,C,E,F}, Xueyan Deng^{2,C-F}

¹ Chongqing Red Cross Hospital, People's Hospital of Jiangbei District, China

² Chongqing Jiulongpo District Second People's Hospital, China

A – research concept and design; B – collection and/or assembly of data; C – data analysis and interpretation;

D – writing the article; E – critical revision of the article; F – final approval of the article

Advances in Clinical and Experimental Medicine, ISSN 1899–5276 (print), ISSN 2451–2680 (online)

Adv Clin Exp Med. 2022;31(8):847–854

Address for correspondence

Xueyan Deng

E-mail: jbq_rmyy@sina.com

Funding sources

None declared

Conflict of interest

None declared

Acknowledgements

The authors are thankful for the medical, non-medical and radiological staff of the Chongqing Jiulongpo District Second People's Hospital, Chongqing, China, and the Chongqing Red Cross Hospital, People's Hospital of Jiangbei District, Chongqing, China.

Received on January 24, 2022

Reviewed on February 10, 2022

Accepted on March 31, 2022

Published online on May 20, 2022

Cite as

Chen L, Cheng Y, Zhou L, Zhang L, Deng X. Quantitative shear wave elastography compared to standard ultrasound (qualitative B-mode grayscale sonography and quantitative power Doppler) for evaluation of achillotendinopathy in treatment-naïve individuals: A cross-sectional study.

Adv Clin Exp Med. 2022;31(8):847–854.

doi:10.17219/acem/147878

DOI

10.17219/acem/147878

Copyright

Copyright by Author(s)

This is an article distributed under the terms of the Creative Commons Attribution 3.0 Unported (CC BY 3.0) (<https://creativecommons.org/licenses/by/3.0/>)

Abstract

Background. Achillotendinopathy is reported as an overuse disorder and/or degeneration change of the tendon. The diagnosis of tendinopathy is not always easy through imaging modalities. The B-mode grayscale sonography and power Doppler are well-established methods aimed at visualising tendon structure, but have limited sensitivity and lack conventional sonographic characteristics in symptomatic patients. Shear wave ultrasound elastography quantitatively assesses tissue stiffness.

Objectives. To compare the diagnostic accuracy of shear wave ultrasound elastography to that of standard ultrasound (combined B-mode grayscale sonography and power Doppler) for diagnosis of achillotendinopathy, considering clinical symptoms as the reference standard.

Materials and methods. Standard questionnaires regarding medical history and the Chinese version of a Victorian Institute of Sports Assessment – Achilles Questionnaires (VISA-AC) score were evaluated for a total of 14 treatment-naïve patients with complaints of localized swelling, and reduced force and/or flexibility of the Achilles tendon(s). The irregular thickening around the Achilles tendon, heterogeneity of echotexture of the tendon and calcification of the calcaneal attachment were considered incidences of tendinopathy in B-mode grayscale sonography. Tendinopathies were considered if tendons were >0.60 cm thick in power Doppler. Shear wave elasticity <350 kpa (10 m/s) was considered tendinopathy.

Results. A total of 28 conditions of both sides were evaluated through standard ultrasound examinations. Eighty-four tendons were assessed using shear wave ultrasound elastography. Asymptomatic tendons were visible as red and symptomatic (VISA-AC score <80) tendons were visible as blue or turquoise in the images. The rigidity of symptomatic tendons was lower than that of asymptomatic tendons ($p < 0.0001$). Sensitivity and accuracy for standard ultrasound were increased by the addition of shear wave ultrasound elastography for both symptomatic and asymptomatic tendons. The VISA-AC score was strongly correlated with the elasticity values ($p = 0.000$, Kendall's tau-beta ($\tau\beta$) = 0.71) of Achilles tendons.

Conclusions. Shear wave ultrasound elastography augments diagnostic confidence of standard ultrasound for the treatment of tendinopathies of Achilles tendons.

Key words: power Doppler, Achilles tendon, B-mode grayscale sonography, shear wave ultrasound elastography, tendinopathies

Background

Achilles tendinopathy (achillotendinopathy) is an orthopedic injury reported due to overuse of lower extremity, especially among athletes (overuse disorder) and elderly people (degeneration change of the tendon).¹ Achilles tendinopathy leads to chronic tendon pain, chronic tendon injury and/or accumulation of subclinical microdamage.² To overcome rupture of a tendon, chronic pain and severe injuries of a tendon, and to provide effective treatment, early diagnosis of tendinopathy is necessary.³ Etiology and pathology of Achilles tendinopathy are not fully understood.⁴ Therefore, it is difficult to choose an appropriate treatment.

Achillotendinopathy is a huge clinical problem and better diagnostic tools would be beneficial for the follow-up of patients with Achilles tendinopathy. The diagnosis of tendinopathy is not always easy using imaging modalities⁵ because 3 different muscles contribute to the Achilles tendons.⁶ The B-mode grayscale sonography and power Doppler are well-established ultrasound techniques, and magnetic resonance imaging (MRI) is used to visualize tendon structure⁷ because heterogeneous echogenicity or hypoechogenicity and increased tendon thickness correlates with tendon functions.⁸ However, their utilization in Achilles tendinopathy diagnosis is controversial⁹ because their sensitivity is limited and Achilles tendinopathy lacks conventional sonographic characters in symptomatic patients.¹⁰

Shear wave ultrasound elastography allows to quantitatively assess tissue stiffness, but is used less often in tendinopathy diagnostics. It is well-established for visualization of stiffness of liver,¹¹ breast,¹² prostate,¹³ thyroid,¹⁴ shoulder tendons,¹⁵ and tongue muscle¹⁶ lesions. It is also regarded as a promising tool for the diagnosis of Achilles tendinopathy and patellar tendons in routine clinical practice.¹⁷

Objectives

The objectives of the retrospective analysis of a cross-sectional study were to compare the diagnostic accuracy of quantitative shear wave ultrasound elastography to that of a standard ultrasound (combined qualitative B-mode grayscale sonography and quantitative power Doppler) for diagnosis of Achilles tendinopathy in treatment-naïve patients, considering clinical symptoms as the reference standard.

Materials and methods

The designed protocol of the study was approved by the ethics committee of the Chongqing Jiulongpo District Second People's Hospital (approval No. CJSPH2123 dated April 20, 2020). The study protocol adheres

to Chinese law and the 2008 Declaration of Helsinki. All studied patients have signed during hospitalization an informed consent form regarding radiological examinations, biochemical tests and publication of anonymized information in the form of a scientific article (1 or more).

The inclusion criteria were as follows: patients from a diabetes clinic with complaints of pain in the Achilles unilateral or bilateral tendon(s), diffuse or localized swelling, reduced force, and/or reduced flexibility of the unilateral or bilateral tendon(s) in the last 6 months.

Patients who had undergone treatment for their clinical symptoms, like physical therapy or medication (systemic, and/or topical) with nonsteroidal anti-inflammatory drugs, were excluded from analysis because symptoms should persist at the time of ultrasound examinations. Patients with tendon rupture or surgery were also excluded from analysis.

Clinical assessment

Standard questionnaires regarding medical history, sports activity and tendon pain (in rest, movement and pressure) were evaluated for all studied patients before ultrasound examinations were performed by orthopedic surgeons. The Chinese version of a Victorian Institute of Sports Assessment – Achilles Questionnaires (VISA-AC) score was used for the evaluation of pain in tendons.¹⁸ The score ranges from 100 to 0, in which 100 means no pain or no impairment in physical activity and 0 means maximum pain or maximum impairment in physical activity. Glycated hemoglobin (%HbA1C), cholesterol, serum triglycerides, fasting blood glucose, and urine albumin levels were evaluated through pathological examinations. Tendons with a VISA-AC score less than 80 were considered symptomatic.³

Ultrasound examinations

All studied patients underwent a bilateral multimodal ultrasound that included B-mode grayscale sonography, power Doppler ultrasound and shear wave ultrasound elastography. Aixplorer (SuperSonic Imagine, Aix-en-Provence, France) ultrasound equipment with 15 MHz linear transducer (SuperLinear SL15-4; SuperSonic Imagine) and 256 bandwidths from a 5–14 MHz range were used. Wall filter, alias threshold and other standardized setting parameters were the same in all studied patients. A gel (Sonogel®; Sonogel Vertriebs GmbH, Bad Camberg, Germany), a cushion delay block (length: 100 × 100 mm) and a 20 mm delay distance between transducer and skin were used to improve docking. All ultrasound examinations were performed by radiologists (blinded to the patients' symptoms) with minimum 5 years of experience.

The Achilles tendons were examined in a relaxed state, in prone position, with foot hanging freely beyond the examination couch.

Standard ultrasound examination

B-mode grayscale sonography in the longitudinal and axial planes was performed. Conditions of the area around the left and right Achilles tendons were evaluated. The irregular thickening around the Achilles tendon, heterogeneity of echotexture of the tendon and calcification of the calcaneal attachment were considered incidences of tendinopathy.³ Then, power Doppler of the whole tendons was performed, and the thickness of the left and right Achilles tendons was evaluated. Achilles tendinopathy was considered if tendons were more than 0.60 cm thick.¹⁹ The representative image for power Doppler of the tendon is presented in Fig. 1.

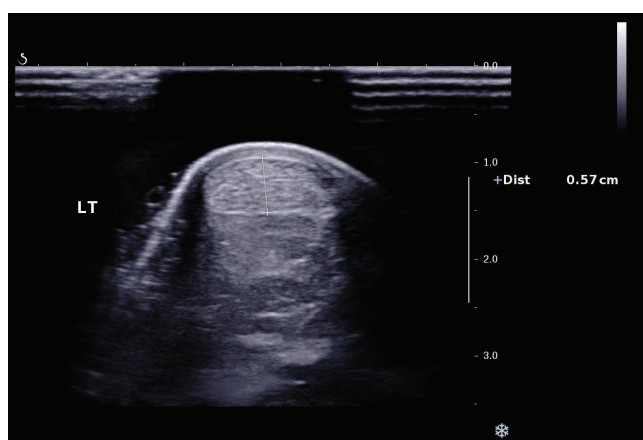


Fig. 1. The power Doppler image of a tendon. The thickness of the left Achilles tendon was 0.57 cm

LT – left tendon.

Shear wave ultrasound elastography

Shear wave ultrasound elastography was performed for the upper left Achilles tendon, middle left Achilles tendon, lower left Achilles tendon, upper right Achilles tendon, middle right Achilles tendon, and lower right Achilles

tendon. It was performed for the most suspicious area detected with the B-mode grayscale sonography. The results were analyzed based on color images (semi-quantitatively) and by rigidity of tissue in the region of interest (ROI; quantitatively). The meaning of the colors is: blue – low rigidity, turquoise – intermediate rigidity, yellow to red – high rigidity. The Young’s modulus was used for a quantitative assessment of shear wave ultrasound elastography. The maximum speed of the shear wave was 500 kPa/13 m/s with 2 cm depth. In the ROI, mean and maximum rigidity and shear wave speed were evaluated. A total of 2 mm was the standard diameter of the ROI.³ The representative images for B-mode grayscale sonography and shear wave ultrasound elastography are presented in Fig. 2. The characteristics of the most auspicious area in the B-mode grayscale sonography were: the irregular thickening around the Achilles tendon, heterogeneity of echotexture of the tendon and calcification of the calcaneal attachment. Shear wave elasticity less than 350 kpa (10 m/s) was considered tendinopathy.

Beneficial score analysis

Working area for treatment of tendinopathy was decided based on Equation 1²⁰:

$$\begin{aligned}
 & \text{Beneficial score analysis} = \\
 & = \left\{ \frac{\text{true positive tendinopathy detected}}{\text{total number of tendons evaluated}} - \right. \\
 & \left. - \left[\frac{\text{false negative tendinopathy detected}}{\text{total number of tendons evaluated}} \right] \times (1) \right. \\
 & \left. \times \frac{\text{level of diagnostic confidence above which}}{\text{1 – level of diagnostic confidence above}} \right\} \left. \begin{array}{l} \text{level of diagnostic confidence above which} \\ \text{treatment for tendinopathy can be} \\ \text{initiated or continued} \end{array} \right\}
 \end{aligned}$$

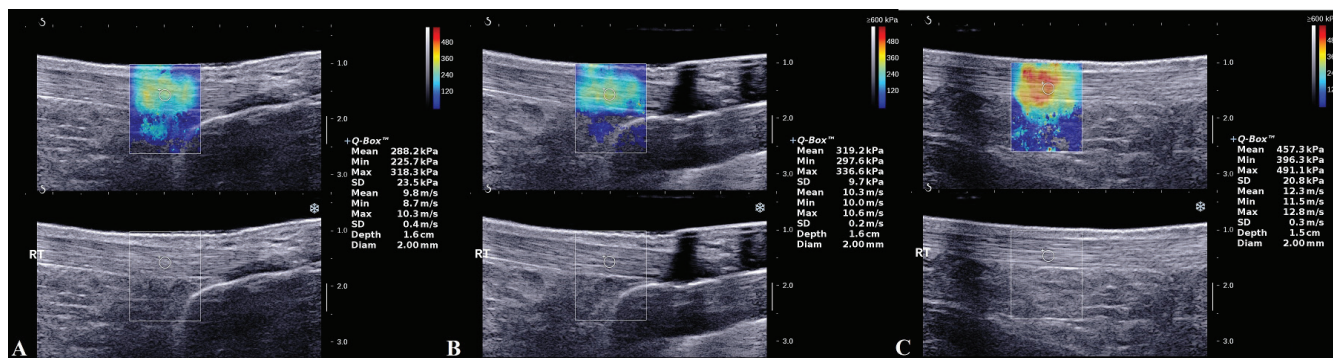


Fig. 2. B-mode grayscale sonography and shear wave ultrasound elastography images of tendons (RT – right tendon). A. Irregular thickening around the Achilles tendon in the B-mode grayscale sonography (blue color image in the shear wave ultrasound elastography signifies low rigidity); B. Heterogeneity of echotexture of the tendon in the B-mode grayscale sonography (turquoise color image in the shear wave ultrasound elastography signifies intermediate rigidity); C. Calcification of the calcaneal attachment in the B-mode grayscale sonography (yellow to the red color image in the shear wave ultrasound elastography signifies high rigidity). A circle in the B-mode grayscale sonography represents the region of interest: 2-mm diameter

Diagnostic parameters

Sensitivity and accuracy were evaluated as in Equation 2,3:

$$\text{sensitivity} = \frac{\text{true positive tendinopathy}}{\text{true positive tendinopathy} + \text{false negative tendinopathy}} \quad (2)$$

$$\text{accuracy} = \frac{\text{true positive tendinopathy} + \text{true negative tendinopathy}}{\text{total number of tendons evaluated}} \quad (3)$$

Statistical analyses

The IBM SPSS v. 26.0 software (IBM Corp., Armonk, USA) was used for statistical analyses. The Mann–Whitney test was performed for continuous data. The Fisher’s exact test was used for categorical data. The Kendall’s tau-beta correlation was developed between VISA-AC score and the ultrasound characteristics of Achilles tendons at 95% confidence interval (95% CI). The Kendall’s tau-beta correlation coefficient ($\tau\beta$) was interpreted as: 0 – no correlation, 0.1–0.39 – weak correlation, 0.4–0.69 – moderate correlation, 0.7–0.89 – strong correlation, and ≥ 0.9 – perfect correlation.²¹ All results were considered significant if the p-value was less than 0.05.

Results

Study population

From April 21, 2020 to May 1, 2021, 32 individuals with complaints of pain, diffuse or localized swelling, reduced force, and/or reduced flexibility of the Achilles tendon(s) were enrolled at the Department of Orthopedics of the Chongqing Jiulongpo District Second People’s Hospital, Chongqing, China, and the Chongqing Red Cross Hospital, People’s Hospital of Jiangbei District, Chongqing, China. Among them, 14 patients had undergone treatment for their clinical symptoms, 3 patients had tendon rupture and 1 patient had undergone surgery. Therefore, data of these patients ($n = 18$) were not included in the analysis. Data on clinical symptoms, pathological examinations, B-mode grayscale sonography, power Doppler ultrasound, and shear wave ultrasound elastography of 14 patients were retrospectively included in the analysis after obtaining written approval from the respective institutions, as it was a retrospective study. The flow diagram of retrospective analysis of the study is presented in Fig. 3.

Clinical symptoms

Clinical symptoms of 14 patients were analyzed. The details of their clinical symptoms are presented in Table 1.

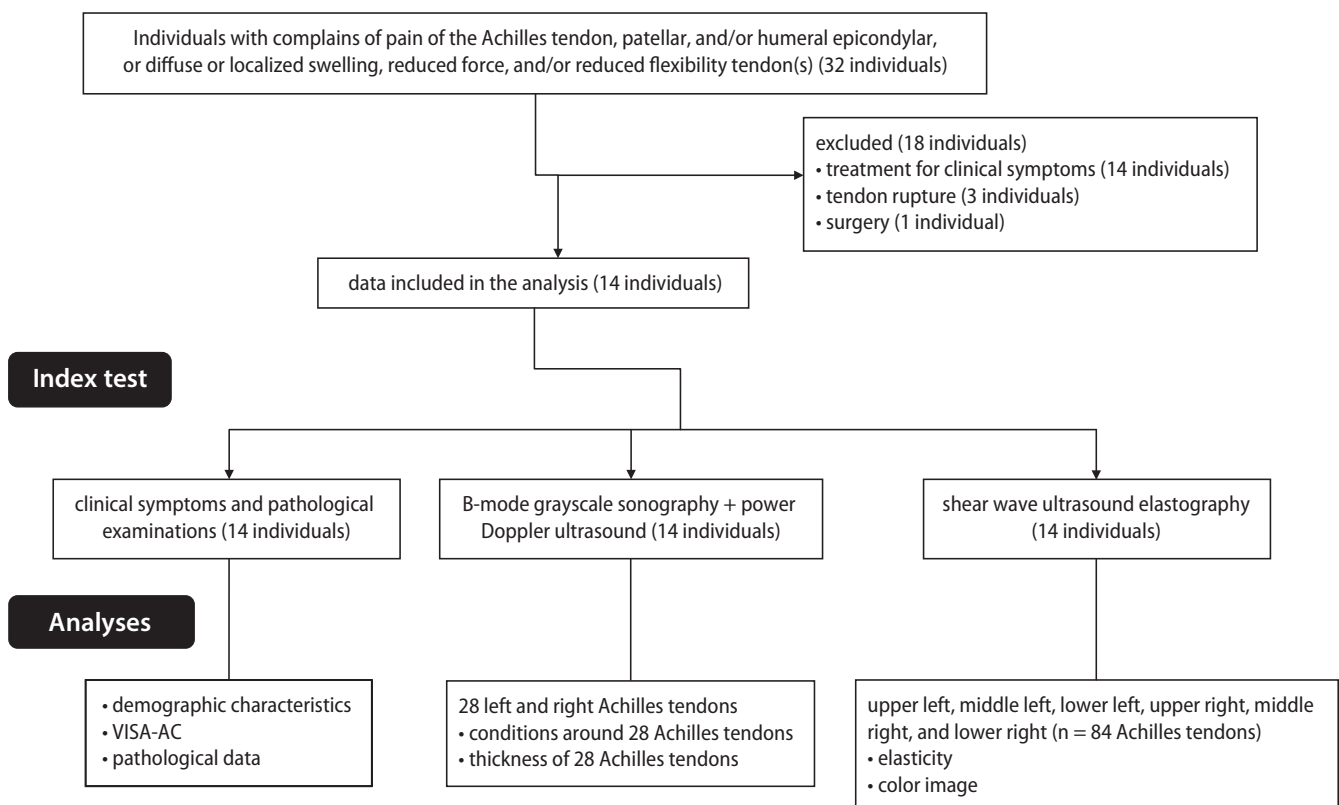


Fig. 3. The flow diagram of retrospective analyses

VISA-AC – Chinese version of a Victorian Institute of Sports Assessment – Achilles Questionnaires.

Table 1. Clinical symptoms of the study group

| Parameters | | Value |
|--|---------------|-------------------|
| Numbers of individuals included in the study | | 14 |
| Gender | male | 8 (57) |
| | female | 6 (43) |
| Age [years] | minimum | 20 |
| | maximum | 77 |
| | mean \pm SD | 54.93 \pm 16.93 |
| Duration of diabetes course | <1 year | 2 (14) |
| | 1–5 years | 4 (29) |
| | 5–10 years | 2 (14) |
| | >10 years | 6 (43) |
| Systolic blood pressure [mm Hg] | minimum | 99 |
| | maximum | 150 |
| | mean \pm SD | 123.5 \pm 13.89 |
| Diastolic blood pressure [mm Hg] | minimum | 57 |
| | maximum | 110 |
| | mean \pm SD | 79.5 \pm 15.29 |
| Height [m] | minimum | 1.55 |
| | maximum | 1.78 |
| | mean \pm SD | 1.69 \pm 0.09 |
| Weight [kg] | minimum | 64 |
| | maximum | 86 |
| | mean \pm SD | 69.4 \pm 6.71 |
| Body mass index [kg/m ²] | minimum | 21.22 |
| | maximum | 30.39 |
| | mean \pm SD | 24.77 \pm 2.90 |
| Ulcers on the feet | | 3 (27) |
| Peripheral neuropathy | | 10 (71) |
| Insulin use | | 7 (50) |
| Oral hypoglycemic drug(s) use | | 13 (93) |
| Glycated hemoglobin [%HbA1C] | minimum | 4.5 |
| | maximum | 13.5 |
| | mean \pm SD | 8.1 \pm 2.15 |
| Total cholesterol [mM/L] | minimum | 1.8 |
| | maximum | 6.5 |
| | mean \pm SD | 3.49 \pm 1.71 |
| Triglycerides [mM/L] | minimum | 0.41 |
| | maximum | 2.8 |
| | mean \pm SD | 1.79 \pm 0.77 |
| Fasting blood glucose [mM/L] | minimum | 4.02 |
| | maximum | 23.9 |
| | mean \pm SD | 12.07 \pm 4.28 |
| Presence of albumin in the urine | | 4 (29) |
| Pain (VISA-AC) score | minimum | 44 |
| | maximum | 94 |
| | mean \pm SD | 83.93 \pm 7.67 |

Constant variables are demonstrated as frequency (percentages) and continuous variables are demonstrated as mean \pm standard deviation (SD). VISA-AC – Chinese version of a Victorian Institute of Sports Assessment – Achilles Questionnaires.

Among these 14 patients, 4 had bilateral tendons and 10 had unilateral tendons. A total of 84 tendons were analyzed. Among them, 11 (13%) were symptomatic and 73 (87%) were asymptomatic.

Standard ultrasound examination

Standard ultrasound examination was performed at left and right Achilles tendons. A total of 28 conditions (left and right) were evaluated using standard ultrasound examination and 14 (50%) of them were reported as tendinopathies. The remaining 14 conditions were diagnosed using ultrasound as asymptomatic.

Shear wave ultrasound elastography

Asymptomatic tendons were visible as red (high rigidity) and symptomatic tendons as blue (low rigidity) or turquoise (intermediate rigidity) images. Tendon rigidity of symptomatic tendons were lower than that of asymptomatic tendons. Shear wave ultrasound elastography results for Achilles tendons was reported in Table 2. According to these measurements, 39 (46%) out of 84 tendons had tendinopathies. Among them, 29 (34%) were asymptomatic and 10 (12%) were symptomatic. The elasticity values of the symptomatic tendons were lower than those of the asymptomatic ones ($p = 0.044$, Mann–Whitney test).

Correlation between pain symptoms and ultrasound examinations

The VISA-AC score had weak correlation with standard ultrasound characteristics ($\tau\beta = 0.31$, degrees of freedom (df) = 83, $p = 0.5467$) and with power Doppler characteristics ($\tau\beta = 0.38$, df = 83, $p = 0.1051$) of Achilles tendons, but that was strongly correlated with the elasticity values ($p = 0.0001$, df = 83, $\tau\beta = 0.71$) of Achilles tendons. The details of the correlation between pain symptoms and ultrasound examinations are reported in Fig. 4.

Diagnostic parameters

All studied patients had mild to moderate complaints about each tendon, and therefore, tendinopathy was clinically considered in all tendons. Sensitivity for standard ultrasound, shear wave ultrasound elastography and standard ultrasound plus shear wave ultrasound elastography for symptomatic tendons were 0, 1 and 1, respectively. Accuracy for standard ultrasound, shear wave ultrasound elastography and standard ultrasound plus shear wave ultrasound elastography for symptomatic tendons were 0, 1 and 1, respectively. Sensitivity for standard ultrasound, shear wave ultrasound elastography and standard ultrasound plus shear wave ultrasound elastography for asymptomatic tendons was 0.58, 0.38 and 0.78, respectively. Accuracy for standard ultrasound, shear wave ultrasound elastography and standard ultrasound plus shear wave ultrasound elastography for asymptomatic tendons was 0.58, 0.38 and 0.78, respectively. Sensitivity for standard ultrasound, shear wave ultrasound elastography and standard

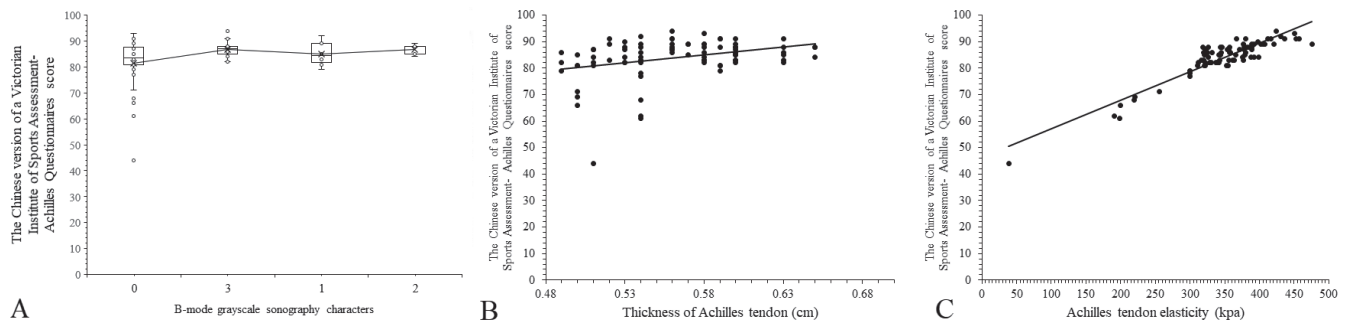


Fig. 4. Correlation between pain symptoms and ultrasound examinations. A. Correlation between VISA-AC score and B-mode grayscale sonography characteristics. Coding of B-mode grayscale sonography characteristics: 0 – none, 1 – blurred Achilles tendon texture, 2 – blurred Achilles tendon texture and bursa effusion behind the calcaneus, 3 – roughness around the Achilles tendon, the blurry texture of the tendon and calcification of the calcaneal attachment; B. Correlation between VISA-AC score and thickness of Achilles tendon; C. Correlation between VISA-AC score and elasticity values

VISA-AC – Chinese version of a Victorian Institute of Sports Assessment – Achilles Questionnaires.

Table 2. Elasticity values of the different types of Achilles tendons

| Elasticity values | Achilles tendon | Type of Achilles tendons | | Comparisons between symptomatic and asymptomatic tendons |
|--------------------|-----------------|--------------------------|--------------|--|
| | | symptomatic | asymptomatic | |
| Numbers of tendons | 84 | 11 | 73 | p-value |
| Minimum [kPa] | 38.6 | 38.6 | 310.8 | <0.0001 |
| Maximum [kPa] | 475.5 | 300.2 | 475.5 | |
| Median [kPa] | 355.5 | 220.4 | 361 | |

Variables are demonstrated as mean \pm standard deviation (SD). The Mann–Whitney test was performed for statistical analysis. Results were considered significant if the p-value was less than 0.05.

Table 3. Diagnostic parameters of index tests for Achilles tendons

| Parameters | | Clinical symptoms | Standard (B-mode grayscale sonography + power Doppler) ultrasound | | Shear wave ultrasound elastography | | Standard ultrasound + shear wave ultrasound elastography | |
|-----------------------------|--------------|-------------------|---|-----------|------------------------------------|-----------|--|-----------|
| | | | | | | | | |
| Numbers of tendons | | 84 | 84 | **p-value | 84 | **p-value | 84 | **p-value |
| True positive tendinopathy | symptomatic | 11 (13) | 0 (0) | <0.0001 | 11 (13) | 0.999 | 11 (13) | 0.999 |
| | asymptomatic | 73 (87) | 42 (50) | <0.0001 | 28 (33) | <0.0001 | 57 (68) | <0.0001 |
| | total | 84 (100) | 42 (50) | <0.0001 | 39 (46) | <0.0001 | 68 (81) | <0.0001 |
| True negative tendinopathy | | 0 (0) | 0 (0) | N/A | 0 (0) | N/A | 0 (0) | N/A |
| False positive tendinopathy | | 0 (0) | 0 (0) | N/A | 0 (0) | N/A | 0 (0) | N/A |
| False negative tendinopathy | symptomatic | 0 (0) | 11 (13) | 0.0007 | 0 (0) | N/A | 0 (0) | N/A |
| | asymptomatic | 0 (0) | 31 (15) | <0.0001 | 45 (54) | <0.0001 | 16 (19) | <0.0001 |
| | total | 0 (0) | 42 (50) | <0.0001 | 45 (54) | <0.0001 | 16 (19) | <0.0001 |
| Sensitivity | symptomatic | 1.00 | 0 | N/A | 1.00 | N/A | 1.00 | N/A |
| | asymptomatic | 1.00 | 0.58 | N/A | 0.38 | N/A | 0.78 | N/A |
| | total | 1.00 | 0.5 | N/A | 0.46 | N/A | 0.81 | N/A |
| Accuracy | symptomatic | 1.00 | 0 | N/A | 1.00 | N/A | 1.00 | N/A |
| | asymptomatic | 1.00 | 0.58 | N/A | 0.38 | N/A | 0.78 | N/A |
| | total | 1.00 | 0.5 | N/A | 0.46 | N/A | 0.81 | N/A |

Variables are demonstrated as frequency (percentages). The Fisher's exact test was performed for statistical analysis. Variables were compared for statistical analysis. Results were considered significant if the p-value was less than 0.05. N/A – not applicable. **with respect to the results of clinical symptoms being reference standards.

ultrasound plus shear wave ultrasound elastography for all Achilles tendons (symptomatic and asymptomatic) was 0.5, 0.46 and 0.81, respectively. Accuracy for standard ultrasound, shear wave ultrasound elastography and standard

ultrasound plus shear wave ultrasound elastography for all Achilles tendons (symptomatic and asymptomatic) was 0.5, 0.46 and 0.81, respectively. The details of diagnostic parameters for index tests are reported in Table 3.

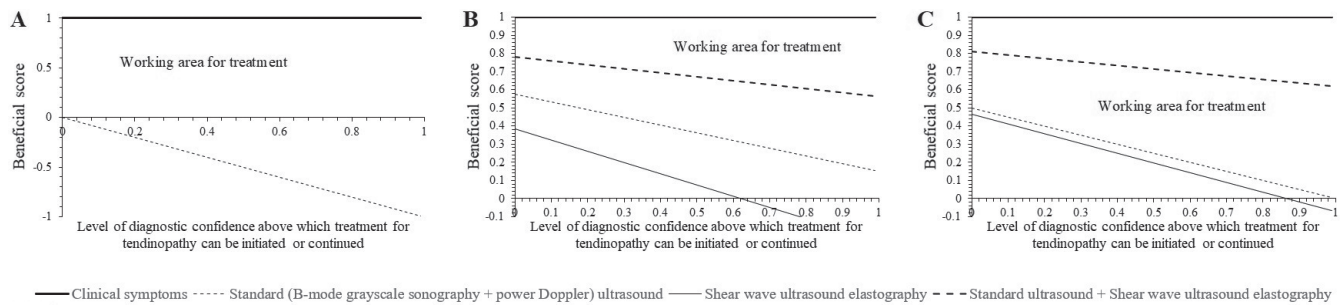


Fig. 5. Beneficial score analyses for index tests. A. For symptomatic Achilles tendons; B. For asymptomatic Achilles tendons; C. For all Achilles tendons (symptomatic plus asymptomatic)

Beneficial score analysis

Working areas for the treatment of tendinopathies of symptomatic Achilles tendons for shear wave ultrasound elastography and standard ultrasound plus shear wave ultrasound elastography were 0–1 diagnostic confidence/tendon (Fig. 5A). Working areas for the treatment of tendinopathy of asymptomatic Achilles tendons for standard ultrasound (B-mode grayscale sonography + power Doppler), shear wave ultrasound elastography and standard ultrasound plus shear wave ultrasound elastography were 0–1 diagnostic confidence/tendon, 0–0.61 diagnostic confidence/tendon and 0–1 diagnostic confidence/tendon, respectively (Fig. 5B). Working areas for the treatment of Achilles tendinopathy of all Achilles tendons (symptomatic plus asymptomatic) for standard ultrasound (B-mode grayscale sonography + power Doppler), shear wave ultrasound elastography and standard ultrasound plus shear wave ultrasound elastography were 0–0.98 diagnostic confidence/tendon, 0–0.86 diagnostic confidence/tendon and 0–1 diagnostic confidence/tendon, respectively (Fig. 5C).

Discussion

The study found that sensitivity and accuracy for standard ultrasound plus shear wave ultrasound elastography were higher for both symptomatic and asymptomatic tendons than those of standard ultrasound. The results of the measurements of diagnostic parameters of the current study are consistent with those of a prospective study³ and a cross-sectional study,¹⁷ but are not consistent with that of another prospective study.⁵ Different study populations are the probable reason for contradictory results. There is a noticeable change in shear wave elasticity values between healthy and diseased tendon(s).⁹ Shear wave ultrasound elastography augments diagnostic confidence for treatment of Achilles tendinopathy.

A study by Visnes et al. reported that standard ultrasound had a higher rate of false negative findings. Also, shear wave ultrasound elastography is not yet standardized to the level of elimination of false negative cases. In clinically symptomatic patients, standard ultrasound often

cannot find sonographic features.¹⁰ Also, inter-observer correlation is an issue for qualitative evaluations of standard ultrasound,²² while shear wave ultrasound elastography provides quantitative information, which has lower inter-observers' variabilities.³ The B-mode grayscale sonography and power Doppler provide limited information on Achilles tendinopathy.

In the present study, the results demonstrated that the pain is strongly correlated to the elasticity of the Achilles tendon but weakly correlated with standard ultrasound. The detected correlations between VISA-AC score and imaging parameters of Achilles tendons of the current study are consistent with those presented in prospective studies^{3,5,23} and a cross-sectional study.¹⁷ Tendon degradation occurs due to loss of fiber, which causes the softening of Achilles tendons, and consequently the patient feels pain.⁹ It is possible to use elasticity as an index to evaluate the pain degree of the patient.

This study found that the elasticity values of symptomatic Achilles tendons were lower than those of the asymptomatic ones. The elasticity values measured in the current study are consistent with a prospective study.³ The possible reasons for parallel results are that the comparisons of the elasticity values of symptomatic and asymptomatic tendons in the current study were performed for individuals in the full age range (28–65 years). The prospective study³ was also performed for individuals in a full age range (mean ± standard deviation (SD) 42 ± 13.4 years, range: 20–71 years).³ The close correlation between the elasticity values of Achilles tendons and clinical symptoms is less pronounced in elderly individuals.³ The tissue rigidity of Achilles tendons is correlated with clinical symptoms in treatment-naïve patients.

Working areas for the treatment of Achilles tendinopathy for standard ultrasound plus shear wave ultrasound elastography were equal to that of clinical symptoms for symptomatic and asymptomatic tendons. Shear wave ultrasound elastography with standard ultrasound can be useful for initiation of treatment for Achilles tendinopathy or monitoring treatment for the same.

In the article, the 3 parts of the tendons assessed using shear wave elastography are considered as 3 different tendons and 14 tendons with both sides are finally considered as 84 tendons. The possible justification is that the elasticity

of different parts and sides of tendons are dissimilar and not correlated with each other. Therefore, it is possible to consider the parts of the tendons as different tendons.

Limitations

The main limitation of this study is that it is a retrospective analysis and not a prospective study. A small sample size (only 14 study patients with 18 painful tendons) led to the type I error. Inter- and intraobserver variabilities were not evaluated (the study was performed by several doctors and the standardization of the study was not performed). The patients' degree of pain was used as the gold standard. However, patients can have symptoms referable to the Achilles tendon but it does not necessarily mean that the patient has Achilles tendinopathy. Pathological diagnostic tests can also be used for diagnosis of tendinopathy and the patient may be asymptomatic early on.

Conclusions

Shear wave ultrasound elastography augments diagnostic confidence for treatment of Achilles tendinopathy. The B-mode grayscale sonography and power Doppler provide limited information for Achilles tendinopathy. The elasticity values of Achilles tendons are correlated with pain. Shear wave ultrasound elastography with standard ultrasound can be useful for initiation or monitoring of treatment of Achilles tendinopathy.

ORCID iDs

Lixiu Chen  <https://orcid.org/0000-0002-1613-2812>
 Ying Cheng  <https://orcid.org/0000-0001-7199-0601>
 Liang Zhou  <https://orcid.org/0000-0002-3863-811X>
 Lei Zhang  <https://orcid.org/0000-0002-9488-3857>
 Xueyan Deng  <https://orcid.org/0000-0002-4999-3811>

References

- Cassel M, Baur H, Hirschi Müller A, Carlsohn A, Fröhlich K, Mayer F. Prevalence of Achilles and patellar tendinopathy and their association to intratendinous changes in adolescent athletes: Tendinopathy in adolescent athletes. *Scand J Med Sci Sports*. 2015;25(3):e310–e318. doi:10.1111/sms.12318
- Patterson-Kane JC, Rich T. Achilles tendon injuries in elite athletes: Lessons in pathophysiology from their equine counterparts. *ILAR J*. 2014;55(1):86–99. doi:10.1093/ilar/ilu004
- Dirrachs T, Quack V, Gatz M, Tingart M, Kuhl CK, Schrading S. Shear wave elastography (SWE) for the evaluation of patients with tendinopathies. *Acad Radiol*. 2016;23(10):1204–1213. doi:10.1016/j.acra.2016.05.012
- Järvinen TA. Neovascularisation in tendinopathy: From eradication to stabilisation? *Br J Sports Med*. 2020;54(1):1–2. doi:10.1136/bjsports-2019-100608
- Gatz M, Bode D, Betsch M, et al. Multimodal ultrasound versus MRI for the diagnosis and monitoring of Achilles tendinopathy: A prospective longitudinal study. *Orthop J Sports Med*. 2021;9(4):232596712110068. doi:10.1177/23259671211006826
- Alfredson H, Masci L, Spang C. Ultrasound and surgical inspection of plantaris tendon involvement in chronic painful insertional Achilles tendinopathy: A case series. *BMJ Open Sport Exerc Med*. 2021;7(1):e000979. doi:10.1136/bmjsem-2020-000979
- McAuliffe S, McCreesh K, Culloty F, Purtill H, O'Sullivan K. Can ultrasound imaging predict the development of Achilles and patellar tendinopathy? A systematic review and meta-analysis. *Br J Sports Med*. 2016;50(24):1516–1523. doi:10.1136/bjsports-2016-096288
- Weinreb JH, Sheth C, Apostolakis J, et al. Tendon structure, disease, and imaging. *Muscles Ligaments Tendons J*. 2014;4(1):66–73. PMID:24932450. PMCID:PMC4049653.
- Klauser AS, Miyamoto H, Tamegger M, et al. Achilles tendon assessed with sonoelastography: Histologic agreement. *Radiology*. 2013;267(3):837–842. doi:10.1148/radiol.13121936
- Visnes H, Tegnander A, Bahr R. Ultrasound characteristics of the patellar and quadriceps tendons among young elite athletes: Ultrasound: patellar and quadriceps tendon. *Scand J Med Sci Sports*. 2015;25(2):205–215. doi:10.1111/sms.12191
- Xiao G, Zhu S, Xiao X, Yan L, Yang J, Wu G. Comparison of laboratory tests, ultrasound, or magnetic resonance elastography to detect fibrosis in patients with nonalcoholic fatty liver disease: A meta-analysis. *Hepatology*. 2017;66(5):1486–1501. doi:10.1002/hep.29302
- Xie X, Zhang Q, Liu S, et al. Value of quantitative sound touch elastography of tissues around breast lesions in the evaluation of malignancy. *Clin Radiol*. 2021;76(1):79.e21–79.e28. doi:10.1016/j.crad.2020.08.016
- Boehm K, Budäus L, Tennstedt P, et al. Prediction of significant prostate cancer at prostate biopsy and per core detection rate of targeted and systematic biopsies using real-time shear wave elastography. *Urol Int*. 2015;95(2):189–196. doi:10.1159/000431233
- Tan S, Sun PF, Xue H, et al. Evaluation of thyroid micro-carcinoma using shear wave elastography: Initial experience with qualitative and quantitative analysis. *Eur J Radiol*. 2021;137:109571. doi:10.1016/j.ejrad.2021.109571
- Hsu PC, Chang KV, Wu WT, Wang JC, Özçakar L. Effects of ultrasound-guided peritendinous and intrabursal corticosteroid injections on shoulder tendon elasticity: A post hoc analysis of a randomized controlled trial. *Arch Phys Med Rehabil*. 2021;102(5):905–913. doi:10.1016/j.apmr.2020.11.011
- Chu CA, Chen YJ, Chang KV, Wu WT, Özçakar L. Reliability of sonoelastography measurement of tongue muscles and its application on obstructive sleep apnea. *Front Physiol*. 2021;12:654667. doi:10.3389/fphys.2021.654667
- Ooi CC, Richards PJ, Maffulli N, et al. A soft patellar tendon on ultrasound elastography is associated with pain and functional deficit in volleyball players. *J Sci Med Sport*. 2016;19(5):373–378. doi:10.1016/j.jsams.2015.06.003
- Chang YP, Shih KS, Chiang H, et al. Characteristics of intratendinous microcirculation shortly after an Achilles rupture and subsequent treatment outcomes. *PM R*. 2017;9(1):32–39. doi:10.1016/j.pmrj.2016.06.011
- Szaro P, Ghali Gataa K. The correlations between dimensions of the normal tendon and tendinopathy changed Achilles tendon in routine magnetic resonance imaging. *Sci Rep*. 2021;11(1):6131. doi:10.1038/s41598-021-85604-9
- Liu T, Ma J, Cao H, Hou D, Xu L. Evaluation of the diagnostic performance of the simple method of computed tomography in the assessment of patients with shoulder instability: A prospective cohort study. *BMC Med Imaging*. 2018;18(1):45. doi:10.1186/s12880-018-0290-4
- Spudić D, Smajla D, David Burnard M, Šarabon N. Muscle activation sequence in flywheel squats. *Int J Environ Res Public Health*. 2021;18(6):3168. doi:10.3390/ijerph18063168
- Sunding K, Fahlström M, Werner S, Forssblad M, Willberg L. Evaluation of Achilles and patellar tendinopathy with greyscale ultrasound and colour Doppler: Using a four-grade scale. *Knee Surg Sports Traumatol Arthrosc*. 2016;24(6):1988–1996. doi:10.1007/s00167-014-3270-4
- Dirrachs T, Quack V, Gatz M, et al. Shear wave elastography (SWE) for monitoring of treatment of tendinopathies: A double-blinded, longitudinal clinical study. *Acad Radiol*. 2018;25(3):265–272. doi:10.1016/j.acra.2017.09.011

Factors predictive of anti-spike antibody titers after COVID-19 vaccination in hemodialysis patients

Mabel Aoun^{1,2,A–F}, Reine-Marie Kahwaji^{3,B,F}, Ghassan Sleilaty^{4,C,F}, Celine Boueri^{2,B,F}, Jenny Hawi^{2,B,F}, Christelle Bou Khalil^{5,B,D,F}, Valerie Hage^{1,6,B,F}

¹ Department of Nephrology, Faculty of Medicine, Saint-Joseph University, Beirut, Lebanon

² Department of Nephrology, Saint-George Hospital Ajaltoun, Lebanon

³ Department of Internal Medicine, Holy Spirit University Kaslik, Lebanon

⁴ Department of Biostatistics and Clinical Research Center, Faculty of Medicine, Saint-Joseph University, Beirut, Lebanon

⁵ Laboratory Department, Saint-George Hospital Ajaltoun, Lebanon

⁶ Department of Nephrology, Centre Hospitalier de Bhannes, Lebanon

A – research concept and design; B – collection and/or assembly of data; C – data analysis and interpretation;

D – writing the article; E – critical revision of the article; F – final approval of the article

Advances in Clinical and Experimental Medicine, ISSN 1899–5276 (print), ISSN 2451–2680 (online)

Adv Clin Exp Med. 2022;31(8):855–861

Address for correspondence

Mabel Aoun

E-mail: aounmabel@yahoo.fr

Funding sources

None declared

Conflict of interest

None declared

Acknowledgements

Authors would like to thank all laboratory doctors and staff who contributed to this work.

Received on December 9, 2021

Reviewed on January 22, 2022

Accepted on March 14, 2022

Published online on April 19, 2022

Cite as

Aoun M, Kahwaji RM, Sleilaty G, et al. Factors predictive of anti-spike antibody titers after COVID-19 vaccination in hemodialysis patients. *Adv Clin Exp Med.* 2022;31(8):855–861. doi:10.17219/acem/147360

DOI

10.17219/acem/147360

Copyright

Copyright by Author(s)

This is an article distributed under the terms of the Creative Commons Attribution 3.0 Unported (CC BY 3.0) (<https://creativecommons.org/licenses/by/3.0/>)

Abstract

Background. Hemodialysis (HD) patients have a high prevalence of severe acute respiratory syndrome coronavirus 2 (SARS-CoV-2) infection and mortality, but they may have a weak response to coronavirus disease 2019 (COVID-19) vaccines.

Objectives. This study aimed to evaluate factors predictive of humoral response in HD patients vaccinated against SARS-CoV-2 infection.

Materials and methods. This is a 2-center observational study including HD patients who received the BNT162b2 mRNA vaccine followed by serological measurements 20 days and 4 weeks after the 1st and 2nd dose, respectively. Healthy controls were included. Anti-spike antibody was measured using the chemiluminescent immunoassay (CLIA) method. The quantile regression analysis was performed to assess factors associated with anti-spike antibody titers.

Results. Seventy-two HD patients and 22 healthy controls were included. Mean age of dialysis patients and controls was 72.5 ± 11.5 years and 45.7 ± 17.4 years, respectively. In the HD group, median levels of anti-spike antibody were 3 (interquartile range (IQR): 0.5–26) UI/mL and 391 (IQR: 55–1642) UI/mL after the 1st and 2nd dose, respectively, with response rates of 62.5% and 96.7%. The median level of the anti-spike antibody after the 1st dose in previously infected patients was 8571 (IQR: 2586–19147) UI/mL. There was a significant correlation between anti-spike antibody levels after the 2nd dose and age and anti-hepatitis B surface (HBs) antibody and serum albumin levels (Spearman's rho: $r = -0.289$, $p < 0.001$; $r = 0.357$, $p = 0.027$; $r = 0.317$; $p = 0.026$, respectively). The regression analysis showed a significant association of previous infection and anti-Hbs antibody level with anti-spike antibody level after the 1st dose of vaccine ($p < 0.001$). After a 5-month follow-up, 2 vaccinated patients contracted COVID-19.

Conclusions. This study showed a response rate of 96.7% to 2 doses of BNT162b2 mRNA vaccine in HD patients and 100% to a single dose in previously infected patients. The level of anti-spike antibody can be predicted by age, anti-Hbs antibodies, serum albumin, and previous infection. Despite the immunization of patients, preventive measures should be maintained in all dialysis units.

Key words: SARS-CoV-2, COVID-19 vaccine, hemodialysis, anti-spike antibody, hepatitis B vaccine

Background

Globally, vulnerable populations were severely afflicted by the severe acute respiratory syndrome coronavirus 2 (SARS-CoV-2) pandemic. Hemodialysis (HD) patients emerged as one of the high-risk groups for coronavirus disease 2019 (COVID-19). Once infected, their mortality rate reached 20–25% in several national and global reports.^{1–3} This led nephrology societies across the globe to call for effective preventive measures in these patients as well as to put them on priority lists for vaccination against COVID-19.^{4–7}

Despite the urgent need to vaccinate HD patients, this comorbid population is known to have low immunity and poor response to vaccines. Since decades, the best practice in HD patients has required administering vaccines against hepatitis B and pneumococcal infection. However, several studies revealed the weak immunization rates, the decline in the antibodies with time and consequently, a lack of chronic protection against the aforementioned diseases.^{8,9} In relation to COVID-19 vaccines, several recent studies showed a diminished humoral response intensity to 2 doses of the COVID-19 BNT162b2 (Pfizer-BioNTech) mRNA vaccine compared to healthy controls.^{10–13} Despite the low levels of antibody titers, the rate of seropositivity seemed to vary between different reports.¹⁴ Moreover, previously infected patients were found to mount their antibodies very early after the 1st dose.^{10,15,16} Therefore, some patients might need 3 doses and others 1 dose only. On another note, the results have been contradictory regarding the correlation between the humoral response to COVID-19 vaccine and previous response to hepatitis B vaccine.^{12,17}

Objectives

This study aims to elucidate the factors affecting the humoral response of HD patients after the COVID-19 mRNA vaccine.

Materials and methods

Study setting

The vaccination campaign against COVID-19 started in Lebanon on February 14, 2021, with a prioritization of healthcare workers and elderly above 75 years of age. Hemodialysis patients received the BNT162b2 mRNA vaccine progressively, based on their age category (category 1A: ≥75 years, category 1B: 55–74 years; patients aged 16–54 years were vaccinated as the last category among HD patients). It took 5 months to cover the vaccination of all HD patients in the country.

The study included all chronic HD patients who received the vaccine and were tested for anti-spike antibody after

vaccination. Nephrologists who participated in the previous national study on COVID-19 prevalence in HD were contacted to include their patients.³ Only 5 nephrologists from 2 units performed serological testing in their patients following vaccination. The HD patients of these 2 units, Saint-George Ajaltoun and Bhanne hospitals, Lebanon, were finally included. These 2 units provided dialysis treatment for 123 patients before their first COVID-19 cases. Among these patients, 33 contracted COVID-19, 12 died from this disease and 9 from other causes. Not all infected patients received the vaccine. Until the end of July 2021, 82 patients received 2 doses of vaccine and 72 patients had the anti-spike antibody level measured.

Healthcare workers, some family members of patients and staff who were vaccinated and serologically tested were included as healthy controls.

Study design and participants

This is a retrospective study that collected data of HD patients who were administered the 1st dose of COVID-19 vaccine between February 15, 2021 and July 31, 2021. All HD patients in Lebanon who were tested for anti-spike protein antibody 20 days after their 1st dose and 4 weeks after their 2nd dose of vaccine were included.

The study got the approval of the ethics committee of Hotel-Dieu de France-affiliated to Saint-Joseph University, Beirut, Lebanon (approval No. CEHDF 1829) and was conducted in agreement with the Declaration of Helsinki of 1975.

Data collection

The outcome variable recorded for each patient was the level of anti-spike antibody after the 1st and 2nd dose of COVID-19 vaccine. Other variables collected were: age, sex, current smoking status, dialysis vintage, frequency of dialysis, number of weeks between the 2 doses of vaccine, comorbidities such as diabetes, hypertension, coronary artery disease (CAD), heart failure, cancer, and whether on immunosuppressive therapy or not. We also collected the hepatitis B vaccination status parameters for each patient: if fully vaccinated (yes/no), if immunized (yes/no) (defined as anti-hepatitis B surface (HBs) antibody levels above 10 UI/mL) and the last measured level of anti-HBs antibody. Symptoms or side effects after vaccination were retrieved from medical charts: fever, myalgia, painful arm, headache, and other symptoms. Laboratory parameters included serum albumin level before vaccination and platelet count 1 month after the 2nd dose.

Anti-spike antibody measurement

The humoral response was evaluated using Elecsys Anti-SARS-CoV-2 S on the cobas e 411 analyzer (Roche Diagnostics, Basel, Switzerland). Elecsys Anti-SARS-CoV-2 S

is an electrochemiluminescence immunoassay (CLIA) intended for detection of antibodies against the receptor binding domain (RBD) of the spike (S) protein in human serum and plasma. The anti-SARS-CoV-2 S detected are mainly immunoglobulin G (IgG), in addition to immunoglobulin A (IgA) and immunoglobulin M (IgM). The Elecsys Anti-SARS-CoV-2 S assay uses a recombinant protein portraying the RBD of the spike antigen in a double-antigen sandwich assay format. Biotinylated SARS-CoV-2 S-RBD-specific recombinant antigen and SARS-CoV-2 S-RBD-specific recombinant antigen labeled with a ruthenium complex are first incubated to form a sandwich complex. During the 2nd incubation, the complex becomes bound to the solid phase via interaction of biotin and streptavidin, after addition of streptavidin-coated microparticles. The reaction mixture is aspirated into the measuring cell where the microparticles are magnetically captured onto the surface of the electrode. Then, application of a voltage to the electrode induces chemiluminescent emission which is measured with a photomultiplier. The results are determined via a calibration curve which is generated by a 2-point calibration and a master curve provided via the reagent barcode or e-barcode. The total duration of the assay is 18 min. When titers were above 250 UI/mL, dilution was performed up to 1/100. A cutoff of 0.8 UI/mL was used for interpretation. The sensitivity of the test is considered to be 89%, 98% and 100% after 14–20 days, 21–27 days and beyond 28 days, respectively. The specificity is almost 100%.

Statistical analyses

Continuous variables were presented as mean \pm standard deviation (SD) if normally distributed, and as median and interquartile range (IQR) if data were skewed; categorical variables were presented as numbers and percentages.

The t independent sample test was used to compare continuous variables that were normally distributed. The Mann–Whitney test was used to compare skewed data. A quantile regression analysis using the median (50th) was performed to assess factors associated with anti-spike antibody levels after the 1st vaccine dose, including all variables that had a p-value less than 0.2 in the univariate analysis. Spearman's rho correlation was used to estimate the association between anti-spike antibody levels after the 2nd dose and serum albumin anti-Hbs antibody levels and other continuous variables. The statistical analysis was performed with IBM SPSS for Windows v. 26 (IBM Corp., Armonk, USA). A p-value ≤ 0.05 was considered statistically significant.

Results

Characteristics of HD patients

A total of 72 HD patients were included. Table 1 summarizes their characteristics. The mean age of patients

was 72.5 \pm 11.5 years and 34.7% of them were females. Among the 60 infection-naïve patients, 2 patients did not get their 2nd dose of vaccine, 1 died and 1 was admitted to the hospital for hip fracture. Among the 12 previously infected patients, only 4 received the 2nd dose of vaccine.

The interval between the 1st dose and 2nd dose was 3 weeks in the eldest patients (those who were administered the vaccine in priority) and it was prolonged to 4–5 weeks in younger patients (based on the decision of the Ministry of Public Health). A total of 34 patients were 75 years old or older, and they completed their vaccination by the end of March 2021.

Two out of the 72 HD patients contracted COVID-19 during the follow-up period that ranged between 1 and 5 months. One of them, a 88-year-old male, who had negative anti-spike antibody titers after 2 doses of vaccine, was diagnosed with COVID-19 4 months after he completed his vaccination. He needed admission to the hospital for cough, dyspnea and oxygen therapy, and recovered after 5 days. Another patient, a 71-year-old female who had anti-spike antibody titers of 237 UI/mL after the 2nd dose, was diagnosed with COVID-19 two months after her 2nd dose. She had mild symptoms and did not require admission.

Characteristics of healthy controls

A total of 22 healthy controls were included with a mean age of 45.7 \pm 17.4 years (22–80 years) and 68.2% of them were females. Among these controls, 31.8% had a previous SARS-CoV-2 infection. All controls received the 2nd dose of vaccine 3 weeks after the 1st dose. The median level of anti-spike antibody following the 1st dose was 150 (IQR: 109.5–571) UI/mL. The median level of anti-spike antibody 1 month after the 2nd dose was 2000 (IQR: 1157–2000) UI/mL (maximum detection in controls was 3500 UI/mL). There was a significant difference in anti-spike antibody levels after the 1st dose of vaccine between previously infected and infection-naïve controls ($N = 21$, $Z = -3.457$, $p < 0.001$, Mann–Whitney test). There was no significant difference in the anti-spike antibody levels after the 2nd dose of vaccine between previously infected and infection-naïve controls ($N = 17$, $Z = -1.213$, $p = 0.225$, Mann–Whitney test).

Comparison between HD patients and healthy controls

The anti-spike antibody levels measured 20 days after the 1st vaccine dose and 4 weeks after the 2nd dose were both significantly higher in healthy controls compared to HD patients (Mann–Whitney test, $p < 0.001$ and $p = 0.001$, respectively). Figure 1 shows the high level of anti-spike antibody in previously infected patients compared to the levels after the 1st dose in healthy controls and infection-naïve HD patients.

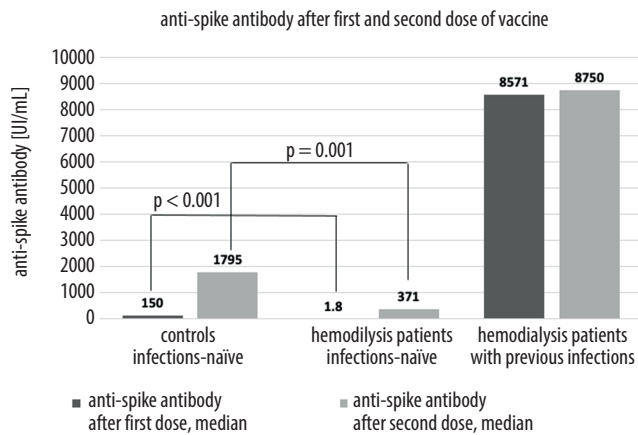


Fig. 1. Anti-spike antibody levels among different groups of patients

Factors associated with anti-spike antibody levels in HD patients

Sex, diabetes or CAD did not significantly affect the anti-spike antibody levels after the 1st and 2nd dose of vaccine. Heart failure patients presented a significantly weaker response with lower anti-spike antibody titers; previous infection caused a higher response of antibodies (Table 2). There was a positive correlation of anti-spike antibody levels after the 1st dose and after the 2nd dose of vaccine with age and anti-HBs antibody and serum albumin levels (Table 3). The median of anti-spike antibodies after the 2nd dose of vaccine was 93.5 (IQR: 20.25–838.5) UI/mL in patients with an interval of 3 weeks between the 1st and

Table 1. Characteristics of hemodialysis (HD) patients and the statistical difference between the compared groups

| Variable | HD patients (total = 72) | HD patients who were infection-naïve (n = 60) | HD patients previously infected (n = 12) | p-value |
|--|------------------------------|---|--|--------------------|
| Age [years], mean ±SD | 72.5 ±11.5 | 73.1 ±11.4 | 69.9 ±11.7 | 0.391* |
| Sex, n (% of females) | 25 (34.7) | 22 (36.7) | 3 (25) | 0.524 |
| Dialysis vintage, median (IQR) | 28 (14–60) | 28 (14.5–60) | 38.5 (9.7–74.2) | 0.976** |
| Smoking status, n (%) | 10 (13.9) | 8 (13.3) | 2 (16.7) | 0.669*** |
| Diabetes, n (%) | 34 (47.2) | 30 (50) | 4 (33.3) | 0.354*** |
| Hypertension, n (%) | 66 (91.7) | 54 (90) | 12 (100) | 0.253 [§] |
| CAD, n (%) | 23 (31.9) | 21 (35) | 2 (16.7) | 0.315*** |
| Heart failure, n (%) | 9 (12.5) | 8 (13.3) | 1 (8.3) | 0.999*** |
| History of cancer, n (%) | 6 (8.3) | 6 (10) | 0 (0) | 0.581*** |
| Serum albumin level [mg/dL], mean ±SD | 37.4 ±5 | 36.9 ±4.6 | 40.1 ±6.3 | 0.120* |
| Vaccinated against hepatitis B, n (%) | 65 (90.3) | 53 (88.3) | 12 (100) | 0.213 [§] |
| Anti-HBs antibody level >10 UI/mL, n (%) | 36 (50) | 27 (45) | 9 (75) | 0.058 [§] |
| Anti-HBs antibody level mean ±SD median (IQR) | 175.6 ±321.7 10.8 (0–109) | 106.9 ±222.6 5.15 (0–50) | 484.7 ±498.9 204 (17.25–818) | <0.001* 0.004** |
| Interval between the 2 doses of vaccine [weeks], mean ±SD | 3.8 ±0.9 | 3.8 ±0.9 | 3.9 ±0.7 | 0.097* |
| Platelet count after the 2 nd vaccine dose, median (IQR) | 181000 (156500–227500) | 177000 (154500–207500) | 208500 (166000–251000) | 0.086** |
| Anti-spike antibody level after the 1 st dose [UI/mL], median (IQR) | 3 (0.5–26) | 1.8 (0.5–7.9) | 8571 (2585–19147) | <0.001** |
| Anti-spike antibody level after the 2 nd dose [UI/mL], median (IQR) | 391 (55–1642) | 371 (50–1157) | 8750 (1936–26250) | 0.003** |
| Anti-spike antibody level titer positive after the 1 st dose, n (%) | 45 (62.5) | 33 (55) | 12 (100) | 0.003 [§] |
| Anti-spike antibody level titer positive after the 2 nd dose (%) | 96.7 (total = 60) | 96.5 (total = 58) | 100 (total = 4) | 0.474*** |
| Adverse events after vaccination | | | | |
| Myalgia, n (%) | 16 (22.2) | 11 (18.3) | 5 (41.7) | 0.091*** |
| Fever, n (%) | 9 (12.5) | 5 (8.3) | 4 (33.3) | 0.030*** |
| Sore arm, n (%) | 27 (37.5) | 24 (40) | 3 (25) | 0.248*** |
| Headache, n (%) | 7 (9.7) | 5 (8.3) | 2 (16.7) | 0.309*** |
| Other – fatigue, n (%) | 12 (16.7) | 11 (18.4) | 1 (8.3) | 0.006 [§] |
| Other – chills, n (%) | 4 (5.6) | 1 (1.7) | 3 (25) | |

*independent t-test was used to compare means of continuous variables with normal distribution; **Mann–Whitney U test was used to compare medians of skewed continuous variables; [§]χ² test and ***Fisher's exact test were used to compare categorical data. SD – standard deviation; IQR – interquartile range; CAD – coronary artery disease; HBs – hepatitis B surface.

Table 2. Assessment of anti-spike antibody levels after the 1st and 2nd dose of vaccine among different groups of categorical variables and the statistical difference between categories

| Variable | Anti-spike antibody level 20 days after the 1 st dose | | | | Anti-spike antibody level 28 days after the 2 nd dose | | | |
|--------------------|--|-------------------|----------|--------|--|--------------------|----------|--------|
| | N (71) | median (IQR) | p-value* | Z | N (61) | median (IQR) | p-value* | Z |
| Sex | | | | | | | | |
| Male | 46 | 2.85 (0.5–26) | 0.652 | −0.452 | 40 | 357.5 (32.05–1049) | 0.120 | −1.556 |
| Female | 25 | 3 (0.7–25.3) | | | 21 | 948.5 (71.91–1932) | | |
| Previous infection | | | | | | | | |
| Yes | 12 | 8571 (3057–17765) | <0.001 | −5.426 | 4 | 8750 (2124–22,500) | 0.001 | −2.928 |
| No | 59 | 1.8 (0.5–7.9) | | | 57 | 371 (52–1119) | | |
| Smoking | | | | | | | | |
| Yes | 10 | 4.8 (0.4–35) | 0.856 | −0.182 | 9 | 1590 (59–2352) | 0.296 | −1.047 |
| No | 61 | 3 (0.6–25.32) | | | 52 | 374 (56.4–1157.5) | | |
| Dialysis frequency | | | | | | | | |
| 2/week | 6 | 1.6 (0.8–7) | 0.579 | −0.579 | 7 | 101 (26–338) | 0.141 | −1.494 |
| 3/week | 65 | 3.2 (0.53–35) | | | 54 | 526 (60.8–1739) | | |
| Diabetes | | | | | | | | |
| Yes | 34 | 1.8 (0.4–14) | 0.127 | −1.526 | 29 | 279 (32–1119) | 0.233 | −1.191 |
| No | 37 | 7.1 (0.8–39) | | | 32 | 743 (86.5–1642) | | |
| Hypertension | | | | | | | | |
| Yes | 65 | 5.9 (0.6–35) | 0.049 | −1.954 | 55 | 391 (60.8–1739) | 0.348 | −0.969 |
| No | 6 | 0.5 (0–1.1) | | | 6 | 295 (19–1032) | | |
| CAD | | | | | | | | |
| Yes | 23 | 0.6 (0.4–23) | 0.058 | −1.899 | 22 | 102 (24–979) | 0.084 | −1.727 |
| No | 48 | 6.5 (0.9–38) | | | 39 | 704 (101–1739) | | |
| Heart failure | | | | | | | | |
| Yes | 9 | 0.6 (0.37–0.9) | 0.029 | −2.187 | 8 | 28 (14–519) | 0.018 | −2.372 |
| No | 62 | 6.6 (0.6–35) | | | 53 | 494 (101–1739) | | |
| History of cancer | | | | | | | | |
| Yes | 6 | 9 (0.6–12) | 0.767 | −0.315 | 5 | 86 (26–1348) | 0.674 | −0.447 |
| No | 64 | 2.75 (0.5–30.2) | | | 56 | 401 (59.9–1642) | | |

*Comparison based on Mann–Whitney test. CAD – coronary artery disease; IQR – interquartile range.

Table 3. Correlation of anti-spike antibody levels after the 1st and 2nd dose of vaccine with different continuous variables

| Variable | Anti-spike antibody level 20 days after the 1 st dose | | | Anti-spike antibody level 28 days after the 2 nd dose | | |
|--|--|---------|----|--|---------|----|
| | correlation coefficient | p-value | n | correlation coefficient | p-value | n |
| Age | −0.289 | 0.015 | 71 | −0.464 | <0.001 | 61 |
| Anti-Hbs antibody level | 0.357 | 0.002 | 71 | 0.283 | 0.027 | 61 |
| Serum albumin level before vaccination | 0.317 | 0.007 | 71 | 0.285 | 0.026 | 61 |
| Dialysis vintage | 0.124 | 0.303 | 71 | 0.208 | 0.108 | 61 |
| Platelet count after 2 nd dose | 0.243 | 0.046 | 68 | 0.207 | 0.110 | 61 |
| Number of weeks between 2 doses of vaccine | 0.158 | 0.212 | 64 | 0.340 | 0.007 | 61 |

Spearman’s rho correlation was used to assess the association between anti-spike antibody levels and different continuous variables; HBS – hepatitis B surface.

2nd dose. It was of 979 (IQR: 308.5–1962.5) UI/mL in patients who received the 2nd dose 4 to 6 weeks after the 1st dose of vaccine.

The quantile regression analysis was used to analyze the association of different factors with the anti-spike antibody levels after the 1st dose of vaccine (Table 4). Previous infection and anti-Hbs levels were significantly associated with higher anti-spike antibody titers after the 1st dose, and remained significant after adjustment to age, sex, diabetes, CAD, heart failure, and serum albumin level.

Discussion

Our study revealed a positive humoral response rate of 96.7% after 2 doses of Pfizer-BioNTech vaccine in HD patients. This is in line with other reports from Europe confirming a good percentage of seropositivity of HD patients after full vaccination. The reported rates in the literature were 82% in a prospective study from Germany,¹⁸ 88% in a trial from Switzerland,¹⁹ 90% in the Romanov study from France,¹⁰ and 97.7% in a prospective multicenter

Table 4. Multivariate quantile regression analysis of factors associated with anti-spike antibody levels 4 weeks after the 1st dose of vaccine

| Variable | Coefficient | SE | df | 95% CI | p-value |
|--------------------------------|-------------|---------|----|----------------------|---------|
| Intercept | 9692.68 | 17.1818 | 53 | [9658.22; 9727.15] | <0.001 |
| Age [years] | 0.006 | 0.1027 | 53 | [-0.200; 0.212] | 0.951 |
| Serum albumin level | 0.257 | 0.2625 | 53 | [-0.270; 0.783] | 0.333 |
| Anti-Hbs antibody level | 0.051 | 0.0039 | 53 | [0.043; 0.059] | <0.001 |
| Sex | | | | | |
| Male | -1.076 | 2.1362 | 53 | [-5.361; 3.209] | 0.616 |
| Female (Ref) | | | | | |
| Previous infection (Ref = yes) | -9700.65 | 3.37 | 53 | [-9707.42; -9693.89] | <0.001 |
| Diabetes (Ref = yes) | -3.479 | 2.1297 | 53 | [-7.750; 0.793] | 0.108 |
| Hypertension (Ref = yes) | -0.617 | 3.6469 | 53 | [-7.931; 6.698] | 0.866 |
| CAD (Ref = yes) | 0.044 | 2.4562 | 53 | [-4.882; 4.971] | 0.986 |
| Heart failure (Ref = yes) | 1.244 | 3.2067 | 53 | [-5.188; 7.676] | 0.700 |

The median (50th) was used for quantile regression analysis. SE – standard error; 95% CI – 95% confidence interval; df – degrees of freedom; CAD – coronary artery disease; HBs – hepatitis B surface.

study from Spain.¹¹ Our findings also highlighted the fact that the 1st dose is not enough to induce an acceptable seroconversion rate or titer in infection-naïve patients. Although 62.5% of patients in our sample developed positive anti-spike antibody levels after the 1st dose, the median of these antibodies was as low as 3 UI/mL (IQR: 0.5–26). This is aligned with the findings of Billany et al. from UK,¹⁶ where antibodies were detectable in 79.8% of patients with a median level of 2.4 (IQR: 8). Lower response rates to the 1st dose of 18%, 21% and 35% were reported by Speer et al.,¹⁸ Longlune et al.¹³ and Torreggiani et al.,²⁰ respectively. They had to administer a 3rd dose of vaccine to patients who did not respond to the routine regimen.¹³ In most of the studies, HD patients had a better response than kidney transplant (TX) patients but worse than healthy controls.^{12,15,17–19,21,22} This was also the case in our sample where healthy controls showed significant higher titers of antibodies.

One interesting finding in our study is the statistically significant association between hepatitis B vaccine response (anti-Hbs antibody levels) and anti-spike antibody levels. To the best of our knowledge, 3 previous studies tried to find out if there was any relation between these 2 variables. Only a French cohort of 78 patients showed a positive correlation between hepatitis B and humoral responses to COVID-19 vaccines, which concurs with our results. In a cohort from Switzerland that studied 1198 HD patients, no such correlation was found.¹⁹ Their patients had longer dialysis vintage than our patients, but were younger. In another study of 81 patients from Switzerland, no association was demonstrated.¹⁷ Their vaccination schedule consisted of 3 doses of Engerix B 40 µg, which is slightly different from our patients' 4 doses. The lack of consistency across studies regarding this association

needs further evaluation by comparing statistical methods used and enrolling more patients from other units worldwide.

In our sample, high serum albumin level was associated with a better response to the COVID-19 vaccine. This parameter is known to predict mortality in HD patients.²³ It has also been demonstrated recently to be associated with COVID-19 vaccine response in HD.¹² Other factors that were highlighted to predict the humoral response to COVID-19 vaccine in other cohorts are age, dialysis vintage and better dialysis quality.^{10–12,19} We showed an inverse correlation between age and anti-spike antibody levels among our patients. However, this was not consistent in the literature. Speer et al. detected lower anti-spike antibody levels at older age in healthy controls but not in HD patients.¹⁸ Stumpf et al. demonstrated age-related differences in TX patients but not in dialysis ones.¹⁹ On the other hand, Jahn et al., Yanay et al. and Attias et al. found significant lower antibody levels in HD patients over 60, 70 and 75 years, respectively.^{21,22,24}

Our results shed light on the distinctive characteristics of patients previously infected with SARS-CoV-2 and their positive response to vaccination. In fact, these patients had higher serum albumin levels, were younger and had significantly higher anti-Hbs antibody titers than infection-naïve patients in our sample. This is most probably due to the natural selection following COVID-19. Those who survived the disease were the ones with more robust immunity parameters. In addition, the strong response of these previously infected patients after a single dose of vaccine and the high incidence of fever following 1 dose suggests that they do not need a 2nd injection. In fact, this 2nd dose can be spared for patients who are non-respondents and would need a 3rd dose.

The pronounced peak of response after 1 dose in patients with a history of COVID-19 has also been demonstrated in several reports from the general population.²⁵

Finally, the fact that one of the immunized patients was diagnosed with COVID-19 two months after the 2nd dose emphasizes the importance of maintaining preventive measures in all dialysis units. This was highlighted as well by Yanay et al. who reported 4% of their patients infected 7 days after the 2nd dose.²²

Limitations

The major limitation of our study is the small sample size. The shortage of serological kits to assess anti-spike antibody levels prevented more units from assessing the humoral response of their patients. However, despite the limited number of patients, this study confirmed once more the good response rate of HD patients to 2 doses of vaccine, highlighted the robust seropositivity after 1 dose of Pfizer-BioNTech vaccine in previously infected patients, and showed the importance of anti-Hbs antibody level as a predictor of the response of patients to COVID-19 vaccine.

Conclusion

In conclusion, this study showed a response rate of 96.7% to 2 doses of BNT162b2 mRNA vaccine in HD patients and of 100% to the 1st dose in previously infected patients. The levels of anti-spike antibody can be predicted by age, anti-Hbs antibody, serum albumin levels, and previous infection. Despite the immunization of patients, preventive measures should be maintained in all dialysis units.

ORCID iDs

Mabel Aoun  <https://orcid.org/0000-0001-9893-5514>

References

- Hilbrands LB, Duivenvoorden R, Vart P, et al; ERACODA collaborators. COVID-19-related mortality in kidney transplant and dialysis patients: Results of the ERACODA collaboration. *Nephrol Dial Transplant*. 2020;35(11):1973–1983. doi:10.1093/ndt/gfaa261
- Jager KJ, Kramer A, Chesnaye NC, et al. Results from the ERA-EDTA registry indicate a high mortality due to COVID-19 in dialysis patients and kidney transplant recipients across Europe. *Kidney Int*. 2020;155: S0085–2538(20)31081–4. doi:10.1016/j.kint.2020.09.006
- Aoun M, Khalil R, Mahfoud W, et al. Age and multimorbidities as poor prognostic factors for COVID-19 in hemodialysis: A Lebanese national study. *BMC Nephrol*. 2021;22:73. doi:10.1186/s12882-021-02270-9
- Combe C, Kirsch AH, Alfano G, et al. At least 156 reasons to prioritize COVID-19 vaccination in patients receiving in-centre haemodialysis. *Nephrol Dial Transplant*. 2021;36(4):571–574. doi:10.1093/ndt/gfab007
- Francis A, Baigent C, Ikizler TA, Cockwell P, Jha V. The urgent need to vaccinate dialysis patients against severe acute respiratory syndrome coronavirus 2: A call to action. *Kidney Int*. 2021;99(4):791–793. doi:10.1016/j.kint.2021.02.003
- ERA-EDTA Council; ERACODA Working Group. Chronic kidney disease is a key risk factor for severe COVID-19: A call to action by the ERA-EDTA. *Nephrol Dial Transplant*. 2021;36(1):87–94. doi:10.1093/ndt/gfaa314
- Sánchez-Álvarez E, Quiroga B, de Sequera P; en representación de la Junta Directiva de Sociedad Española de Nefrología. Position statement of the Spanish Society of Nephrology on the SARS-CoV-2 vaccines. *Nefrología*. 2021;S0211-6995(20)30211-3. doi:10.1016/j.nefro.2020.12.002
- Yousaf F, Gandham S, Galler M, Spinowitz B, Charytan C. Systematic review of the efficacy and safety of intradermal versus intramuscular hepatitis B vaccination in end-stage renal disease population unresponsive to primary vaccination series. *Ren Fail*. 2015;37(7):1080–1088. PMID:26258528.
- Mitra S, Stein GE, Bhupalam S, Havlichek DH. Immunogenicity of 13-valent conjugate pneumococcal vaccine in patients 50 years and older with end-stage renal disease and on dialysis. *Clin Vaccine Immunol*. 2016;23(11):884–887. doi:10.1128/CVI.00153-16
- Espi M, Charmetant X, Barba T, et al. The ROMANOV study found impaired humoral and cellular immune responses to SARS-Cov-2 mRNA vaccine in virus unexposed patients receiving maintenance hemodialysis. *Kidney Int*. 2021;100(4):928–936. doi:10.1016/j.kint.2021.07.005
- Broseta JJ, Rodríguez-Espinosa D, Rodríguez N, et al. Humoral and cellular responses to mRNA-1273 and BNT162b2 SARS-CoV-2 vaccines administered to hemodialysis patients. *Am J Kidney Dis*. 2021; 78(4):571–581. doi:10.1053/j.ajkd.2021.06.002
- Danthu C, Hantz S, Dahlem A, et al. Humoral response after SARS-CoV-2 mRNA vaccine in a cohort of hemodialysis patients and kidney transplant recipients. *J Am Soc Nephrol*. 2021;32(9):2153–2158. doi:10.1681/ASN.2021040490
- Longlune N, Nogier MB, Miedougé M, et al. High immunogenicity of a messenger RNA based vaccine against SARS-CoV-2 in chronic dialysis patients. *Nephrol Dial Transplant*. 2021;36(9):1704–1709. doi:10.1093/ndt/gfab193
- Ikizler TA, Coates PT, Rovin BH, Ronco P. Immune response to SARS-CoV-2 infection and vaccination in patients receiving kidney replacement therapy. *Kidney Int*. 2021;99(6):1275–1279. doi:10.1016/j.kint.2021.04.007
- Speer C, Göth D, Benning L, et al. Short-term antibody response after 1 dose of BNT162b2 vaccine in patients receiving hemodialysis. *CMAJ*. 2021;193(22):E793–E800. doi:10.1503/cmaj.210673
- Billany RE, Selvaskandan H, Adenwalla SF. Seroprevalence of antibody to S1 spike protein following vaccination against COVID-19 in patients on hemodialysis: A call to arms. *Kidney Int*. 2021;99(6): 1492–1494. doi:10.1016/j.kint.2021.04.008
- Simon B, Rubey H, Treipl A, et al. Haemodialysis patients show a highly diminished antibody response after COVID-19 mRNA vaccination compared to healthy controls. *Nephrol Dial Transplant*. 2021;36(9): 1709–1716. doi:10.1093/ndt/gfab179
- Speer C, Göth D, Benning L, et al. Early humoral responses of hemodialysis patients after COVID-19 vaccination with BNT162b2. *Clin J Am Soc Nephrol*. 2021;16(7):1073–1082. doi:10.2215/CJN.03700321
- Stumpf J, Siepmann T, Lindner T, et al. Humoral and cellular immunity to SARS-CoV-2 vaccination in renal transplant versus dialysis patients: A prospective, multicenter observational study using mRNA-1273 or BNT162b2 mRNA vaccine. *Lancet Reg Health Eur*. 2021;9:100178. doi:10.1016/j.lanpe.2021.100178
- Torreggiani M, Bianchi S, Fois A. Neutralizing SARS-CoV-2 antibody response in dialysis patients after the first dose of the BNT162b2 mRNA COVID-19 vaccine: The war is far from being won. *Kidney Int*. 2021;99(6):1494–1496. doi:10.1016/j.kint.2021.04.010
- Jahn M, Korth J, Dorsch O, et al. Humoral response to SARS-CoV-2-vaccination with BNT162b2 (Pfizer-BioNTech) in patients on hemodialysis. *Vaccines (Basel)*. 2021;9(4):360. doi:10.3390/vaccines9040360
- Yanay NB, Freiman S, Shapira M. Experience with SARS-CoV-2 BNT162b2 mRNA vaccine in dialysis patients. *Kidney Int*. 2021;99(6):1496–1498. doi:10.1016/j.kint.2021.04.006
- Mehrotra R, Duong U, Jiwakanon S, et al. Serum albumin as a predictor of mortality in peritoneal dialysis: Comparisons with hemodialysis. *Am J Kidney Dis*. 2011;58(3):418–428. doi:10.1053/j.ajkd.2011.03.018
- Attias P, Sakhi H, Rieu P, et al. Antibody response to the BNT162b2 vaccine in maintenance hemodialysis patients. *Kidney Int*. 2021;99(6): 1490–1492. doi:10.1016/j.kint.2021.04.009
- Fraley E, LeMaster C, Geanes E, et al. Humoral immune responses during SARS-CoV-2 mRNA vaccine administration in seropositive and seronegative individuals. *BMC Med*. 2021;19(1):169. doi:10.1186/s12916-021-02055-9

Gastrointestinal hemorrhage as an acute-on-chronic liver failure trigger in cirrhotic patients

Paweł Rogalski^{A–D,F}, Marta Zaborowska^{B–F}, Maria Mazur^{B–F}, Żaneta Jankowska^{B,C,E,F}, Alicja Piszczyk^{B,C,E,F}, Edyta Mermer^{B,C,E,F}, Andrzej Dąbrowski^{C,E,F}, Jarosław Daniluk^{C,E,F}

Department of Gastroenterology and Internal Medicine, Medical University of Białystok, Poland

A – research concept and design; B – collection and/or assembly of data; C – data analysis and interpretation; D – writing the article; E – critical revision of the article; F – final approval of the article

Advances in Clinical and Experimental Medicine, ISSN 1899–5276 (print), ISSN 2451–2680 (online)

Adv Clin Exp Med. 2022;31(8):863–871

Address for correspondence

Paweł Rogalski
E-mail: progalsky@gmail.com

Funding sources

None declared

Conflict of interest

None declared

Received on August 15, 2021

Reviewed on December 21, 2021

Accepted on March 18, 2022

Published online on April 19, 2022

Abstract

Background. Acute-on-chronic liver failure (ACLF) is a syndrome characterized by acute decompensation of chronic liver disease associated with organ failures and very high short-term mortality.

Objectives. To assess the incidence and factors predisposing to ACLF in patients with liver cirrhosis hospitalized due to acute gastrointestinal bleeding (GIB).

Materials and methods. We collected and retrospectively analyzed the data of 89 consecutive patients (59 males (66.2%), median age 53 years (range: 44–62 years), mean Model for End-Stage Liver Disease (MELD) score 14.42 ± 6.5 , median Child–Turcotte–Pugh score 10 (range: 8–11), and acute GIB (72 variceal bleeding and 17 non-variceal bleeding cases). Acute-on-chronic liver failure was diagnosed based on European Association for the Study of the Liver – Chronic Liver Failure Consortium definition.

Results. Twenty-seven (30.33%) patients met the criteria of ACLF during hospitalization: 8 (30%) had ACLF grade 1, 13 (48%) had ACLF grade 2 and 6 (22%) had ACLF grade 3. The most frequent organ failures were respiratory (22 (25%)), kidney (18 (20.23%)) and brain (17 (19.1%)) failure. The MELD score value, creatinine level and presence of hepatic encephalopathy (HE) on admission were significant predictors of ACLF in the multivariate logistic regression model with optimal cutoff point for MELD score of 18.313 and optimal cutoff point for creatinine level of 1.35 mg/dL.

Conclusions. In-hospital risk of ACLF in cirrhotic patients hospitalized for acute gastrointestinal hemorrhage is high despite successful arrest of bleeding. Elevated creatinine level, MELD score and the presence of HE on admission are the best predictors of ACLF during hospitalization in such patients.

Key words: liver cirrhosis, gastrointestinal bleeding, organ failure, gastrointestinal hemorrhage, acute-on-chronic liver failure

Cite as

Rogalski P, Zaborowska M, Mazur M, et al. Gastrointestinal hemorrhage as an acute-on-chronic liver failure trigger in cirrhotic patients. *Adv Clin Exp Med.* 2022;31(8):863–871. doi:10.17219/acem/147464

DOI

10.17219/acem/147464

Copyright

Copyright by Author(s)

This is an article distributed under the terms of the Creative Commons Attribution 3.0 Unported (CC BY 3.0) (<https://creativecommons.org/licenses/by/3.0/>)

Background

The natural history of liver cirrhosis includes compensated and decompensated phase. The classic hallmarks of decompensated liver cirrhosis are variceal bleeding, ascites and hepatic encephalopathy (HE). Acute-on-chronic liver failure (ACLF) is a syndrome characterized by acute decompensation (AD) of chronic liver disease associated with organ failures. While the predicted survival of patients with decompensated cirrhosis is 3–5 years, ACLF has very high short-term mortality exceeding 25%, with a prognosis comparable to the acute liver failure.^{1,2} The European Association for the Study of the Liver-Chronic Liver Failure (EASL-CLIF) Consortium and the EASL-CLIF Acute-on-Chronic Liver Failure in Cirrhosis (CANONIC) study provided the evidence-based definition of ACLF in 2013.³ This definition is based on the existence of the failure of 1 of the 6 major organ systems (liver, kidney, brain, coagulation, circulation, and respiration) in patients with acutely decompensated cirrhosis (with or without prior episodes of decompensation).^{3,4} The failure of individual organ systems in these patients is assessed using the CLIF-C Organ Failure scale. As defined by EASL-CLIF, ACLF is divided into 3 grades of increasing severity, based on the number of organ system failure.

The Personalised Responses to Dietary Composition Trial (PREDICT) study showed that AD without organ failure (without ACLF) is a heterogeneous condition with 3 major clinical courses: 1) pre-ACLF with high risk of ACLF and high 3-month and 1-year mortality rates; 2) unstable decompensated cirrhosis (UDC) with intermediate mortality rates, high risk of ≥ 1 readmission, but not leading to ACLF; 3) stable decompensated cirrhosis (SDC) neither requiring readmission to hospital nor leading to ACLF, and showing the lowest mortality.⁵ Based on results of CANONIC and PREDICT studies, we can identify cirrhotic patients with AD with a high risk of short-term mortality due to ACLF.

In patients with compensated cirrhosis, the major determinants of decompensation are clinically significant portal hypertension and the degree of liver failure. Traditionally, portal hypertension, portosystemic shunting, and hepatic and extrahepatic organ perfusion disorders have been recognized for decades as the main risk factors for complications of cirrhosis. The current view of the physiological mechanism of AD assumes a crucial role of systemic inflammation in the development of AD subphenotypes, including AD-ACLF.⁶ Systemic inflammation increases across AD-no-ACLF phenotypes from the lowest degree of inflammation in SDC, through moderate in UDC to the highest in pre-ACLF.^{7,8} In patients with AD-ACLF, the degree of systemic inflammation correlates also with the number of organ failures, severity of the clinical course and prognosis.^{6,9} Variceal bleeding, which is a major complication of portal hypertension, occurs more frequently in UDC than in other AD-no-ACLF phenotypes.¹⁰ This phenotype has a complicated clinical

course and a relatively high mortality rate, with moderate systemic inflammation at hospital admission. In patients with variceal bleeding and AD-ACLF phenotype, the clinical course seems to depend on the evolution of systemic inflammation.

Objectives

The aim of the study was to assess the incidence and factors predisposing to ACLF in the cohort of patients with liver cirrhosis, hospitalized due to acute gastrointestinal bleeding (GIB) effectively treated endoscopically. The primary endpoint was the occurrence of ACLF in these patients. Secondary endpoints were in-hospital mortality, days of intensive care unit (ICU)/hospital stay, 5-day treatment failure, the rate of repeat endoscopy within 72 h for rebleeding, the need for salvage therapy, and blood transfusion requirements.

Materials and methods

The medical records of patients hospitalized in our department from August 2015 to December 2018 were searched using International Classification of Diseases (ICD)-10 codes (see Supplementary material for codes and their explanations: <https://doi.org/10.5281/zenodo.6374308>). Data on age, sex, etiology and severity of cirrhosis, sources of acute GIB, and organ failure were collected. We collected and analyzed both the results of laboratory tests on admission and during hospitalization in order to determine ACLF predictors on admission and the incidence of ACLF on admission and during hospitalization.

Definitions

The definitions are presented in the Supplementary material: <https://doi.org/10.5281/zenodo.6374308>.

Inclusion and exclusion criteria

Inclusion criteria were as follows: 1) cirrhosis diagnosed based on clinical, laboratory and imaging evidence; 2) acute upper GIB confirmed endoscopically and based on clinical symptoms (see above); 3) effective initial resuscitation and successful endoscopic treatment or no need for endoscopic treatment. Exclusion criteria were as follows: 1) admission for scheduled procedure or treatment; 2) hepatocellular carcinoma outside Milan criteria; 3) severe chronic extrahepatic diseases; 4) ongoing immunosuppressive treatments; 5) human immunodeficiency virus (HIV) infection.¹¹

The study was approved by Ethics Committee of Medical University of Białystok, Poland (resolution

No. R-I-002/336/2019, of June 27, 2019). The study was conducted in accordance with the principles of the Helsinki Declaration. Due to the retrospective design of the study, informed consent of the subjects was not required.

Statistical analyses

Continuous variables were tested for normality using the Shapiro–Wilk test and Lilliefors test, and expressed as means (\pm standard deviation (SD)) or median (interquartile range (IQR)), as appropriate. The equality of variance in the tested samples was assessed with the Levene's test. Categorical variables were reported as counts (percentage). Continuous data were analyzed with either t-test or Mann–Whitney U test, as appropriate. Categorical variables were analyzed using χ^2 test. The p-values of <0.05 were considered statistically significant. The additional analysis included a stepwise multivariate logistic regression, which was used to identify the best combination of parameters predicting ACLF presence. Only variables which were significantly different between analyzed groups were included into the regression model as predictors. Model was assessed with χ^2 test, R^2 Nagelkerky coefficient and Hosmer–Lemeshow goodness of fit (GOF) test. The receiver operating characteristic (ROC) curves were prepared. Cut-off point calculation was based on Youden's criterion. Statistical analyses were performed with the STATISTICA v. 13.3 software package (StatSoft Inc., Tulsa, USA).

Results

Of the 1902 hospitalizations identified based on ICD-10 codes (384 hospitalizations due to decompensated liver cirrhosis and 1518 hospitalizations due to acute GIB – see the Supplementary material: <https://doi.org/10.5281/zenodo.6374308>), we collected and retrospectively analyzed data of 89 consecutive patients of Caucasian ethnicity (59 males (66.2%), median age 53 (44–62) years), with cirrhosis (mean Model for End-Stage Liver Disease (MELD) score 14.42 ± 6.5 , median Child–Turcotte–Pugh score 10 (8–11) of various etiologies, and acute GIB, hospitalized from August 2015 to December 2018 at our department.

Twenty-seven (30.33%) patients met the ACLF criteria during hospitalization: 8 (30%) had ACLF grade 1, 13 (48%) ACLF grade 2 and 6 (22%) ACLF grade 3. We were able to confirm ACLF in 7 (7.86%) patients on admission to hospital, based on the available data. Patient data were analyzed considering the presence of ACLF. Demographic, clinical and laboratory characteristics are shown in Table 1.

Acute gastrointestinal bleeding

Seventy-two patients (80.89%) had variceal bleeding, while 17 patients (19.1%) had non-variceal bleeding. Twenty-one (29.1%) patients with variceal bleeding and

6 (35.29%) patients with non-variceal bleeding had ACLF. Esophageal varices were the most common source of variceal bleeding, while gastric ulcers, erosive esophagitis, duodenal ulcers, and Mallory–Weiss tear were the most common causes of non-variceal bleeding. We found no relationship between the type (variceal compared to non-variceal) and the source of bleeding, and the occurrence of ACLF (Table 2).

Acute cirrhosis decompensation

Forty-three (50%) patients had overt HE, 23 patients (26.44%) had HE grades I/II and 20 patients (23.26%) had HE grades III/V. Hepatic encephalopathy was diagnosed in 24 (40%) patients without ACLF and in 19 (73.08%) patients with ACLF ($p = 0.0048$).

Ascites was present in 48 patients (54.55%) – 26 (42.58%) non-ACLF patients and 22 (81.48%) ACLF patients ($p = 0.0023$). Fifty-seven (66.28%) patients were on diuretics (34 (57.63%) in the non-ACLF group compared to 23 (85.19%) in the ACLF group ($p = 0.0121$). The need for therapeutic paracentesis during hospitalization was observed in 6 patients – 3 (4.92%) patients without and 3 (11.11%) patients with ACLF ($p = 0.2878$).

A total of 12 (13.48%) patients were diagnosed with clinically significant infections. The most common infections were pneumonia (5 (5.62%)) and urinary tract infection (5 (5.62%)), followed by bacteremia (3 (3.37%)), spontaneous bacterial peritonitis (2 (2.25%)) and *Clostridium difficile* intestinal infection (2 (2.25%)). Infections were more common in the ACLF group compared to patients in the non-ACLF group (8 (29.63%) compared to 4 (6.45%), $p = 0.006$). Antibiotics were administered in 73 (82.95%) patients (64 (91.43%) patients with variceal bleeding and 9 (52.94%) patients with non-variceal bleeding). Antibiotics were used more frequently in the ACLF group compared to the non-ACLF group (26 (96.3%) compared to 47 (77.05%), $p = 0.0268$).

Previous episodes of acute decompensation

Fifty (56.18%) patients had a history of previous AD. Of the patients with previous episodes of AD, 16 (32%) had ACLF, while 11 (28%) patients had ACLF despite no prior AD. The history of previous AD did not affect the occurrence of ACLF during current hospitalization ($p = 0.699$).

Organ failures

The most frequent organ failures as defined by EASL-CLIF score were respiratory (22 (25%)), kidney (18 (20.23%)) and brain (17 (19.1%)) failures, followed by coagulation (7 (7.87%)), circulation (6 (6.98%)) and liver (4 (4.49%)) failures (Table 3). Among patients with organ failures, 20

Table 1. Demographic, clinical and laboratory characteristics

| Variable | No ACLF (n = 62) | ACLF (n = 27) | Test statistics | df | Mean (95% CI) | p-value |
|---------------------------------|---------------------|---------------------|-------------------|--------|-------------------------|---------|
| Age [years] | 50.0 (43–62) | 54 (48–61) | U = 751 | – | – | 0.4478 |
| Sex, n (%) | | | | | | |
| Men | 44 (70.97) | 15 (55.56) | $\chi^2 = 1.999$ | 1 | – | 0.1574 |
| Women | 18 (29.03) | 12 (44.44) | | | | |
| Days of hospitalization (IQR) | 8 (5–9) | 10 (6–16) | U = 579.5 | – | – | 0.0209 |
| Etiology | | | | | | |
| Alcohol, n (%) | 44 (70.97) | 17 (62.96) | $\chi^2 = 6.1357$ | 4 | – | 0.1892 |
| Viral, n (%) | 5 (8.06) | 0 | | | | |
| Cholestatic, n (%) | 3 (4.84) | 1 (3.7) | | | | |
| Other, n (%) | 9 (14.52) | 9 (33.33) | | | | |
| Child–Pugh score | 9 (8–11) | 11 (10–12) | U = 227.5 | – | – | 0.0059 |
| MELD _{Na} score | 10.75 (8.45–14.89) | 24.06 (18.4–27.05) | U = 132 | – | – | <0.0001 |
| MELD score | 11.82 ± 4.62 | 20.32 ± 6.37 | t = 6.1258 | 37.081 | 14.42 [13.017; 15.825] | <0.0001 |
| Hemoglobin (IQR) [g/dL] | 8.7 (7.6–10.10) | 8.55 (6.7–9.8) | U = 725 | – | – | 0.4640 |
| RBC ±SD [10 ⁶ /UL] | 3.0 ± 0.66 | 2.76 ± 0.96 | t = –1.3793 | 86 | 2.9302 [2.7680; 3.0924] | 0.1714 |
| WBC (IQR) [10 ³ /UL] | 7.035 (4.92–9.59) | 8.425 (6.74–12.03) | U = 573.5 | – | – | 0.0329 |
| PLT (IQR) [10 ³ /UL] | 96.79 (59–122) | 106.58 (69–116) | U = 757 | – | – | 0.6593 |
| PT (IQR) (%) | 60.0 (50.0–70.0) | 46.0 (33.5–68.0) | U = 511.5 | – | – | 0.0307 |
| Fibrinogen (IQR) [mg/dL] | 217.5 (176.0–263.0) | 216.5 (162.0–373.0) | U = 566 | – | – | 0.4438 |
| Albumin (IQR) [g/dL] | 2.94 (2.67–3.11) | 2.65 (2.65–2.76) | U = 12 | – | – | 0.0897 |
| Ammonia | 55.5 (40.8–62.7) | 61.7 (44.5–112.7) | U = 138 | – | – | 0.1731 |
| Bilirubin (IQR) [mg/dL] | 2.04 (1.28–3.54) | 2.8 (1.92–5.87) | U = 598 | – | – | 0.0574 |
| AST (IQR) [IU/L] | 67.0 (42–118.0) | 76.0 (46.0–157.0) | U = 558.5 | – | – | 0.2814 |
| ALT (IQR) [IU/L] | 29.0 (21.0–49.0) | 35.5 (19.5–55.0) | U = 581.00 | – | – | 0.4053 |
| Urea (IQR) [mg/dL] | 43.0 (27.0–75.0) | 76.0 (42.5–123.5) | U = 405 | – | – | 0.0020 |
| BUN [mg/dL] | 20.07 (12.6–33.6) | 26.6 (19.6–57.4) | U = 414.5 | – | – | 0.0343 |
| Creatinine (IQR) [mg/dL] | 0.79 (0.72–1.04) | 1.47 (0.85–2.66) | U = 351 | – | – | <0.0001 |
| Na [mmol/L] | 138 (135–141.0) | 134 (127.0–140.0) | U = 345 | – | – | 0.0532 |
| K [mmol/L] | 4.25 (3.73–4.61) | 4.51 (4.02–5.73) | U = 307.5 | – | – | 0.0185 |
| CRP (IQR) [mg/L] | 4.8 (2.0–20.7) | 18.4 (7.8–30.11) | U = 412.5 | – | – | 0.0077 |

Data presented as mean ± standard deviation (SD) or median (1st quartile (Q1), 3rd quartile (Q3)), unless indicated otherwise. IQR – interquartile range; t – Student's t-test; U – Mann–Whitney U test; df – degrees of freedom; 95% CI – 95% confidence interval; ACLF – acute-on-chronic liver failure; BUN – blood urea nitrogen; MELD – Model for End-Stage Liver Disease; WBC – white blood cells; RBC – red blood cells; PLT – platelet count; PT – prothrombin time; AST – aspartate transaminase; ALT – alanine transaminase; CRP – C-reactive protein.

(52.63%) patients had single organ failure, 13 (34.21%) patients had 2 organs failures, 2 (5.26%) patients had 3 or 4 organs failures, and 1 (2.63%) patient had failure of 5 organs.

In-hospital mortality

There were 7 deaths in the study group: 6 (24.0%) in patients with ACLF and 1 (1.61%) in a patient without ACLF. Estimated probability of dying in the ACLF group calculated based on CLIF-C ACLF score, age and white blood cell (WBC) count was: 24.0% (range: 13–41%), 42.0% (range: 31–61%), 47.0% (range: 41.0–66.0%), and 56.0% (range: 50.0–73.0%) at 1, 3, 6, and 12 months, respectively. The estimated probability of death based on the CLIF AD

score in the non-ACLF group was: 3.0% (range: 1.0–5.0%), 8.0% (range: 5.0–14.0%), 13.5% (range: 9.0–21.0%), and 24.5% (range: 18.0–34.0%) at 1, 3, 6, and 12 months, respectively. Both CLIF-C ACLF score and CLIF AD score (at 1 month) allowed for a reliable assessment of probability of death during hospitalization in patients with ACLF and patients with AD without ACLF, respectively. There were no statistically significant differences in the number of deaths <5 days between the groups – 1 (1.67%) ACLF patient compared to 1 (4%) non-ACLF patient; p = 0.5. However, the overall number of in-hospital deaths was significantly higher in the ACLF group compared to the non-ACLF group: 6 (24%) compared to 1 (1.61%), respectively (p = 0.002).

Table 2. Sources of bleeding

| Source of bleeding | No ACLF (n = 62) | ACLF (n = 27) | Pearson's χ^2 | df | p-value |
|----------------------------------|------------------|---------------|--------------------|----|---------|
| Variceal | 51 (82.25) | 21 (77.78) | 0.04 | 1 | 0.8407 |
| Non-variceal | 11 (17.74) | 6 (22.22) | | | |
| Variceal | | | | | |
| Esophageal varices, n (%) | 38 (61.29) | 15 (55.56) | 1.39 | 3 | 0.7081 |
| Gastric varices, n (%) | 6 (9.68) | 3 (11.11) | | | |
| Gastro-esophageal varices, n (%) | 2 (3.23) | 2 (7.41) | | | |
| NS, n (%) | 5 (8.06) | 1 (3.7) | | | |
| Non-variceal | | | | | |
| Erosive esophagitis, n (%) | 4 (6.45) | 0 | 8.83 | 5 | 0.1162 |
| Gastric ulcer, n (%) | 3 (4.84) | 2 (7.41) | | | |
| Duodenal ulcer, n (%) | 0 | 3 (11.11) | | | |
| Mallory–Weiss tear, n (%) | 2 (3.23) | 1 (3.7) | | | |
| Dieulafoy lesion, n (%) | 1 (1.61) | 0 | | | |
| NS, n (%) | 1 (1.61) | 0 | | | |

df – degrees of freedom; NS – not specified; ACLF – acute-on-chronic liver failure.

Table 3. Organ failures according to European Association for the Study of Liver-Chronic Liver Failure (EASL-CLIF) definition

| Organ/system | No ACLF (n = 62) | ACLF (n = 27) | df | Pearson's χ^2 | p-value |
|--------------------|------------------|---------------|----|--------------------|---------|
| Liver | | | | | |
| Bilirubin <12 | 62 (100) | 23 (85) | 1 | 9.62 | 0.0019 |
| Bilirubin >12 | 0 | 4 (15) | | | |
| Brain | | | | | |
| HE 0–2 | 57 (92) | 15 (56) | 1 | 16.1 | 0.0001 |
| HE 3–4 | 5 (8) | 12 (44) | | | |
| Coagulation | | | | | |
| 0 | 61 (98) | 21 (78) | 1 | 11.2 | 0.0009 |
| 1 | 1 (2) | 6 (22) | | | |
| Kidney | | | | | |
| Creatinine <1.5 | 58 (94) | 13 (48) | 2 | 30.64 | <0.0001 |
| Creatinine 1.5–1.9 | 4 (6) | 3 (11) | | | |
| Creatinine >1.9 | 0 | 11 (41) | | | |
| Circulation | | | | | |
| 0 | 61 (100) | 19 (76) | 1 | 15.74 | 0.0001 |
| 1 | 0 | 6 (24) | | | |
| Respiratory | | | | | |
| 0 | 52 (85) | 14 (52) | 1 | 11.13 | 0.0009 |
| 1 | 9 (15) | 13 (48) | | | |

ACLF – acute-on-chronic liver disease; HE – hepatic encephalopathy; df – degrees of freedom.

5-day treatment failure

Five-day treatment failure was found significantly more frequently in patients with ACLF compared to non-ACLF group: 6 (22.2%) compared to 2 (3.23%), respectively (p = 0.008). The rate of repeat endoscopy within 72 h for rebleeding was significantly higher in the ACLF group compared to the non-ACLF group: 7 (25.93%) compared

to 3 (4.84%), respectively (p = 0.0075). No statistically significant differences were found in the need for salvage therapy.

The use of blood products

Red blood cell concentrate was used significantly more frequently in the ACLF group compared to the non-ACLF

group: 33 (53.23%) compared to 21 (80.77%), respectively ($p = 0.017$). The frequency of using fresh frozen plasma, platelet concentrate and cryoprecipitate were comparable between groups (11 (18.03%) compared to 8 (29.63%) ($p = 0.265$), 13 (21.31%) compared to 4 (14.81%) ($p = 0.568$) and 0 (0%) compared to 1 (3.7%) ($p = 0.307$), respectively).

Multivariate logistic regression

Parameters which were significantly different between the groups were included into the multivariate logistic regression model with ACLF as outcome variable. Stepwise logistic regression recommended a model with 10 parameters: the presence of HE, ascites, infection, rebleeding during hospitalization, the use of diuretics, red blood cell concentrate, the value of the MELD score, and WBC, creatinine and C-reactive protein (CRP) levels.

The MELD score, creatinine level and presence of HE were significant in the model (Table 4). The model was validated with χ^2 test, which confirmed that all variables jointly are significant ($p < 0.001$). The R^2 Nagelkerky coefficient was on a moderate level (63%). The additional assessment with Hosmer–Lemeshow GOF test ($p = 0.495$) confirmed good fit of the model to the data.

To ascertain the optimal cutoff point for MELD score and creatinine level as predictors for ACLF, ROC curves were prepared (Fig. 1,2). For MELD score, the analysis resulted in the area under the curve (AUC) = 0.853, 95% confidence interval (95% CI): [0.759; 0.948]. The optimal cutoff point for MELD score was 18.313, with ACLF prediction for MELD score ≥ 18.313 . Sensitivity and specificity of the analysis were 69.2% and 91.5%, respectively. Accuracy of the test (ACC) was on the level of 84.7%, meaning 84.7% of all patients were correctly identified as ACLF patients based on the MELD score cutoff point of 18.313. For creatinine level, the analysis resulted in the AUC = 0.779, 95% CI: [0.656; 0.902]. The optimal cutoff point for creatinine level was 1.35 mg/dL, with ACLF prediction for creatinine ≥ 1.35 mg/dL. Sensitivity of the analysis was 61.5% and specificity was 95.1%. The ACC was on the level of 85.1%.

Discussion

The efficacy of endoscopic and pharmacological treatment of acute GIB has improved significantly during the last decades.¹² Nevertheless, despite high efficiency of current methods in achieving hemostasis and reducing

Table 4. Multivariate logistic regression model for acute-on-chronic liver failure (ACLF)

| Characteristic | Coefficient | SE | p-value | OR | 95% CI for OR |
|--------------------------|-------------|-------|---------|-------|-----------------|
| HE | 2.028 | 0.949 | 0.0325 | 7.601 | [1.184; 48.810] |
| MELD | 0.0162 | 0.081 | 0.0461 | 1.176 | [1.003; 1.379] |
| Creatinine level [mg/dL] | 2.117 | 0.911 | 0.0202 | 8.304 | [1.392; 49.548] |
| Constant | -7.229 | 1.671 | <0.0001 | 0.001 | [0.000; 0.019] |

SE – standard error; OR – odds ratio; 95% CI – 95% confidence interval; HE – hepatic encephalopathy; MELD – Model for End-Stage Liver Disease.

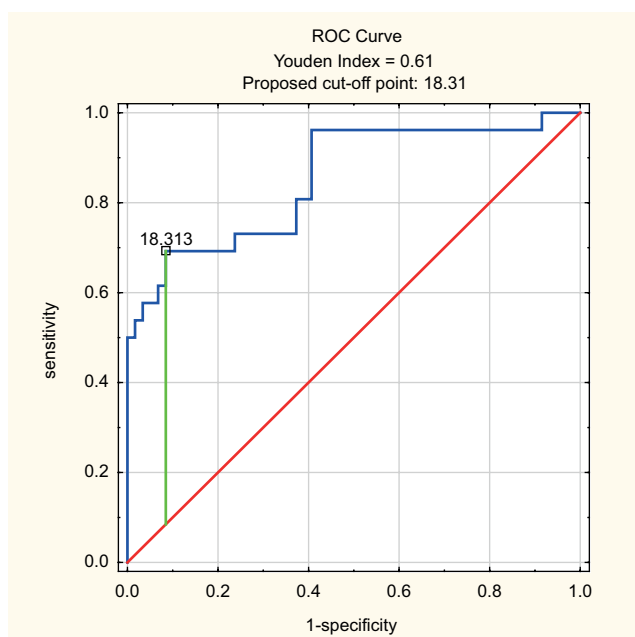


Fig. 1. Receiver operating characteristic (ROC) curve for the Model for End-Stage Liver Disease (MELD)

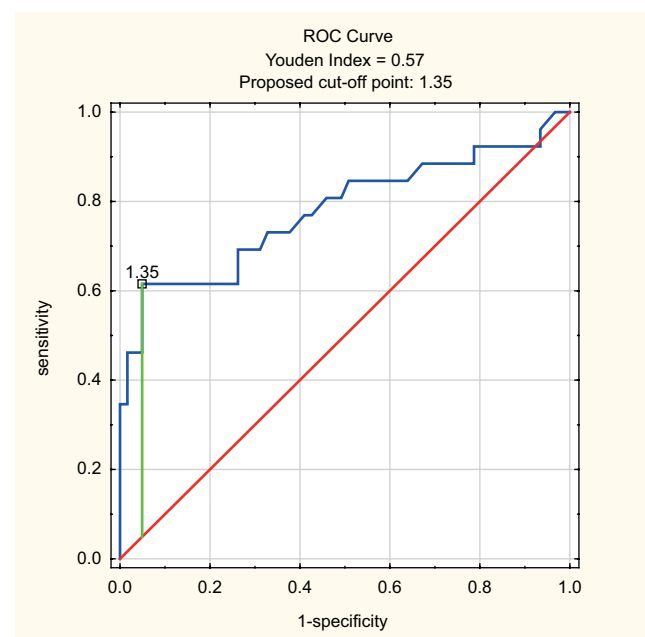


Fig. 2. Receiver operating characteristic (ROC) curve for creatinine level

the frequency of early bleeding relapses, mortality in cirrhotic patients with acute gastrointestinal bleeding remains high.¹³ This disparity indicates that the clinical outcome depends not only on successful stopping of bleeding, but primarily on the severity of underlying chronic liver disease and the development of complications.^{14,15} Acute-on-chronic liver failure is one such complication which potentially can contribute to increased mortality after GIB. Gastrointestinal hemorrhage is a known trigger of ACLF. However, the relationship between GIB in cirrhotic patients and ACLF is not well understood.

In this study, we analyzed the data of 89 consecutive cirrhotic patients admitted to our hospital due to gastrointestinal hemorrhage. All patients included in the study were subsequently hospitalized in our department after fluid resuscitation and achieving hemostasis. The incidence of ACLF in these patients during hospitalization was very high (30.33%), despite effective initial treatment of GIB. The in-hospital mortality in patients with ACLF was also high and exceeded 24%. On the other hand, in-hospital mortality in patients without ACLF was 8 times lower. These data indicate that cirrhotic patients with acute GIB are a heterogeneous group in terms of prognosis, and the risk of death in these patients depends primarily on the occurrence of ACLF. Of the organ failures, respiratory failure was most frequently found, followed by kidney and brain failure.

The relationship between the type and number of precipitants and the clinical course of patients hospitalized with AD-no-ACLF and AD-ACLF phenotypes has been investigated previously. The PREDICT study identified 4 precipitants associated with the AD-ACLF phenotype: proven bacterial infections, severe alcoholic hepatitis, GIB with shock, and toxic encephalopathy.⁶ In the present study, we identified 3 major risk factors for ACLF in patients admitted to hospital for gastrointestinal hemorrhage: high MELD score value, elevated creatinine and HE. Two of the 3 parameters (bilirubin and International Normalized Ratio (INR)) assessed in MELD are used in Maddrey's discriminant function for alcoholic hepatitis. Therefore, a high MELD score could, in fact, indirectly indicate a higher frequency of alcoholic hepatitis in the ACLF group. Nevertheless, due to the small group of patients, it was not possible to perform separate analyses in subgroups of different etiology. Increased creatinine level could indicate a higher frequency of prerenal renal failure in the ACLF group, resulting from more severe bleeding. Finally, some cases of HE may in practice be a toxic, drug-induced encephalopathy – due to the retrospective design of the study we were unable to distinguish between these cases.

On account of the dynamic clinical course of AD-ACLF, precipitants most often occur in close association with ACLF.⁶ However, to the best of our knowledge, the exact time interval from triggering to ACLF has not been investigated so far. The assessment of the temporal relationship

between the precipitant and ACLF is an interesting issue that requires a new prospective study with close monitoring of parameters of organ systems failure.

In addition to more severe liver failure, higher CRP and WBC values were found in the ACLF group compared to non-ACLF group on the admission. In our study, bacterial infections were more common, and antibiotics were also more often used in the ACLF group compared to non-ACLF group. The effectiveness of antibiotic prophylaxis in reducing the mortality, the incidence of infections and the recurrence of bleeding in cirrhotic patients with upper GIB has been confirmed previously in a meta-analysis of 12 studies.¹⁶ However, studies included in the meta-analysis did not assess the effect of antibiotic prophylaxis on the incidence of ACLF. Antibiotic prophylaxis (ceftriaxone or ciprofloxacin) has been used in most patients with variceal bleeding and in a significant proportion of patients with non-variceal bleeding in our study. Interestingly, ACLF occurred despite the widespread, prophylactic use of antibiotics. This may indicate the need to individualize antibiotic prophylaxis in cirrhotic patients with GIB at highest risk of ACLF.

The issue of identifying patients with the highest risk of mortality and recurrent bleeding is currently of great interest. In a recent study, it was shown that ACLF in patients with acute variceal bleeding almost doubled the risk of recurrent bleeding.¹⁷ Furthermore, ACLF was, along with hepatocellular carcinoma, the strongest predictor of short-term mortality in these patients, with an almost threefold increased risk. Interestingly, it was also shown that transjugular intrahepatic portosystemic shunt (TIPSS) could improve survival in patients with ACLF and acute variceal bleeding. Kumar et al. analyzed the determinants of mortality in patients with cirrhosis and uncontrolled variceal bleeding.¹⁸ The ACLF was found in the majority (68.4%) of patients during hospitalization and it was the strongest determinant of the 42-day and 1-year mortality rates that increased with increasing ACLF grades. Other mortality predictors identified were age and systemic inflammation reflected by the WBC. Importantly, the beneficial effect of the rescue TIPSS was also shown in this study, but only in patients with ACLF. The authors concluded that TIPSS should be offered to these patients. In turn, Lv et al. showed that Chronic Liver Failure Consortium Acute Decompensation Score (CLIF-C ADS) outperforms active bleeding at endoscopy and other prognostic models in predicting 6-week and 1-year mortality.¹⁹ This model may be useful in qualifying patients with Child–Pugh B cirrhosis and acute variceal bleeding for early TIPSS. Finally, in a recent study, it was shown that variceal bleeding has increased mortality compared to non-variceal bleeding only in males.²⁰ Therefore, the authors suggest a particularly close follow-up after endoscopy in this group of patients with cirrhosis. Nevertheless, in our study, we did not confirm the relationship between the sex and the outcome.

Recent studies suggest comparable mortality after variceal and non-variceal bleeding in cirrhotic patients.^{15,16} The type of GIB (variceal compared to non-variceal) seemed not to significantly affect the risk of ACLF in our study, which indirectly confirms the results of recent studies.^{21,22} On the other hand, the risk of ACLF depended on the severity of the bleeding, reflected by 5-day treatment failure and rebleeding rate. The rate of repeat endoscopy within 72 h for rebleeding and 5-day treatment failure (defined as death within 5 days and active bleeding such as spurting or oozing blood or fresh blood contents in the stomach on repeat endoscopy) were significantly higher in the ACLF group compared to the non-ACLF group. The second investigation derived from the PREDICT study showed that GIB with shock is a significant risk factor for AD-ACLF phenotype.⁶ According to the current study protocol, patients were enrolled after hemodynamic stabilization and stopping GIB, which was performed in the ICU. Therefore, we were unable to directly analyze the impact of hemorrhagic shock on the incidence of ACLF.

Limitations

There are several limitations of our study. First, the study was retrospective, and the data obtained were limited to patients' medical records. Second, the number of patients with variceal bleeding was relatively small. Therefore, results regarding the effect of the type of bleeding on ACLF should be interpreted with caution. Third, ACLF was diagnosed in only a few patients on admission to hospital. We are aware that in some of them, the bleeding was a complication of ACLF and not a trigger of ACLF. Based on the available data, we were not able to determine which patients developed ACLF following a hemorrhage prior to hospitalization and in which bleeding was a complication of ACLF. Although the latter situation probably concerned only a few patients with ACLF at admission, this should be considered when interpreting our results. And finally, this is a single-center study with a relatively small number of patients.

Conclusions

In conclusion, in-hospital risk of ACLF in cirrhotic patients hospitalized for acute gastrointestinal hemorrhage is high despite successful bleeding arrest and widespread use of antibiotics. Elevated creatinine levels and MELD score, and the presence of HE on admission are the best predictors of ACLF during hospitalization in these patients. Patients with liver cirrhosis after gastrointestinal hemorrhage are particularly at risk for respiratory failure, followed by kidney and brain failure.


Data availability


The Supplementary data are available at <https://doi.org/10.5281/zenodo.6374308>. The package consists of the following files:


1. Supplementary definitions.
2. Explanations of ICD-10 codes.
3. Fig. S1. Search results of the medical records of patients hospitalized in the department from August 2015 to December 2018.
4. Supplementary Table 1. Verification of assumptions of statistical tests (t-test or Mann–Whitney U test).


ORCID iDs

Paweł Rogalski  <https://orcid.org/0000-0002-1884-2500>


Marta Zaborowska  <https://orcid.org/0000-0002-3879-9722>


Maria Mazur  <https://orcid.org/0000-0001-8982-6033>

Żaneta Jankowska  <https://orcid.org/0000-0001-8531-6159>

Alicja Piszczczyk  <https://orcid.org/0000-0003-2317-3062>

Edyta Mermer  <https://orcid.org/0000-0002-3685-9904>

Andrzej Dąbrowski  <https://orcid.org/0000-0002-5996-394X>

Jarosław Daniluk  <https://orcid.org/0000-0002-0787-1461>

References

1. Jalan R, Gines P, Olson JC, et al. Acute-on-chronic liver failure. *J Hepatol.* 2012;57(6):1336–1348. doi:10.1016/j.jhep.2012.06.026
2. Hernaez R, Kramer JR, Liu Y, et al. Prevalence and short-term mortality of acute-on-chronic liver failure: A national cohort study from the USA. *J Hepatol.* 2019;70(4):639–647. doi:10.1016/j.jhep.2018.12.018
3. Moreau R, Jalan R, Gines P, et al. Acute-on-chronic liver failure is a distinct syndrome that develops in patients with acute decompensation of cirrhosis. *Gastroenterology.* 2013;144(7):1426–1437.e9. doi:10.1053/j.gastro.2013.02.042
4. Zaccherini G, Weiss E, Moreau R. Acute-on-chronic liver failure: Definitions, pathophysiology and principles of treatment. *JHEP Rep.* 2021; 3(1):100176. doi:10.1016/j.jhepr.2020.100176
5. Trebicka J, Fernandez J, Papp M, et al. The PREDICT study uncovers three clinical courses of acutely decompensated cirrhosis that have distinct pathophysiology. *J Hepatol.* 2020;73(4):842–854. doi:10.1016/j.jhep.2020.06.013
6. Trebicka J, Fernandez J, Papp M, et al. PREDICT identifies precipitating events associated with the clinical course of acutely decompensated cirrhosis. *J Hepatol.* 2021;74(5):1097–1108. doi:10.1016/j.jhep.2020.11.019
7. Arroyo V, Moreau R, Jalan R. Acute-on-chronic liver failure. *N Engl J Med.* 2020;382(22):2137–2145. doi:10.1056/NEJMra1914900
8. Clària J, Stauber RE, Coenraad MJ, et al. Systemic inflammation in decompensated cirrhosis: Characterization and role in acute-on-chronic liver failure. *Hepatology.* 2016;64(4):1249–1264. doi:10.1002/hep.28740
9. Trebicka J, Amorós A, Pitarch C, et al. Addressing profiles of systemic inflammation across the different clinical phenotypes of acutely decompensated cirrhosis. *Front Immunol.* 2019;10:476. doi:10.3389/fimmu.2019.00476
10. Jalan R, D'Amico G, Trebicka J, Moreau R, Angeli P, Arroyo V. New clinical and pathophysiological perspectives defining the trajectory of cirrhosis. *J Hepatol.* 2021;75:514–526. doi:10.1016/j.jhep.2021.01.018
11. Heimbach JK, Kulik LM, Finn RS, et al. AASLD guidelines for the treatment of hepatocellular carcinoma. *Hepatology.* 2018;67(1):358–380. doi:10.1002/hep.29086
12. Mallet M, Rudler M, Thabut D. Variceal bleeding in cirrhotic patients. *Gastroenterol Rep (Oxf).* 2017;5(3):185–192. doi:10.1093/gastro/gox024
13. de Franchis R. Expanding consensus in portal hypertension. *J Hepatol.* 2015;63(3):743–752. doi:10.1016/j.jhep.2015.05.022

14. Rogalski P, Rogalska-Płońska M, Wróblewski E, et al. Laboratory evidence for hypercoagulability in cirrhotic patients with history of variceal bleeding. *Thromb Res.* 2019;178:41–46. doi:10.1016/j.thromres.2019.03.021
15. Rogalski P, Rogalska-Płońska M, Wróblewski E, et al. Blood platelet function abnormalities in cirrhotic patients with esophageal varices in relation to the variceal bleeding history. *Scand J Gastroenterol.* 2019;54(3):311–318. doi:10.1080/00365521.2019.1578822
16. Chavez-Tapia NC, Barrientos-Gutierrez T, Tellez-Avila F, et al. Meta-analysis: Antibiotic prophylaxis for cirrhotic patients with upper gastrointestinal bleeding. An updated Cochrane review. *Aliment Pharmacol Ther.* 2011;34(5):509–518. doi:10.1111/j.1365-2036.2011.04746.x
17. Trebicka J, Gu W, Ibáñez-Samaniego L, et al. Rebleeding and mortality risk are increased by ACLF but reduced by pre-emptive TIPS. *J Hepatol.* 2020;73(5):1082–1091. doi:10.1016/j.jhep.2020.04.024
18. Kumar R, Kerbert AJC, Sheikh MF, et al. Determinants of mortality in patients with cirrhosis and uncontrolled variceal bleeding. *J Hepatol.* 2021;74(1):66–79. doi:10.1016/j.jhep.2020.06.010
19. Lv Y, Wang Z, Li K, et al. Risk stratification based on Chronic Liver Failure Consortium Acute Decompensation Score in patients with Child–Pugh B cirrhosis and acute variceal bleeding. *Hepatology.* 2021;73(4):1478–1493. doi:10.1002/hep.31478
20. Erasmus HP, Bektas R, Orland K, et al. Variceal bleeding has increased mortality compared to nonvariceal bleeding only in males. *Eur J Gastroenterol Hepatol.* 2021;33(15):e94–e101. doi:10.1097/MEG.0000000000001964
21. Ardevol A, Ibáñez-Sanz G, Profitos J, et al. Survival of patients with cirrhosis and acute peptic ulcer bleeding compared with variceal bleeding using current first-line therapies. *Hepatology.* 2018;67(4):1458–1471. doi:10.1002/hep.29370
22. Tandon P, Bishay K, Fisher S, et al. Comparison of clinical outcomes between variceal and non-variceal gastrointestinal bleeding in patients with cirrhosis: Outcomes of UGIB in cirrhosis. *J Gastroenterol Hepatol.* 2018;33(10):1773–1779. doi:10.1111/jgh.14147

Impact of moderately reduced renal function on the diagnostic and prognostic value of galectin-3 in patients with exertional dyspnea

Bożena Karolko^{A–F}, Adam Serafin^{A–F}, Monika Przewłocka-Kosmala^{A–F}

Institute of Heart Diseases, Wrocław Medical University, Poland

A – research concept and design; B – collection and/or assembly of data; C – data analysis and interpretation; D – writing the article; E – critical revision of the article; F – final approval of the article

Advances in Clinical and Experimental Medicine, ISSN 1899–5276 (print), ISSN 2451–2680 (online)

Adv Clin Exp Med. 2022;31(8):873–879

Address for correspondence

Monika Przewłocka-Kosmala
E-mail: monika.przewlocka-kosmala@umed.wroc.pl

Funding sources

None declared

Conflict of interest

None declared

Received on February 7, 2022
Reviewed on February 20, 2022
Accepted on March 24, 2022

Published online on April 25, 2022

Cite as

Karolko B, Serafin A, Przewłocka-Kosmala M. Impact of moderately reduced renal function on the diagnostic and prognostic value of galectin-3 in patients with exertional dyspnea. *Adv Clin Exp Med.* 2022;31(8):873–879. doi:10.17219/acem/147665

DOI

10.17219/acem/147665

Copyright

Copyright by Author(s)
This is an article distributed under the terms of the Creative Commons Attribution 3.0 Unported (CC BY 3.0) (<https://creativecommons.org/licenses/by/3.0/>)

Abstract

Background. Blood concentration of galectin-3 (Gal-3) – a biomarker of fibrosis useful in diagnostics and prognostication in heart failure (HF) – is known to be elevated in patients with renal impairment, a condition which often accompanies cardiac insufficiency.

Objectives. To investigate the effect of moderately reduced renal function (estimated glomerular filtration rate (eGFR) 30–60 mL/min/1.73 m²) on the diagnostic and prognostic utility of circulating Gal-3 in patients with HF with preserved ejection fraction (HFpEF).

Materials and methods. Clinical, biochemical and echocardiographic variables were collected at baseline in 154 patients with HFpEF: 101 with normal and 53 with moderately reduced renal function, who were followed up for 48 (24–60) months for HF hospitalization and cardiovascular (CV) death (composite endpoint).

Results. Patients with moderately impaired renal function were characterized by higher age, Meta-Analysis Global Group in Chronic Heart Failure (MAGGIC) risk score, Gal-3, B-type natriuretic peptide (BNP) and New York Heart Association (NYHA) class, lower hemoglobin, and more advanced left ventricular diastolic dysfunction. Older age, female sex and deeper impairment of renal performance were determinants of higher Gal-3 blood concentrations. Lower exercise capacity (lower peak VO₂) was associated with higher Gal-3 level and more pronounced renal impairment. Multivariable regression analysis demonstrated the significance of renal dysfunction as a determinant of lower exercise capacity and revealed a significant interaction between Gal-3 and eGFR with respect to peak VO₂. The addition of Gal-3 to the prognostic models based on clinical data improved their predictive power for the study endpoint. The Kaplan–Meier analysis revealed that the presence of moderately reduced renal function with eGFR 30–60 mL/min/1.73 m² did not enhance the increased risk of adverse outcome associated with Gal-3 above the median.

Conclusions. In patients with HFpEF, the coexistence of moderate renal dysfunction does not deteriorate the prognostic usefulness of circulating Gal-3. However, renal impairment modifies the association between Gal-3 and exercise capacity, which supports the need to adjust for kidney function when interpreting the contribution of Gal-3 to exercise intolerance in this population.

Key words: prognosis, galectin-3, renal dysfunction, heart failure with preserved ejection fraction

Background

Galectin-3 (Gal-3), a member of the beta-galactoside-binding lectin family, is a multifunctional protein secreted by activated macrophages, fibroblasts and vascular cells, and involved in the regulation of pro-inflammatory and profibrotic signaling.¹ The pathophysiological relevance of Gal-3 for the heart has been documented in animal investigations showing the promotion of myocardial fibrosis by exogenous Gal-3,² as well as the regression of fibrotic changes in response to Gal-3 inhibition.³ Given that cardiac fibrosis and inflammation play major roles in the development of heart failure (HF), especially the category with preserved ejection fraction (HFpEF), Gal-3 has emerged as an attractive biomarker in diagnostics and prognostication in this disease entity.⁴

Accumulating evidence from experimental and human studies indicates that Gal-3 can be useful in the diagnostic and prognostic strategies both in the preclinical and clinical phase of HF.^{2,5} Circulating Gal-3 levels have been found to be associated with cardiovascular and all-cause mortality in HF population and general population, with exercise intolerance and treatment effects of angiotensin receptor blockers and statins.^{6–10} However, Gal-3 is not a cardiac-specific marker. Chiefly, decreased renal function has been shown to contribute to Gal-3 overexpression in the blood.¹¹ This interference may provide a confounding effect, decreasing the diagnostic and prognostic usefulness of Gal-3 since renal impairment frequently accompanies HF.¹²

According to the existing evidence, advanced kidney compromise with estimated glomerular filtration rate (eGFR) <30 mL/min/m² is associated with a significant increase in circulating Gal-3 of noncardiac origin.¹³ However, data reporting the impact of the coexistence of a lesser degree of renal insufficiency on the accuracy of Gal-3 as a cardiac marker are scarce.

Objectives

In view of this, we sought to investigate the effect of moderately reduced renal function (eGFR 30–60 mL/min/1.73 m²) on the diagnostic and prognostic utility of circulating Gal-3 in patients with exertional dyspnea categorized as having HFpEF.

Materials and methods

Patient selection

In this study, we enrolled 154 patients who were diagnosed at a tertiary cardiology center between 2012 and 2015 due to exertional dyspnea, and fulfilled the HFpEF criteria in place at the time of recruitment¹⁴: 1) signs of HF classified as New York Heart Association (NYHA) functional class II or III; 2) exercise capacity below normal (<100% of age- and sex-predicted normal ranges for peak

oxygen consumption; 3) preserved left ventricle ejection fraction (>50%); and 4) evidence of the left ventricular diastolic dysfunction (LVDD). The exclusion criteria included: 1) atrial fibrillation or flutter (irregular heart rhythm decreases the accuracy of echocardiographic evaluation); 2) significant ischemic heart disease (defined by the presence of atherosclerotic lesions on coronary angiography or inducible ischemia during exercise testing); 3) moderate or severe valvular heart disease; 4) obesity (body mass index (BMI) >36 kg/m²); 5) anemia (hemoglobin (Hb) <11 g/dL); and 6) suspected or confirmed pulmonary, liver, rheumatic, oncological, skeletal, or kidney (creatinine eGFR < 30 mL/min/1.73 m²) disease. The study cohort was divided into 2 subgroups: with eGFR > 60 mL/min/1.73 m² (n = 101) and with eGFR 30–60 mL/min/1.73 m² (n = 53).

The study protocol comprised medical interview and examination, cardiopulmonary exercise testing, echocardiography, and assessment of blood biomarkers: serum Gal-3 and plasma B-type natriuretic peptide (BNP).

All enrollees provided written informed consent following obtaining full information on the essence of the study. Investigations were approved by the institutional review board (Wrocław Medical University Bioethics Committee approval No. 731/2018) and were conducted in accordance with the Declaration of Helsinki.

Outcome

Enrollees were followed up over a median period of 48 (24–60) months for the composite endpoint of HF hospitalization (defined as hospital admission due to HF worsening requiring intensification of diuretic therapy) or cardiovascular (CV) death. The event rate was verified through systematic contact with patients or their authorized relatives. A standard clinical history was taken, including information about risk factors, etiology and treatment.

Standard equipment (Vivid e9; General Electric Medical Systems, Milwaukee, Wisconsin) with a phased array 2.5-MHz multifrequency transducer was used for echocardiographic imaging. Ultrasound data were saved in the digital format on a secure server and analyzed offline.

Cardiopulmonary exercise testing and blood assays

A symptom-limited exercise testing was performed on a treadmill, according to Bruce protocol, with standard ECG and blood pressure monitoring. Ventilation, oxygen uptake and carbon dioxide production were monitored continuously, and peak oxygen uptake (peak VO₂) was computed as the average oxygen consumption during the last 30 s of exercise. Peripheral venous blood samples were drawn between 8:00 and 9:00 AM after 30 min of rest in the supine position, and subsequently frozen at –70°C. Serum Gal-3 levels were estimated using enzyme-linked immunosorbent assay (ELISA) kits from BioVendor, Inc. (Brno, Czech

Republic). Intra- and inter-assay coefficients of variation were 6.4% and 11.4%, respectively. Serum BNP levels were quantified using commercially available fluorescence immunoassay from Biosite Diagnostics Inc. (San Diego, USA).

Risk stratification

Based on the age, sex, presence of diabetes, and chronic obstructive pulmonary disease (COPD), current smoking status, duration of HF, HF functional class, use of β -blockers and angiotensin converting enzyme inhibitors/angiotensin receptor blockers, systolic blood pressure (SBP), BMI, serum creatinine, and left ventricular ejection fraction, the Meta-Analysis Global Group in Chronic Heart Failure (MAGGIC) risk score was calculated.¹⁵

Statistical analyses

Data are presented as mean \pm standard deviation (SD) for normally distributed variables, as median (interquartile range (IQR)) for skewed variables (Gal-3, BNP), and as counts and percentages for categorical variables. Before being analyzed, the BNP was subjected to logarithmic transformation and Gal-3 to Box–Cox transformation. Between-group comparisons were performed with an unpaired two-sided Student's *t*-test. Associations between variables were evaluated using univariable and stepwise multiple regression analysis. The interaction between Gal-3 and eGFR with respect to prediction of exercise capacity was tested using a general linear model. Nested Cox regression models were built to evaluate the incremental value of BNP, eGFR and Gal-3 for prediction of the composite endpoint. In the 1st analysis, the base model included the MAGGIC risk score, and BNP and Gal-3 were successively added in the next steps. In the 2nd analysis, eGFR and Gal-3 were consecutively added to patient age. The change in overall log-likelihood ratio χ^2 value was used to estimate the increase in predictive power after the addition of subsequent parameter. To evaluate model performance, the Harrell's *C*-statistic was used. Univariable and multivariable Cox proportional hazards models were used to assess the associations of analyzed parameters with the study endpoint. Event-free survival curves were estimated using the Kaplan–Meier method, and differences were assessed with the log-rank test. All calculations were carried out using standard statistical software (STATISTICA v. 13; TIBICO Software Inc., Palo Alto, USA). The level of statistical significance was set at *p*-value <0.05.

Results

Patient characteristics

A total of 154 patients were finally enrolled into the study and divided into 2 subgroups: with moderately reduced renal function (eGFR 30–60 mL/min/1.73 m² (n = 53)) and normal

renal function (eGFR > 60 mL/min/1.73 m² (n = 101)). The demographic and clinical profile of the studied population presented in Table 1 was typical of HFpEF, with the predominance of female sex, hypertension and overweight/obesity. There were significant differences between groups: the subgroup with reduced renal function was characterized by older age, higher MAGGIC risk score and Gal-3 and BNP concentration, lower hemoglobin level, more advanced exertional dyspnea as expressed by NYHA class, and lower exercise capacity as assessed by peak oxygen uptake. Echocardiographic characteristics of study population are presented in Table 1. Patients with reduced renal function demonstrated abnormalities of left ventricle (LV) diastolic parameters: peak early diastolic tissue velocity of the mitral annulus (*e'*) and the ratio of peak early diastolic mitral inflow velocity of the mitral annulus (*E*) to *e'*. There were no significant differences in other demographic, clinical and echocardiographic variables between both subgroups.

Determinants of Gal-3 concentration in HFpEF population

Univariable and multivariable linear regression analysis revealed that older age, female sex and deeper impairment of renal function were significant independent determinants of higher Gal-3 concentration in the studied population (Table 2).

Gal-3 and renal function as determinants of exercise capacity in HFpEF population

Univariable linear regression analysis demonstrated significant associations of Gal-3 and eGFR with exercise capacity expressed by peak VO₂. Multivariable linear regression model revealed the presence of significant interaction between Gal-3 and eGFR with respect to peak VO₂ (Table 3).

Prognostic utility of Gal-3 in the prediction of HF hospitalization and CV death in HFpEF patients

Univariable associations of demographic and clinical predictors of the study composite endpoint (HF hospitalization or CV death) in Cox proportional hazards analysis are presented in Table 4. A higher risk of the adverse outcome significantly correlates with higher Gal-3 and BNP concentration, more advanced age, higher MAGGIC risk score, and more severe renal function impairment.

In the sequential Cox analysis presented in Fig. 1A, the addition of Gal-3 to the model including MAGGIC risk score and BNP improved the predictive power for HF hospitalization or CV death. Analogically, the addition of Gal-3 to the model including patient age and eGFR provided an incremental predictive benefit for the composite study endpoint (Fig. 1B).

Table 1. Demographic, clinical and echocardiographic characteristics of the study population according to renal function

| Variable | eGFR \geq 60 mL/min/1.73 m ² (n = 101) | eGFR < 60 mL/min/1.73 m ² (n = 53) | Test value | p-value |
|------------------------------------|--|--|------------|------------------|
| Age [years] | 63.2 \pm 8.4 | 67.7 \pm 7.5 | 10.2 | 0.002 |
| Men, n (%) | 30 (30) | 12 (23) | 0.87 | 0.35 |
| BMI [kg/m ²] | 29.8 \pm 4.4 | 29.5 \pm 4.3 | 0.13 | 0.72 |
| Diabetes, n (%) | 36 (36) | 20 (38) | 0.07 | 0.80 |
| Hypertension, n (%) | 91 (90) | 51 (96) | 1.82 | 0.18 |
| NYHA class II, n (%) | 81 (80) | 34 (64) | 4.73 | 0.030 |
| NYHA class III, n (%) | 20 (20) | 19 (36) | N/A | |
| Systolic BP [mm Hg] | 127 \pm 14 | 127 \pm 17 | 0.04 | 0.84 |
| Diastolic BP [mm Hg] | 75 \pm 9 | 72 \pm 9 | 3.3 | 0.07 |
| Glucose [mg/dL] | 119 \pm 30 | 118 \pm 33 | 0.01 | 0.93 |
| Hemoglobin [g/dL] | 13.8 \pm 1.1 | 13.4 \pm 0.9 | 6.7 | 0.010 |
| Creatinine [mg/dL] | 0.92 \pm 0.12 | 1.23 \pm 0.25 | 115.7 | <0.001 |
| eGFR [mL/min/1.73 m ²] | 73.3 \pm 12.0 | 50.6 \pm 6.9 | 161.6 | <0.001 |
| Galectin-3 [ng/mL] | 1.07 (0.83–1.82) | 2.04 (1.00–2.46) | 12.4 | <0.001 |
| BNP [pg/mL] | 41 (20–90) | 70 (32–123) | 7.4 | 0.007 |
| peak VO ₂ [mL/min/kg] | 16.3 \pm 4.8 | 13.1 \pm 4.4 | 17.2 | <0.001 |
| MAGGIC risk score | 14.0 \pm 4.9 | 17.7 \pm 4.6 | 19.8 | <0.001 |
| ACEI/ARB, n (%) | 100 (99) | 53 (100) | 0.53 | 0.47 |
| β -blockers, n (%) | 83 (82) | 41 (77) | 0.51 | 0.47 |
| Ca-blockers, n (%) | 42 (42) | 22 (42) | 0.0 | 0.99 |
| Thiazides, n (%) | 52 (51) | 29 (55) | 0.15 | 0.70 |
| Loop diuretics, n (%) | 7 (7) | 8 (15) | 2.63 | 0.10 |
| LVEDD [mm] | 49.4 \pm 4.3 | 48.8 \pm 4.5 | 0.58 | 0.45 |
| LVMI [g/m ^{2.7}] | 53.2 \pm 13.4 | 55.3 \pm 12.5 | 0.88 | 0.35 |
| LAVI [mL/m ²] | 32.8 \pm 8.5 | 33.3 \pm 12.3 | 0.09 | 0.76 |
| EF [%] | 73.3 \pm 8.3 | 73.6 \pm 7.8 | 0.03 | 0.85 |
| E/A | 0.97 \pm 0.40 | 0.94 \pm 0.58 | 0.23 | 0.64 |
| DT [ms] | 233 \pm 52 | 249 \pm 51 | 3.5 | 0.063 |
| e' septal [cm/s] | 6.12 \pm 1.40 | 5.45 \pm 1.24 | 8.6 | 0.003 |
| e' lateral [cm/s] | 8.30 \pm 1.81 | 7.16 \pm 2.14 | 12.0 | <0.001 |
| E/e' | 11.1 \pm 3.2 | 12.7 \pm 4.9 | 5.7 | 0.01 |

Values are presented as mean \pm standard deviation (SD), n (%), or median (interquartile range (IQR)). The p-values in bold indicate the statistical significance of differences. A – late diastolic mitral inflow velocity; ACEI – angiotensin-converting enzyme inhibitor; ARB – angiotensin receptor blocker; BMI – body mass index; BNP – B-type natriuretic peptide; BP – blood pressure; DT – deceleration time of E wave; E – peak early diastolic mitral flow velocity; e' – peak early diastolic mitral annular velocity; EF – ejection fraction; eGFR – estimated glomerular filtration rate; LAVI – left atrial volume index; LVEDD – left ventricular end-diastolic diameter; LVMI – left ventricular mass index; MAGGIC – The Meta-Analysis Global Group in Chronic Heart Failure; NYHA – New York Heart Association; VO₂ – oxygen uptake; N/A – not applicable.

Survival free of the study endpoint is shown in Fig. 2. Patients with Gal-3 concentration above the median (1.30 ng/mL) were at higher risk for HF hospitalization or CV death in comparison with patients with Gal-3 concentration below the median ($p = 0.009$; Fig. 2A). There was a trend towards a higher incidence of the study endpoint in patients with eGFR 30–60 mL/min/1.73 m² compared to patients with normal renal function ($p = 0.066$; Fig. 2B). The increased risk for adverse outcome associated with higher (above the median) Gal-3 was not amplified by the coexistence of moderate renal impairment (eGFR 30–60 mL/min/1.73 m²; $p = 0.60$; Fig. 2C).

Discussion

The major findings of this study are that in patients with exertional dyspnea and possible HFpEF, Gal-3 provides prognostic information that is independent from and incremental to clinical data and BNP, and the value of this marker in predicting adverse outcome is similar between subjects with normal and moderately reduced (eGFR 30–60 mL/min/1.73 m²) renal function. The association between Gal-3 and exercise capacity is modified by renal function; therefore, kidney performance should

Table 2. Univariable and multivariable associations of galectin-3

| Parameter | β | SE | p-value |
|--|---------|------|--------------|
| Univariable linear regression | | | |
| eGFR | -0.20 | 0.08 | 0.01 |
| Age | 0.24 | 0.08 | 0.002 |
| Female sex | 0.20 | 0.08 | 0.01 |
| Multivariable linear regression ($R^2 = 0.13$) | | | |
| eGFR | -0.20 | 0.08 | 0.02 |
| Age | 0.20 | 0.08 | 0.01 |
| Female sex | 0.25 | 0.08 | 0.003 |

The p-values in bold indicate the statistical significance of differences. eGFR – estimated glomerular filtration rate; SE – standard error.

Table 3. Univariable and multivariable associations of exercise capacity (peak oxygen uptake) with galectin-3 and eGFR

| Parameter | β | SE | p-value |
|--|---------|------|------------------|
| Univariable linear regression | | | |
| Galectin-3 | -0.21 | 0.08 | 0.008 |
| eGFR | 0.37 | 0.08 | <0.001 |
| Multivariable linear regression ($R^2 = 0.16$) | | | |
| Galectin-3 | -0.15 | 0.08 | 0.065 |
| eGFR | 0.34 | 0.08 | <0.001 |
| Interaction galectin-3*eGFR | -0.20 | 0.08 | 0.016 |

The p-values in bold indicate the statistical significance of differences. eGFR – estimated glomerular filtration rate; SE – standard error.

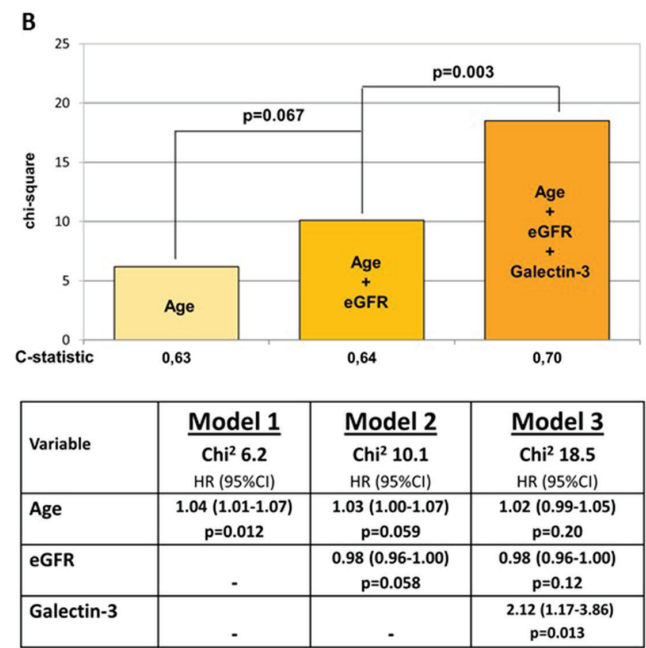
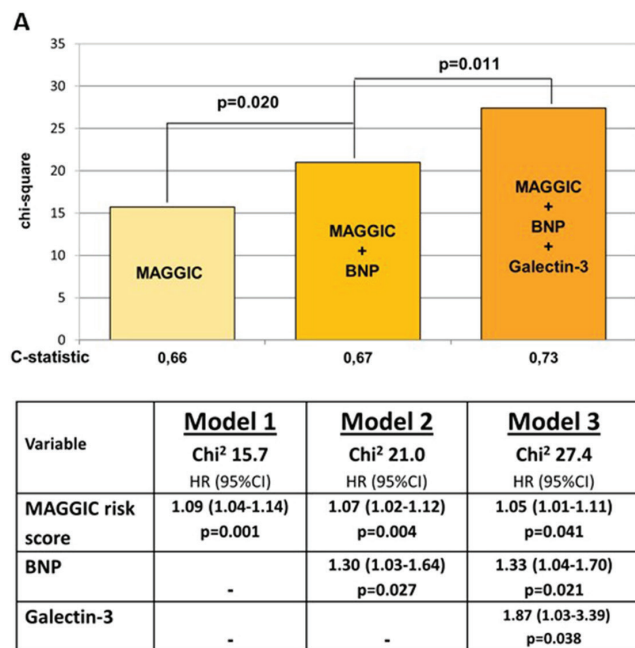


Fig. 1. A. Incremental value of galectin-3 (Gal-3) over Meta-Analysis Global Group in Chronic Heart Failure (MAGGIC) risk score and B-type natriuretic peptide (BNP) for prediction of heart failure (HF) hospitalization or cardiovascular (CV) death; B. Incremental value of Gal-3 over patient age and estimated glomerular filtration rate (eGFR) for prediction of HF hospitalization or CV death

HR – hazard ratio; 95% CI – 95% confidence interval.

Table 4. Demographic and clinical predictors of the study endpoint (HF hospitalization or CV death) in univariable Cox proportional hazards models

| Parameter | HR | 95% CI | p-value |
|-------------------|------|--------------|------------------|
| Galectin-3 | 2.67 | [1.51; 4.73] | <0.001 |
| Age | 1.04 | [1.01; 6.25] | 0.01 |
| eGFR | 0.98 | [0.96; 0.99] | 0.01 |
| MAGGIC risk score | 1.09 | [1.04; 1.14] | <0.001 |
| BNP | 1.46 | [1.18; 1.80] | <0.001 |

eGFR – estimated glomerular filtration rate; MAGGIC – The Meta-Analysis Global Group in Chronic Heart Failure; HF – heart failure; 95% CI – 95% confidence interval; CV – cardiovascular; HR – hazard ratio; BNP – B-type natriuretic peptide. The p-values in bold indicate the statistical significance of differences.

be taken into account when using Gal-3 for defining the pathophysiologic phenotype of exercise intolerance in this population.

Galectin-3 is implicated in the fibrotic and inflammatory processes, and its expression is increased in damaged and remodeling tissues, irrespective of the affected organ and etiology of injury. The contribution to the blood Gal-3 pool can come from a variety of sources of increased fibrosis. Accordingly, the coexistence of multiple organ diseases, one of the most frequent of which is cardiorenal syndrome, constrains the diagnostic ability of circulating Gal-3 to track specific pathologies, as well as specific organ-related outcomes.

The clearance of Gal-3 is thought to be largely hepatic; however, renal excretion of this protein also appears to play a role.^{1,16} Some data indicate that the urinary elimination of Gal-3 is impaired in HF even if the kidney function is normal.¹¹ It has been postulated that the impact of renal disease on HF worsening may in part be mediated

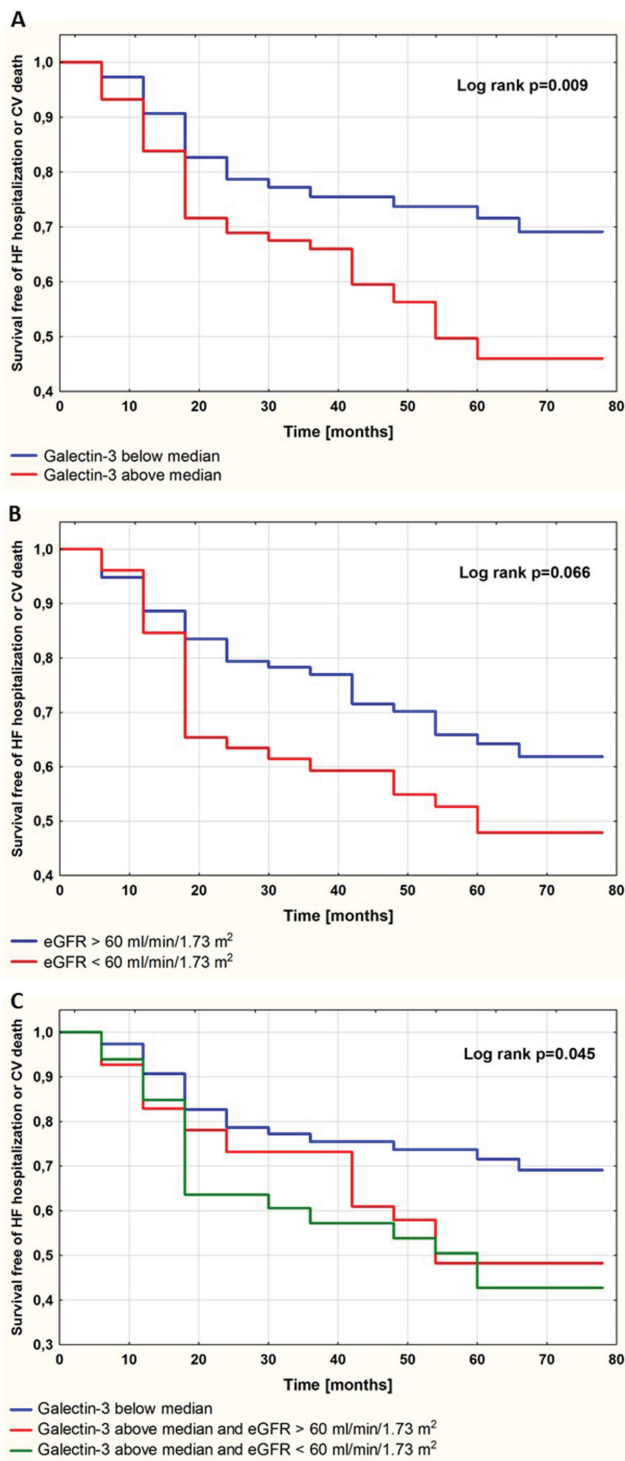


Fig. 2. A. Survival free of heart failure (HF) hospitalization or cardiovascular (CV) death in the study population stratified according to the median galectin-3 (Gal-3) concentration (1.30 ng/mL); B. Survival free of HF hospitalization or CV death in the study population stratified according to estimated glomerular filtration rate (eGFR); C. Survival free of HF hospitalization or CV death in the study population stratified according to Gal-3 concentration and eGFR

Subset (a) – Gal-3 below the median value ($n = 77$); Subset (b) – Gal-3 above the median value and eGFR > 60 mL/min/1.73 m² ($n = 43$); Subset (c) – Gal-3 above the median value and eGFR 30–60 mL/min/1.73 m² ($n = 34$).

Log rank p -values: subset (a) compared to subset (b) $p = 0.046$; subset (a) compared to subset (c) $p = 0.013$; subset (b) compared to subset (c) $p = 0.60$.

by the Gal-3 pathways that aggravate cardiac remodeling and dysfunction.^{17–19}

The prognostic significance of Gal-3 has been demonstrated both in acute and chronic HF across a wide spectrum of kidney function.^{20–23} However, in multivariate adjustments including renal impairment, the significance of independent predictive contribution from Gal-3 was lost in some studies.^{13,24,25} Interestingly, the association of higher Gal-3 with adverse outcome in predialysis cohorts was preserved for all-cause mortality but not for HF progression, which might suggest that in patients with more severe renal dysfunction, the prognostic profile of Gal-3 becomes less cardiac-oriented.²⁶

The commonly believed notion that in the setting of advanced chronic kidney disease (CKD) Gal-3 is not a useful marker of cardiac injury, does not exclude the possibility that a lesser degree of renal impairment can be more neutral in terms of limiting the diagnostic utility of Gal-3 in cardiovascular disease (CVD). The current study demonstrated that in patients with exertional dyspnea satisfying the former criteria for HFpEF and having only a moderately reduced kidney function, circulating Gal-3 is a robust prognostic marker, providing predictive information independent from demographic and clinical data, including renal function status. It is worth emphasizing that the prognostic significance of Gal-3 was corroborated after adjustment for the MAGGIC risk score – a widely approved risk-stratifying tool in HF, including several risk-associated variables.

The incremental value of Gal-3 in predicting adverse outcome was evident despite the association of this biomarker with eGFR, which, however, was weaker than that reported in prior studies including subjects with more advanced renal impairment. Thus, our results support the use of Gal-3 in the prognostic assessment of patients suspected of having HFpEF in the absence of severe kidney dysfunction.

The association between Gal-3 and exercise capacity has a pathophysiological basis. Higher Gal-3 reflects more intense myocardial fibrosis, which is a substrate for increased LV stiffness, leading to LV filling pressure elevation and pulmonary congestion. Abnormal LV filling is exaggerated by exercise, which is clinically evidenced as exertional dyspnea. On the other hand, renal disease can contribute to myocardial dysfunction through a number of mechanisms, including changes in neurohormonal, metabolic and pro-inflammatory milieu, as well as in cardiac loading conditions.

This study revealed that both Gal-3 and eGFR were associated with peak oxygen consumption. The presence of significant interaction between these predictors in multivariable analysis suggests the interplay of fibrosis and renal impairment in their effect on exercise capacity. This finding indicates that the role of Gal-3 in the pathophysiology of exercise intolerance should be considered in the context of kidney function.

Limitations


First, the analysis in this paper was limited to the demographic, clinical and laboratory factors. The contribution of echocardiographic parameters to the discussed aspects was presented in the previous papers analyzing the currently studied population.^{27,28} Second, the clinical profile of this study population, with exclusions of atrial fibrillation, coronary artery disease (CAD) and COPD, may constrain the extrapolation of our findings to other patient cohorts with exercise intolerance, suspected of HFpEF. Third, the enrollment of patients from a single academic center might limit the generalizability of our results.


Conclusions

In patients with exertional dyspnea classified as HFpEF, the coexistence of moderately reduced renal function does not deteriorate the prognostic usefulness of circulating Gal-3. However, renal impairment modifies the association between Gal-3 and exercise capacity, which supports the need to adjust for kidney function when interpreting the contribution of Gal-3 to exercise intolerance in this population.

ORCID iDs

Bożena Karolko  <https://orcid.org/0000-0001-6253-1817>

Adam Serafin  <https://orcid.org/0000-0002-4391-9223>

Monika Przewłocka-Kosmala  <https://orcid.org/0000-0002-4054-6521>

References

- Yang RY, Rabinovich GA, Liu FT. Galectins: Structure, function and therapeutic potential. *Expert Rev Mol Med*. 2008;10:e17. doi:10.1017/S1462399408000719
- Sharma UC, Pokharel S, van Brakel TJ, et al. Galectin-3 marks activated macrophages in failure-prone hypertrophied hearts and contributes to cardiac dysfunction. *Circulation*. 2004;110(19):3121–3128. doi:10.1161/01.CIR.0000147181.65298.4D
- Liu YH, D'Ambrosio M, Liao TD, et al. N-acetyl-seryl-aspartyl-lysyl-proline prevents cardiac remodeling and dysfunction induced by galectin-3, a mammalian adhesion/growth-regulatory lectin. *Am J Physiol Heart Circ Physiol*. 2009;296(2):H404–H412. doi:10.1152/ajpheart.00747.2008
- de Boer RA, Lok DJ, Jaarsma T, et al. Predictive value of plasma galectin-3 levels in heart failure with reduced and preserved ejection fraction. *Ann Med*. 2011;43(1):60–68. doi:10.3109/07853890.2010.538080
- de Boer RA, Voors AA, Muntendam P, van Gilst WH, van Veldhuisen DJ. Galectin-3: A novel mediator of heart failure development and progression. *Eur J Heart Fail*. 2009;11(9):811–817. doi:10.1093/eurjhf/hfp097
- de Boer RA, van Veldhuisen DJ, Gansevoort RT, et al. The fibrosis marker galectin-3 and outcome in the general population. *J Intern Med*. 2012;272(1):55–64. doi:10.1111/j.1365-2796.2011.02476.x
- Felker GM, Fiuzat M, Shaw LK, et al. Galectin-3 in ambulatory patients with heart failure: Results from the HF-ACTION study. *Circ Heart Fail*. 2012;5(1):72–78. doi:10.1161/CIRCHEARTFAILURE.111.963637
- Anand IS, Rector TS, Kuskowski M, Adourian A, Muntendam P, Cohn JN. Baseline and serial measurements of galectin-3 in patients with heart failure: Relationship to prognosis and effect of treatment with valsartan in the Val-HeFT. *Eur J Heart Fail*. 2013;15(5):511–518. doi:10.1093/eurjhf/hfs205
- Gullestad L, Ueland T, Kjekshus J, et al. The predictive value of galectin-3 for mortality and cardiovascular events in the Controlled Rosuvastatin Multinational Trial in Heart Failure (CORONA). *Am Heart J*. 2012;164(6):878–883. doi:10.1016/j.ahj.2012.08.021
- Kosmala W, Przewłocka-Kosmala M, Rojek A, Marwick TH. Comparison of the diastolic stress test with a combined resting echocardiography and biomarker approach to patients with exertional dyspnea: Diagnostic and prognostic implications. *JACC Cardiovasc Imaging*. 2019;12(5):771–780. doi:10.1016/j.jcmg.2017.10.008
- Meijers WC, van der Velde AR, Ruifrok WP, et al. Renal handling of galectin-3 in the general population, chronic heart failure, and hemodialysis. *J Am Heart Assoc*. 2014;3(5):e000962. doi:10.1161/JAHA.114.000962
- Gopal DM, Kommineni M, Ayalon N, et al. Relationship of plasma galectin-3 to renal function in patients with heart failure: Effects of clinical status, pathophysiology of heart failure, and presence or absence of heart failure. *J Am Heart Assoc*. 2012;1(5):e000760. doi:10.1161/JAHA.112.000760
- Zamora E, Lupón J, de Antonio M, et al. Renal function largely influences galectin-3 prognostic value in heart failure. *Int J Cardiol*. 2014;177(1):171–177. doi:10.1016/j.ijcard.2014.09.011
- Paulus WJ, Tschöpe C, Sanderson JE, et al. How to diagnose diastolic heart failure: A consensus statement on the diagnosis of heart failure with normal left ventricular ejection fraction by the Heart Failure and Echocardiography Associations of the European Society of Cardiology. *Eur Heart J*. 2007;28(20):2539–2550. doi:10.1093/eurheartj/ehm037
- Rich JD, Burns J, Freed BH, Maurer MS, Burkhoff D, Shah SJ. Meta-Analysis Global Group in Chronic (MAGGIC) Heart Failure Risk Score: Validation of a simple tool for the prediction of morbidity and mortality in heart failure with preserved ejection fraction. *J Am Heart Assoc*. 2018;7(20):e009594. doi:10.1161/JAHA.118.009594
- Desmedt V, Desmedt S, Delanghe JR, Speeckaert R, Speeckaert MM. Galectin-3 in renal pathology: More than just an innocent bystander. *Am J Nephrol*. 2016;43(5):305–317. doi:10.1159/000446376
- Bansal N, Zelnick L, Go A, et al. Cardiac biomarkers and risk of incident heart failure in chronic kidney disease: The CRIC (Chronic Renal Insufficiency Cohort) study. *J Am Heart Assoc*. 2019;8(21):e012336. doi:10.1161/JAHA.119.012336
- Prud'homme M, Coutrot M, Michel T, et al. Acute kidney injury induces remote cardiac damage and dysfunction through the galectin-3 pathway. *JACC Basic Transl Sci*. 2019;4(6):717–732. doi:10.1016/j.jacbt.2019.06.005
- Mueller T, Leitner I, Egger M, Haltmayer M, Dieplinger B. Association of the biomarkers soluble ST2, Galectin-3 and growth-differentiation factor-15 with heart failure and other non-cardiac diseases. *Clin Chim Acta*. 2015;445:155–160. doi:10.1016/j.cca.2015.03.033
- van Kimmenade RR, Januzzi JL, Ellinor PT, et al. Utility of aminoterminal pro-brain natriuretic peptide, galectin-3, and apelin for the evaluation of patients with acute heart failure. *J Am Coll Cardiol*. 2006;48(6):1217–1224. doi:10.1016/j.jacc.2006.03.061
- Shah RV, Chen-Tournoux AA, Picard MH, van Kimmenade RR, Januzzi JL. Galectin-3, cardiac structure and function, and long-term mortality in patients with acutely decompensated heart failure. *Eur J Heart Fail*. 2010;12(8):826–832. doi:10.1093/eurjhf/hfq091
- Fermann GJ, Lindsell CJ, Storrow AB, et al. Galectin 3 complements BNP in risk stratification in acute heart failure. *Biomarkers*. 2012;17(8):706–713. doi:10.3109/1354750X.2012.719037
- Tang WH, Shrestha K, Shao Z, et al. Usefulness of plasma galectin-3 levels in systolic heart failure to predict renal insufficiency and survival. *Am J Cardiol*. 2011;108(3):385–390. doi:10.1016/j.amjcard.2011.03.056
- Drechsler C, Delgado G, Wanner C, et al. Galectin-3, renal function, and clinical outcomes: Results from the LURIC and 4D studies. *J Am Soc Nephrol*. 2015;26(9):2213–2221. doi:10.1681/ASN.2014010093
- Zhang R, Zhang Y, An T, et al. Prognostic value of sST2 and galectin-3 for death relative to renal function in patients hospitalized for heart failure. *Biomark Med*. 2015;9(5):433–441. doi:10.2217/bmm.15.12
- Tuegel C, Katz R, Alam M, et al. GDF-15, galectin 3, soluble ST2, and risk of mortality and cardiovascular events in CKD. *Am J Kidney Dis*. 2018;72(4):519–528. doi:10.1053/j.ajkd.2018.03.025
- Jasic-Szpak E, Marwick TH, Donal E, et al. Prediction of atrial fibrillation in HFpEF: Incremental value of left atrial strain. *JACC Cardiovasc Imaging*. 2021;14(1):131–144. doi:10.1016/j.jcmg.2020.07.040
- Goździk A, Marwick TH, Przewłocka-Kosmala M, Jankowska EA, Ponikowski P, Kosmala W. Comparison of left ventricular longitudinal systolic function parameters in the prediction of adverse outcome in heart failure with preserved ejection fraction. *ESC Heart Fail*. 2021;8(2):1531–1540. doi:10.1002/ehf2.13247

mGluR5 promotes the progression of multiple myeloma in vitro via Ras–MAPK signaling pathway

Wei Kou^{A,E,F}, Haibin Huang^{B–D}, Shuangwu Dai^{B–D}, Xinmei Tan^{B–E}, Qi Chen^{B–E}, Renwei Huang^{A,C–F}, Hequn Zou^{A,C,E,F}

Third Affiliated Hospital of Southern Medical University, Guangzhou, China

A – research concept and design; B – collection and/or assembly of data; C – data analysis and interpretation; D – writing the article; E – critical revision of the article; F – final approval of the article

Advances in Clinical and Experimental Medicine, ISSN 1899–5276 (print), ISSN 2451–2680 (online)

Adv Clin Exp Med. 2022;31(8):881–888

Address for correspondence

Wei Kou
E-mail: vh56982@126.com

Funding sources

None declared

Conflict of interest

None declared

Received on June 5, 2020

Reviewed on July 2, 2020

Accepted on October 7, 2020

Published online on April 8, 2022

Abstract

Background. Multiple myeloma (MM) is a malignant plasma cancer which remains difficult to be cured. Recently, numerous research studies have appeared, exploring MM from molecular level. However, there is no study about the impact of metabotropic glutamate receptors (mGluRs), especially *mGluR5*, on MM progression. Thus, the present research was dedicated to the exploration of the influence of mGluR5 on MM.

Objectives. In this research, we used quantitative real-time polymerase chain reaction (qRT-PCR) to check the gene expression in MM, western blot assay to check the protein expression of the gene, MTT assay to quantify the cell viability, and flow cytometry (FCM) apoptosis method to evaluate cell apoptosis in order to acquire the results. The purpose was to assess the role of *mGluR5* in MM cells.

Materials and methods. The qRT-PCR was used and it was found that *mGluR5* was overexpressed in MM cell lines and MM tissues compared to normal ones. To better observe the function of *mGluR5* in MM, cell viability and apoptosis were checked using MTT and FCM apoptosis assays after the treatment with agonists and antagonists.

Results. Agonist-induced *mGluR5* upregulation could promote MM cell viability and inhibit apoptosis. The same results were obtained through MTT and FCM apoptosis assays after upregulation and down-regulation of *mGluR5* by transfection. To further investigate the inner mechanism, the effect of *mGluR5* on Ras–MAPK pathway was checked using western blot. It was found that the upregulation of *mGluR5* could activate the Ras–MAPK pathway.

Conclusions. The *mGluR5* might be involved in promoting cell proliferation and inhibiting cell apoptosis in MM. It can be an essential biomarker in the screening for MM and a potential part of future MM therapies.

Key words: apoptosis, multiple myeloma, viability, *mGluR5*

Cite as

Kou W, Huang H, Dai S, et al. *mGluR5* promotes the progression of multiple myeloma in vitro via Ras–MAPK signaling pathway. *Adv Clin Exp Med.* 2022;31(8):881–888. doi:10.17219/acem/130445

DOI

10.17219/acem/130445

Copyright

Copyright by Author(s)

This is an article distributed under the terms of the Creative Commons Attribution 3.0 Unported (CC BY 3.0) (<https://creativecommons.org/licenses/by/3.0/>)

Background

Multiple myeloma (MM) is recognized as plasma cell myeloma, myelomatosis or Kahler's disease.¹ It is an age-related plasma cell cancer and a clonal plasma cell malignancy that is responsible for approx. 10% of hematologic malignancies.² The latest drug discoveries could lead to greatly improved survival percentages.³ Even though previous research on therapies such as immunomodulatory drugs (IMiDs) and proteasome inhibitors have benefited the MM patients, the development mechanism of this disease still remains to be explored.^{4,5} Until now, the frequently discussed genes in MM include *KRAS*, *NRAS*, *TP53*, *BRAF*, and *CCND1*.⁶ It has been widely reported that the mutations in *KRAS* and *NRAS* could regulate the cell apoptosis of MM cells.^{6,7} The *TP53*, a classic tumor suppressor, is also correlated with cellular apoptosis in MM.⁸

Metabotropic glutamate receptors (mGluRs), as G-protein coupling receptors, have been extensively studied in correlation with cell survival and death, and Group I consists of *mGluR1* and *mGluR5* subtypes (*mGluR1/5*), which are coupled to $G\alpha_{q/11}$ proteins.⁹ Both *mGluR1* and *mGluR5* have been reported to be expressed in a variety of tumors, including lung cancer¹⁰ and osteosarcoma,¹¹ among others. It has been confirmed that *mGluR5* is involved in the osteosarcoma cell proliferation and its inhibition reduces cell proliferation.¹¹ Similarly, *mGluR5* antagonist was found to suppress cell proliferation in laryngeal cancer.¹² Apart from that, *mGluR5* was also discovered to be expressed in MM.

However, there has been no further research on MM regarding *mGluR5*. Oncomine (<https://www.oncomine.org>) online analysis showed that *mGluR5* ranked the top 10% of the significantly upregulated genes in MM tissues compared to normal ones, suggesting that *mGluR5* might play an oncogenic part in MM. Therefore, we hypothesized that *mGluR5* might be involved in the occurrence and progression of MM and tried to explore whether *mGluR5* regulates the cell apoptosis and proliferation and also the functional mechanism beneath MM.

Objectives

The aim of this study was to investigate the role of *mGluR5* in MM and also explore its regulatory mechanism.

Materials and methods

Cell culture

The MM cell lines (MM1S, OPM-2, NCI-H929, U266, and RPMI-8226) and normal human umbilical vein endothelial cells (HUVECs) were bought from the American Type Cell Culture (ATCC; Manassas, USA). The MM1S,

OPM-2, NCI-H929, U266, and RPMI-8226 are different B lymphocytes derived from MM patients. The cells were cultured in RPMI-1640 medium (Thermo Fisher Scientific, Waltham, USA) supplemented with 10% fetal bovine serum (FBS; Invitrogen, Shanghai, China) and 1% penicillin/streptomycin at 37°C in 5% CO₂.

qRT-PCR

Total RNA was extracted from cells using Triazole reagent (Thermo Fisher Scientific). The cDNA was reversely transcribed as a template. A Roche LC480 real-time polymerase chain reaction (RT-PCR) machine and a SYBR Green kit (both from Qiagen, Düsseldorf, Germany) were utilized to perform the quantitative RT-PCR (qRT-PCR) analysis. A total of 10 µL of the SYBR Green PCR master mix, 50 ng cDNA and 250 nM of each primer were mixed and diluted to a total volume of 20 µL. Each group was analyzed in triplicate and the process was repeated 3 times. The conditions for thermal cycling were as follows: 10 min at 95°C, followed by 40 cycles of 95°C for 15 s and 60°C for 60 s. The 2^{-ΔΔC_q} method was used. Primer sequences were as follows: *mGluR5*: forward, 5'-TGAGGGTTGTGCCTTCAGAT-3', reverse, 5'-AAGAGTGGGCGATGCAAATC-3'. The *GAPDH* was used as an internal control and its primer sequences were as follows, forward, 5'-GTCGGAGTCAACGGATTTGG-3', reverse, 5'-TGACGGTGCCATGGAATTTG-3'.

Cell treatment

After qRT-PCR detected the differential expression of *mGluR5* in the 4 MM cell lines, we selected the cell line with the highest *mGluR5* expression to knock down the gene expression through its antagonist or inhibitor (OPM2) and the cell line with the lowest *mGluR5* expression (MM1S) to upregulate the expression of *mGluR5* by treating it with its agonist or oe-*mGluR5*. Therefore, *mGluR5* siRNA plasmid, lentivirus plasmid and respective empty vectors (Santa Cruz Biotechnology, Santa Cruz, USA) were used to regulate the expression levels of *mGluR5* in MM1S and OPM2 cells. The MM1S cells were treated with 50 nmol/L agonist (S)-3,5-dihydroxyphenylglycine (DHPG) (Santa Cruz Biotechnology), with the group treated with dimethyl sulfoxide (DMSO, 10 ng/mL; Santa Cruz Biotechnology) as a positive control. The OPM2 cells were treated with *mGluR5* antagonist 1 (2-methyl-6-(phenylethynyl)-pyridine – MPEP; 50 nmol/L; Santa Cruz Biotechnology) and the other group of OPM2 cells – with *mGluR5* antagonist 2 (3-[(2-methyl-1,3-thiazol-4-yl) ethynyl]pyridine – MTEP, 50 nmol/L, ab 144307; Abcam, Cambridge, UK), with the DMSO-treated (10 ng/mL) group as a positive control.

Western blot assay

The separation of protein was conducted with ProteoJET Mammalian Cell Lysis Reagent (Thermo Fisher Scientific).

This was completed step by step according to the manufacturer's guidelines. Then, the centrifugation (15 min, 4°C) was performed. The proteins were denatured and forced to undergo sodium dodecyl sulfate-polyacrylamide gel electrophoresis (SDS-PAGE). The *mGluR5* primary antibodies – Rabbit Anti-Metabotropic Glutamate Receptor 5 antibodies (ab27190, 1:2000) were purchased from Abcam. The antibodies related to the rest proteins were also bought from Abcam: RAS primary antibody – Rabbit Anti-Ras antibody (ab69747, 1.0 µg/mL); Raf1 primary antibody – Rabbit Anti-Raf1 antibody (ab230850, 1:1000); Rabbit Anti-beta Actin antibody (ab8227, 1:2000); and secondary antibody Goat Anti-Rabbit IgG H&L (HRP) (ab205718, 1:2000). The resulting bands (RAS, Raf1 and b-actin) were analyzed with electrochemiluminescence (ECL) (Thermo Fisher Scientific) and densitometry analysis using ImageJ software (Bharti Airtel Ltd., New Delhi, India).

MTT assay

The MTT assay was utilized to evaluate the cell viability. Shortly thereafter, MM1S and OPM2 cells were placed in 96-well plates and treated with actinomycin for 0 h, 2 h, 4 h, and 8 h; then, 20 µL of MTT reagent (5 mg/mL; Abcam) was applied to each plate, after which they were incubated for 3–4 h, and the absorbance was measured at 495 nm using a microplate reader (Thermo Fisher Scientific).

Flow cytometry method for apoptosis assay

The cell apoptosis was evaluated with the flow cytometry (FCM) method. Annexin V PE and 7AAD (eBioscience, San Diego, USA) were utilized to stain cells in accordance with the instructions of the manufacturers. The percentages of apoptotic cells (annexin V PE+/7AAD–) were evaluated using Cell Quest software in a FACScan cytometer (Becton Dickinson Bioscience, Franklin Lakes, USA).

Statistical analyses

The Graphpad Prism v. 8.2 (GraphPad Software, San Diego, USA) was applied for statistical analysis. The Kruskal–Wallis test (K–W) followed by Dunn's post hoc and Kolmogorov–Smirnov test (K–S) were applied in the statistical analysis. The experiments were repeated 3 times independently.

Results

mGluR5 is upregulated in MM cell lines

The *mGluR5* expression in MM cells lines MM1S, OPM2, U266, NCI-H929, and RPMI-8226 and normal cell line HUVECs was measured using qRT-PCR (Fig. 1A). The results

revealed that the *mGluR5* expression was higher in MM cells compared to the normal cells. Among the MM cell lines, *mGluR5* expression in MM1S cells was the highest and in OPM2 was the lowest, though still higher than in HUVECs. Therefore, we selected MM1S cell line for *mGluR5* downregulation and OPM2 for upregulation in the following assays. The MM1S cells treated with *mGluR5* agonist DHPG, and OPM2 cells treated with *mGluR5* antagonist MPEP and MTEP were measured using qRT-PCR with the DMSO groups as controls in both cell lines. The *mGluR5* was increased in DHPG agonist group compared to the DMSO group of the MM1S, while *mGluR5* had low expression in both the MPEP and MTEP antagonist groups (Fig. 1B,C). Furthermore, we measured the relative protein levels of *mGluR5* in all the groups of both cell lines. The results showed that *mGluR5* was downregulated in the MPEP and MTEP, and upregulated in the DHPG compared to the DMSO positive controls, which was consistent with the qRT-PCR findings (Fig. 1D,E).

Agonist-induced upregulation of *mGluR5* promotes cell viability in MM cells

The MTT assay revealed that the DHPG group had higher viability than the DMSO group in MM1S cells (Fig. 2A), while the MPEP and MTEP groups had lower cell viability than the control group in OPM2 cells (Fig. 2B) due to the regulation of the *mGluR5* expression.

Agonist-induced *mGluR5* upregulation inhibited apoptosis in MM cells

The cell apoptosis was evaluated in the groups of both MM1S and OPM2 cell lines using FCM apoptosis assays. The apoptosis rates in the *mGluR5* agonist group were lower than those of the control group in MM1S cells (Fig. 3A). Higher apoptosis was found in the groups of MTEP and MPEP in comparison with the DMSO control group (Fig. 3B). The results pointed out that the agonist-induced upregulation of *mGluR5* could decrease the cell apoptosis, while the antagonist-induced downregulation of *mGluR5* could elevate the cell apoptosis in MM cells.

Transfection-induced upregulation of *mGluR5* promotes cell viability and curbs cell apoptosis of MM cells

After MM1S cells were transfected with oe-*mGluR5*, oe-NC and OPM2, the cells were transfected with si-*mGluR5* and si-NC, and qRT-PCR was used to confirm the regulation of *mGluR5* expression in different groups. It was verified that the oe-*mGluR5* group had a high expression of *mGluR5*, while the si-*mGluR5* group had a lower *mGluR5* expression compared to their control groups (Fig. 4A). The MTT assay revealed that the oe-*mGluR5* induced an increase in cell viability, while si-*mGluR5*

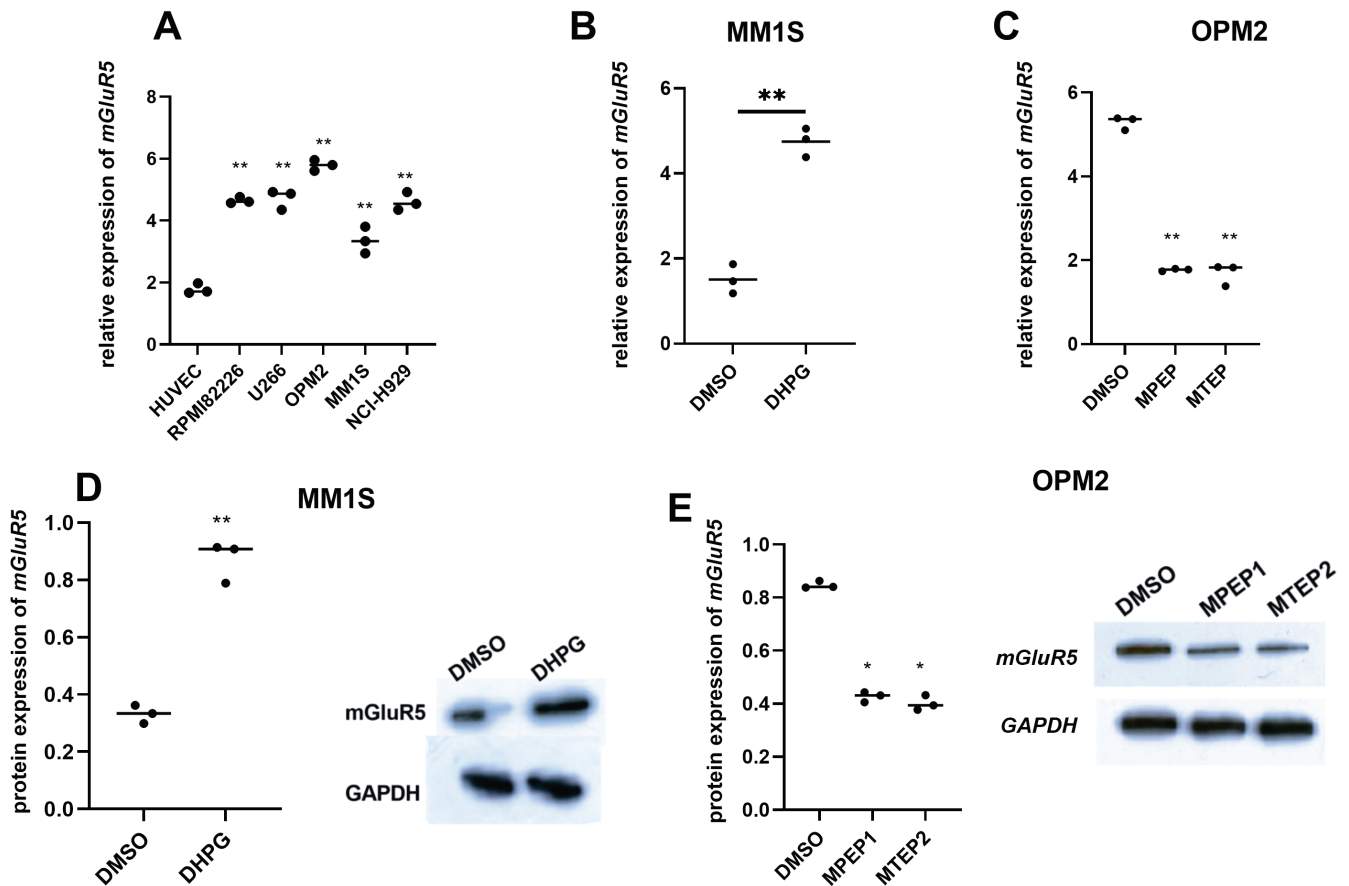


Fig. 1. *mGluR5* had higher expression in multiple myeloma (MM) cell lines. A. Quantitative real-time polymerase chain reaction (qRT-PCR) was applied to evaluate the *mGluR5* expression in MM cell lines and MM1S, OPM-2, U266, NCI-H929, and RPMI-8226, and normal cell line CD143; B,D. MM1S cell line was treated with dimethyl sulfoxide (DMSO) as a control group and 3,5-dihydroxyphenylglycine (DHPG) as an agonist group. The qRT-PCR was used to measure *mGluR5* RNA expression in each group in MM1S cell line. Western blot was used to measure *mGluR5* protein expression in each group in MM1S cell line; C,E. OPM2 cell line was treated with DMSO as a control group, 2-methyl-6-(phenylethynyl)-pyridine (MPEP) or 3-[(2-methyl-1,3- thiazol-4-yl) ethynyl]pyridine (MTEP) as antagonist groups. The qRT-PCR was used to measure *mGluR5* RNA expression in each group in the MM1S cell line. Western blot was used for *mGluR5* protein expression in each group in MM1S cell line. Each assay was performed thrice independently. Kruskal–Wallis test (K–W) with Dunn’s post hoc test and Kolmogorov–Smirnov test (K–S) were applied in the statistical analysis (Fig. 1A. human umbilical vein endothelial cells (HUVECs) compared to RPMI82226, $p = 0.0197$; HUVECs compared to U266, $p = 0.0324$; HUVECs compared to OPM2, $p = 0.0029$; HUVECs compared to MM1S, $p = 0.0452$; HUVECs compared to NCI-H929, $p = 0.0298$; K–W, Dunn’s post hoc. Fig. 1B. $p = 0.0237$, K–S; Fig. 1C. DMSO compared to MPEP, $p = 0.0376$; DMSO compared to MTEP, $p = 0.0425$; K–W, Dunn’s post hoc; Fig. 1D. $p = 0.0198$, K–S; Fig. 1E. DMSO compared to MPEP1. $p = 0.0487$; DMSO compared to MTEP2, $p = 0.0341$; K–W, Dunn’s post hoc)

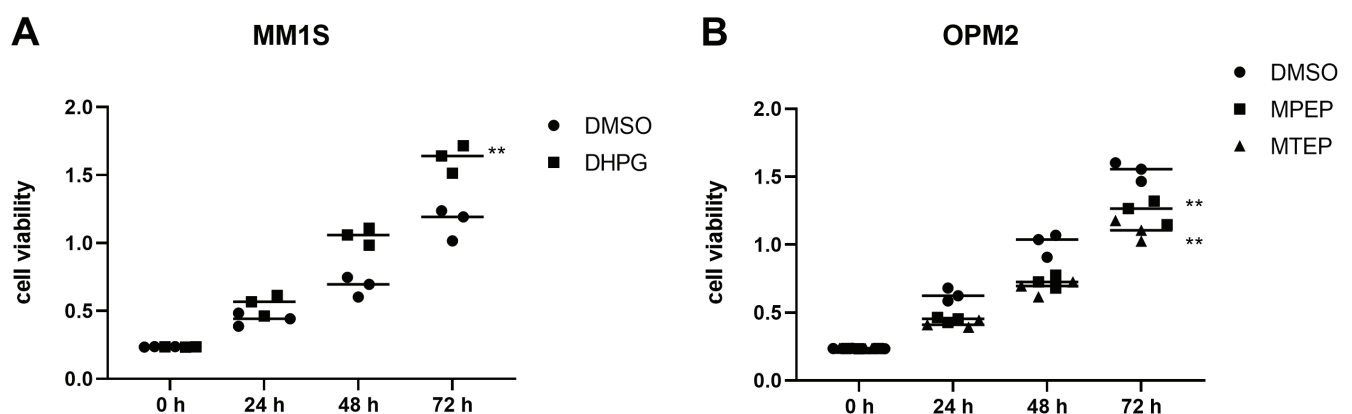


Fig. 2. Agonist-induced *mGluR5* upregulation promoted cell viability in multiple myeloma (MM) cells. A,B. The MTT assay measured the cell viability situation when MM1S cell line was treated with dimethyl sulfoxide (DMSO) as a control group and 3,5-dihydroxyphenylglycine (DHPG) as an agonist group, and OPM2 cell line was treated with DMSO as control group, with 2-methyl-6-(phenylethynyl)-pyridine (MPEP) or 3-[(2-methyl-1,3- thiazol-4-yl) ethynyl]pyridine (MTEP) as antagonist groups. Each assay was performed thrice independently. Kruskal–Wallis test (K–W) with Dunn’s post hoc test and Kolmogorov–Smirnov test (K–S) were applied in the statistical analysis (Fig. 2A. $p = 0.0032$, K–S; Fig. 2B. DMSO compared to MPEP, $p = 0.0356$; DMSO compared to MTEP, $p = 0.0225$; K–W, Dunn’s post hoc)

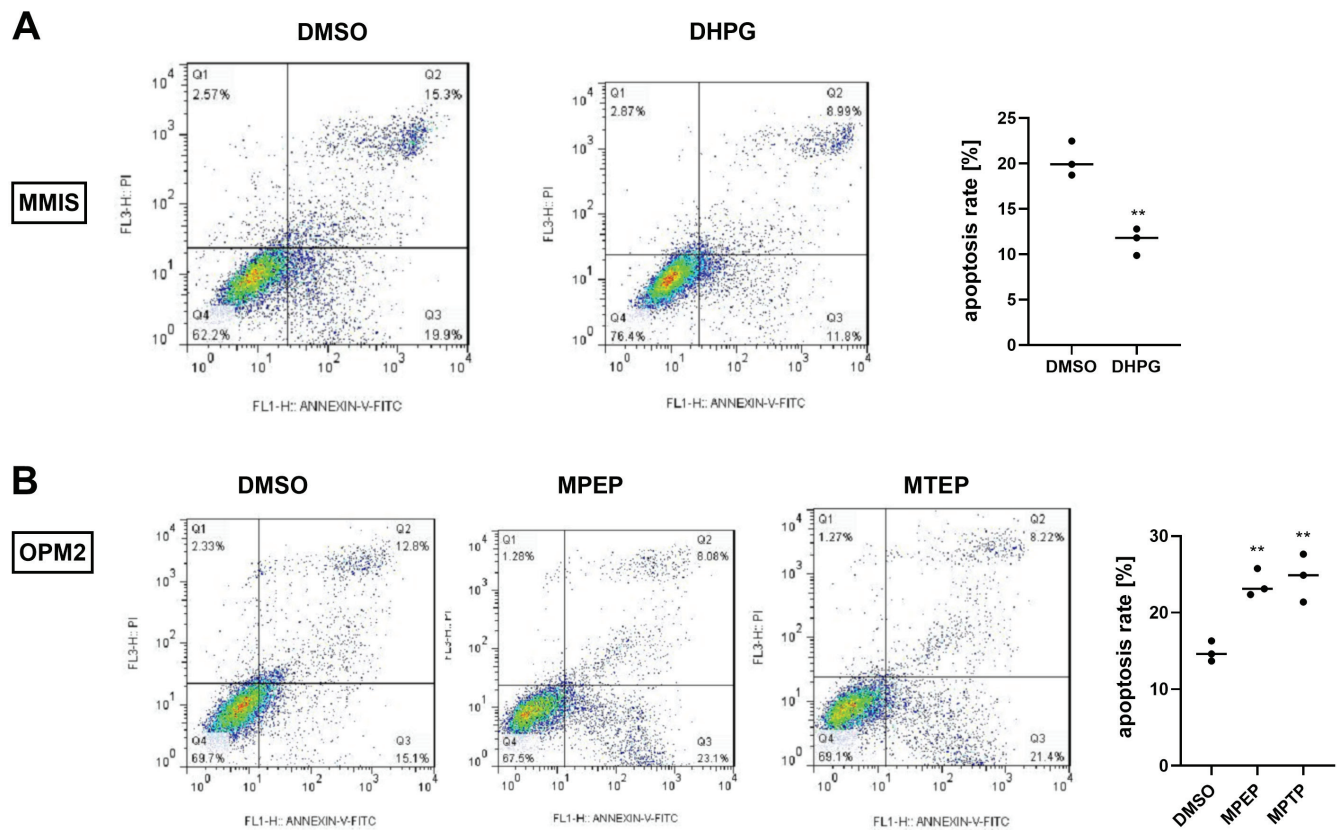


Fig. 3. Agonist-induced *mGluR5* upregulation inhibited apoptosis in multiple myeloma (MM) cells. A,B. Flow cytometry (FCM) apoptosis assays measured the cell apoptosis changes when MM1S cell line was treated with dimethyl sulfoxide (DMSO) as a control group and 3,5-dihydroxyphenylglycine (DHPG) as an agonist group, and OPM2 cell line was treated with DMSO as a control group, with 2-methyl-6-(phenylethynyl)-pyridine (MPEP) or 3-[[2-methyl-1,3-thiazol-4-yl)ethynyl]pyridine (MTEP) as antagonist groups. Each assay was performed thrice independently. Kruskal–Wallis test (K–W) with Dunn’s post hoc test and Kolmogorov–Smirnov test (K–S) were applied in the statistical analysis (Fig. 3A. $p = 0.0269$, K–S; Fig. 3B. DMSO compared to MPEP, $p = 0.0274$; DMSO compared to MTEP, $p = 0.0225$; K–W, Dunn’s post hoc)

lowered cell viability compared with the control groups (Fig. 4B). On the other hand, FCM apoptosis assays found that the oe-*mGluR5* group displayed lower cell apoptosis rate, while the si-*mGluR5* group presented higher cell apoptosis in MM cell lines compared to their control groups (Fig. 4C,D). The MTT assay revealed that the oe-*mGluR5* induced an increase in cell viability, while si-*mGluR5* lowered cell viability compared with the control groups (Fig. 4B).

mGluR5 upregulation activates the Ras signaling pathway in MM cells

Western blot assays revealed that in the oe-*mGluR5* group, the protein expression of *mGluR5* was upregulated in comparison to the oe-NC, while in the si-*mGluR5* group, the *mGluR5* protein expression was downregulated (Fig. 5A,D). The investigation into the correlation between *mGluR5* and Quantitative real-time polymerase chain reaction (qRT-PCR) signaling was carried out in MM cells. The protein levels of Ras, p-Raf1 and Raf1 were measured using western blot. The inhibition of *mGluR5* in MM1S cells showed decreased protein levels of Ras and phosphorylated Raf1, and the upregulation of *mGluR5* in OPM2 cells had an opposite effect

on the protein levels of the signaling pathway (Fig. 5B–D). These data indicated that the upregulation of *mGluR5* in MM cells could activate the Ras–MAPK pathway by promoting Ras and the phosphorylation of Raf1 in MM cells (Fig. 5B–D).

Discussion

Previous studies have demonstrated that *mGluR5* plays different roles in various human diseases. Studies verified that *mGluR5* was upregulated in human tongue cancer and its overexpression promoted cell invasion, migration and adhesion.¹³ As displayed by Oncomine online tool, *mGluR5* is aberrantly upregulated in MM compared to normal tissues. Therefore, we presumed that *mGluR5* might serve as an oncogenic gene in MM, similarly to its role in tongue cancer and prostate cancer.¹⁴ Yet, there have been few research studies concerning the impact of *mGluR5* on MM. Therefore, our study was dedicated to explore how *mGluR5* regulated the cell apoptosis and proliferation of the MM and the possible mechanisms beneath. Firstly, through qRT-PCR we confirmed the expression of *mGluR5* in various cell lines of MM and the control cell line HUVEC, and we discovered that *mGluR5* was upregulated in MM

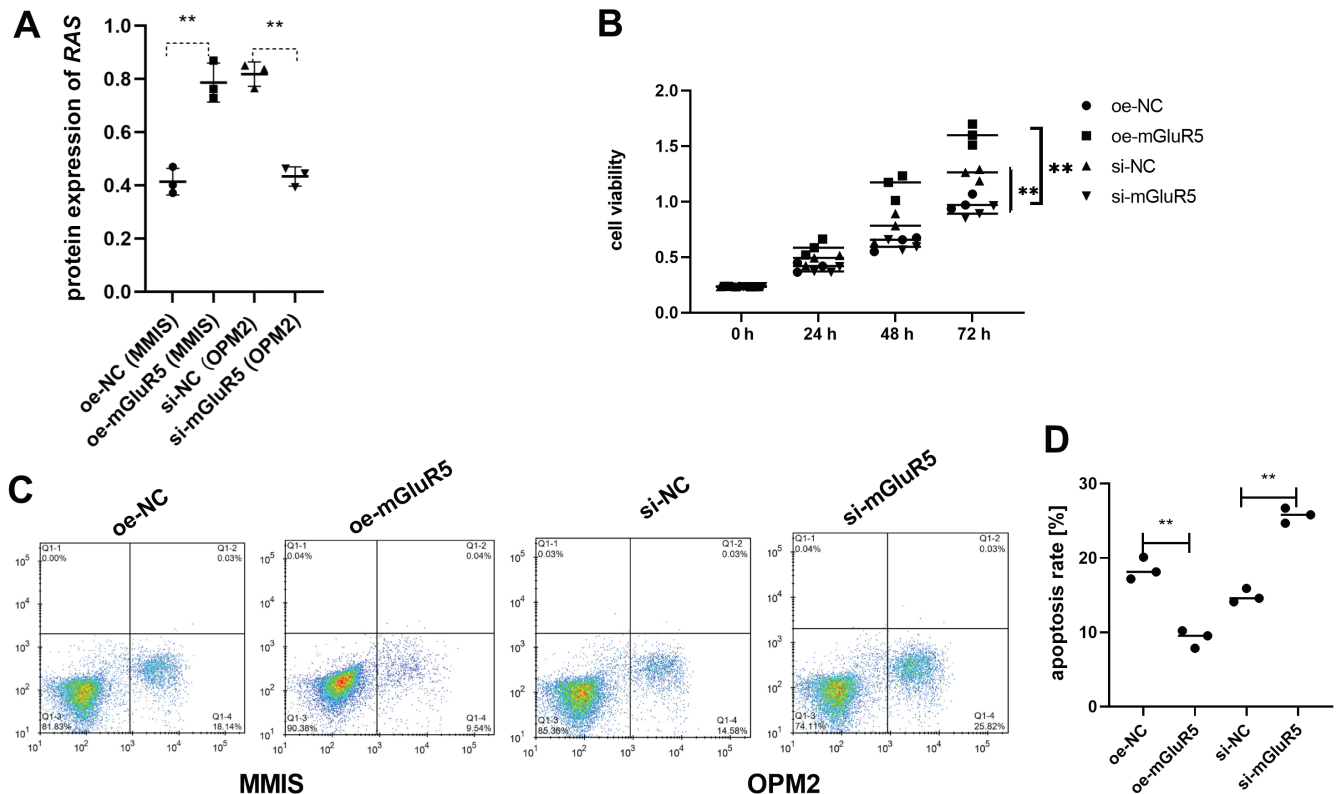


Fig. 4. Transfection-induced upregulation of *mGluR5* promoted cell viability and inhibited cell death in multiple myeloma (MM) cells. MM1S cell line was transfected with si-NC or si-mGluR5 plasmids while OPM2 cell line was selected to knock down by transfection with oe-NC and oe-mGluR5 plasmids. **A.** Quantitative real-time polymerase chain reaction (qRT-PCR) was performed to evaluate the relative *mGluR5* mRNA expression among all the groups in both cell lines; **B.** Cell viability was measured with MTT method; **C, D.** Flow cytometry (FCM) apoptosis assay was used to measure cell apoptosis. Each assay was performed thrice independently. Kruskal–Wallis test (K–W) with Dunn’s post hoc test and Kolmogorov–Smirnov test (K–S) were applied in the statistical analysis (Fig. 4A. oe-NC (MM1S) compared to oe-mGluR5 (MM1S), $p = 0.0163$; si-NC (OPM2) compared to si-mGluR5 (OPM2), $p = 0.0319$; K–W, Dunn’s post hoc; Fig. 4B. oe-NC (MM1S) compared to oe-mGluR5 (MM1S), $p = 0.0094$; si-NC (OPM2) compared to si-mGluR5 (OPM2), $p = 0.0308$; K–W, Dunn’s post hoc. Fig. 4C; oe-NC (MM1S) compared to oe-mGluR5 (MM1S), $p = 0.0268$; si-NC (OPM2) compared to si-mGluR5 (OPM2), $p = 0.0325$; K–W, Dunn’s post hoc).

cells compared to the HUVECs, which was consistent with OncoPrint analysis and also suggested that *mGluR5* might be an oncogene in MM. Among all the MM cell lines, OPM2 presented the highest expression of *mGluR5*, while MM1S the lowest. Furthermore, we decided to differentiate the expression of *mGluR5* in MM cell lines, selecting OPM2 and MM1S cell lines. To inhibit or stimulate the *mGluR5* expression in cells, transfection with si-mGluR5 and oe-mGluR5, and treatments with inhibitors or agonists are available. As for *mGluR5*, DHPG is commonly used to activate *mGluR1/5*^{15,16}; MPEP and MTEP are effective inhibitors of *mGluR5*.^{17,18} In addition, it has been discovered that *mGluR5* takes part in central nervous system (CNS) disorders that are induced by the hypersecretion of glutamate, such as epilepsy, neurogenic or inflammatory pain, dyskinesia, headaches, drug addiction, and psychosis.^{19,20} In this study, we adopted both the transfection and treatments with agonist DHPG and inhibitors MPEP and MTEP in MM cells in order to upregulate *mGluR5* in MM1S and downregulate *mGluR5* in OPM2. The qRT-PCR and western blot confirmed the upregulation of *mGluR5* by agonist DHPG or oe-mGluR5 in MM1S, and inhibition of *mGluR5* by antagonists MPEP and MTEP and si-mGluR5 in OPM2 cells in mRNA and protein levels. After confirmation,

we carried out MTT and apoptosis assays to measure the changes in cell viability and apoptosis. The results indicated that the upregulation of *mGluR5* by oe-mGluR5 or DHPG in MM1S promoted the cell viability and inhibited cell apoptosis compared with the DMSO control group, which supported the claim that *mGluR5* behaved as an oncogene in the MM cell lines. Likewise, it was revealed that the downregulation of *mGluR5* by si-mGluR5 and antagonists MPEP and MTEP in OPM2 cells suppressed cell viability and induced cell apoptosis. The results verified that *mGluR5* acted as oncogene in MM, which was in accordance with our hypothesis. To investigate the potential mechanism involved, we did further research with regard to Ras–MAPK signaling.

Ras–mitogen activated protein kinase pathway is an essential intracellular signaling pathway that regulates multiple cellular functions, including cell proliferation and apoptosis.²¹ The most frequently mutated gene concerning the MAPK signaling pathway is *Ras*, which is related to the superfamily of small GTPases and is the first intracellular effector of the Ras–MAPK signaling pathway.²² *Ras* can be stimulated by many extracellular stimuli, which helps to transform *Ras* from a GDP-bound inactivated form to a GTP-bound activated form, and recruit

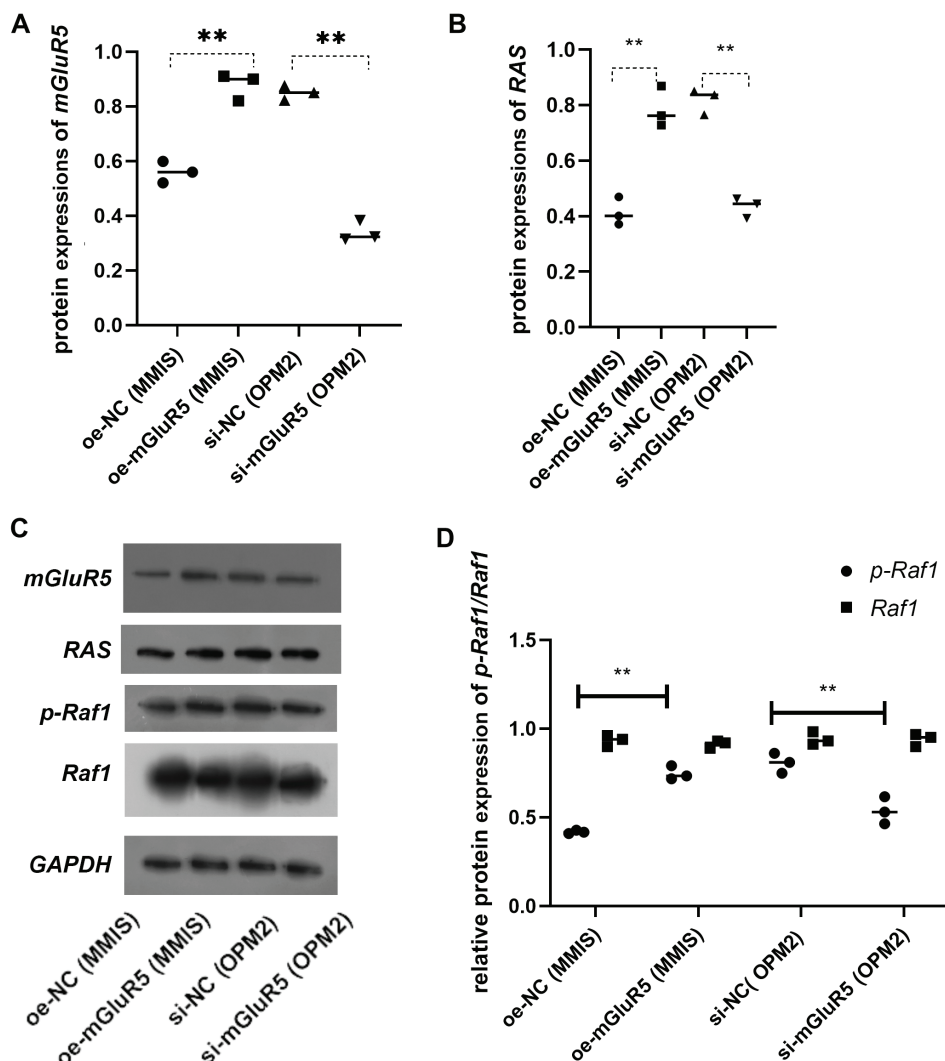


Fig. 5. Transfection-induced upregulation activated the Ras–mitogen activated protein kinase (MAPK) signaling pathway in multiple myeloma (MM) cells. MM1S cell line was transfected with si-NC or si-*mGluR5* plasmids, while the OPM2 cell line was selected to be knocked down by transfection with oe-NC and oe-*mGluR5* plasmids. Western blot was used to examine the protein levels of *mGluR5* (A) and RAS (B) as well as phosphorylation of Raf1 (C) among all the groups in both cell lines after transfection. Each assay was performed thrice independently. Kruskal–Wallis test (K–W) with Dunn’s post hoc test and Kolmogorov–Smirnov test (K–S) were applied in the statistical analysis (Fig. 5A. oe-NC (MM1S) compared to oe-*mGluR5* (MM1S), $p = 0.0039$, si-NC (OPM2) compared to si-*mGluR5* (OPM2), $p = 0.0254$; K–W, Dunn’s post hoc; Fig. 5B. oe-NC (MM1S) compared to oe-*mGluR5* (MM1S), $p = 0.0174$, si-NC (OPM2) compared to si-*mGluR5* (OPM2), $p = 0.0232$; K–W, Dunn’s post hoc; Fig. 5D. oe-NC (MM1S) compared to oe-*mGluR5* (MM1S), $p = 0.0094$, si-NC (OPM2) compared to si-*mGluR5* (OPM2), $p = 0.0163$; K–W, Dunn’s post hoc)

the Raf-1 kinase to the plasma membrane.²³ The activation of the Ras–MAPK pathway is an early event in cancers and a promoter to chemoresistance.²⁴ In MM, previous studies showed that Ras–MAPK pathway is activated in MM patients and its activation could promote the progression of MM.²⁵

In the present study, western blot was used to determine the changes in *Ras* and p-Raf1/Raf1 in response to *mGluR5* regulation in MM1S and OPM2 cells. It was found that the upregulation of *mGluR5* could activate the Ras–MAPK pathway, exerting a promotive impact on MM cell proliferation and a suppressive effect on apoptosis.

Limitations

This study only focused on the in vitro cellular model, which makes the results and findings relatively limited.

Conclusion

The results from the present research indicate that the overexpression of *mGluR5* promoted cell proliferation

and inhibited apoptosis by activating Ras–MAPK pathway in MM. The findings suggest that *mGluR5* inhibitors MPEP or MTEP might be used in the future as a tumor suppressor in MM after extensive in vivo research and clinical trials.

ORCID iDs

- Wei Kou <https://orcid.org/0000-0001-7576-3270>
- Haibin Huang <https://orcid.org/0000-0001-8402-4883>
- Shuangwu Dai <https://orcid.org/0000-0003-4906-1421>
- Xinmei Tan <https://orcid.org/0000-0002-9869-3647>
- Qi Chen <https://orcid.org/0000-0001-9480-9449>
- Renwei Huang <https://orcid.org/0000-0002-9798-5795>
- Hequn Zou <https://orcid.org/0000-0001-6422-6090>

References

1. Raab MS, Podar K, Breitkreutz I, Richardson PG, Anderson KC. Multiple myeloma. *Lancet*. 2009;374(9686):324–339. doi:10.1016/S0140-6736(09)60221-X
2. Rajkumar SV, Dimopolulos MA, Palumbo A, et al. International Myeloma Working Group updated criteria for the diagnosis of multiple myeloma. *Lancet Oncol*. 2014;15(12):e538–e548. doi:10.1016/S1470-2045(14)70442-5
3. Zhang Z, Li Z, Chen W. Downregulated G protein-coupled receptor kinase 6 leads to apoptosis in multiple myeloma MM1R cells. *Exp Ther Med*. 2018;16(5):4253–4259. doi:10.3892/etm.2018.6722
4. Rajkumar SV, Kumar S. Multiple myeloma: Diagnosis and treatment. *Mayo Clin Proc*. 2016;91(1):101–119. doi:10.1016/j.mayocp.2015.11.007

5. Kazandjian D. Multiple myeloma epidemiology and survival: A unique malignancy. *Semin Oncol*. 2016;43(6):676–681. doi:10.1053/j.seminoncol.2016.11.004
6. Weaver CJ, Tariman JD. Multiple myeloma genomics: A systematic review. *Semin Oncol Nurs*. 2017;33(3):237–253. doi:10.1016/j.soncn.2017.05.001
7. Ramakrishnan VG, Miller KC, Macon EP, et al. Histone deacetylase inhibition in combination with MEK or BCL-2 inhibition in multiple myeloma. *Haematologica*. 2019;104(10):2061–2074. doi:10.3324/haematol.2018.211110
8. Jovanović KK, Escure G, Demonchy J, et al. Deregulation and targeting of TP53 pathway in multiple myeloma. *Front Oncol*. 2018;8:665. doi:10.3389/fonc.2018.00665
9. Conn PJ, Pin JP. Pharmacology and functions of metabotropic glutamate receptors. *Annu Rev Pharmacol Toxicol*. 1997;37:205–237. doi:10.1146/annurev.pharmtox.37.1.205
10. Rosenfeld MR, Titulaer MJ, Dalmau J. Paraneoplastic syndromes and autoimmune encephalitis: Five new things. *Neurol Clin Pract*. 2012;2(3):215–223. doi:10.1212/CPJ.0b013e31826af23e
11. Liao S, Ruiz Y, Gulzar H, et al. Osteosarcoma cell proliferation and survival requires mGluR5 receptor activity and is blocked by riluzole. *PLoS One*. 2017;12(2):e0171256. doi:10.1371/journal.pone.0171256
12. Stepulak A, Luksch H, Uckermann O, et al. Glutamate receptors in laryngeal cancer cells. *Anticancer Res*. 2011;31(2):565–573. PMID:21378340.
13. Park SY, Lee SA, Han IH, et al. Clinical significance of metabotropic glutamate receptor 5 expression in oral squamous cell carcinoma. *Oncol Rep*. 2007;17(1):81–87. PMID:17143482.
14. Pissimissis N, Papageorgiou E, Lembessis P, Armakolas A, Koutsilieris M. The glutamatergic system expression in human PC-3 and LNCaP prostate cancer cells. *Anticancer Res*. 2009;29(1):371–377. PMID:19331175.
15. Wang W, Duclot F, Groverman B, et al. Hippocampal protein kinase D1 is necessary for DHPG-induced learning and memory impairments in rats. *PLoS One*. 2018;13(4):e0195095. doi:10.1371/journal.pone.0195095
16. Feng X, Bader BM, Yang F, et al. Improvement of impaired electrical activity in NPC1 mutant cortical neurons upon DHPG stimulation detected by micro-electrode array. *Brain Res*. 2018;1694:87–93. doi:10.1016/j.brainres.2018.05.009
17. López-Zapata A, León-Navarro DA, Crespo M, Albasanz JL, Martín M. Chronic oral administration of MPEP, an antagonist of mGlu₅ receptor, during gestation and lactation alters mGlu₅ and A₂A receptors in maternal and neonatal brain. *Neuroscience*. 2017;344:187–203. doi:10.1016/j.neuroscience.2016.12.019
18. Huang Y, Shu H, Li L, et al. L-DOPA-induced motor impairment and overexpression of corticostriatal synaptic components are improved by the mGluR5 antagonist MPEP in 6-OHDA-lesioned rats. *ASN Neuro*. 2018;10:1759091418811021. doi:10.1177/1759091418811021
19. Brauner-Osborne H, Egebjerg J, Nielsen EO, Madsen U, Krosgaard-Larsen P. Ligands for glutamate receptors: Design and therapeutic prospects. *J Med Chem*. 2000;43(14):2609–2645. doi:10.1021/jm00007r
20. Spooren W, Ballard T, Gasparini F, Amalric M, Mutel V, Schreiber R. Insight into the function of Group I and Group II metabotropic glutamate (mGlu) receptors: Behavioural characterization and implications for the treatment of CNS disorders. *Behav Pharmacol*. 2003;14(4):257–277. doi:10.1097/01.fbp.0000081783.35927.8f
21. Roberts AE, Allanson JE, Tartaglia M, Gelb BD. Noonan syndrome. *Lancet*. 2013;381(9863):333–342. doi:10.1016/S0140-6736(12)61023-X
22. Tajan M, Paccoud R, Branka S, Edouard T, Yart A. The RASopathy family: Consequences of germline activation of the RAS/MAPK pathway. *Endocr Rev*. 2018;39(5):676–700. doi:10.1210/er.2017-00232
23. Dhawan NS, Scopton AP, Dar AC. Small molecule stabilization of the KSR inactive state antagonizes oncogenic Ras signalling. *Nature*. 2016;537(7618):112–116. doi:10.1038/nature19327
24. Hrustanovic G, Bivona TG. Ras–MAPK signaling influences the efficacy of ALK-targeting agents in lung cancer. *Mol Cell Oncol*. 2016;3(2):e1091061. doi:10.1080/23723556.2015.1091061
25. Chang-Yew Leow C, Gerondakis S, Spencer A. MEK inhibitors as a chemotherapeutic intervention in multiple myeloma. *Blood Cancer J*. 2013;3(3):e105. doi:10.1038/bcj.2013.1

RPS27 selectively regulates the expression and alternative splicing of inflammatory and immune response genes in thyroid cancer cells

Jing Wan^{1,B–D,F}, Juan Lv^{1,B,C}, Chun Wang^{2,B,C}, Li Zhang^{1,A,E,F}

¹ Ultrasound Department, People's Hospital of Xinjiang Uygur Autonomous Region, China

² Pathology Department, People's Hospital of Xinjiang Uygur Autonomous Region, China

A – research concept and design; B – collection and/or assembly of data; C – data analysis and interpretation; D – writing the article; E – critical revision of the article; F – final approval of the article

Advances in Clinical and Experimental Medicine, ISSN 1899–5276 (print), ISSN 2451–2680 (online)

Adv Clin Exp Med. 2022;31(8):889–901

Address for correspondence

Li Zhang
E-mail: springwch@126.com

Funding sources

This research was funded by Natural Science Foundation of Xinjiang Uygur Autonomous Region (contract No. 2017D01C120). The funder had no role in study design, data collection and analysis, decision to publish, or preparation of the manuscript.

Conflict of interest

None declared

Received on August 16, 2021

Reviewed on October 7, 2021

Accepted on March 10, 2022

Published online on May 12, 2022

Cite as

Wan J, Lv J, Wang C, Zhang L. RPS27 selectively regulates the expression and alternative splicing of inflammatory and immune response genes in thyroid cancer cells.

Adv Clin Exp Med. 2022;31(8):889–901.

doi:10.17219/acem/147271

DOI

10.17219/acem/147271

Copyright

Copyright by Author(s)

This is an article distributed under the terms of the Creative Commons Attribution 3.0 Unported (CC BY 3.0) (<https://creativecommons.org/licenses/by/3.0/>)

Abstract

Background. The expression of ribosomal protein S27 (RPS27) is upregulated in multiple human malignancies. In thyroid cancer, the expression of RPS27 is associated with patient outcomes. However, the carcinogenic mechanisms of RPS27 and functions of RPS27 in the initiation and progression of thyroid cancer are still not clear.

Objectives. To investigate the carcinogenic mechanisms of RPS27 and functions of RPS27 in the initiation and progression of thyroid cancer.

Materials and methods. The RPS27 gene was overexpressed in BTH101 cells and the influence on the level of gene expression and alternative splicing (AS) was then analyzed by comparing the transcriptomes of the overexpressing cells with the controls. The procedures included cloning and plasmid construction of RPS27, cell culture and transfection, evaluation of RPS27 overexpression, library preparation and sequencing, RNA-Seq raw data clean and alignment, differentially expressed genes (DEGs) analysis, AS analysis, quantitative real-time polymerase chain reaction (qRT-PCR) validation of DEGs and AS events (ASEs), and functional enrichment analysis.

Results. The results demonstrated that RPS27 could selectively regulate the expression of genes associated with autoimmune thyroid disease, inflammatory/immune response and AS of genes associated with TRIF-dependent toll-like receptor signaling pathway and apoptotic process. The genes in question are *BMP6*, *SERPINA3*, *IL17B*, *IL17RN*, *HLA-B*, *PF4*, *HLA-DOB*, *MADCAM1*, *HLA-DQA1*, *TPO*, *HLA-B*, *HLA-DQA1*, *HLA-DOB*, *HLA-C*, *KRT8*, *CFLAR*, *HMGAI1*, *CASP8*, *CCNH*, *UBE2D3*, and *MAPK9*, among others.

Conclusions. The RPS27 selectively regulated the expression and alternative splicing of genes involved in inflammatory/immune response and TRIF-dependent toll-like receptor signaling pathway, which were tightly associated with the initiation and progression of thyroid cancer. These results extend our knowledge on the molecular functions of RPS27 in thyroid cancer cells and have a potential value in thyroid cancer treatment.

Key words: gene expression, thyroid cancer, alternative splicing, ribosomal protein S27, overexpression

Background

Thyroid cancer is a common endocrine tumor with an increasing incidence worldwide.¹ The age-standardized incidence rate of thyroid cancer rose by 20% from 1990 to 2013.² In China, a recent investigation reported a rapidly increasing number of thyroid cancer cases.³ The immune system plays a crucial role in prevention of tumors, as well as in their initiation and progression.⁴ Some tumor types are strongly correlated with chronic infectious or inflammatory diseases, whereas others are not, but inflammatory components are present in most of human neoplastic lesions. Studies have demonstrated that thyroid cancer can be associated with thyroid autoimmunity, even if the exact mechanisms remain poorly elucidated.^{5,6}

Ribosomal protein S27 (RPS27), also known as metalloproteinase-1 (MPS-1), is a multifunctional protein ubiquitously expressed in most of the human normal tissues and primarily located in the cytoplasm.⁷ It serves as an RNA-binding protein (RBP) and subsequently affects the translation and degradation of many mRNAs.⁸ In addition to translation-related functions, ribosomal proteins are also associated with plenty of biological process functions, including apoptosis, genomic stability, development, and cell proliferation.⁹ The expression of RPS27 is upregulated in multiple human malignancies, including liver, prostate, colon, stomach, and head and neck cancers.^{10–12} In thyroid cancer, the expression of RPS27 is associated with patient outcomes.¹³ However, the carcinogenic mechanisms of RPS27 and functions of RPS27 in the initiation and progression of thyroid cancer are still not clear.

Therefore, in this study, the *RPS27* gene was overexpressed in BTH101 cells and the influence on the gene expression level and alternative splicing (AS) was then analyzed through comparing the transcriptomes of the overexpressing cells with the controls.

Objectives

The objectives were to investigate the carcinogenic mechanisms of *RPS27* and functions of *RPS27* in the initiation and progression of thyroid cancer.

Materials and methods

Cloning and plasmid construction of RPS27

CE Design v. 1.04 (Vazyme Biotech, Nanjing, China) was employed to design the primer pairs for Hot Fusion. Each of the primers consists of a fragment of gene-specific sequence and a 17–30 bp sequence of the pIRES-hrGFP-1a vector:

F-primer: agcccgggcgatccgaattc
ATGCCTCTCGCAAAGGATCTC
R-primer: gtcaccttgtagctctgag
GTGCTGCTTCCTCCTGAAGGA.

The pIRES-hrGFP-1a vector was digested with EcoRI and XhoI (New England Biolabs (NEB), Ipswich, USA) for 2–3 h at 37°C. The enzyme-digested vector was then run on 1.0% agarose gel and purified with the Qiagen column kit (Qiagen, Hilden, Germany). Total RNA was extracted from BHT101 cells with TRIzol (Ambion, Invitrogen, Carlsbad, USA). The purified RNA was reversely transcribed for cDNA with oligo dT primer. The inserted fragment was synthesized through polymerase chain reaction (PCR) amplification. The ClonExpress® II One Step Cloning Kit (Vazyme Biotech, Nanjing, China) was used to ligate the linearized vector digested with EcoRI and XhoI and PCR insert. Plasmids were introduced into *Escherichia coli* strain through chemical transformation. Cells were plated onto Luria broth (LB) agar plates containing 1 µL/mL ampicillin, and incubated overnight at 37°C. Colonies were screened through colony PCR (28 cycles) with universal primers located on the backbone vector. Sanger sequencing was used to verify the insert sequence.

Cell culture and transfection

Chinese Academy of Sciences Cell Bank (Shanghai, China) provided the human thyroid cancer cell line BHT101. The BHT101 cells were cultured with 5% CO₂ at 37°C in Dulbecco's modified Eagle's medium (DMEM) containing 10% fetal bovine serum (FBS), 100 µg/mL of streptomycin and 100 U/mL of penicillin. Lipofectamine 2000 (Invitrogen) was employed to conduct plasmid transfection of BHT101 cells following the manufacturer's protocol, and transfected cells were harvested after 48 h for quantitative real-time PCR (qRT-PCR) and western blot analysis. This study complied with the Declaration of Helsinki and the study protocol was approved by the Ethical Committee of People's Hospital of Xinjiang Uygur Autonomous Region, China (approval No. KY20180118148).

Evaluation of RPS27 overexpression

The evaluation of RPS27 overexpression was performed by means of qRT-PCR and western blot analysis, using glyceraldehyde-3-phosphate dehydrogenase (GAPDH) as the control. The synthesis of cDNA was conducted through standard procedures, and qRT-PCR was performed on the Bio-Rad S1000 Thermal Cycler (Bio-Rad, Hercules, USA) with Bestar SYBR Green RT-PCR Master Mix (DBI Bioscience, Shanghai, China). The primers of RPS27 were 5'-TCCTTCATCCCTCTCCAGAA-3' (forward) and 5'-GTAGGCTGGCAGAGGACAGT-3' (reverse), respectively; and the primers of GAPDH were 5'-CGGAGTCAACGGATTGGTCGTAT-3' (forward) and 5'-AGCCTTCTCCATGGTGGTGAAGAC-3' (reverse), respectively. The 2^{-ΔΔCt} method was employed to evaluate the relative expression level of RPS27. The paired Student's t-test was used to perform the comparison between RPS27-overexpressed cells and control cells.

For western blot analysis, to prepare the total cell lysates, RPS27-overexpressed and control BHT101 cells were lysed in radioimmunoprecipitation assay (RIPA) buffer, containing 150 mM NaCl, 50 mM Tris-HCl (pH 7.4), 0.1% sodium dodecyl sulfate (SDS), 1.0% deoxycholate, 1 mM ethylenediaminetetraacetic acid (EDTA), and 1% Triton X-100. The samples were centrifuged at $12,000 \times g$ for 5 min. The supernatants were analyzed using a 10% SDS polyacrylamide gel electrophoresis (SDS-PAGE) gel and then transferred onto a polyvinylidene difluoride (PVDF) membrane (Merck Millipore, Burlington, USA). The RPS27 was detected with a monoclonal Flag antibody (Sigma-Aldrich, St. Louis, USA) diluted in Tris-buffered saline with Tween 20 (TBST) (1:2000), and GAPDH (ABclonal Technology, Cumming Park, USA) was used as the loading control (1:2000).

Library preparation and sequencing

Total RNA extracted from BHT101 cells was purified using 2 phenol-chloroform treatments and then treated using RQ1 DNase (Promega, Madison, USA) to remove DNA. The Smartspec Plus (Bio-Rad) was employed to evaluate the quality and quantity of the purified RNA by measuring the absorbance at 260 nm/280 nm (A260/A280), and 1.5% agarose gel electrophoresis was used to verify the integrity of the RNA.

The VAHTS Stranded mRNA-seq Library Prep Kit (Vazyme Biotech) was used to perform RNA-seq library preparation with 1 μ g of the total RNA. Polyadenylated mRNAs were converted into double-stranded cDNAs after purification and fragmentation. The DNAs were then ligated to VAHTS RNA Adapters (Vazyme Biotech) following end repair and A tailing. Purified ligation products ranging from 200 bps to 500 bps were digested using heat-labile uracil-DNA glycosylase (UDG), and the single-stranded cDNA was amplified, purified, quantified, and stored at -80°C before high-throughput sequencing.

For high-throughput sequencing, the libraries were prepared according to the instructions of the manufacturer and applied to Illumina HiSeq X Ten system (Illumina, Inc., San Diego, USA) for 150 nt paired-end sequencing.

RNA-Seq raw data clean and alignment

Raw reads with more than 2-N bases in raw sequencing reads were excluded. FASTX-Toolkit v. 0.0.13 (http://hannonlab.cshl.edu/fastx_toolkit/index.html) was then used to trim adaptors and low-quality bases. The short reads with less than 16 nt were also discarded. After that, clean reads were aligned to the GRCh38 genome with tophat2,¹⁴ allowing 4 mismatches. Uniquely mapped reads were used for calculation of gene reads number and fragments per kilobase of transcript per million fragments mapped (FPKM).¹⁵

Alternative splicing analysis

As described previously, the ABL alternative splicing (ABLAs) pipeline was employed to define and quantify the alternative splicing events (ASEs) between the samples.¹⁶ Briefly, the detection of 10 types of ASEs was based on the splice junction reads, including exon skipping (ES), alternative 5' splice site (A5SS), alternative 3' splice site (A3SS), intron retention (IR), mutually exclusive exons (MXE), mutually exclusive 5'UTRs (5pMXE), mutually exclusive 3'UTRs (3pMXE), cassette exon, A3SS&ES, and A5SS&ES.

qRT-PCR validation of differentially expressed genes and ASEs

In order to elucidate the validity of the RNA-seq data, the qRT-PCR was conducted for some of the differentially expressed genes (DEGs). The information of primers was demonstrated in Supplementary File 1. Total RNA remaining from RNA-seq library preparation was used for qRT-PCR. The RNA was reversely transcribed into cDNA using a M-MLV Reverse Transcriptase (Vazyme Biotech). The qRT-PCR was conducted on the StepOne Real-Time PCR System using the SYBR Green PCR Reagents Kit (Yeasen, Shanghai, China). The qRT-PCR conditions consisted of denaturing at 95°C for 10 min, 40 cycles of denaturing at 95°C for 15 s, and annealing and extension at 60°C for 1 min. The qRT-PCR amplifications were performed in triplicate for each sample. The expression levels of all selected DEGs were normalized against that of GAPDH.

Meanwhile, a qRT-PCR assay was also conducted for alternative splicing event (ASE) validation. The primers used were also presented in Supplementary File 1. To detect alternative isoforms, we used a boundary-spanning primer for the sequence encompassing the junction of constitutive exon and alternative exon, as well as an opposing primer in a constitutive exon. The boundary-spanning primer of alternative exon was designed according to “model exon” to detect model splicing or “altered exon” to detect altered splicing.

Statistical analyses

The R Bioconductor package edgeR (<https://bioconductor.org/packages/release/bioc/html/edgeR.html>) was employed to screen out the DEGs whose expression levels were assessed using FPKM.¹⁷ A false discovery rate (FDR) <0.05 and fold change (FC) >2 or <0.5 were set as the cutoff criteria for identifying DEGs. The Student's t-test was performed to evaluate the significance of the ratio alteration of ASEs between RPS27-overexpressed and control cells. Regulated alternative splicing events (RASEs) were identified when $p \leq 0.05$. To sort out functional categories of DEGs, Gene Ontology (GO) terms and Kyoto

Encyclopedia of Genes and Genomes (KEGG) pathways were identified using KOBAS 2.0 server (<http://kobas.cbi.pku.edu.cn/>).¹⁸ The hypergeometric test and Benjamini–Hochberg FDR controlling procedure were employed to define the enrichment of each term. The expression levels of RPS27, selected DEGs and ASEs were compared using the Student's t-test. Significance was set at $p < 0.05$.

Results

RNA-seq data analysis

The qRT-PCR and western blot were used to evaluate the efficacy of RPS27 overexpression (Fig. 1A,B). Six cDNA libraries were constructed and then sequenced for paired-end reads of each sample. The average high-quality reads of these 6 samples was 78.47 ± 3.92 million (Supplementary File 2). Among these reads, 94.04–96.39% were aligned and about 89.14–94.42% were uniquely aligned when they were mapped onto the reference genome with TopHat 2 (Supplementary File 2). Robust expression results for 20,994 genes were obtained from RNA-seq data (Supplementary File 3). A correlation matrix was computed with FPKM values for all 20,994 genes according to the Pearson's correlation coefficient (Fig. 1C).

RPS27 overexpression in BHT101 cell selectively regulates the expression of inflammatory and immune response genes

A total of 1504 genes were differentially expressed, including 604 upregulated and 900 downregulated. Supplementary File 4 provides the details of all the DEGs. A volcano plot (Fig. 1D) demonstrated the DEGs regulated by RPS27 overexpression. Figure 1E shows the hierarchical clustering of DEGs in control and RPS27 overexpression samples. These results showed that RPS27 overexpression extensively regulated gene expression in BHT101 cells.

According to the cutoff criteria, the upregulated and downregulated DEGs were enriched in 44 and 112 GO terms, respectively (Supplementary Files 5 and 6). Interestingly, the upregulated genes in the biological process terms of the GO analysis were mainly associated with the inflammatory and immune response (Fig. 1F), including *BMP6*, *SERPINA3*, *IL17B*, *IL1RN*, *HLA-B*, *PF4*, *HLA-DOB*, *MADCAM1*, and *HLA-DQA1*. Conversely, the downregulated genes were primarily involved in mitosis and mitotic cell cycle.

When the corrected p-values of the KEGG pathways were set at <0.05 , the upregulated and downregulated DEGs were enriched in 166 and 211 pathways, respectively (Supplementary Files 7 and 8). Strikingly, the upregulated genes were primarily associated with autoimmune thyroid disease (Fig. 1G), including *TPO*, *HLA-B*,

HLA-DQA1, and *HLA-DOB*. In contrast, the downregulated genes were primarily associated with pathways in cancer, HTLV-I infection and regulation of actin cytoskeleton (Fig. 1G).

The expression of the DEGs involved in the inflammatory and immune response and angiogenesis was quantified using RNA sequencing data, including *BMP6*, *SERPINA3*, *IL17B*, *IL1RN*, *HLA-B*, *PF4*, *HLA-DOB*, *MADCAM1*, *HLA-DQA1*, and *TPO*. The results demonstrated that their expressions were significantly upregulated (Fig. 2). Among them, we selected *BMP6*, *HLA-B*, *HLA-DQA1*, *IL17B*, and *SERPINA3* for further qRT-PCR validation analysis. The PCR primers were demonstrated in Supplementary File 1. The qRT-PCR results were in agreement with the sequencing data (Fig. 3).

RPS27 regulates the alternative splicing of a large number of immune-response genes

Among the 66.7 ± 3.0 million uniquely mapped reads, 47.08–47.97% were junction reads (Supplementary File 2). Compared with the reference genome annotation through the use of the Tophat2 pipeline, there were 62.69% annotated exons (230,287 out of 367,321 annotated exons), 152,726 known splice junctions and 111,776 novel splice junctions.

There were 16,925 known ASEs in the model gene which was termed as the reference genome, and 45,772 novel ASEs excluding intron retention events (Supplementary Files 9 and 10).

A total of 735 RASEs were identified, including 401 upregulated and 334 downregulated (Supplementary Files 11 and 12). The RPS27-regulated ASEs mainly included the A5SS (157), A3SS (146), ES (120), and cassette exon (73) (Fig. 4A). These results implied that RPS27 overall regulated ASEs in BHT101 cell. The genes whose levels of AS and expression were both regulated by RPS27 were overlapped in order to determine whether the increase in ASEs could be attributed to altered transcription,¹⁹ and 3 such genes were identified (Fig. 4B), including *ITGA1*, *NPNT* and *MACF1*. This result suggested that AS and transcriptional regulation might be partially coupled.

Interestingly, among the genes regulated by RPS27-mediated AS, most were enriched in “viral reproduction”, “TRIF-dependent toll-like receptor signaling pathway” and “MyD88-independent toll-like receptor signaling pathway”, including *HLA-C*, *KRT8*, *CFLAR*, *HMGAI*, *CASP8*, *CCNH*, *UBE2D3*, and *MAPK9* (Fig. 4C). In contrast, enriched KEGG pathways ($p < 0.05$) mainly included those associated with “pyrimidine metabolism”, “purine metabolism” and “ribosome” (Fig. 4D).

The ASEs of the genes involved in thyroid cancer were quantified using RNA sequencing data, including *HLA-C*, *KRT8*, *CFLAR*, *HMGAI*, *CASP8*, *CCNH*, *UBE2D3*, and *MAPK9*. The results showed that they were significantly upregulated (Fig. 5). To validate the ASEs identified from

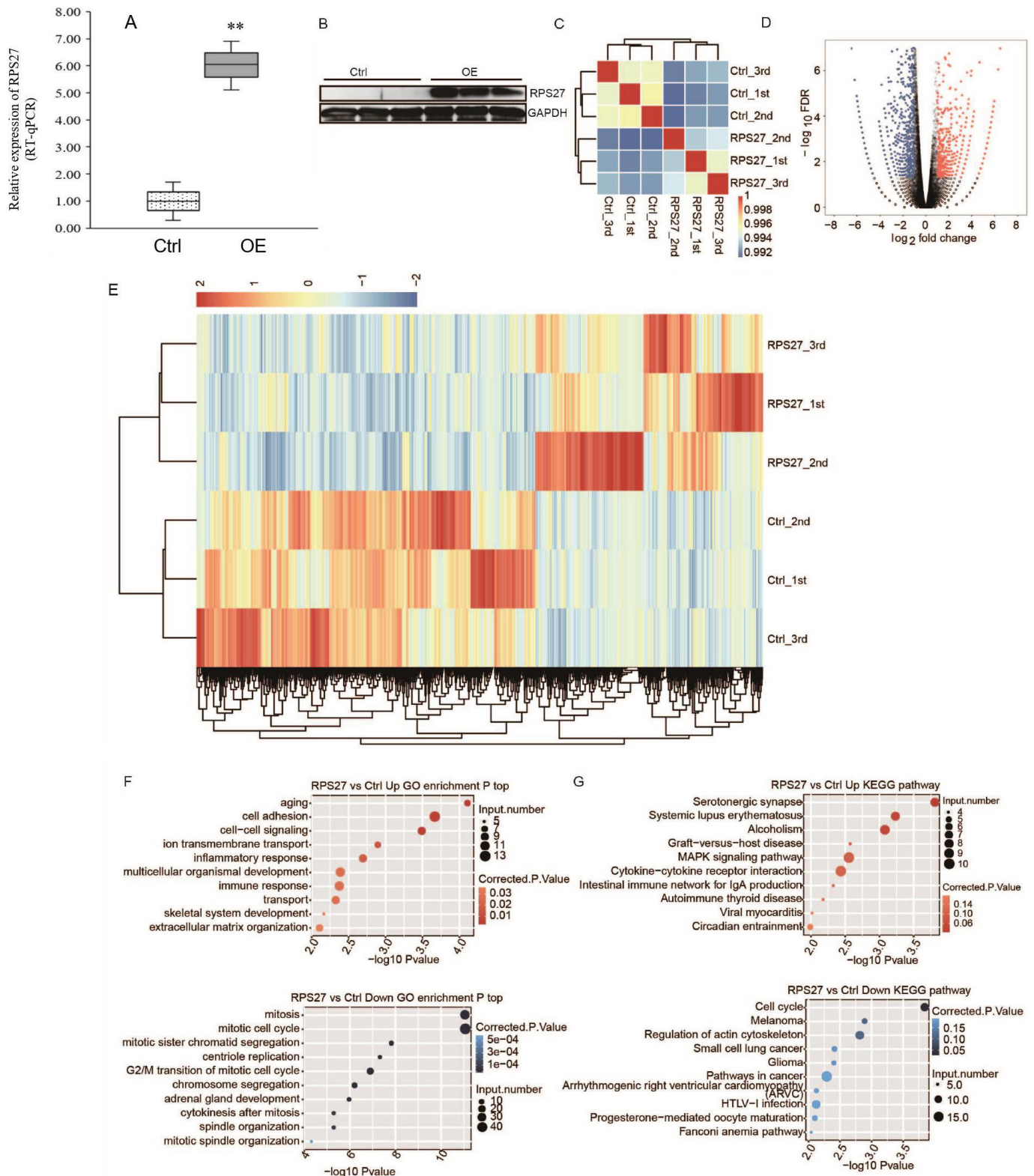


Fig. 1. RNA-seq analysis of ribosomal protein S27 (RPS27)-regulated transcriptome. A. RPS27 expression was quantified using quantitative real-time polymerase chain reaction (qRT-PCR); $t = -7.618$; $p = 0.002$; $**p < 0.01$; B. RPS27 expression was quantified using western blot; C. Heat map showing the hierarchically clustered Pearson's correlation matrix resulting from comparing the transcript expression values of the control cells with RPS27 overexpression cells; D. Identification of RPS27-regulated genes. Upregulated genes were labeled in red, whereas downregulated genes were labeled in blue in the volcano plot; E. Hierarchical clustering of differentially expressed genes (DEGs) in the control cells and RPS27 overexpression cells. Fragments per kilobase of transcript per million fragments mapped (FPKM) values were log₂-transformed and then median-centered by each gene; F. The top 10 representative Gene Ontology (GO) biological processes of up- or downregulated genes; G. The top 10 representative Kyoto Encyclopedia of Genes and Genomes (KEGG) pathways of up- or downregulated genes.

Control (Ctrl) – BHT101 cells without RPS27 overexpression; OE – BHT101 cells with RPS27 overexpression; GAPDH – glyceraldehyde-3-phosphate dehydrogenase; FDR – false discovery rate; IgA – immunoglobulin A.

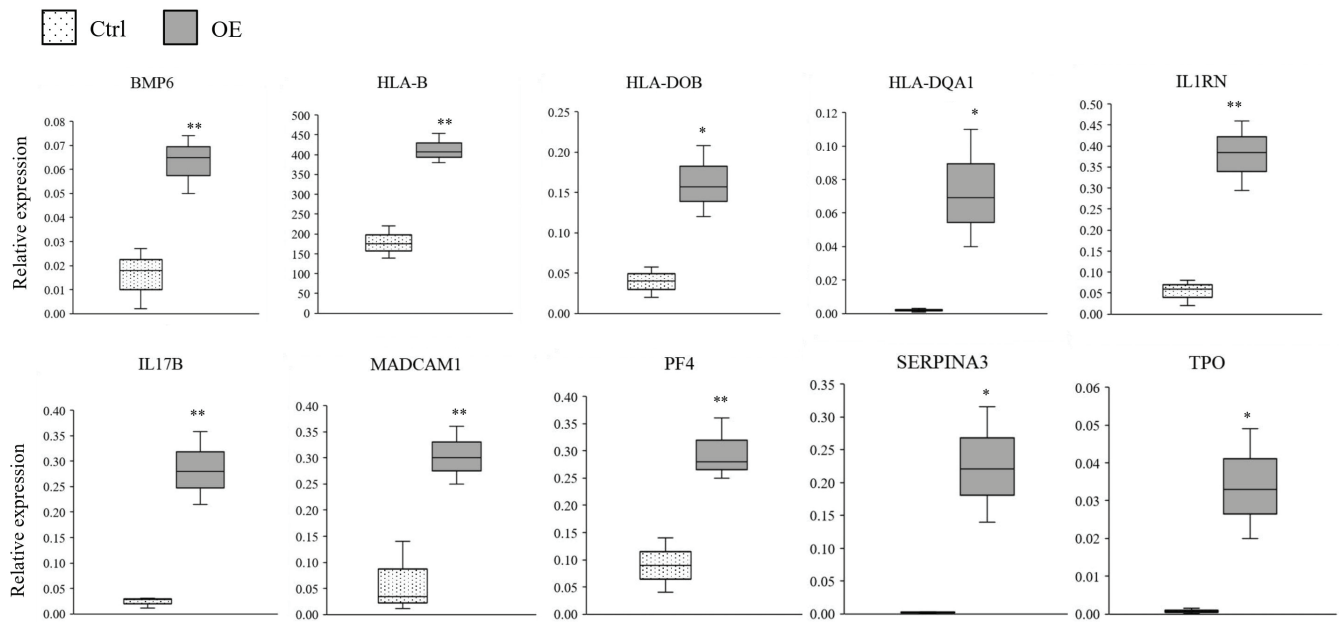


Fig. 2. Ribosomal protein S27 (RPS27) regulated the expression of the genes involved in the inflammatory and immune response and angiogenesis. Gene expression was quantified using RNA sequencing data. Fragments per kilobase of transcript per million fragments mapped (FPKM) values were calculated as explained in Materials and methods section; $t = -4.677, -7.468, -4.405, -3.495, -6.424, -6.243, -4.758, -4.727, -4.397, -3.955$; $p = 0.009, 0.002, 0.012, 0.025, 0.003, 0.003, 0.009, 0.009, 0.012, 0.017$; ** $p < 0.01$; * $p < 0.05$.

Control (Ctrl) – BHT101 cells without RPS27 overexpression; OE – BHT101 cells with RPS27 overexpression.

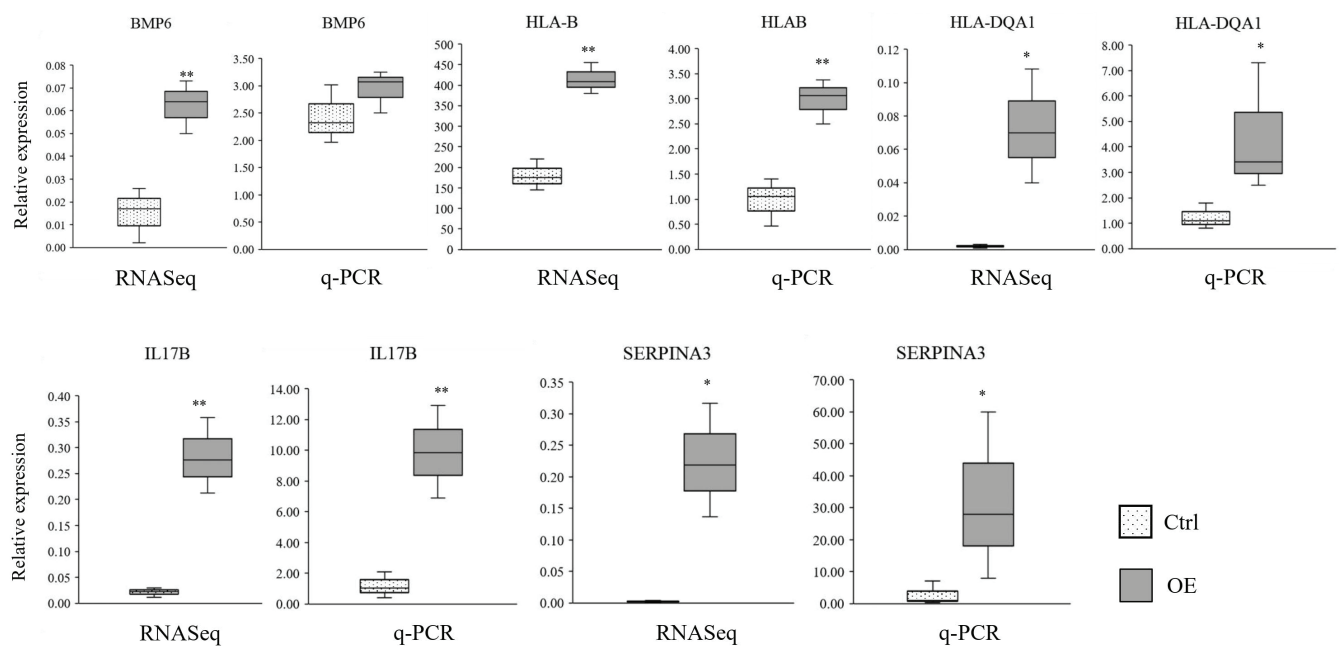


Fig. 3. Ribosomal protein S27 (RPS27) regulated the expression of *BMP6*, *HLA-B*, *HLA-DQA1*, *IL17B*, and *SERPINA3*. Both the RNA-seq and quantitative real-time polymerase chain reaction (qRT-PCR) validation are shown; $t = -4.677, -1.316, -7.468, -5.373, -3.495, -3.254, -6.243, -4.829, -4.397$; $p = 0.009, 0.259, 0.002, 0.006, 0.025, 0.026, 0.003, 0.008, 0.012$; $Z = -2.235$; $p = 0.043$; ** $p < 0.01$; * $p < 0.05$.

Control (Ctrl) – BHT101 cells without RPS27 overexpression; OE – BHT101 cells with RPS27 overexpression.

the RNA-Seq data, 4 potential ASEs were analyzed using qRT-PCR. They were located in *KRT8*, *CFLAR*, *CASP8*, and *CCNH* genes, respectively. The PCR primers were also demonstrated in Supplementary File 1. All the 4 ASEs validated with qRT-PCR were highly consistent with the sequencing results (Fig. 4E,F, Fig. 6).

Discussion

In this study, we profiled the entire transcriptome in BHT101 cells with the overexpression of RPS27, allowing for the decoding of RPS27-mediated regulation for gene expression and AS. Strikingly, the expression of genes

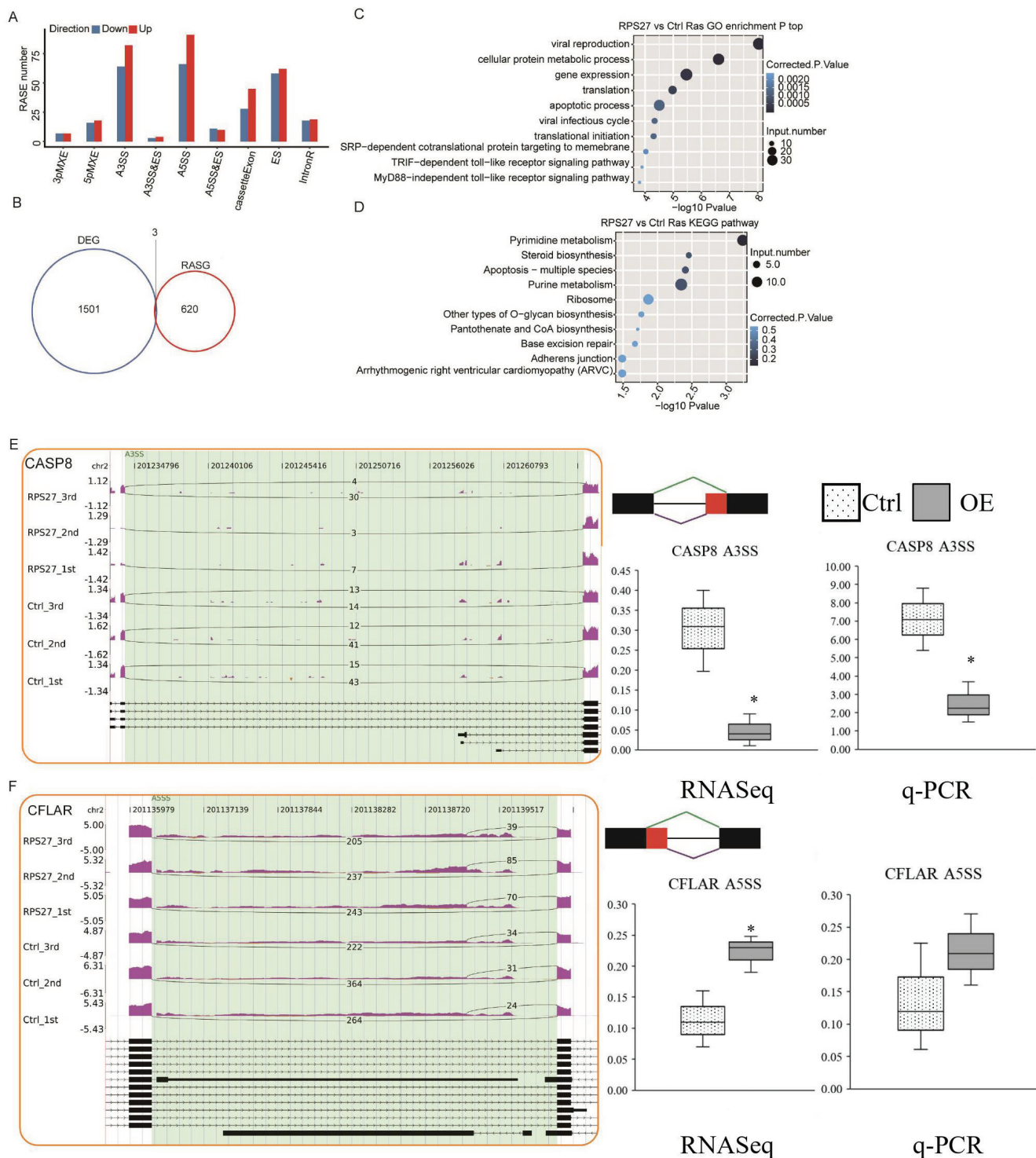


Fig. 4. Ribosomal protein S27 (RPS27) regulated alternative splicing events (ASEs) in BHT101 cells. **A.** Classification of RPS27-regulated ASEs; **B.** The overlap analysis between RPS27-regulated differentially expressed genes (DEGs) and alternative splicing genes (RASGs); **C.** The top 10 enriched Gene Ontology (GO) biological processes of RPS27-regulated alternative splicing genes; **D.** The top 10 enriched Kyoto Encyclopedia of Genes and Genomes (KEGG) pathways of RPS27-regulated alternative splicing (AS) genes; **E.** RPS27 regulated AS of CASP8, with IGV-Sashimi plot showing an alternative 3' splice sites (A3SS) event. Both RNA-seq quantification and quantitative real-time polymerase chain reaction (qRT-PCR) validation are presented; **F.** RPS27-regulated AS of CFLAR, with IGV-Sashimi plot showing an alternative 5' splice sites (A5SS) event. Both RNA-seq quantification and qRT-PCR validation are presented. Reads distribution of each ASE was plotted in the left panel with the transcripts of each gene shown below. The schematic diagrams depict the structures of ASEs, AS1 (purple line) and AS2 (green line). The constitutive exon sequences were denoted by black boxes, intron sequences by horizontal line (right panel, top), while alternative exon by red box and intron by purple box. The RNA-seq quantification is shown at the bottom of the right panel; $t = 4.406, 3.930, -3.058, -1.349$; $p = 0.016, 0.017, 0.025, 0.249$; * $p < 0.05$.

Control (Ctrl) – BHT101 cells without RPS27 overexpression; OE – BHT101 cells with RPS27 overexpression; 5pMXE – mutually exclusive 5'UTRs; 3pMXE – mutually exclusive 3'UTRs; ES – exon skipping.

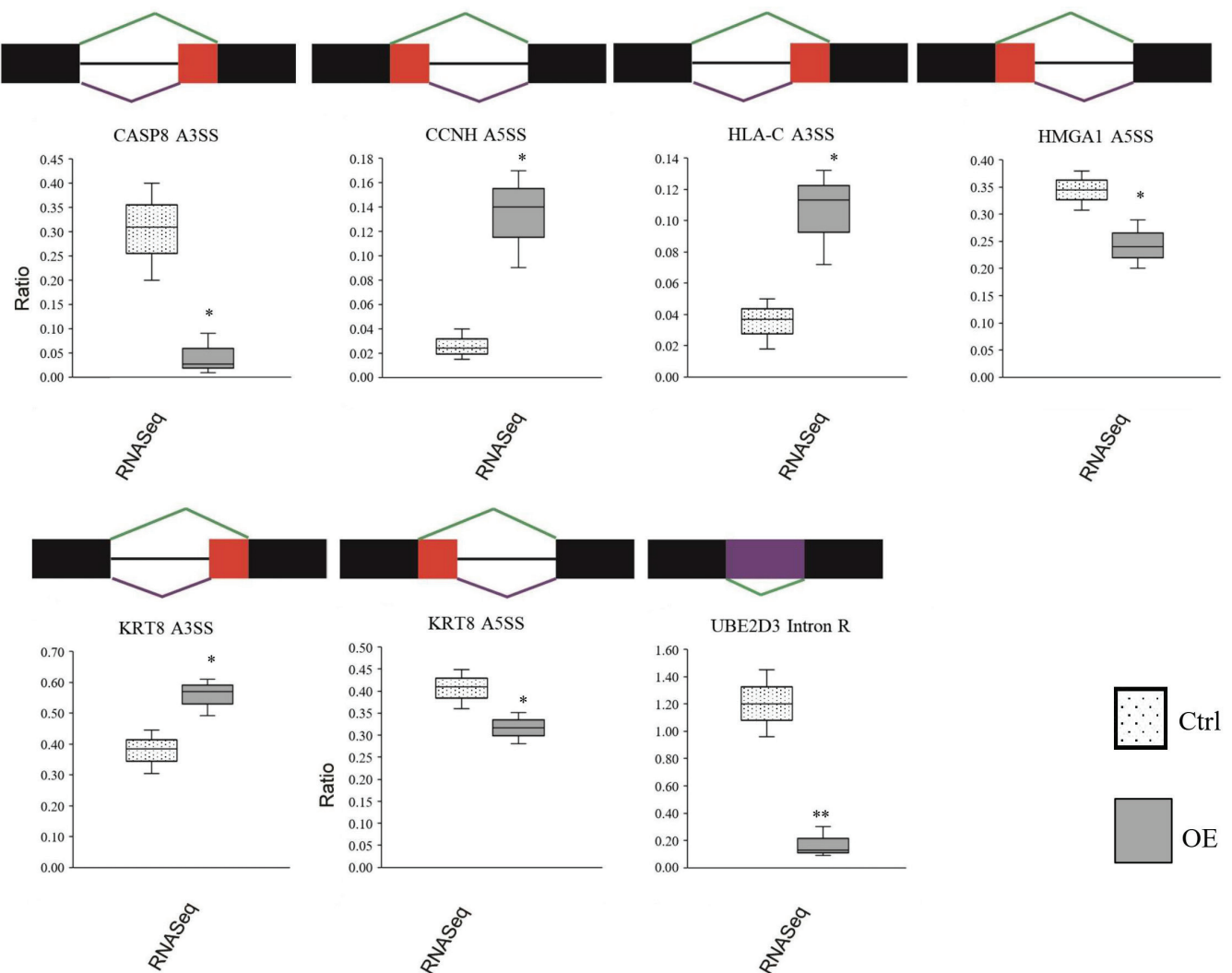


Fig. 5. Ribosomal protein S27 (RPS27) regulated alternative splicing (AS) of the genes associated with thyroid cancer, with alternative 3' splice sites (A3SS) for CASP8, alternative 5' splice sites (A5SS) for CCNH, A3SS for HLA-C, A5SS for HMGA1, A3SS for KRT8, A5SS for KRT8, and intron retention (IR) for UBE203. RNA-seq quantification is presented; $t = 4.159, -4.376, -3.534, 3.032, -3.337, 2.971, 6.627$; $p = 0.014, 0.012, 0.024, 0.039, 0.029, 0.042, 0.003$; ** $p < 0.01$; * $p < 0.05$.

Control (Ctrl) – BHT101 cells without RPS27 overexpression; OE – BHT101 cells with RPS27 overexpression.

involved in the inflammatory and immune response and autoimmune thyroid disease were selectively upregulated following RPS27 overexpression. Meanwhile, the genes whose AS was specifically regulated by RPS27 were enriched in the positive regulation of viral reproduction, apoptotic process, TRIF-dependent toll-like receptor signaling pathway, MyD88-independent toll-like receptor signaling pathway, and so forth. These results demonstrated that RPS27 was involved in the initiation and progression of thyroid cancer, possibly through regulating the expression of genes associated with autoimmune thyroid disease, and inflammatory and immune response and AS of genes associated with TRIF-dependent toll-like receptor signaling pathway and apoptotic process.

The upregulated genes associated with the inflammatory and immune response included *BMP6*, *SERPINA3*, *IL17B*, *IL1RN*, *HLA-B*, *PF4*, *HLA-DOB*, *MADCAM1*, and *HLA-DQA1*. Bone morphogenetic proteins (BMPs) are believed

to have complex roles in cancer progression.²⁰ Bentley et al. showed that BMP-6 was correlated with bone metastases in prostate cancer.²¹ Katsuta et al. found that a high expression of BMP6 was correlated with higher immune cell infiltration and better prognosis in estrogen receptor-positive breast cancer, whereas it was correlated with a worse prognosis in estrogen receptor-negative breast cancer.²² The expression of SERPINA3 has been detected in many tumor cells, including hepatocellular carcinoma, breast cancer, lung adenocarcinoma, and prostate cancer. Ko et al. indicated that SERPINA3 could promote hepatocellular carcinoma (HCC) cell survival and proliferation through upregulating the transcriptional activity of HNRNP-K.²³ Cao et al. demonstrated that the expression of SERPINA3 was higher in colon cancer tissues than in adjacent normal tissues, and silencing of SERPINA3 had significant effects on inhibiting the migration and invasion of colon cancer cells.²⁴ Recent studies have emphasized the potential role

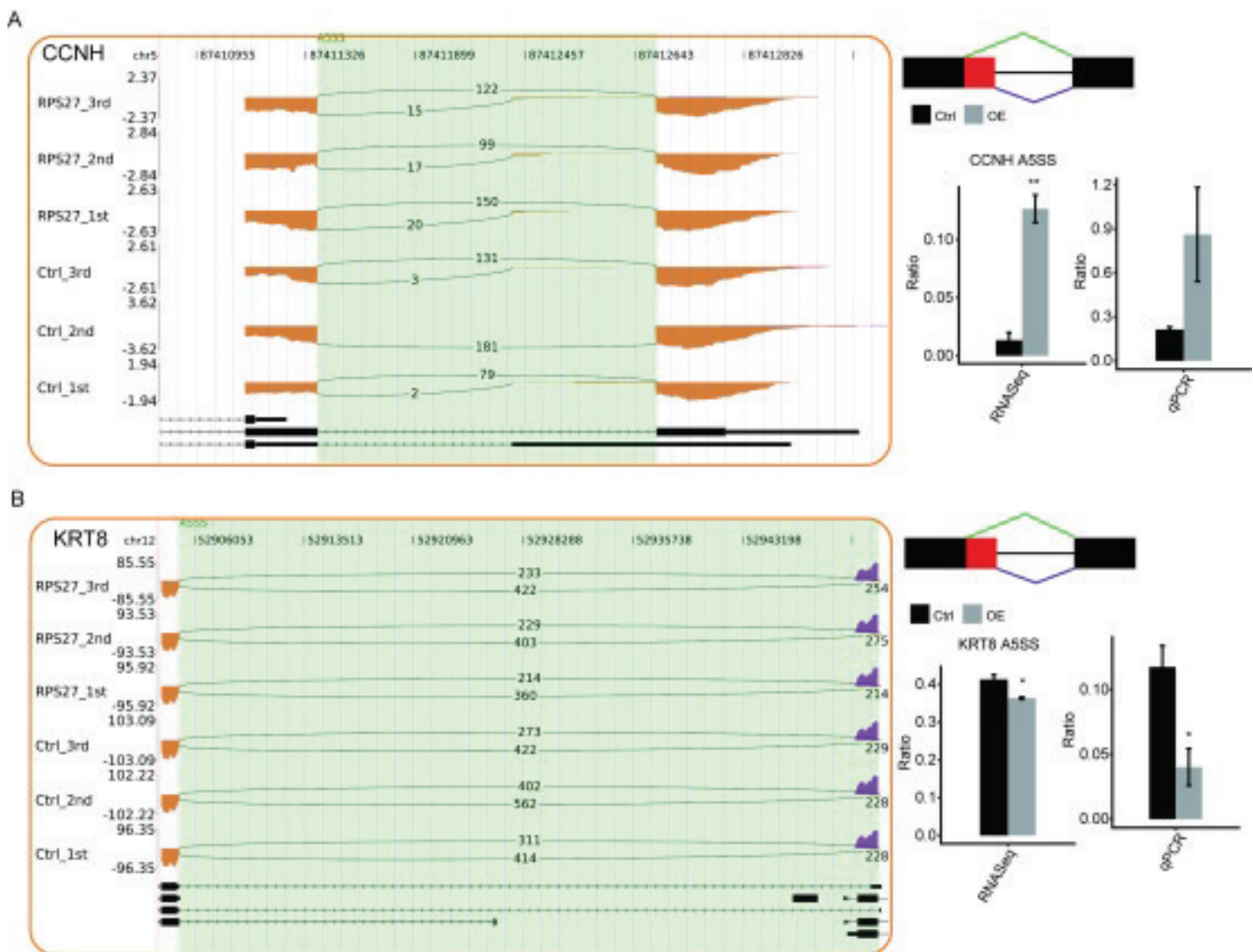


Fig. 6. Alternative splicing (AS) events of CCNH and KRT8 validated using quantitative real-time polymerase chain reaction (qRT-PCR) were highly consistent with the sequencing results

Control (Ctrl) – BHT101 cells without RPS27 overexpression; OE – BHT101 cells with RPS27 overexpression; A5SS – alternative 5' splice sites.

of the IL-17B/IL-RB pathway in cancer. The upregulated expression of IL-17B or its receptor has been correlated with a poor prognosis of various cancer types.^{25–27} In vitro cell assays demonstrate that IL-17B can promote the survival of breast cancer cells through enhancing the expression of anti-apoptotic Bcl-2 family members and activating the NF-κB and ERK pathways.^{28,29} In thyroid cancer, IL-17B is confirmed to be able to promote the growth, invasion and migration of cancer cells in a dose-dependent manner.³⁰ The *IL1RN* (interleukin-1 receptor antagonist) gene plays a role in the pathogenesis of many autoimmune diseases. The *IL1RN*(VNTR) polymorphism may be correlated with susceptibility for Hashimoto’s thyroiditis, a complex genetic autoimmune thyroid disease.³¹ The *IL1RN* polymorphisms are also associated with the susceptibility for cancers. Wang et al. found that *IL1RN* rs315919, rs452204 and rs3181052 polymorphisms were associated with a decreased risk of esophageal cancer in a Northwest Han Chinese population.³² Niedźwiecki et al. suggested that interleukin-1 receptor antagonist (IL-1ra) might have a critical

role in the development of anaplastic thyroid carcinoma and follicular thyroid carcinoma.³³ As a chemokine, platelet factor 4 (PF4, *CXCL4*) is involved in the pathogenesis of autoimmune thyroid diseases. Circulating PF4 levels are decreased in subclinically hypothyroid autoimmune thyroiditis (AIT).³⁴ Additionally, PF4 can regulate the inflammation within the tumor microenvironment, tumor angiogenesis, and, in turn, tumor growth.³⁵

The upregulated and downregulated DEGs were enriched in 166 and 211 pathways, respectively. Strikingly, the upregulated genes were associated with autoimmune thyroid disease, including *TPO*, *HLA-B*, *HLA-DQA1*, and *HLA-DOB*. The *TPO* plays a critical role in the production of thyroid hormones through catalyzing the iodination and coupling of tyrosyl residues to thyroglobulin.^{36,37} Many a study has investigated *TPO* as a marker for thyroid cancer. It is used as a thyroid differentiation marker,³⁶ and its expression is decreased in thyroid carcinoma.^{36,37} The human leukocyte antigen (*HLA*) gene is involved in the recognition and presentation of foreign antigens to the natural killer

cells (NK) and T lymphocytes, which is the starting point of the immune response.³⁸ This gene participates in tumor immunity and is a susceptibility gene for many cancers, including thyroid tumors.^{39,40} Some HLA alleles are risk factors for some tumors, whereas some have a protective role in tumorigenesis. Shuxian et al. showed that HLA-B*51:01 may be a susceptible allele for papillary thyroid carcinoma in the Chinese Han population of the Shandong coastal areas.⁴¹ The HLA-DQA1 is located on chromosome 6p21 and belongs to the MHC Class II family.⁴² It has a role in the progression of esophageal squamous-cell carcinoma (ESCC) and may be a biomarker for ESCC diagnosis and prognosis, as well as a potential target for the treatment of ESCC patients.⁴³ As the β -subunit of the HLA-DO class II paralogs, HLA-DOB has a negative regulation for major histocompatibility complex class II molecules through inhibiting HLA-DM molecules.⁴⁴ The DO:DM ratio defines major histocompatibility complex class II restricted-antigen presentation efficiency. Evidence has demonstrated that the dysregulation of the antigen presentation pathway has influence on development of cancer.⁴⁵ A report indicated that the single nucleotide polymorphism (SNP) of HLA-DOB rs2071554 was correlated with overall survival in patients with advanced non-small cell lung cancer treated with first-line chemotherapy.⁴⁶ Additionally, certain HLA-C alleles are also predisposing factors for papillary thyroid carcinoma.⁴⁷

Among the genes regulated by RPS27-mediated AS, some were enriched in “viral reproduction”, “TRIF-dependent toll-like receptor signaling pathway” and “MyD88-independent toll-like receptor signaling pathway”, including *HLA-C*, *KRT8*, *CFLAR*, *HMGAI*, *CASP8*, *CCNH*, *UBE2D3*, and *MAPK9*. Bromodomain-containing protein 4 (BRD4), belonging to the bromodomain and extra terminal domain family, has been reported to have important roles in various cancers. The abnormal expression of BRD4 is associated with tumor progression in thyroid cancer.⁴⁸ It can suppress tumor cell proliferation to inhibit the recruitment of BRD4 to the promoter complex of the *Ccnd1* and *Myc* genes in rat thyroid follicular PCCL3 cells.⁴⁹ In prostate cancer, the inhibition of BRD4 can suppress cell proliferation by regulating FOXO1-p21-Myc signaling.⁵⁰ In Merkel cell carcinoma, the disruption of BRD4 can inhibit MCC-3 xenograft tumor growth, possibly through downregulating c-Myc expression.⁵¹ Keratin8 (KRT8), the major component of the intermediate filament cytoskeleton, is correlated with progression and metastasis of several tumors. In gastric cancer, the abnormal expression of KRT8 can promote proliferation and migration of cancer cells through upregulating *MMP2*, *MMP9*, *PCNA*, and *TIMP1*.⁵² In lung adenocarcinoma, the expression of KRT8 is significantly elevated and may act as an independent prognostic factor for poor overall survival and recurrence-free survival.⁵³ In anaplastic thyroid carcinoma (ATC), the expression of KRT8 is upregulated, and upregulated KRT8 expression is critical for survival of ATC tumor

cells since siRNA-mediated knockdown of KRT8 expression leads to loss of cell viability and increased apoptosis in ATC-derived cells in vitro.⁵⁴ Mitogen-activated protein kinases (MAPKs) are associated with a large number of biological processes such as proliferation, differentiation, growth, migration, and apoptosis.⁵⁵ As a result, aberrant expression of MAPKs results in various diseases, including cancers.⁵⁶ The Mapk9, also named as JNK2, is a kinase from JNK subfamily. The function of JNK2 in cancers is still controversial. Several studies demonstrated that JNK2 acted as a tumor promoter in multiple myeloma, epidermal neoplasia, glioblastoma, breast cancer, and lung cancer.^{57–59} However, in bladder cancer and some lung and breast cancers, JNK2 appears to act as a suppressor.^{60,61} The high mobility group A1 (HMGA1) is an important member of superfamily of nonhistone chromatin binding proteins and plays a role in many cellular biology processes, such as embryogenesis, transcriptional regulation, viral integration, transformation, DNA repair, cell cycle regulation, and differentiation.⁶² The expression of HMGA1 is significantly upregulated in plenty of cancers, including thyroid, lung, colon, pancreas, breast, and ovary cancers.^{63–65} In addition, HMGA1 is confirmed to be correlated with high invasion and metastasis of thyroid cancer.^{65,66} The upregulated expression of HMGA1 can foster carcinogenesis and tumor progression via dysregulation of Wnt signaling and other developmental transcriptional networks.⁶⁷ Ubiquitin-conjugating enzyme E2D3 (UBE2D3) belongs to ubiquitin-conjugating enzyme (E2) family and is a critical component in ubiquitin (Ub) proteasome system (UPS).⁶⁸ Ubiquitin-dependent proteolysis by the 26S proteasome has a crucial role in the occurrence of tumors.⁶⁹ Guan et al. indicated that UBE2D3 might be a positive prognostic factor and might be associated with the expression of hTERT in esophageal cancer patients.⁷⁰ Additionally, the downregulation of UBE2D3 enhances radioresistance of esophageal cancer cells through prolonging IR-induced G2/M arrest and increasing telomere homeostasis,⁷¹ whereas its overexpression enhances radiosensitivity through degrading hTERT.⁷² Caspase 8 is an important component of the caspases family proteins that are the main regulatory and executive enzymes in the apoptosis pathway.⁷³ Apoptosis is associated with prevention from overproliferation in normal cells,⁷⁴ and the aberration of the apoptosis pathway is involved in the development of cancers.⁷⁵ Caspase 8 regulates the extrinsic apoptosis pathway,⁷⁶ and the *CASP8* -652 6N ins/del polymorphism is correlated with a decreased risk of various cancers.⁷⁷

The *CFLAR* gene encodes the apoptosis modulator protein c-FLIP, which has a critical role in regulating cell death.⁷⁸ One mechanism c-FLIP uses is forming heterodimers with caspase 8.⁷⁹ In HCC cells, the expression of *CFLAR* is significantly elevated, and the inhibition of *CFLAR* expression can reduce the proliferation of cancer cells.⁸⁰

In summary, the overexpression of RPS27 selectively regulated the expression and AS of inflammatory and immune response genes in thyroid cancer cells, whereas these genes had been confirmed to be involved in occurrence and development of cancer. Therefore, RPS27 was involved in the initiation and progression of thyroid cancer, possibly through regulating the expression of genes associated with autoimmune thyroid disease, and inflammatory and immune response and AS of genes associated with TRIF-dependent toll-like receptor signaling pathway and apoptotic process. These results broaden the current understanding on functions of RPS27 in the initiation and progression of thyroid cancer.

As for selection of cell lines, the objectives of this study were to investigate the carcinogenic mechanisms of RPS27 and functions of RPS27 in the initiation and progression of thyroid cancer, so selecting the normal cell line might not be enough. Meanwhile, we analyzed the expression of RPS27 in thyroid cancer through The Cancer Genome Atlas (TCGA). The results showed that the expression level of RPS27 in thyroid cancer tissues was not significantly different from normal tissues, but the upregulated expression of RPS27 in thyroid cancer tissues was associated with the prognosis of thyroid cancer patients. Therefore, we selected the BHT101 cells for this study.

Limitations

The limitations of this study mainly included 2 aspects. One aspect was that only a few DEGs and ASEs were validated through qRT-PCR, and the other aspect was that in vivo study was not performed.

Conclusions

THE RPS27 was involved in the initiation and progression of thyroid cancer, possibly through regulating the expression of genes associated with autoimmune thyroid disease and inflammatory and immune response, and the AS of genes associated with TRIF-dependent toll-like receptor signaling pathway and apoptotic process.

Data availability

The Supplementary Files are available at <https://doi.org/10.5281/zenodo.6324826>. The contents of the deposit are as follows:

Supplementary File 1. Primers used in qRT-PCR validation.

Supplementary File 2. Summary for RNA-seq reads used in this analysis.

Supplementary File 3. Robust expression results for 20,994 genes were obtained from RNA-seq data.

Supplementary File 4. The details of all the differentially expressed genes (DEGs).

Supplementary File 5. The upregulated differentially expressed genes (DEGs) were enriched in 44 GO terms.

Supplementary File 6. The downregulated differentially expressed genes (DEGs) were enriched in 112 Gene Ontology (GO) terms.

Supplementary File 7. The upregulated differentially expressed genes (DEGs) were enriched in 166 pathways.

Supplementary File 8. The downregulated differentially expressed genes (DEGs) were enriched in 211 pathways.

Supplementary File 9. There were 16,925 known alternative splicing events (ASEs) in the model gene which was termed as the reference genome.

Supplementary File 10. There were 45,772 novel alternative splicing events (ASEs) excluding intron retention events.


Supplementary File 11. Four hundred and one upregulated Regulated alternative splicing events (RASEs) were identified.

Supplementary File 12. Three hundred and thirty-four downregulated Regulated alternative splicing events (RASEs) were identified.

Supplementary File 13. Levene's test for equality of variances, Kolmogorov–Smirnov test and Student's t-test or Mann–Whitney U test.

ORCID iDs

Jing Wan  <https://orcid.org/0000-0002-3032-5047>

Juan Lv  <https://orcid.org/0000-0003-2758-4651>

Chun Wang  <https://orcid.org/0000-0002-0467-1093>

Li Zhang  <https://orcid.org/0000-0001-8541-0065>

References

- Harmer C. Foreword for special issue on thyroid cancer 2017. *Clin Oncol (R Coll Radiol)*. 2017;29(5):275. doi:10.1016/j.clon.2017.01.008
- Kim J, Gosnell JE, Roman SA. Geographic influences in the global rise of thyroid cancer. *Nat Rev Endocrinol*. 2020;16(1):17–29. doi:10.1038/s41574-019-0263-x
- Du L, Wang Y, Sun X, et al. Thyroid cancer: Trends in incidence, mortality and clinical-pathological patterns in Zhejiang province, South-east China. *BMC Cancer*. 2018;18(1):291. doi:10.1186/s12885-018-4081-7
- Galdiero MR, Varricchi G, Marone G. The immune network in thyroid cancer. *Oncoimmunology*. 2016;5(6):e1168556. doi:10.1080/2162402X.2016.1168556
- Ferrari SM, Fallahi P, Elia G, et al. Thyroid autoimmune disorders and cancer. *Semin Cancer Biol*. 2020;64:135–146. doi:10.1016/j.semcancer.2019.05.019
- Krátký J, Jiskra J. Autoimmune thyroiditis and thyroid cancer [in Czech]. *Vnitř Lek*. 2015;61(10):878–881. PMID:26486481.
- Feldheim J, Kessler AF, Schmitt D, et al. Ribosomal protein S27/metallopanstimulin-1 (RPS27) in glioma: A new disease biomarker? *Cancers (Basel)*. 2020;12(5):E1085. doi:10.3390/cancers12051085
- Revenkova E, Masson J, Koncz C, et al. Involvement of *Arabidopsis thaliana* ribosomal protein S27 in mRNA degradation triggered by genotoxic stress. *EMBO J*. 1999;18(2):490–499. doi:10.1093/emboj/18.2.490
- Zhou X, Liao WJ, Liao JM, et al. Ribosomal proteins: Functions beyond the ribosome. *J Mol Cell Biol*. 2015;7(2):92–104. doi:10.1093/jmcb/mjv014
- Atsuta Y, Aoki N, Sato K, et al. Identification of metallopanstimulin-1 as a member of a tumor associated antigen in patients with breast cancer. *Cancer Lett*. 2002;182(1):101–107. doi:10.1016/s0304-3835(02)00068-x
- Lee WJ, Keefer K, Hollenbeak CS, et al. A new assay to screen for head and neck squamous cell carcinoma using the tumor marker metallopanstimulin. *Otolaryngol Head Neck Surg*. 2004;131(4):466–471. doi:10.1016/j.otohns.2004.03.011

12. Wang YW, Qu Y, Li JF, et al. In vitro and in vivo evidence of metallopainstimulin-1 in gastric cancer progression and tumorigenicity. *Clin Cancer Res*. 2006;12(16):4965–4973. doi:10.1158/1078-0432.CCR-05-2316
13. Floristán A, Morales L, Hanniford D, et al. Functional analysis of RPS27 mutations and expression in melanoma. *Pigment Cell Melanoma Res*. 2020;33(3):466–479. doi:10.1111/pcmr.12841
14. Kim D, Pertea G, Trapnell C, et al. TopHat2: Accurate alignment of transcriptomes in the presence of insertions, deletions and gene fusions. *Genome Biol*. 2013;14(4):R36. doi:10.1186/gb-2013-14-4-r36
15. Trapnell C, Williams BA, Pertea G, et al. Transcript assembly and quantification by RNA-Seq reveals unannotated transcripts and isoform switching during cell differentiation. *Nat Biotechnol*. 2010;28(5):511–515. doi:10.1038/nbt.1621
16. Xia H, Chen D, Wu Q, et al. CELF1 preferentially binds to exon-intron boundary and regulates alternative splicing in HeLa cells. *Biochim Biophys Acta Gene Regul Mech*. 2017;1860(9):911–921. doi:10.1016/j.bbagr.2017.07.004
17. Robinson MD, McCarthy DJ, Smyth GK. edgeR: A bioconductor package for differential expression analysis of digital gene expression data. *Bioinformatics*. 2010;26(1):139–140. doi:10.1093/bioinformatics/btp616
18. Xie C, Mao X, Huang J, et al. KOBAS 2.0: A web server for annotation and identification of enriched pathways and diseases. *Nucleic Acids Res*. 2011;39(Web Server issue):W316–W322. doi:10.1093/nar/gkr483
19. Nafelberg S, Schor IE, Ast G, et al. Regulation of alternative splicing through coupling with transcription and chromatin structure. *Annu Rev Biochem*. 2015;84:165–198. doi:10.1146/annurev-biochem-060614-034242
20. Guo X, Wang XF. Signaling cross-talk between TGF- β /BMP and other pathways. *Cell Res*. 2009;19(1):71–88. doi:10.1038/cr.2008.302
21. Bentley H, Hamdy FC, Hart KA, et al. Expression of bone morphogenetic proteins in human prostatic adenocarcinoma and benign prostatic hyperplasia. *Br J Cancer*. 1992;66(6):1159–1163. doi:10.1038/bjc.1992.427
22. Katsuta E, Maawy AA, Yan L, et al. High expression of bone morphogenetic protein (BMP) 6 and BMP7 are associated with higher immune cell infiltration and better survival in estrogen receptor-positive breast cancer. *Oncol Rep*. 2019;42(4):1413–1421. doi:10.3892/or.2019.7275
23. Ko E, Kim JS, Bae JW, et al. SERPINA3 is a key modulator of HNRNP-K transcriptional activity against oxidative stress in HCC. *Redox Biol*. 2019;24:101217. doi:10.1016/j.redox.2019.101217
24. Cao LL, Pei XF, Qiao X, et al. SERPINA3 silencing inhibits the migration, invasion, and liver metastasis of colon cancer cells. *Dig Dis Sci*. 2018;63(9):2309–2319. doi:10.1007/s10620-018-5137-x
25. Yang YF, Lee YC, Lo S, et al. A positive feedback loop of IL-17B-IL-17RB activates ERK/ β -catenin to promote lung cancer metastasis. *Cancer Lett*. 2018;422:44–55. doi:10.1016/j.canlet.2018.02.037
26. Al-Samadi A, Moossavi S, Salem A, et al. Distinctive expression pattern of interleukin-17 cytokine family members in colorectal cancer. *Tumour Biol*. 2016;37(2):1609–1615. doi:10.1007/s13277-015-3941-x
27. Leivonen SK, Pollari M, Brück O, et al. T-cell inflamed tumor microenvironment predicts favorable prognosis in primary testicular lymphoma. *Haematologica*. 2019;104(2):338–346. doi:10.3324/haematol.2018.200105
28. Laprevotte E, Cochaud S, du Manoir S, et al. The IL-17B-IL-17 receptor B pathway promotes resistance to paclitaxel in breast tumors through activation of the ERK1/2 pathway. *Oncotarget*. 2017;8(69):113360–113372. doi:10.18632/oncotarget.23008
29. Huang CK, Yang CY, Jeng YM, et al. Autocrine/paracrine mechanism of interleukin-17B receptor promotes breast tumorigenesis through NF- κ B-mediated antiapoptotic pathway. *Oncogene*. 2014;33(23):2968–2977. doi:10.1038/ncr.2013.268
30. Ren L, Xu Y, Liu C, et al. IL-17RB enhances thyroid cancer cell invasion and metastasis via ERK1/2 pathway-mediated MMP-9 expression. *Mol Immunol*. 2017;90:126–135. doi:10.1016/j.molimm.2017.06.034
31. Zaaber I, Mestiri S, Marmouch H, et al. Polymorphisms in *TSHR* and *IL1RN* genes and the risk and prognosis of Hashimoto's thyroiditis. *Autoimmunity*. 2014;47(2):113–118. doi:10.3109/08916934.2013.866101
32. Wang T, Feng Y, Zhao Z, et al. IL1RN polymorphisms are associated with a decreased risk of esophageal cancer susceptibility in a Chinese population. *Chemotherapy*. 2019;64(1):28–35. doi:10.1159/000496400
33. Niedźwiecki S, Stepień T, Kuzdak K, et al. Serum levels of interleukin-1 receptor antagonist (IL-1ra) in thyroid cancer patients. *Langenbecks Arch Surg*. 2008;393(3):275–280. doi:10.1007/s00423-007-0251-9
34. Görar S, Ademoğlu E, Çarlıoğlu A, et al. Low levels of circulating platelet factor 4 (PF4, CXCL4) in subclinically hypothyroid autoimmune thyroiditis. *J Endocrinol Invest*. 2016;39(2):185–189. doi:10.1007/s40618-015-0348-x
35. Pilatova K, Greplova K, Demlova R, et al. Role of platelet chemokines, PF-4 and CTAP-III, in cancer biology. *J Hematol Oncol*. 2013;6:42. doi:10.1186/1756-8722-6-42
36. Caballero Y, López-Tomassetti EM, Favre J, et al. The value of thyroperoxidase as a prognostic factor for differentiated thyroid cancer: A long-term follow-up study. *Thyroid Res*. 2015;8:12. doi:10.1186/s13044-015-0022-6
37. Huang L, Wang X, Huang X, et al. Diagnostic significance of CK19, galectin-3, CD56, TPO and Ki67 expression and BRAF mutation in papillary thyroid carcinoma. *Oncol Lett*. 2018;15(4):4269–4277. doi:10.3892/ol.2018.7873
38. Robinson J, Halliwell JA, McWilliam H, et al. The IMGT/HLA database. *Nucleic Acids Res*. 2013;41(Database issue):D1222–D1227. doi:10.1093/nar/gks949
39. Ahn S, Choi HB, Kim TG. HLA and disease associations in Koreans. *Immune Netw*. 2011;11(6):324–335. doi:10.4110/in.2011.11.6.324
40. Amoli MM, Yazdani N, Amiri P, et al. HLA-DR association in papillary thyroid carcinoma. *Dis Markers*. 2010;28(1):49–53. doi:10.3233/DMA-2010-0683
41. Shuxian J, Xiaoyun C, Zhihui F, et al. Association of HLA-B*51:01 with papillary thyroid carcinoma in the Chinese Han population of the Shandong coastal areas. *Thyroid*. 2014;24(5):867–871. doi:10.1089/thy.2013.0130
42. Wu C, Wang Z, Song X, et al. Joint analysis of three genome-wide association studies of esophageal squamous cell carcinoma in Chinese populations. *Nat Genet*. 2014;46(9):1001–1006. doi:10.1038/ng.3064
43. Shen FF, Pan Y, Li JZ, et al. High expression of HLA-DQA1 predicts poor outcome in patients with esophageal squamous cell carcinoma in Northern China. *Medicine (Baltimore)*. 2019;98(8):e14454. doi:10.1097/MD.00000000000014454
44. Denzin LK, Sant'Angelo DB, Hammond C, et al. Negative regulation by HLA-DO of MHC class II-restricted antigen processing. *Science*. 1997;278(5335):106–109. doi:10.1126/science.278.5335.106
45. Seliger B. Different regulation of MHC class I antigen processing components in human tumors. *J Immunotoxicol*. 2008;5(4):361–367. doi:10.1080/15476910802482870
46. Pu X, Hildebrandt MA, Lu C, et al. Inflammation-related genetic variations and survival in patients with advanced non-small cell lung cancer receiving first-line chemotherapy. *Clin Pharmacol Ther*. 2014;96(3):360–369. doi:10.1038/clpt.2014.89
47. Haghpanah V, Khalooghi K, Adabi K, et al. Associations between HLA-C alleles and papillary thyroid carcinoma. *Cancer Biomark*. 2009;5(1):19–22. doi:10.3233/CBM-2009-0564
48. Gao X, Wu X, Zhang X, et al. Inhibition of BRD4 suppresses tumor growth and enhances iodine uptake in thyroid cancer. *Biochem Biophys Res Commun*. 2016;469(3):679–685. doi:10.1016/j.bbrc.2015.12.008
49. Zhu X, Enomoto K, Zhao L, et al. Bromodomain and extraterminal protein inhibitor JQ1 suppresses thyroid tumor growth in a mouse model. *Clin Cancer Res*. 2017;23(2):430–440. doi:10.1158/1078-0432.CCR-16-0914
50. Tan Y, Wang L, Du Y, et al. Inhibition of BRD4 suppresses tumor growth in prostate cancer via the enhancement of FOXO1 expression. *Int J Oncol*. 2018;53(6):2503–2517. doi:10.3892/ijo.2018.4577
51. Sengupta D, Kannan A, Kern M, et al. Disruption of BRD4 at H3K27Ac-enriched enhancer region correlates with decreased c-Myc expression in Merkel cell carcinoma. *Epigenetics*. 2015;10(6):460–466. doi:10.1080/15592294.2015.1034416
52. Fang J, Wang H, Liu Y, et al. High KRT8 expression promotes tumor progression and metastasis of gastric cancer. *Cancer Sci*. 2017;108(2):178–186. doi:10.1111/cas.13120
53. Xie L, Dang Y, Guo J, et al. High KRT8 expression independently predicts poor prognosis for lung adenocarcinoma patients. *Genes (Basel)*. 2019;10(1):36. doi:10.3390/genes10010036
54. Guo D, Xu Q, Pabla S, et al. Cytokeratin-8 in anaplastic thyroid carcinoma: More than a simple structural cytoskeletal protein. *Int J Mol Sci*. 2018;19(2):577. doi:10.3390/ijms19020577

55. Dhillon AS, Hagan S, Rath O, et al. MAP kinase signalling pathways in cancer. *Oncogene*. 2007;26(22):3279–3290. doi:10.1038/sj.onc.1210421
56. Bubici C, Papa S. JNK signalling in cancer: In need of new, smarter therapeutic targets. *Br J Pharmacol*. 2014;171(1):24–37. doi:10.1111/bph.12432
57. Barbarulo A, Iansante V, Chaidos A, et al. Poly(ADP-ribose) polymerase family member 14 (PARP14) is a novel effector of the JNK2-dependent pro-survival signal in multiple myeloma. *Oncogene*. 2013;32(36):4231–4242. doi:10.1038/onc.2012.448
58. Nitta RT, Del Vecchio CA, Chu AH, et al. The role of the c-Jun N-terminal kinase 2- α -isoform in non-small cell lung carcinoma tumorigenesis. *Oncogene*. 2011;30(2):234–244. doi:10.1038/onc.2010.414
59. Cantrell MA, Ebel ND, Pfefferle AD, et al. c-Jun N-terminal kinase 2 prevents luminal cell commitment in normal mammary glands and tumors by inhibiting p53/Notch1 and breast cancer gene 1 expression. *Oncotarget*. 2015;6(14):11863–11881. doi:10.18632/oncotarget.3787
60. Cellurale C, Weston CR, Reilly J, et al. Role of JNK in a Trp53-dependent mouse model of breast cancer. *PLoS One*. 2010;5(8):e12469. doi:10.1371/journal.pone.0012469
61. Pan CW, Liu H, Zhao Y, et al. JNK2 downregulation promotes tumorigenesis and chemoresistance by decreasing p53 stability in bladder cancer. *Oncotarget*. 2016;7(23):35119–35131. doi:10.18632/oncotarget.9046
62. Resar LM. The high mobility group A1 gene: Transforming inflammatory signals into cancer? *Cancer Res*. 2010;70(2):436–439. doi:10.1158/0008-5472.CAN-09-1212
63. Shah SN, Cope L, Poh W, et al. HMGA1: A master regulator of tumor progression in triple-negative breast cancer cells. *PLoS One*. 2013;8(5):e63419. doi:10.1371/journal.pone.0063419
64. Belton A, Gabrovsky A, Bae YK, et al. HMGA1 induces intestinal polyposis in transgenic mice and drives tumor progression and stem cell properties in colon cancer cells. *PLoS One*. 2012;7(1):e30034. doi:10.1371/journal.pone.0030034
65. Chiappetta G, Tallini G, De Biasio MC, et al. Detection of high mobility group 1 HMGI(Y) protein in the diagnosis of thyroid tumors: HMGI(Y) expression represents a potential diagnostic indicator of carcinoma. *Cancer Res*. 1998;58(18):4193–4198. PMID:9751634.
66. Zhong J, Liu C, Zhang QH, et al. TGF- β 1 induces HMGA1 expression: The role of HMGA1 in thyroid cancer proliferation and invasion. *Int J Oncol*. 2017;50(5):1567–1578. doi:10.3892/ijo.2017.3958
67. Resar L, Chia L, Xian L. Lessons from the crypt: HMGA1-amping up Wnt for stem cells and tumor progression. *Cancer Res*. 2018;78(8):1890–1897. doi:10.1158/0008-5472.CAN-17-3045
68. Wu K, Kovacev J, Pan ZQ. Priming and extending: A UbcH5/Cdc34 E2 handoff mechanism for polyubiquitination on a SCF substrate. *Mol Cell*. 2010;37(6):784–796. doi:10.1016/j.molcel.2010.02.025
69. Kraus WE, Muoio DM, Stevens R, et al. Metabolomic quantitative trait loci (mQTL) mapping implicates the ubiquitin proteasome system in cardiovascular disease pathogenesis. *PLoS Genet*. 2015;11(11):e1005553. doi:10.1371/journal.pgen.1005553
70. Guan GG, Wang WB, Lei BX, et al. UBE2D3 is a positive prognostic factor and is negatively correlated with hTERT expression in esophageal cancer. *Oncol Lett*. 2015;9(4):1567–1574. doi:10.3892/ol.2015.2926
71. Yang H, Wu L, Ke S, et al. Downregulation of ubiquitin-conjugating enzyme UBE2D3 promotes telomere maintenance and radioresistance of Eca-109 human esophageal carcinoma cells. *J Cancer*. 2016;7(9):1152–1162. doi:10.7150/jca.14745
72. Gao X, Wang W, Yang H, et al. UBE2D3 gene overexpression increases radiosensitivity of EC109 esophageal cancer cells in vitro and in vivo. *Oncotarget*. 2016;7(22):32543–32553. doi:10.18632/oncotarget.8869
73. Yu J, Zhang L, Hwang PM, et al. PUMA induces the rapid apoptosis of colorectal cancer cells. *Mol Cell*. 2001;7(3):673–682. doi:10.1016/s1097-2765(01)00213-1
74. Hengartner MO. The biochemistry of apoptosis. *Nature*. 2000;407(6805):770–776. doi:10.1038/35037710
75. Thompson CB. Apoptosis in the pathogenesis and treatment of disease. *Science*. 1995;267(5203):1456–1462. doi:10.1126/science.7878464
76. Tummers B, Green DR. Caspase-8: Regulating life and death. *Immunol Rev*. 2017;277(1):76–89. doi:10.1111/imr.12541
77. Cai J, Ye Q, Luo S, et al. CASP8-652 6N insertion/deletion polymorphism and overall cancer risk: Evidence from 49 studies. *Oncotarget*. 2017;8(34):56780–56790. doi:10.18632/oncotarget.18187
78. Faiz A, Heijink IH, Vermeulen CJ, et al. Cigarette smoke exposure decreases CFLAR expression in the bronchial epithelium, augmenting susceptibility for lung epithelial cell death and DAMP release. *Sci Rep*. 2018;8(1):12426. doi:10.1038/s41598-018-30602-7
79. Ueffing N, Singh KK, Christians A, et al. A single nucleotide polymorphism determines protein isoform production of the human c-FLIP protein. *Blood*. 2009;114(3):572–579. doi:10.1182/blood-2009-02-204230
80. Wang Y, Zhao YR, Zhang AY, et al. Targeting of miR-20a against CFLAR to potentiate TRAIL-induced apoptotic sensitivity in HepG2 cells. *Eur Rev Med Pharmacol Sci*. 2017;21(9):2087–2097. PMID:28537677.

Arsenic trioxide induces the differentiation of retinoic acid-resistant neuroblastoma cells via upregulation of *HoxC9*

Chunmou Li^{1,B–D}, Chuchu Feng^{1,B,D}, Yantao Chen^{2,B,C}, Pingping Wu^{1,B,D},
Peng Li^{3,B,C}, Xilin Xiong^{1,B,C}, Xiaomin Peng^{1,B}, Zhixuan Wang^{1,C}, Yang Li^{1,A,E,F}

¹ Pediatric Hematology/Oncology, Children's Medical Center, Sun Yat-Sen Memorial Hospital, Sun Yat-Sen University, Guangzhou, China

² Department of Orthopaedics, Sun Yat-Sen Memorial Hospital, Sun Yat-Sen University, Guangzhou, China

³ Key Laboratory of Regenerative Biology, South China Institute for Stem Cell Biology and Regenerative Medicine, Guangzhou Institutes of Biomedicine and Health, Chinese Academy of Sciences, China

A – research concept and design; B – collection and/or assembly of data; C – data analysis and interpretation; D – writing the article; E – critical revision of the article; F – final approval of the article

Advances in Clinical and Experimental Medicine, ISSN 1899–5276 (print), ISSN 2451–2680 (online)

Adv Clin Exp Med. 2022;31(8):903–911

Address for correspondence

Yang Li
E-mail: drliyang@126.com

Funding sources

Grants No. 2017A030313806 and No. 2020A1515010127 from the Guang Dong Natural Science Foundation, and grant No. SYS-C-202007 from Sun Yat-Sen Clinical Research Cultivating Program.

Conflict of interest

None declared

Received on December 4, 2021

Reviewed on December 13, 2021

Accepted on March 18, 2022

Published online on April 25, 2022

Cite as

Li C, Feng C, Chen Y, et al. Arsenic trioxide induces the differentiation of neuroblastoma cells with retinoic acid-resistant via upregulation of *HoxC9*. *Adv Clin Exp Med*. 2022;31(8):903–911. doi:10.17219/acem/147463

DOI

10.17219/acem/147463

Copyright

Copyright by Author(s)

This is an article distributed under the terms of the Creative Commons Attribution 3.0 Unported (CC BY 3.0) (<https://creativecommons.org/licenses/by/3.0/>)

Abstract

Background. Neuroblastoma (NB) is one of the most common extracranial tumors with limited therapeutic options. Retinoic acid (RA) has been identified to play anticancer role against NB cells by inducing the differentiation and apoptosis of immature neuroblasts. However, silencing *HoxC9* promoter by *EZH2*-induced H3K27me3 hypermethylation can lead to RA resistance. Previous studies have suggested that arsenic trioxide (ATO), an inhibitor of DNA methylation, could downregulate the expression of *EZH2* in breast cancer cells.

Objectives. In our study, we attempted to obtain some insight into the mechanisms of differentiation of RA-resistant NB cells by detecting the expressions of *HoxC9* and *EZH2* in NB cells treated with ATO, so as to provide a basis for the subsequent treatment of RA-resistant NB by ATO.

Materials and methods. Two NB cell lines, SK-N-AS (retinoic acid-resistant neuroblastoma cells) and SK-N-SH (retinoic acid-sensitive neuroblastoma cells), were used in our experiments. Cell proliferation and apoptosis were respectively determined with Cell Counting Kit-8 (CCK-8) assay kit and Annexin V staining. The inverted phase contrast microscope was used to observe cell growth and measure the total length of nerve synapses. We employed label-free quantitative proteomic analysis to profile ATO-dependent changes in the proteome of NB cells. Western blot was used to detect the expressions of *HoxC9*, *HoxD8* and *EZH2*.

Results. Arsenic trioxide inhibited the cell proliferation and increased apoptosis and total length of synapses in two NB cell lines. The expressions of *HoxC9* and *HoxD8* were upregulated, while the expression of *EZH2* was downregulated in the SK-N-AS cell line. No significant changes in the 3 proteins mentioned above were observed in the SK-N-SH cell line after ATO treatment.

Conclusions. Arsenic trioxide may reactivate the expression of *HoxC9* by downregulating *EZH2*, which leads to restoring RA sensitivity and promoting the differentiation and apoptosis of RA-resistant NB cells.

Key words: neuroblastoma, arsenic trioxide, retinoic acid resistance, *EZH2* gene, *HoxC9* promoter

Background

Neuroblastoma (NB), which results from the improper differentiation of neural crest progenitors, is the 2nd most frequent extracranial pediatric cancer,¹ accounting for about 10% of all malignancies in children and 15% of all cancer-related deaths in this population.^{2,3} Although new treatment options constantly emerge over the past years, the long-term overall survival (OS) of high-risk NB is still below 50%.⁴

Retinoic acid (RA) can modulate the expression of its target genes in order to regulate the differentiation, apoptosis and proliferation in numerous types of cells.^{5,6} As an effective inducer of cell differentiation, RA has been used for the treatment of high-risk NB.^{7,8} Thus, RA-resistant NB may significantly contribute to minimal residual disease during RA maintenance therapy, even with more than 50% of the patients developing recurrent disease.⁹ Patients with relapsed or refractory NB have, in general, poor prognosis and more than 60% of them will eventually die due to deteriorating health conditions within a few years.^{10,11}

Homeobox (*Hox*) genes are well known for their ability to regulate embryogenesis and induce tissue differentiation.¹² It is currently assumed that *HoxC9* can activate the intrinsic pathway of apoptosis and is associated with spontaneous regression in NB.^{13,14} The expression of *HoxC9*-induced genes can significantly downregulate the oncogenic marker paired-like homeobox 2b (PHOX2B) in BE(2)-C and other NB cells, and upregulate the neuronal differentiation markers, like neurofilament medium (NEFM) and microtubule-associated protein 2 (MAP2).¹⁴ The NEFM has been confirmed to be the target gene of *HoxC9*, and *HoxC9* was confirmed to be a direct target gene of *HoxD8*.^{14,15} However, to the best of our knowledge, the expression of *Hox* genes was not observed in RA-resistant NB cells during retinoic acid-therapy.¹⁴ In addition, zeste homolog 2 (*EZH2*), as a methyltransferase, can extend gene silencing of *Hox* genes by trimethylating histone H3 lysine 27 (H3K27me3) in NB cells.^{16–18}

Arsenic trioxide (ATO) is an ancient drug from China which currently entered the clinical arena as a Food and Drug Administration (FDA)-approved drug for the treatment of acute promyelocytic leukemia (APL).^{19,20} One study has suggested that ATO could significantly upregulate *HoxB8* in both mRNA and protein levels during hematopoietic stem cell (HSC) differentiation into the colony forming unit-granulocyte (CFU-G).²¹ As a methylation inhibitor, ATO could also provoke the expression or reactivation of tumor suppressor genes (*GSTP1*, *RASSF1A*, etc.) with CpG islands demethylation by suppressing DNA methyltransferases (DNMT) in liver cancer.²²

Objectives

In our study, we detected the expressions of *Hox* genes and *EZH2* in RA-resistant NB cells to elucidate whether ATO could reactivate the expression of *HoxC9*

by downregulating *EZH2*, leading to the restoration of RA sensitivity and promotion of the differentiation and apoptosis of RA-resistant NB cells. With this experimental setup, we attempt to provide a novel therapeutic intervention for NB patients with RA-resistant feature.

Materials and methods

Materials

Dulbecco's modified Eagle's medium (DMEM) and heat-inactivated fetal bovine serum (FBS) were purchased from Gibco (Waltham, USA). Arsenic trioxide was purchased from Harbin Yida Pharmaceutical Co., Ltd. (Harbin, China). Cell Counting Kit-8 Assay (CCK-8) was purchased from APEX BIO (Houston, USA). Annexin V-FITC Apoptosis Detection Kit (Annexin V-FITC/PI) was purchased from Beyotime Biotechnology (Beijing, China). The BCA kit was purchased from Beyotime Biotechnology. Anti-*HoxC9*, anti-*HoxD8* and anti-*EZH2* antibodies were purchased from Abcam (Cambridge, UK). The horseradish peroxidase (HRP)-linked whole antibody anti-mouse immunoglobulin G (IgG) was purchased from Cell Signaling Technology (CST, Darmstadt, Germany). The protein markers were purchased from Thermo Fisher Scientific (Waltham, USA). The Click-it EdU Alexa Fluor 488 Flow Cytometry Assay was purchased from Invitrogen (Waltham, USA). All procedures were performed according to the manufacturers' protocols.

Cell cultures

For this study, we chose 2 human NB cell lines for culture: SK-N-AS (retinoic acid-resistant neuroblastoma cells) and SK-N-SH (retinoic acid-sensitive neuroblastoma cells), both obtained from the Sun Yat-Sen University (Guangzhou, China). Cell line authentication to confirm genomic identity was performed and the continual tests of mycoplasma contamination were run after each thaw. Both cell lines were cultured in DMEM (with 10% FBS and 1% penicillin-streptomycin) at 37°C in a 5% CO₂ incubator. After growing as a monolayer and multilayers with 70–80% confluence in T75 cell culture flasks with 15 mL of media, the cells were adjusted at a density of 1 × 10⁴/mL and then transferred to a 96-well plate.

Cytotoxicity assay

The CCK-8 assay was used to detect cell cytotoxicity. Both cell lines were seeded in 96-well plates with 1000 cells (1 × 10⁴/mL; 100 μL) per well separately. Arsenic trioxide treatment was performed in triplicate 24 h later. Based on our previous experience, the 50% inhibitory concentration of ATO (IC₅₀_{ATO}) value of NB cells was set at 2–128 μM for 24 h. Thus, we chose the ATO

concentrations of 1–256 μM for this experiment. The cells, drugs, medium, and CCK-8 reagent were contained in experimental wells; control wells set with the cells, medium and CCK-8 reagent; blank control contained no cells. After incubation for 60 min in the dark, the optical density (OD) value was measured at a 450 nm wavelength using a microplate reader (SpectraMax Plus 384; Molecular Devices, Sunnyvale, USA), and the relative viability was calculated as follows:

the relative viability = [(experimental absorbance – background absorbance)/(untreated control absorbance – background absorbance)] \times 100%.

In our experiment, to assess the effect of ATO on NB cells differentiation, the synaptic growth was chosen as a representative feature. After both cell lines were cultured with ATO for 24 h in IC50 (95.36 μM in SK-N-AS, 5.52 μM in SK-N-SH), apoptotic NB cells became round and suspended. Thus, we reduced the concentration of ATO and tried to find a proper one in order to obtain a better observation result of synapses. To achieve this purpose, we cultured them with their $1/2$ IC50 (48 μM in SK-N-AS cells, 2.7 μM in SK-N-SH cells), $1/3$ IC50 (32 μM in SK-N-AS, 1.9 μM in SK-N-SH), $1/6$ IC50 (16 μM in SK-N-AS, 0.9 μM in SK-N-SH), and $1/12$ IC50 (8 μM in SK-N-AS, 0.5 μM in SK-N-SH) concentrations to find out the optimal one by comparison.

Cell morphology

Both cell lines in the logarithmic growth phase were seeded in 6-well microplates (6×10^5 cells/well) as a single-cell suspension and cultured for 24 h to attach to the plate. Then, they were treated with or without ATO and grown in DMEM with 10% FBS and 1% penicillin-streptomycin for 24 h at 37°C in a 5% CO₂ cell culture incubator (HERA Cell 240i; Thermo Fisher Scientific). To avoid the interference of apoptosis on the observation of differentiation, by comparison, $1/6$ IC50 concentration (16 μM) of SK-N-AS cells and $1/2$ IC50 concentration (2.7 μM) of SK-N-SH cells were chosen for observation of cell morphology. After 24-hour treatment with or without ATO (the cells were adherent to walls at this time), we used inverted phase contrast microscopy (DP50 digital camera; Olympus Corp., Tokyo, Japan) to evaluate the cellular morphological changes. The length of neurites was tallied using the ImageJ program v. 1.51 (National Institutes of Health (NIH), Bethesda, USA) with the assistance of the NeuronJ Plugin, which can provide semi-automated tracing.

Apoptosis assay

We used flow cytometry (FCM) assay purchased from Invitrogen to conduct the apoptosis assay. The experiment was carried out in accordance with the manufacturer's instructions. After the treatment with ATO, trypsinization was used to harvest the cells, which were

then collected by centrifugation at 1000 rpm for 5 min. The cells were rinsed in PBS once more before the collection by centrifugation.

The both collected cell lines were suspended in 400 μL Ca²⁺ Binding Buffer (Abcam) and split equally into 2 tubes. One tube was supplemented with 5 μL of fluorescein isothiocyanate (FITC) reagents, and the other one was used as a blank control group without any treatment. Then, 10 μL of propidium iodide (PI) dyes were applied to each sample and the samples were incubated at room temperature for 15 min in the dark.

Two different markers (FITC conjugated to Annexin V as an apoptotic cell marker and PI as a dead cell marker) were contained in Annexin V-FITC/PI Apoptosis Detection Assay Kit (Invitrogen). In this test, the ratio of fluorescence intensities excited at 488 nm was monitored at an emission wavelength of 515 nm for FITC and 560 nm for PI. Apoptotic cells were collected and at least 10,000 cells were counted for all FCM experiments to ensure the accuracy. The experiment was repeated in triplicate.

Phosphoproteomic analysis

Both cell lines in the logarithmic growth phase were processed to single-cell suspension and cultured in 15-centimeter cell culture dishes ($2 \times 10^6/\text{mL}$, 20 mL). Cells were incubated using the method described in the cell morphology subsection. After the cells adhered to the walls of the dishes, they were treated with or without ATO for 24 h, and then collected for measuring protein abundances with mass spectroscopy analysis at PTM Biolabs, Inc. (Hangzhou, China).

Protein extraction

All operations were carried out on ice. The cells were sonicated 3 times with a high-intensity ultrasonic processor (SCIENTZ-1200E; Ningbo Scientz Biotechnology Co., Ltd., Ningbo, China) in lysis buffer (8 M urea and 1% Protease Inhibitor Cocktail; Roche, Basel, Switzerland). The supernatant was collected after centrifugation at $12,000 \times g$ for 10 min at 4°C (in order to remove the residual debris). The BCA kit was then used to determine the protein content.

Trypsin digestion

The protein solution was alkylated with 11 mM iodoacetamide for 15 min at room temperature in darkness after being reduced with 5 mM dithiothreitol for 30 min at 56°C. The protein sample was then diluted with 100 mM triethylammonium bicarbonate (TEAB) to achieve a lower urea content (less than 2 M). Following the aforementioned process, trypsin was introduced at a 1:50 trypsin-to-protein mass ratio for the 1st overnight digestion, and a 1:100 trypsin-to-protein mass ratio for the 2nd 4-hour digestion.

Mass spectroscopy analysis

The tryptic peptides were separated using an EASY-nLC 1000 UPLC machine (Thermo Fisher Scientific) after being dissolved in 0.1 percent formic acid (solvent A; Thermo Fisher Scientific). The peptides were evaluated using tandem mass spectroscopy (MS) in Q Exactive™ Plus mass spectrometer (Thermo Fisher Scientific) linked online to the ultra-performance liquid chromatography (UPLC) with the nanospray ionization source. The pieces were identified in the Orbitrap (Thermo Fisher Scientific) at 17,500 resolutions using a normalized collision energy value of 28 for UPLC-tandem mass spectrometry (UPLC-MS/MS). One MS scan was followed by 20 MS/MS scans with 15.0 s dynamic exclusion in a data-dependent method. Automatic gain control (AGC) was set to 5E4 (automatic gain control); 100 m/z was chosen as the fixed initial mass.

Database search

The MS/MS data were analyzed using the Maxquant search engine v. 1.5.2.8 (<https://www.maxquant.org/>). Tandem mass spectra were compared to the Uniprot Human database (<https://www.uniprot.org/>), which was combined with the reverse decoy database (unip_Anas_8839 database). Trypsin/P was chosen as the cleavage enzyme, allowing for up to 4 missed cleavages. The mass tolerance for precursor ions was set to 20 ppm in the First search and 5 ppm in the Main search. Additionally, the mass tolerance for fragment ions was set to 0.02 Da. Carbamidomethylation on cysteine (Cys) was designated as a fixed modification, whereas acetylation and oxidation on methionine (Met) were designated as variable modifications. False discovery rate (FDR) was adjusted to <1% and a score greater than 40 was set for modified peptides.

Bioinformatics methods

The Gene Ontology (GO) annotation covers cellular composition (CC), molecular function (MF) and biological process (BP), and it is applied for bioinformatics analysis by evaluating differentially expressed genes (DEGs) and associated gene modules, based on the substantial enrichment of GO functions. The UniProt-GOA database (<http://www.ebi.ac.uk/GOA/>) was used for the GO annotation proteome by identifying protein IDs, converting them to UniProt IDs, and then mapping them to GO IDs by protein ID. If any of the proteins were not annotated by the UniProt-GOA database, the InterProScan online software (<http://www.ebi.ac.uk/InterProScan/>) was used as a substitute method based on protein sequence alignment technique.

Western blot

Whole-cell lysates from both cell lines (with or without ATO) were investigated using standard western blotting techniques. Both cell lines were seeded in 6-well microplates (6×10^5 cells/well) as a single-cell suspension and cultured for 24 h. After the cells adhered to the walls of the plates and were treated with or without ATO for 24 h, 2–3 mL of precooled PBS were added to wash the cells, and then the samples were immediately placed on ice. After that, 100 μ L of lysate was added for 30 min in order to achieve full lysis. Protein lysates were denatured at 95°C for 5 min after being collected and centrifuged (1200 r/min, 4°C) for 5 min, and then they were stored at –80°C. Protein concentration was measured using BCA protein assay. The absorbance was measured with enzyme labeling instrument at 592 nm wavelength, and concentration of each sample was calculated based on standard curve analysis. Approximately 20 μ g of protein were run on 4–15% gradient Tris-Glycine Gels (Thermo Fisher Scientific). Before being transferred with the Trans-Blot Turbo transfer system (Bio-Rad, Hercules, USA), the concentrated gel was run at 80 V and separation gel at 120 V constant pressure electrophoresis. After blocking the membranes for 1 h at room temperature with 5% skim milk powder, the membranes were incubated with the 1st antibody (1:1000) in Tris-buffered saline containing 0.1% Tween20 (TBST) overnight at 4°C. The membrane was washed 3 times with TBST, incubated for 1 h with the 2nd antibody of HRP-labeled anti-mouse IgG (1:2000), and rinsed 3 times with TBST before using electrochemiluminescence (ECL) reagent to visualize the blots. A gel documentation system (Biozym, Hessisch Oldendorf, Germany) was applied to quantify the scanned film, following gel electrophoresis.

Statistical analyses

We used IBM SPSS v. 25.0 (IBM Corp., Armonk, USA) and GraphPad Prism software v. 8.0 (GraphPad Software, San Diego, USA) to analyze the data. Before applying parametric statistics, we used Levene's test for the homogeneity of variance and Kolmogorov–Smirnov tests combined with QQ-plots for the normality of data. If the quantitative data fulfilled the necessary conditions, the Student's t-test was used. The rank-sum test was performed if the normal distribution or the homogeneity of the variance was not met. Values of $p < 0.0500$ were considered to indicate statistically significant differences. The IC₅₀ values are not cases of simple linear regression, but they reflect non-linear parameter optimization and fit using a sigmoidal dose-response model. In our experiment, a 4-parameter logistic equation was employed using Microsoft Excel 2019 (Microsoft Corp., Redmond, USA) and GraphPad Prism for curve fitting analysis to determine IC₅₀ values.

Results

SK-N-AS and SK-N-SH cells growth inhibition with different concentration of ATO

In order to evaluate the cytotoxicity of ATO, both SK-N-AS and SK-N-SH cells were seeded in 96-well cell culture plates with 1000 cells (1×10^4 /mL; 100 μ L) per well separately and treated with different concentration of ATO ranging from 1 μ M to 2⁸ μ M. The CCK-8 assay was used to detect cell cytotoxicity. In SK-N-AS cells, the inhibition rate (mean \pm standard deviation (SD)) was 1.1 \pm 5.1%, 8.5 \pm 0.7%, 17.1 \pm 4.5%, 25.9 \pm 0.2%, 37.5 \pm 2.1%, 44 \pm 1.0%, 48.3 \pm 1.9%, 48.9 \pm 0.9%, and 55.9 \pm 0.8% in different ATO concentrations (1 μ M, 2 μ M, 4 μ M, 8 μ M, 16 μ M, 32 μ M, 64 μ M, 128 μ M, and 256 μ M) at 24 h. The inhibition rate of proliferation markedly elevated from 4 μ M to 128 μ M and plateaued thereafter (Fig. 1). The IC₅₀_{ATO} value of SK-N-AS cells was 95.36 μ M at 24 h, calculated with GraphPad Prism. The IC₅₀_{ATO} value (5.52 μ M) of SK-N-SH cells was obtained the same way as above (Fig. 1), which corresponded with our previous experimental results.²³ To avoid

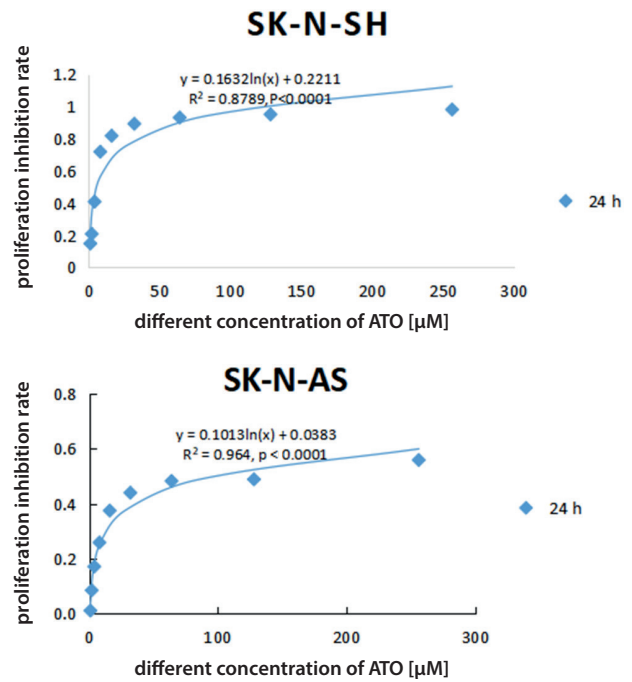
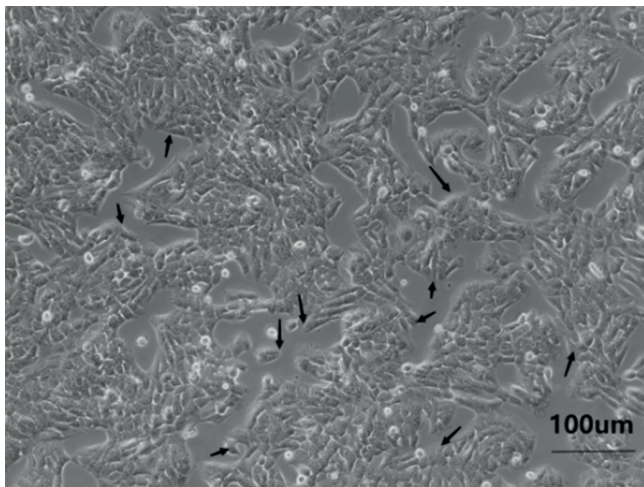
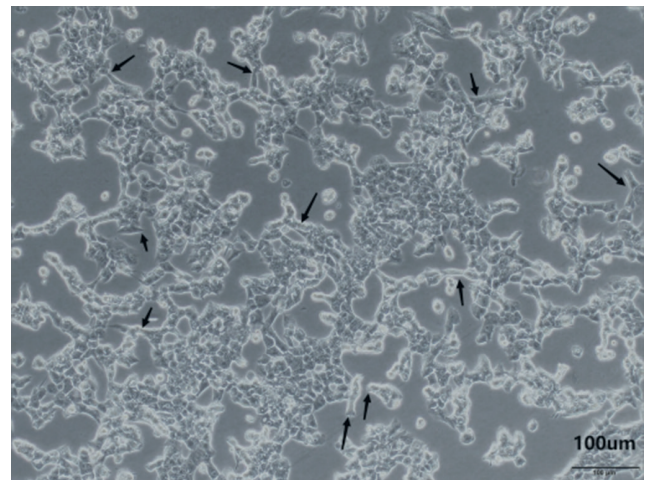


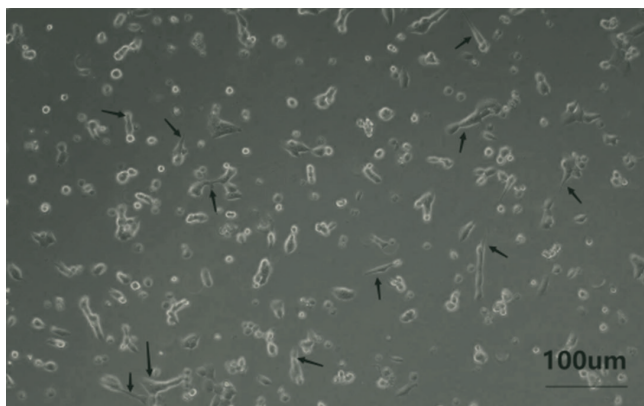
Fig. 1. Proliferation inhibition rate of SK-N-AS (retinoic acid-resistant neuroblastoma) and SK-N-SH (retinoic acid-sensitive neuroblastoma) cells with different concentration of arsenic trioxide (ATO) at 24 h



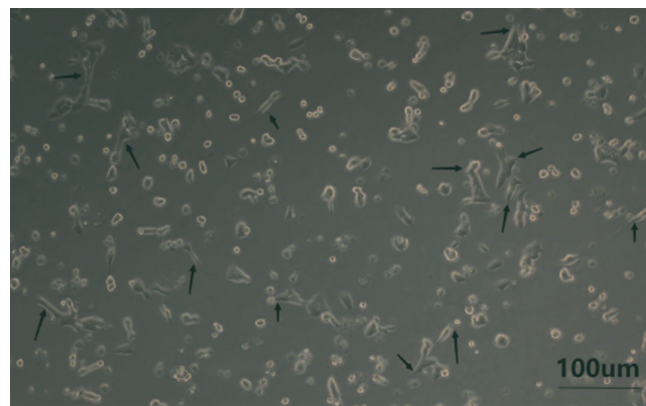
The control group of SK-N-AS (without ATO)



The experimental group of SK-N-AS (with ATO)



The control group of SK-N-SH (without ATO)



The experimental group of SK-N-SH (with ATO)

Fig. 2. Cell morphology of SK-N-AS (retinoic acid-resistant neuroblastoma) and SK-N-SH (retinoic acid-sensitive neuroblastoma) cells with or without arsenic trioxide (ATO)

the interference of apoptosis on the observation of differentiation, by comparison, $1/6$ IC50 concentration (16 μM) of SK-N-AS cells and $1/2$ IC50 concentration (2.7 μM) of SK-N-SH cells were chosen for observation of cell morphology, apoptosis assay, phosphoproteomic analysis, and western blot.

ATO accelerated synaptic growth of SK-N-AS and SK-N-SH cells

To assess the effect of ATO on NB cells differentiation, the synaptic growth was chosen as a representative feature (longer synapses represents better differentiation). We cultured both cell lines with or without ATO for 24 h, and more synapses in 2 cell lines were observed in the experimental group (with ATO) than the control group (without ATO) using inverted phase contrast microscopy (Fig. 2). In both cell lines, using ImageJ program with NeuronJ Plugin, we found that the length of synapses (1 field was randomly selected under microscope with $\times 100$ magnification) grew longer with time in culture in both cells, and the total length of synapses in the experimental group significantly increased compared to the control group (Table 1,2). We can conclude that ATO could morphologically promote the differentiation of NB cells.

ATO promoted apoptosis of SK-N-AS and SK-N-SH cells

We cultured both cell lines with or without ATO for 24 h and the apoptotic rates of the 2 groups were analyzed with FCM. Results were expressed as mean \pm SD. We found that the apoptotic rate of SK-N-AS cells in the experimental group was significantly higher (Fig. 3)

Table 1. Total lengths of synapses of SK-N-AS and SK-N-SH cells with or without ATO

| Time [h] | Total lengths of synapses [μM] | | | |
|----------|---|---------|-------------------------------|---------|
| | control group (without ATO) | | experimental group (with ATO) | |
| | SK-N-AS | SK-N-SH | SK-N-AS | SK-N-SH |
| 0 | 0 | 0 | 0 | 0 |
| 24 | 96 | 84 | 723 | 435 |

Table 2. The p-value of normality test and homogeneity test

| Group | Total lengths of synapses | | Apoptosis rate | |
|--|---------------------------|-------------|----------------|-------------|
| | normality | homogeneity | normality | homogeneity |
| Control group (without ATO) of SK-N-AS cells | 0.826 | 0.050 | 0.718 | 0.050 |
| Experimental group (with ATO) of SK-N-AS cells | 0.126 | | 0.085 | |
| Control group (without ATO) of SK-N-SH cells | 0.157 | 0.050 | 1.000 | 0.050 |
| Experimental group (with ATO) of SK-N-SH cells | 0.194 | | 0.680 | |

ATO – arsenic trioxide; SK-N-AS – retinoic acid-resistant neuroblastoma cells; SK-N-SH – retinoic acid-sensitive neuroblastoma cells.

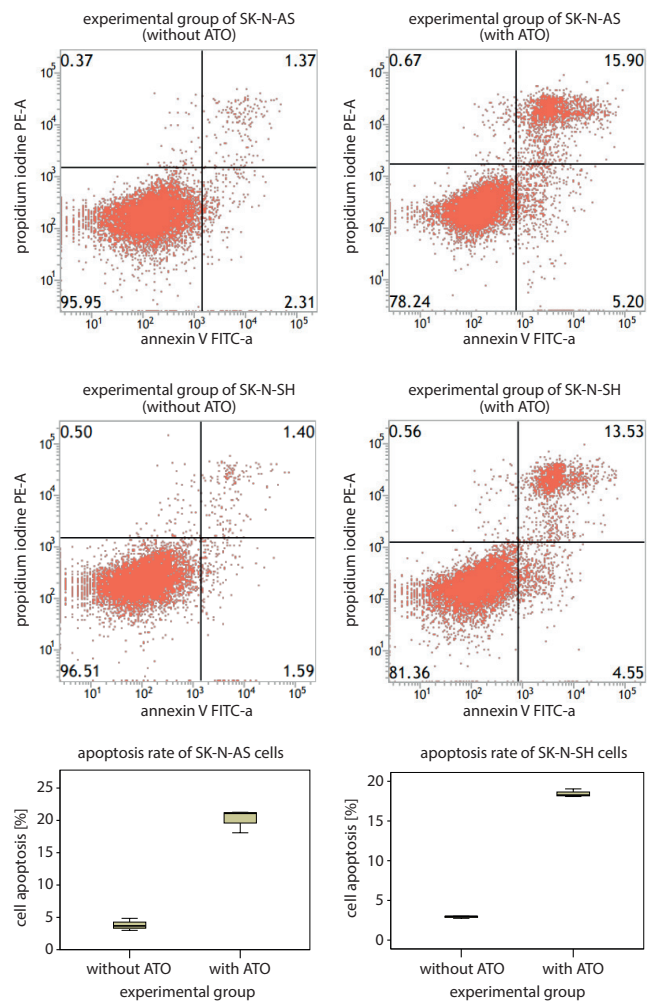


Fig. 3. The apoptosis rate of SK-N-AS (retinoic acid-resistant neuroblastoma) and SK-N-SH (retinoic acid-sensitive neuroblastoma) cells with or without arsenic trioxide (ATO)

than that in the control group (20.15 \pm 1.79% compared to 3.84 \pm 0.94%, $p < 0.0001$). In SK-N-SH cells, a significant increase of apoptosis could also be observed in the experimental group compared to the control group.

Different intracellular protein expressions between the experimental group and control group of SK-N-AS and SK-N-SH cells

In order to figure out the different intracellular protein expressions before and after the treatment with ATO,

we compared intracellular protein expressions of SK-N-AS and SK-N-SH cells between the experimental group (with ATO) and control group (without ATO). We identified quantitative information for 6424 proteins in the SK-N-AS cell line and 4638 proteins in the SK-N-SH cell line. Differentially expressed protein (DEP) was identified by comparison of the signal values between the 2 groups based on $p < 0.05$ using t-test. In SK-N-AS cells, we identified that the neuronal markers MAPT and NEFM were upregulated, and the tumorigenic marker PHOX2B was downregulated in the ATO-treated group. As compared with the control group, we found that EZH2 (FC = 0.552) and PHOX2B (an oncogenic marker, FC = 0.142) were significantly downregulated, while the markers related to the normal differentiation of neurons were upregulated, like MAPT (FC = 1.21), NEFM (FC = 1.547) and MAP2 (FC = 2.669) in the experimental group. In SK-N-SH cells, the same changing trends of the markers mentioned above (PHOX2B was not detected in SK-N-SH cells), but the disparity coefficients of most proteins were smaller than in the SK-N-AS cells, such as for EZH2 (FC = 0.691), MAPT (FC = 1.312), NEFM (FC = 1.146), MAP2 (FC = 1.086), and others. We tested the protein expressions of HoxC9, HoxD8 and EZH2 in SK-N-AS with or without ATO using western blot. We found that, compared to control group, ATO could upregulate HoxC9 and HoxD8, and down-regulate EZH2 (Fig. 4, 5).

Discussion

The NB, which derives from embryonic neural crest, has self-renewable capacities and can differentiate multidirectionally during dorsal migration from the neural tube to the ventral side.²³ When neuroblasts fail to migrate

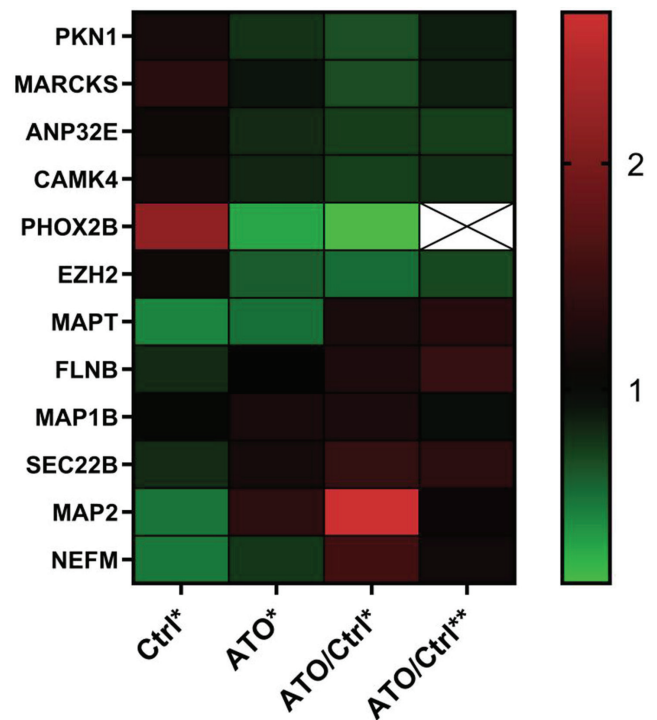


Fig. 4. Differential protein expressions in both cell lines (heat map)

Ctrl* – the control group (without ATO) in the SK-N-AS (retinoic acid-resistant neuroblastoma) cells; ATO* – the experimental group (with ATO) in the SK-N-AS cells; ATO/Ctrl* – ratio of protein expression in the experimental group to the control group in the SK-N-AS (retinoic acid-sensitive neuroblastoma) cells; ATO/Ctrl** – ratio of protein expression in the experimental group to the control group in the SK-N-SH cells; ATO – arsenic trioxide.

correctly and remain undifferentiated, NB occurs.²⁴ The degree of differentiation is assessed by the total neurite length, co-expression of neurofilament and synaptic vesicles, and shape of the cone.²⁵ Notably, total neurite length is directly involved in the neural differentiation.^{26,27} The MAP2,

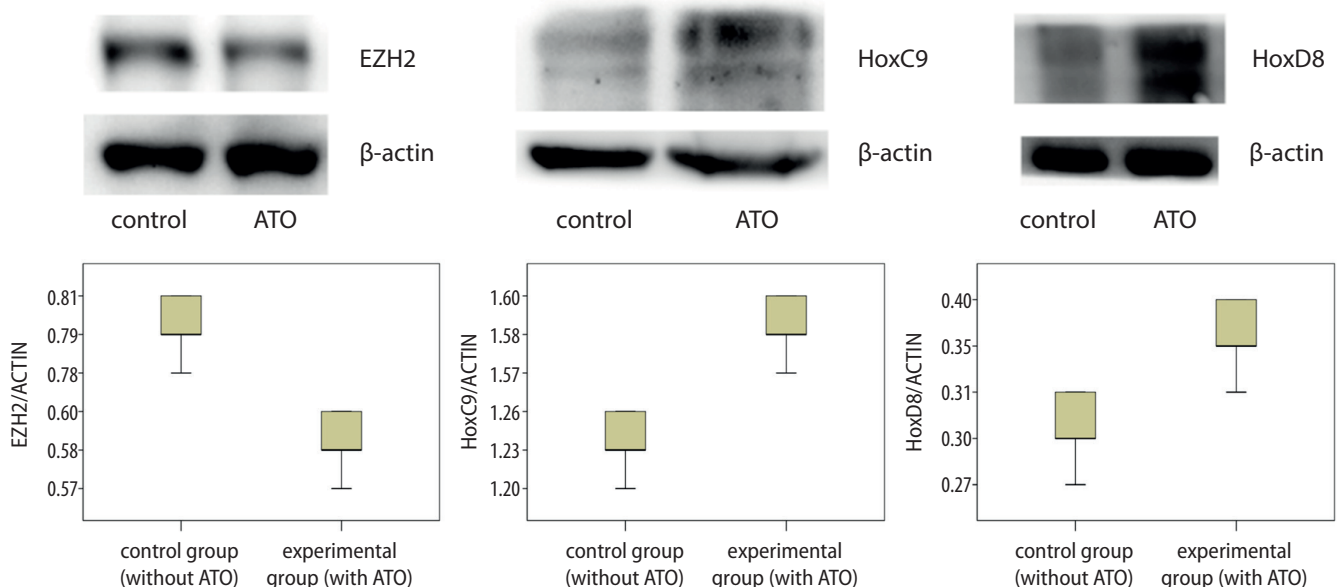


Fig. 5. Different protein expressions of HoxC9, HoxD8 and EZH2 in SK-N-AS (retinoic acid-resistant neuroblastoma) cells with arsenic trioxide (ATO)

as a neuronal differentiation marker, can maintain neuronal dendritic spines by interacting with microtubules.²⁸ It has been reported that the expression of MAP2 could be upregulated by RA through brain-derived neurotrophic factor (BDNF) in SH-SY5Y cells.^{29,30} A study on whole genome sequencing of fetal adrenal cells has found that PHOX2B is a marker of sympathetic progenitors, which is significantly downregulated during the differentiation process of sympathetic nerves.³¹ The *NEFM* gene encodes a subunit of neuron-specific intermediate filaments³²; its expression was reduced after ATO administration.³³ The NEFM was verified to be the target of RA in NB cells, as well as the direct target of *HoxC9*.⁷ Our study verified that expressions of *HoxC9* and *HoxD8* in SK-N-AS cells were upregulated. Label-free quantitative proteomic technology identified that tumorigenic marker PHOX2B was significantly downregulated, while the markers for differentiation of sympathetic neurons (NEFM, MAP2, MAPT) were upregulated. Similarly to the results of previous studies, the expressions of NEFM, MAP2 and MAPT were decreased after RA treatment in SH-SY5Y cells.³⁴ The above results suggest that low doses of ATO could reprogram RA-resistant NB cells differentiation, which may be due to the upregulation of *HoxC9*. In SK-N-SH cell line, the same changing trends of the markers mentioned above, except PHOX2B, *HoxC9* and *HoxD8* (not detected), were observed after ATO treatment, but the disparity coefficients of most proteins were smaller compared to the SK-N-AS cell line. However, in our view, this phenomenon can be explained. The SK-N-SH cell line, with RA-sensitive feature, might not possess the inhibition of *HoxC9* pathway, and thus ATO could not ameliorate the differentiation by the mechanism of enhancing *HoxC9* (via disinhibition). The H3K27me3 is a repressive histone mark, frequently seen in various kinds of tumors and associated with poor prognosis.³⁵ The H3K4me3, a silencing marker of *HoxC9* promoter, is represented in an activated state in RA-resistant NB cells and conversely silenced in RA-sensitive cell lines.¹⁴ This may partly explain why RA could not induce the expression of *HoxC9* in SK-N-AS cell line. The methylation of histone is catalyzed by 2 different families: the protein arginine methyltransferases (RMTs) and the histone lysine methyltransferases (KMTs). Among them, methyltransferase EZH2 is known to be closely associated with the tumorigenesis and tumor development.³⁶ Previous studies showed that histone deacetylase inhibitors (HDACi) targets EZH2 and SUZ12, which are the major components of the PRC2 complex, ultimately reducing the H3K27me3 methylation.^{37,38}

Our phosphoproteomic analysis revealed that ATO downregulates the expression of EZH2 in both cell lines; western blotting also confirmed this result, accompanied by the overexpression of *HoxC9* in SK-N-AS cells. Based on existing literature, we speculate that ATO may act through a mechanism similar to HDACi, which could reduce repressive H3K27me3 through downregulating the expression of EZH2, and then reactivate *HoxC9*.









Limitations

However, there are also some shortcomings of this experiment. First, only 2 human NB cell lines were chosen, which could affect the robustness of the results. Second, the results confirm that ATO could upregulate the expression of *HoxC9* and enhance neuronal differentiation, but we did not confirm the direct relationship between *HoxC9* and neuronal differentiation. Finally, we mentioned that ATO might reduce repressive H3K27me3 through downregulating the expression of EZH2, and then reactivate *HoxC9*, but methylation assays were not performed to confirm this result.

Conclusion

The ATO-mediated EZH2 suppression of RA-resistant NB cells induces *HoxC9* expression that, in turn, ameliorates differentiation and enhances cell apoptosis. Further study is necessary to compensate for the abovementioned limitations and support our conclusion.

ORCID iDs

Chunmou Li  <https://orcid.org/0000-0001-8279-5115>
 Chuchu Feng  <https://orcid.org/0000-0002-0322-2544>
 Yantao Chen  <https://orcid.org/0000-0001-9638-2661>
 Pingping Wu  <https://orcid.org/0000-0002-1822-4294>
 Peng Li  <https://orcid.org/0000-0003-4530-2400>
 Xilin Xiong  <https://orcid.org/0000-0002-5634-0544>
 Xiaomin Peng  <https://orcid.org/0000-0002-0376-9400>
 Zhixuan Wang  <https://orcid.org/0000-0002-5721-8639>
 Yang Li  <https://orcid.org/0000-0002-1756-5847>

Reference

- Halakos EG, Connell AJ, Glazewski L, Wei S, Mason RW. Bottom up proteomics reveals novel differentiation proteins in neuroblastoma cells treated with 13-cis retinoic acid. *J Proteomics*. 2019;209:103491. doi:10.1016/j.jprot.2019.103491
- Maris JM, Hogarty MD, Bagatell R, Cohn SL. Neuroblastoma. *Lancet*. 2007;369(9579):2106–2120. doi:10.1016/S0140-6736(07)60983-0
- Smith V, Foster J. High-risk neuroblastoma treatment review. *Children*. 2018;5(9):114. doi:10.3390/children5090114
- Pinto NR, Applebaum MA, Volchenboum SL, et al. Advances in risk classification and treatment strategies for neuroblastoma. *J Clin Oncol*. 2015;33(27):3008–3017. doi:10.1200/JCO.2014.59.4648
- Karapolat S, Sanli A, Onen A, Acikel U, Sivrikoz O. Effects of retinoic acid on compensatory lung growth. *J Cardiothorac Surg*. 2008;3(1):37. doi:10.1186/1749-8090-3-37
- Theodosiou M, Laudet V, Schubert M. From carrot to clinic: An overview of the retinoic acid signaling pathway. *Cell Mol Life Sci*. 2010;67(9):1423–1445. doi:10.1007/s00018-010-0268-z
- Park JR, Eggert A, Caron H. Neuroblastoma: Biology, prognosis, and treatment. *Hematol Oncol Clin North Am*. 2010;24(1):65–86. doi:10.1016/j.hoc.2009.11.011
- Volchenboum SL, Cohn SL. Progress in defining and treating high-risk neuroblastoma: Lessons from the bench and bedside. *J Clin Oncol*. 2009;27(7):1003–1004. doi:10.1200/JCO.2008.20.2739
- Nguyen T, Hocker JE, Thomas W, et al. Combined RAR α - and RXR-specific ligands overcome N-myc-associated retinoid resistance in neuroblastoma cells. *Biochem Biophys Res Commun*. 2003;302(3):462–468. doi:10.1016/S0006-291X(03)00177-3
- Keshelava N, Davicioni E, Wan Z, et al. Histone deacetylase 1 gene expression and sensitization of multidrug-resistant neuroblastoma cell lines to cytotoxic agents by depsipeptide. *J Natl Cancer Inst*. 2007;99(14):1107–1119. doi:10.1093/jnci/djm044

11. Lau DT, Hesson LB, Norris MD, Marshall GM, Haber M, Ashton LJ. Prognostic significance of promoter DNA methylation in patients with childhood neuroblastoma. *Clin Cancer Res.* 2012;18(20):5690–5700. doi:10.1158/1078-0432.CCR-12-0294
12. Berletch JB, Deng X, Nguyen DK, Distèche CM. Female bias in RhoX6 and 9 regulation by the histone demethylase KDM6A. *PLoS Genet.* 2013;9(5):e1003489. doi:10.1371/journal.pgen.1003489
13. Kocak H, Ackermann S, Hero B, et al. Hox-C9 activates the intrinsic pathway of apoptosis and is associated with spontaneous regression in neuroblastoma. *Cell Death Dis.* 2013;4(4):e586–e586. doi:10.1038/cddis.2013.84
14. Mao L, Ding J, Zha Y, et al. HoxC9 links cell-cycle exit and neuronal differentiation and is a prognostic marker in neuroblastoma. *Cancer Res.* 2011;71(12):4314–4324. doi:10.1158/0008-5472.CAN-11-0051
15. Zha Y, Ding E, Yang L, et al. Functional dissection of HOXD cluster genes in regulation of neuroblastoma cell proliferation and differentiation. *PLoS One.* 2012;7(8):e40728. doi:10.1371/journal.pone.0040728
16. Wan C, Liu X, Bai B, Cao H, Li H, Zhang Q. Regulation of the expression of tumor necrosis factor related genes by abnormal histone H3K27 acetylation: Implications for neural tube defects. *Mol Med Rep.* 2018;17(6):8031–8038. doi:10.3892/mmr.2018.8900
17. Ziegler C, Finke J, Grüllich C. Features of cell death, mitochondrial activation and caspase dependence of rabbit anti-T-lymphocyte globulin signaling in lymphoblastic Jurkat cells are distinct from classical apoptosis signaling of CD95. *Leuk Lymphoma.* 2016;57(1):177–182. doi:10.3109/10428194.2015.1044449
18. Kanduri M, Sander B, Ntoufa S, et al. A key role for EZH2 in epigenetic silencing of HOX genes in mantle cell lymphoma. *Epigenetics.* 2013;8(12):1280–1288. doi:10.4161/epi.26546
19. Au WY, Li CK, Lee V, et al. Oral arsenic trioxide for relapsed acute promyelocytic leukemia in pediatric patients. *Pediatr Blood Cancer.* 2012;58(4):630–632. doi:10.1002/pbc.23306
20. Iland HJ, Bradstock K, Supple SG, et al. All-trans-retinoic acid, idarubicin, and IV arsenic trioxide as initial therapy in acute promyelocytic leukemia (APML4). *Blood.* 2012;120(8):1570–1580. doi:10.1182/blood-2012-02-410746
21. Liu WJ, Jiang NJ, Guo QL, Xu Q. ATRA and As₂O₃ regulate differentiation of human hematopoietic stem cells into granulocyte progenitor via alteration of HoxB8 expression. *Eur Rev Med Pharmacol Sci.* 2015;19(6):1055–1062. PMID:25855932.
22. Cui X, Wakai T, Shirai Y, Yokoyama N, Hatakeyama K, Hirano S. Arsenic trioxide inhibits DNA methyltransferase and restores methylation-silenced genes in human liver cancer cells. *Hum Pathol.* 2006;37(3):298–311. doi:10.1016/j.humpath.2005.10.013
23. Qi K, Li Y, Huang K, et al. Pre-application of arsenic trioxide may potentiate cytotoxic effects of vinorelbine/docetaxel on neuroblastoma SK-N-SH cells. *Biomed Pharmacother.* 2019;113:108665. doi:10.1016/j.biopha.2019.108665
24. Palacios-Moreno J, Foltz L, Guo A, et al. George L neuroblastoma tyrosine kinase signaling networks involve FYN and LYN in endosomes and lipid rafts. *PLoS Comput Biol.* 2015;11(4):e1004130. doi:10.1371/journal.pcbi.1004130
25. Anitha M, Shahnavaz N, Qayed E, et al. BMP2 promotes differentiation of nitrergic and catecholaminergic enteric neurons through a Smad1-dependent pathway. *Am J Physiol Gastrointest Liver Physiol.* 2010;298(3):G375–G383. doi:10.1152/ajpgi.00343.2009
26. Teppola H, Sarkanen JR, Jalonen TO, Linne ML. Morphological differentiation towards neuronal phenotype of SH-SY5Y neuroblastoma cells by estradiol, retinoic acid and cholesterol. *Neurochem Res.* 2016;41(4):731–747. doi:10.1007/s11064-015-1743-6
27. Thiele CJ, Reynolds CP, Israel MA. Decreased expression of N-myc precedes retinoic acid-induced morphological differentiation of human neuroblastoma. *Nature.* 1985;313(6001):404–406. doi:10.1038/313404a0
28. Clagett-Dame M, McNeill EM, Muley PD. Role of all-trans retinoic acid in neurite outgrowth and axonal elongation. *J Neurobiol.* 2006;66(7):739–756. doi:10.1002/neu.20241
29. Shelton MA, Newman JT, Gu H, et al. Loss of microtubule-associated protein 2 immunoreactivity linked to dendritic spine loss in schizophrenia. *Biol Psychiatry.* 2015;78(6):374–385. doi:10.1016/j.biopsych.2014.12.029
30. Constantinescu R, Constantinescu AT, Reichmann H, Janetzky B. Neuronal differentiation and long-term culture of the human neuroblastoma line SH-SY5Y. In: Gerlach M, Deckert J, Double K, Koutsilieri E, eds. *Neuropsychiatric Disorders An Integrative Approach.* Vienna, Austria: Springer Vienna; 2007:17–28. doi:10.1007/978-3-211-73574-9_3
31. Encinas M, Iglesias M, Liu Y, et al. Sequential treatment of SH-SY5Y cells with retinoic acid and brain-derived neurotrophic factor gives rise to fully differentiated, neurotrophic factor-dependent, human neuron-like cells. *J Neurochem.* 2002;75(3):991–1003. doi:10.1046/j.1471-4159.2000.0750991.x
32. Dong R, Yang R, Zhan Y, et al. Single-cell characterization of malignant phenotypes and developmental trajectories of adrenal neuroblastoma. *Cancer Cell.* 2020;38(5):716–733.e6. doi:10.1016/j.ccell.2020.08.014
33. Uchida A, Brown A. Arrival, reversal, and departure of neurofilaments at the tips of growing axons. *Mol Biol Cell.* 2004;15(9):4215–4225. doi:10.1091/mbc.e04-05-0371
34. Scheibe RJ, Ginty DD, Wagner JA. Retinoic acid stimulates the differentiation of PC12 cells that are deficient in cAMP-dependent protein kinase. *J Cell Biol.* 1991;113(5):1173–1182. doi:10.1083/jcb.113.5.1173
35. Murillo JR, Goto-Silva L, Sánchez A, Nogueira FCS, Domont GB, Junqueira M. Quantitative proteomic analysis identifies proteins and pathways related to neuronal development in differentiated SH-SY5Y neuroblastoma cells. *EuPA Open Proteomics.* 2017;16:1–11. doi:10.1016/j.euprot.2017.06.001
36. Wang C, Liu Z, Woo CW, et al. EZH2 mediates epigenetic silencing of neuroblastoma suppressor genes *CASZ1*, *CLU*, *RUNX3*, and *NGFR*. *Cancer Res.* 2012;72(1):315–324. doi:10.1158/0008-5472.CAN-11-0961
37. Simon JA, Lange CA. Roles of the EZH2 histone methyltransferase in cancer epigenetics. *Mutat Res.* 2008;647(1–2):21–29. doi:10.1016/j.mrfmmm.2008.07.010
38. Yin X, Yang S, Zhang M, Yue Y. The role and prospect of JMJD3 in stem cells and cancer. *Biomed Pharmacother.* 2019;118:109384. doi:10.1016/j.biopha.2019.109384

Trimethylamine N-oxide in cardiovascular disease

Radosław Andrzej Konieczny^{1,A–D}, Wiktor Kuliczkowski^{2,C,E,F}

¹ Clinical Department of Gastroenterology and Hepatology, Wrocław Medical University, Poland

² Institute for Heart Diseases, Wrocław Medical University, Poland

A – research concept and design; B – collection and/or assembly of data; C – data analysis and interpretation;

D – writing the article; E – critical revision of the article; F – final approval of the article

Advances in Clinical and Experimental Medicine, ISSN 1899–5276 (print), ISSN 2451–2680 (online)

Adv Clin Exp Med. 2022;31(8):913–925

Address for correspondence

Radosław Andrzej Konieczny
E-mail: rkonieczny.med@gmail.com

Funding sources

None declared

Conflict of interest

None declared

Received on December 20, 2021

Reviewed on March 17, 2022

Accepted on March 24, 2022

Published online on April 19, 2022

Abstract

Although traditional cardiovascular risk factors are well established and understood, mortality and morbidity in patients with cardiovascular disease (CVD) remains high. Exploring new pathophysiological pathways enables a better understanding of CVD at both the molecular and clinical levels. Gut microbiota as a potential modulator of CVD are the subject of extensive research. In recent years, trimethylamine N-oxide (TMAO), a biologically active molecule generated by the gut microbiota, has been widely tested in studies on various populations of patients. The ultimate TMAO levels depend on individual features and gut microbiota composition. Most of the research on TMAO has focused on atherosclerotic CVD and heart failure (HF). Studies conducted so far support the use of TMAO as a prognostic marker in CVD. Several studies describe diverse interventions aimed at reducing the concentration of TMAO and its harmful effects. This article summarizes the findings from research, discusses the major insights into TMAO metabolism and related pathophysiological processes, as well as indicates the directions for future research.

Key words: gut microbiota, coronary artery disease, heart failure, TMAO, trimethylamine oxide

Cite as

Konieczny RA, Kuliczkowski W. Trimethylamine N-oxide in cardiovascular disease. *Adv Clin Exp Med.* 2022;31(8):913–925. doi:10.17219/acem/147666

DOI

10.17219/acem/147666

Copyright

Copyright by Author(s)

This is an article distributed under the terms of the Creative Commons Attribution 3.0 Unported (CC BY 3.0) (<https://creativecommons.org/licenses/by/3.0/>)

Introduction

According to the World Health Organization (WHO), cardiovascular disease (CVD) remains the major cause of death and disability worldwide.¹ Exploring new pathophysiological pathways enables a better understanding of CVD at both the molecular and clinical levels. Owing to the development of metabolomics and metagenomics, the intestinal microbiota have been indicated as a potential modulator of the course of CVD. Trimethylamine N-oxide (TMAO) is a gut-derived metabolite whose usefulness has been evaluated in numerous studies. Despite promising results, TMAO is an example of a deeply researched gut microbiome biomarker which is still not used in everyday clinical practice. In order to determine the utility of a new biomarker, it is first necessary to assess its metabolism and related pathophysiological processes, followed by clinical trials.² This review summarizes extensive literature on TMAO and indicates gaps in knowledge existing after more than 10 years of research.

Objectives

The purpose of this article was to provide an overview of the metabolism of TMAO and associated pathophysiological processes, and the results of major studies. An attempt was also made to indicate the direction of further research.

Methodology

Literature search was carried out in the PubMed database on November 3, 2021 using the queries: “(TMAO) AND (atherosclerosis)”, “(TMAO) AND (coronary artery disease)”, “(TMAO) AND (atrial fibrillation)”, “(TMAO) AND (heart failure)”, and “(TMAO) AND (gut microbiota)”. Selected key studies concern diverse groups of patients with CVD. Their results are discussed in the text and presented in tables below.

Metabolism of TMAO

The TMAO is an organic compound with the chemical formula of $(\text{CH}_3)_3\text{NO}$. It is commonly found in the tissues of marine organisms, where it mitigates the adverse effects of temperature, salinity, as well as high urea and hydrostatic pressure.³ In humans, TMAO is produced by the oxidation of trimethylamine (TMA) and is absorbed directly from food. The TMAO is most abundant in fish and seafood.⁴ Gut microbiota produce TMA from the dietary precursors: choline, L-carnitine, and betaine. These TMA precursors are most abundant in red meat and eggs.⁵ The most recent research indicates that the intake of foods rich in TMA precursors does not translate directly

into an increase in plasma TMAO level because it depends on individual metabolic features, such as hepatic enzymes activity and gut microbiota composition.^{6,7}

Carnitine metabolism is key to human TMAO production and 3 major bacterial metabolic pathways leading to TMA synthesis from dietary precursors were described⁸:

- a) anaerobic choline degradation by choline TMA-lyase;
- b) hydroxylation of L-carnitine to TMA by carnitine oxidoreductase; and
- c) conversion of L-carnitine to γ -butyrobetaine, which is then converted to TMA.

Trimethylamine produced by gut microbiota is excreted from the gut via 3 mechanisms: it can be absorbed to the circulation, excreted with stool or used by other bacteria in the process of syntrophy. Trimethylamine that has been absorbed to the circulation is oxidized to TMAO by hepatic flavin-containing monooxygenase (FMO).⁵ Trimethylamine absorption occurs in the small intestine (Fig. 1).⁹ After absorption, TMA is almost immediately oxidized to TMAO. Following the oral intake of phosphatidylcholine, the highest plasma and urinary TMAO levels are observed after 12 h and 24 h, respectively. After 48 h from intake, the plasma TMAO level returns to baseline.⁹ The TMAO taken with food is absorbed through the intestinal barrier and is detectable in blood after 15 min. The maximum blood concentration is reached after 1 h and is maintained for approx. 6 h. After 24 h, 96% of the TMAO dose taken with food is excreted with urine, mostly in an unchanged form.¹⁰

To determine the concentration of TMAO, liquid chromatography coupled with tandem mass spectrometry and automated nuclear magnetic resonance spectrometry are most often used.⁴ Due to the need of specialized equipment, reliable TMAO determination is possible in research or academic facilities; however, mentioned methods become more available.

The effect of TMAO on pathophysiological processes

The first studies reporting the negative effects of TMAO were conducted on an animal model and focused on atherogenesis. Initially, it was determined that TMAO accelerates the production of foam cells from macrophages. The TMAO was shown to promote the upregulation of the scavenger receptors CD36 and SR-A1¹¹ as well as induce inflammation¹² via the MAPK/JNP pathway, which regulates the synthesis of pro-inflammatory cytokines – tumor necrosis factor alpha (TNF- α), interleukin 6 (IL-6) and intercellular adhesion molecule 1 (ICAM-1). This leads to cholesterol overload in macrophage foam cells and their faster migration and adhesion to endothelial cells. A study on human umbilical vein endothelial cells (HUVECs) confirmed a link between high plasma TMAO levels and the development of atherosclerosis. Moreover, it indicated that TMAO impaired endothelial self-repair

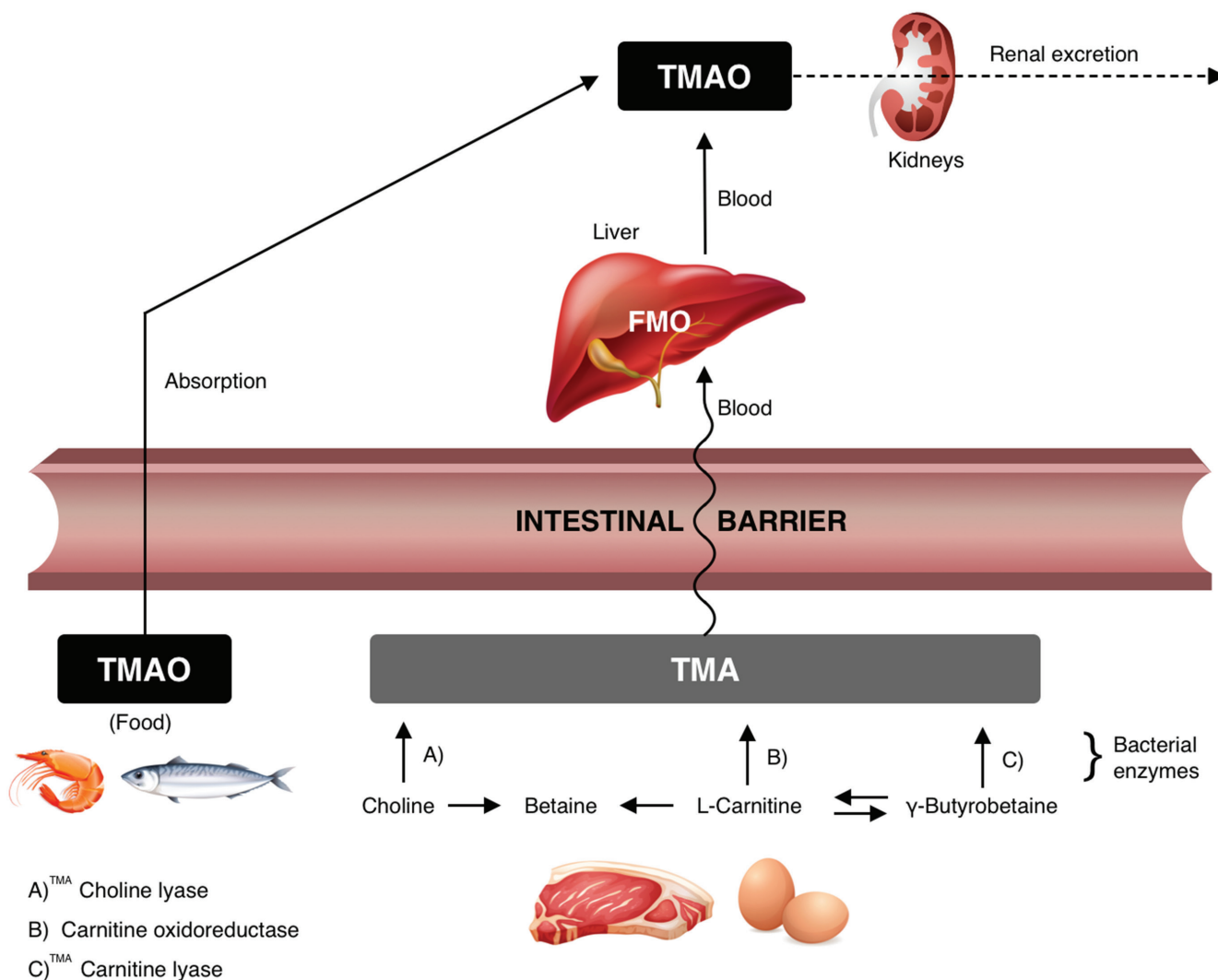


Fig. 1. Schematic presentation of the intestinal absorption of TMA and TMAO

TMA – trimethylamine; TMAO – trimethylamine N-oxide; FMO – flavin-containing monooxygenase.

already in the early stages of atherogenesis.¹³ This is due to the inhibitory effect of TMAO on endothelial cell proliferation during the G0/G1 phase of the cell cycle¹⁴ as well as its cytotoxic effect on circulating endothelial progenitor cells.¹⁵ This cascade of events is accompanied by increased oxidative stress, another postulated effect of chronically elevated TMAO levels, observed also in healthy individuals.¹⁶ The effect of TMAO on pathophysiological processes is depicted in Fig. 2.

At a systemic level, TMAO promotes atherogenesis by altering lipid metabolism. In a study on a mice model, Koeth et al. demonstrated that TMAO inhibited the expression of the Cyp7a1 enzyme and bile acid transport proteins.¹⁷ The Cyp7a1 is responsible for bile acid synthesis and inhibition of cholesterol catabolism. The lack of Cyp7a1 leads to the reduced bile acid synthesis and secretion, resulting in atherosclerosis progression. At the same time, a reduction in the expression of bile acid transporter proteins in the liver negatively affects the major pathway of elimination of cholesterol from the body.¹⁷

Along with research on atherosclerosis, there have been studies investigating the prothrombotic effect of TMAO. Impaired intracellular calcium ion transport in platelets, heightened platelet reactivity and increased platelet adhesion to collagen fibers were reported.¹⁸ In endothelial cells, an increased tissue factor synthesis and downregulation of thrombomodulin were described.¹⁹

Direct cardiotoxic and proarrhythmic effects of TMAO

The cardiotoxicity of TMAO was confirmed in morphological and functional studies, mainly in animal models. By activating the inflammatory pathways, TMAO promotes cardiac fibrosis, heart weight gain and cardiac remodeling.²⁰ At a cellular level, TMAO impairs the intracellular microtubule network and alters calcium concentration control in cardiac muscle cells. This leads to a decrease in contraction amplitude, longer time of peak and reduced

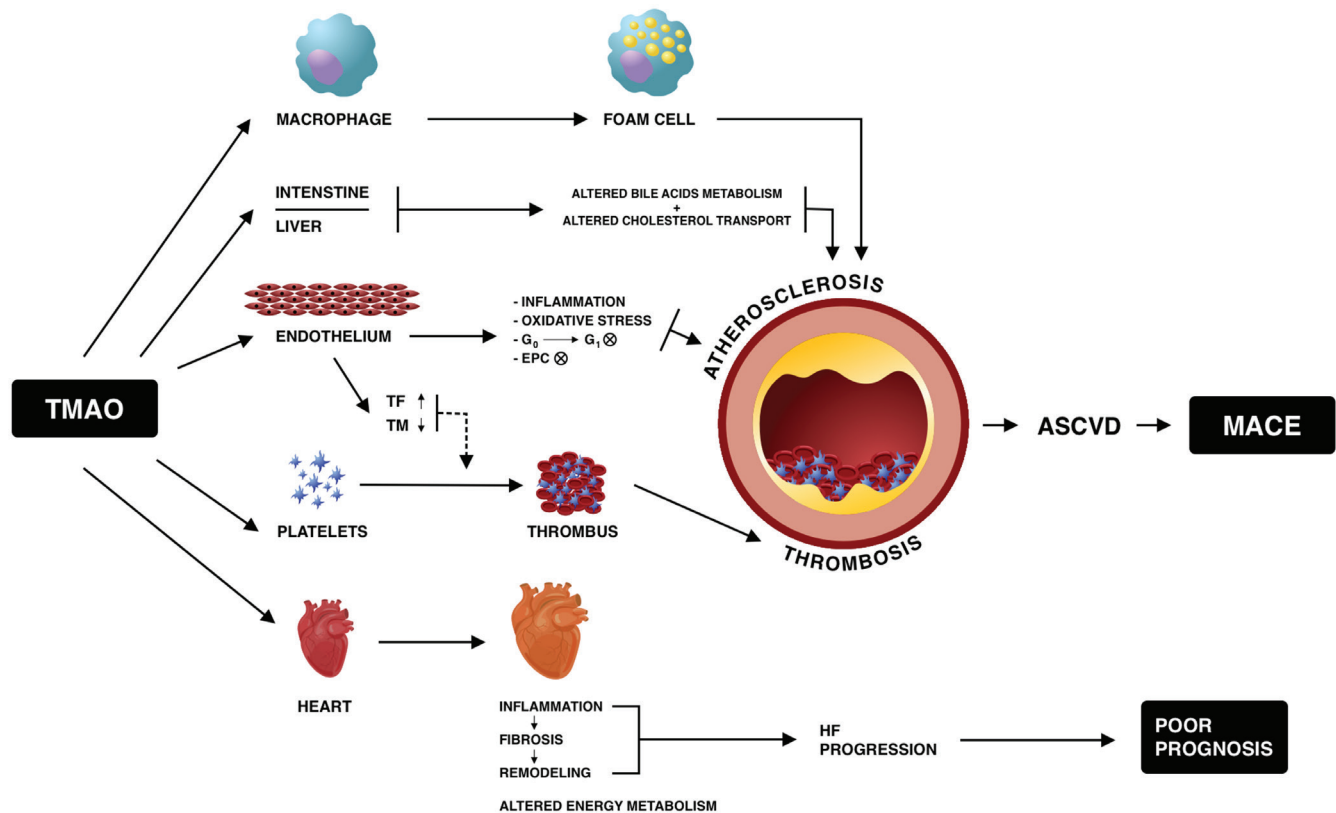


Fig. 2. Effect of TMAO on pathophysiological processes

TMAO – trimethylamine N-oxide; ASCVD – atherosclerotic cardiovascular disease; EPC – endothelial progenitor cells; HF – heart failure; MACE – major cardiovascular events; TF – tissue factor; TM – thrombomodulin.

| DRUGS | SURGERY | DIET | GUT MICROBIOTA MODIFICATION |
|---|---|---|--|
| <ul style="list-style-type: none"> • STATIN⁵⁶ • ASPIRIN⁵⁷ • RIFAXIMIN⁶⁰ • RESVERATROL⁶⁴ • MELDONIUM⁶⁵ | <ul style="list-style-type: none"> • GASTRIC BYPASS⁶³ • DUODENAL SWITCH⁶³ | <ul style="list-style-type: none"> • DISCONTINUATION OF RED MEAT⁵ | <ul style="list-style-type: none"> • Probiotics: <ul style="list-style-type: none"> -Saccharomyces Boulardi⁶⁰ -VSL#3⁶¹ • Fecal microbiota transplant⁶² |

Fig. 3. Therapeutic strategies affecting TMAO levels and metabolism in humans. Detailed information included in Table 3, with consistent reference numbers
TMAO – trimethylamine N-oxide.

synchronization.²¹ Similar TMAO-induced abnormalities in contractility were also reported in ex-vivo human cardiac tissue.²²

Results from studies on TMAO

Over the past 10 years, numerous studies investigating the prognostic value of TMAO have been conducted. The research included various populations of patients, both with acute and chronic illness. Most of those studies

enrolled patients with coronary artery disease (CAD) and heart failure (HF). Selected studies are discussed below and summarized in Table 1.

The first meaningful study on the effect of TMAO in CAD was published in 2013.²³ Tang et al. demonstrated that higher plasma TMAO levels correlated with an increased risk of major adverse cardiovascular events (MACEs) during a 3-year follow-up in 4007 patients referred for elective coronary angiography.²³ The correlation was revealed even after adjustment for traditional risk factors. Similar findings were reported by Senthong et al.

in a study of 2235 patients with significant coronary artery stenosis receiving optimal treatment. Higher TMAO levels predicted mortality independent of traditional risk factors during a 5-year follow-up.²⁴ In a longitudinal study

by Lee et al.,²⁵ a significant association between higher levels of TMAO and increased risk of incident and recurrent atherosclerotic CVD was shown.²⁵ Another large community-based study of middle-aged participants revealed that

Table 1. Results of studies on the association of TMAO with cardiovascular risk

| Author | Type of study | Population characteristics | Follow-up | Study endpoint | Results HR/OR (95% CI) | TMAO [μmol/L], median (IQR) |
|--------------------------------|--|--|-------------------|--|---|---|
| Coronary artery disease | | | | | | |
| Tang et al. ²³ | prospective study | n = 4007; patients undergoing elective coronary angiography USA age: 63 ± 11 male sex: 64% | 3 years | MACE (death, myocardial infarction, stroke) | TMAO Q4 compared to Q1 MACE n = 513, HR 2.54 [1.96; 3.28]; p < 0.001 multivariate HR 1.43 [1.05; 1.94] death HR 3.37 [2.39; 4.75]; p < 0.001 nonfatal myocardial infarction or stroke HR 2.13 [1.48; 3.05]; p < 0.001 | 3.7 (2.4–6.20) MACE 5.0 (3.0–8.8) no MACE 3.5 μM (2.4–5.9); p < 0.001 |
| Senthong et al. ²⁴ | prospective study | n = 2235; patients with stable coronary artery disease who underwent elective coronary angiography USA age: 63 ± 11 years male sex: 71% | 5 years | death (all-cause) | TMAO Q4 compared to Q1 death n = 338 HR 3.90 [2.78; 5.48]; p < 0.0001 | 3.8 (2.5–6.5) Q4 > 6.5; 9.7 (7.7–14.9) |
| Lee et al. ²⁵ | prospective multicenter community-based cohort study | n = 5580 USA age: 72 ± 5.3 years male sex: 36% a) participants free of prevalent cardiovascular disease (n = 4131) age: 72.2 ± 5.3 years male sex: 36% b) participants with prevalent cardiovascular disease (n = 1449) age: 73.6 ± 5.8 years male sex = 53% | 15 years | ASCVD defined as MI (fatal and nonfatal), fatal coronary heart disease, stroke (fatal and nonfatal), sudden cardiac death, and other atherosclerotic death | quintile 5 compared to quintile 1 multivariable HR 1.23 [1.04; 1.45]; p = 0.028 multivariable, diet and renal function adjusted HR 1.08 [0.91; 1.29]; p = 0.579 a) multivariable, diet and continuous eGFR, adjusted HR 1.07 [0.90; 1.27]; p = 0.516 b) multivariable HR 1.25 [1.01; 1.56]; p = 0.009 multivariable, diet and continuous eGFR, HR 1.10 [0.87; 1.39]; p = 0.179 | 4.7 (3.2–7.7) quintile 1 = 2.29 (1.84–2.61) quintile 5 = 13.2 (10.4–19.9) a) 4.72 (3.19–7.69) eGFR 70.1 (16.2) b) 5.43 (3.57–8.74) eGFR 63.8 (17.9) |
| Tang et al. ²⁶ | nested case-control study | n = 2181; healthy individuals Europe age: 65 ± 8 years male sex: 65% | 8 years | CAD – hospital admission and/or death with CAD as underlying cause (ICD9 Code 410–414) | Q4 compared to Q1 n = 908 OR 1.86 [1.46; 2.37]; p < 0.001 adjusted for traditional risk factors OR 1.58 [1.21; 2.06]; p < 0.001 | 3.4 (2.3–5.7) |
| Suzuki et al. ²⁷ | retrospective study | n = 1079; acute MI patients UK age: 67 (57–77) years male sex: 72% | 2 years | all-cause mortality death/MI | TMAO T3 compared to T1 n = 292 events all-cause mortality n = 119 HR 1.21 [0.98; 1.48] p = 0.074 death/MI n = 232 HR 1.40 [1.26; 1.55] p < 0.0005 multivariate HR 1.21 [1.03; 1.4] p = 0.023 | 3.7 (4.6–6.4) T3 > 5.1; 8.5 (6.2–15.0) |
| Matsuzawa et al. ²⁸ | observational study | n = 112; STEMI patients who underwent primary PCI Japan age: 63 (56–71) years male sex: 88% | median: 5.4 years | cardiovascular events | death n = 5 nonfatal myocardial infarction n = 5, unstable angina requiring revascularization n = 2 nonfatal stroke n = 5 TMAO > 6.76 compared to < 6.76 adjusted HR 6.21 [1.69; 30.285]; p = 0.005 adjusted HR for 0.1 increase in log TMAO 1.343 [1.122; 1.636]; p = 0.001 | 6.76 (3.82–12.53) |

Table 1. Results of studies on the association of TMAO with cardiovascular risk – cont.

| Author | Type of study | Population characteristics | Follow-up | Study endpoint | Results HR/OR (95% CI) | TMAO [$\mu\text{mol/L}$], median (IQR) |
|-------------------------------|--|---|---|---|---|--|
| Li et al. ²⁹ | prospective study | n = 530; patients presenting to the emergency department with chest pain of suspected cardiac origin (112 troponin T-positive) USA age: 62.4 \pm 13.9 years male sex: 57.5% n = 1683 who underwent coronary angiography for ACS Switzerland age: 63.9 \pm 12.4 years male sex: 77.8% | 1 month, 6 months, 7 years, 1 year | MACE defined as a composite of MI, stroke, revascularization, or all-cause mortality (1 month, 6 months), all-cause mortality (7 years) | TMAO Q4 compared to Q1 MACE 1 month OR 6.30 [1.89; 21.0]; p < 0.01 MACE 6 months n = 220 (death n = 29) OR 5.65 [1.91; 16.7]; p < 0.01 mortality 7 years HR 1.81 [1.04; 3.15]; p < 0.05 MACE n = 119 (death n = 79) (1 year Q4 HR 1.57 [1.03; 2.41]; p < 0.05 | 4.28 (2.55–7.91) 2.87 (1.94–4.85) |
| Sheng et al. ³⁰ | prospective observational study | n = 335; patients with STEMI China age: 58.7 \pm 12.1 years male sex: 80.6% | N/A | SYNTAX Score \geq 23 presence of multivessel disease | adjusted OR 1.16 [1.06; 1.29]; p = 0.001 r = 0.237, p < 0.001 AUC 0.656 [0.591; 0.722]; p < 0.001 adjusted OR 1.15 [1.01; 1.32]; p = 0.035 r = 0.192, p < 0.001 | 2.18 (1.34–3.90) |
| Senthong et al. ³¹ | prospective cohort study | n = 353; stable patients with CAD detected by elective coronary angiography USA age: 65.0 \pm 11.0 years male sex: 79% | N/A | SYNTAX Score SYNTAX Score II presence of diffuse lesions | SYNTAX Score (r = 0.61) p < 0.0001 adjusted OR 4.82; p < 0.0001 SYNTAX Score II (r = 0.62) p < 0.0001 adjusted OR = 1.88; p = 0.0001 8.4 [5.7; 14.0] compared to 4.4 [5.2; 13.5] adjusted OR 2.05 [1.45; 2.90], p = 0.0001 | 5.5 mM (3.4–9.8) |
| Fu et al. ³² | observational study | n = 26 patients with CAD who underwent optical coherence tomography China age: 60 \pm 10 years male sex: 77% n = 12 – plaque rupture group n = 14 – non-plaque rupture group | N/A | TMAO concentration in rupture compared to non-rupture TMAO concentration and plaque composition | TMAO level – lipid arc (r = 0.43, p = 0.031), lipid volume index (r = 0.39, p = 0.048) | rupture compared to no rupture 8.6 \pm 4.8 compared to 4.2 \pm 2.4; p = 0.011 |
| Tan et al. ³³ | prospective observational study | n = 146; STEMI with pre-intervention optical coherence tomography China age: 57.0 \pm 11.0 years male sex: 82.2% n = 77 – plaque rupture n = 69 – plaque erosion | N/A | TMAO rupture compared to erosion | rupture adjusted OR 4.06 [2.38; 6.91]; p < 0.001 AUROC 0.89, 1.95 μM sensitivity = 88.3%, specificity = 76.8% | rupture compared to erosion 3.33 (2.48–4.57) compared to 1.21 (0.86–1.91); p < 0.001 |
| Heart failure | | | | | | |
| Tang et al. ³⁷ | single-center prospective cohort study | n = 720; stable subjects with HF, patients with ACS within the preceding 30 days excluded USA age: 66 \pm 10 years male sex: 59% | 5 years | all-cause mortality | death n = 207 Q4 compared to Q1 adjusted for traditional risk factors and BNP HR 2.2 [1.42; 3.43]; p < 0.001 adjusted for renal function HR 1.75 [1.07; 2.86]; p < 0.001 | 5.0 (3.0–8.5) |
| Trøseid et al. ³⁸ | prospective observational study | n = 155; patients with stable HF for >6 months (NYHA class II–IV) Europe age: 57 \pm 11 years male sex: 83% n = 73 – CAD n = 75 – DCM n = 7 – other | median: 5.2 years | all-cause and anticipated mortality, i.e., HTx | death (n = 39) HTx (n = 16) T3 compared to T1 unadjusted HR 2.24 [1.28; 3.92]; p = 0.005 adjusted HR 1.79 [0.90; 1.79]; p = 0.097 NYHA class II/III/IV r = 0.15, p < 0.05 | CAD – 12.1 \pm 19.5 DCM – 9.2 \pm 8.5 healthy control – 7.9 \pm 8.9 |

Table 1. Results of studies on the association of TMAO with cardiovascular risk – cont.

| Author | Type of study | Population characteristics | Follow-up | Study endpoint | Results HR/OR (95% CI) | TMAO [μmol/L], median (IQR) |
|------------------------------|---|---|---|---|---|---|
| Zhou et al. ³⁹ | prospective cohort study | n = 1208; patients with chronic HF after MI China age: 73 (64–80) years male sex: 68.5% | median: 1.84 years | MACE, all-cause mortality, HF rehospitalization, recurrent MI all-cause mortality | Q4 compared to Q1 MACE n = 507 death n = 56 readmitted with HF n = 384 recurrent MI n = 67 unadjusted HR 3.15 [2.09; 4.73]; p < 0.01 adjusted HR 2.31 [1.42; 3.59]; p < 0.01 all-cause mortality HR 2.15 [1.37; 3.24]; p < 0.01 | Q4 > 7.92 Q1 < 2.83 |
| Schuett et al. ⁴⁰ | retrospective study | n = 2490; LURIC population Europe n = 823 – HF patients: HF rEF (n = 428) and HF pEF (n = 395) | mean: 9.7 years | all-cause mortality death due to cardiovascular causes | all patients T3 compared to T1 death n = 728 1.70 [1.41; 2.04]; p < 0.001 cardiovascular death n = 446 1.87 [1.48; 2.38] HF rEF T3 compared to T1 death 2.33 [1.67; 3.24]; p < 0.001 cardiovascular death 2.27 [1.52; 3.37] HF pEF – ns | T3 ≥ 5.92 T1 ≤ 3.90 |
| Suzuki et al. ⁴¹ | retrospective study | n = 972; patients with acute HF UK age: 78 (69–84) years male sex: 61% | 1 year | all-cause mortality (death) composite death or rehospitalization due to HF (death/HF) | death n = 268 T3 compared to T1 univariate HR 1.35 [1.21; 1.51]; p < 0.0005 n = 384 death/HF HR 1.33 [1.20; 1.46]; p < 0.0005 adjusted for renal function – ns | 5.6 (3.4–10.5) T3 = 14.2 (8.2–151.5) T1 = 2.9 (0.5–4.0) |
| Israr et al. ⁴² | retrospective study | n = 806; patients with acute HF UK age: 78 (69–84) years male sex: 61% | 1 year | death at 30 days n = 62 death at 1 year n = 213 death/HF at 30 days n = 98 death/HF at 1 year n = 313 | T3 compared to T1 HR 1.39 [1.05; 1.84]; p = 0.022 HR 1.26 [1.08; 1.47] p = 0.004 HR 1.38 [1.10; 1.73] p = 0.006 HR 1.25 [1.09; 1.42] p = 0.001 adjusted for renal function – ns | 10.2 (5.8–18.7) |
| Suzuki et al. ⁴³ | multicenter prospective study (BIOSTAT-CHF) | n = 2234; patients with progressive worsening or new-onset symptoms of HF UK age: 70 (61–78) years male sex: 74% | 3 years | all-cause mortality (3 years) composite event of mortality combined with rehospitalization due to HF (3 years) | unadjusted HR 2.27 [1.90; 2.72]; p < 0.001 adjusted HR 1.42 [1.13; 1.80]; p = 0.003 unadjusted HR 1.93 [1.66; 2.23]; p < 0.001 adjusted HR 1.21 [1.00; 1.46]; p = 0.054 | 5.9 (3.6–10.8) |
| Wei et al. ⁴⁴ | prospective study | n = 915; chronic HF patients with reduced ejection fraction China age: 57.1 ± 14.1 years male sex: 69.9% | median: 33 months, max. 7 years | cardiovascular death or HTx (n = 314) recurrence of HF + first rehospitalization for cardiovascular causes | T3 compared to T1 HR 1.47 [1.13; 1.91]; p = 0.004 adjusted HR 1.33 [1.01; 1.74]; p = 0.039 high dose-dependent association: first rehospitalization for cardiovascular causes (p = 0.002) recurrence of HF (p = 0.003) | 2.52 (1.20–4.76) T3 > 3.770 T1 ≤ 1.574 |
| Atrial fibrillation | | | | | | |
| Svingen et al. ⁴⁷ | retrospective cohort study | n = 3797; patients with suspected stable angina Europe n = 3143; community-based control population Europe | median: 7.3 years community control 10.8 years | diagnosis of AF during hospitalization | m = 412 Q4 compared to Q1 adjusted HR 1.16 [1.05; 1.28]; p = 0.0009 community control n = 484 adjusted HR 1.10 [1.004; 1.19] per 1 standard deviation increase in log-transformed plasma TMAO | Q4 > 15.8 (11.9–23.5) Q1 < 2.7 (2.2–3.2) |

Table 1. Results of studies on the association of TMAO with cardiovascular risk – cont.

| Author | Type of study | Population characteristics | Follow-up | Study endpoint | Results HR/OR (95% CI) | TMAO [$\mu\text{mol/L}$], median (IQR) |
|---------------------------|--|--|-----------|---|---|--|
| Gong et al. ⁴⁹ | prospective observational cohort study | n = 117; consecutive rheumatic heart disease patients with AF age: 57 (50–64) years male sex: 41% n = 25 – patients with cardiac thrombi n = 92 – patients without cardiac thrombi | N/A | comparison of TMAO concentration between 2 groups | TMAO, group I compared to group II: 4.55 [3.19; 4.83] compared to 3.53 [2.96; 4.25]; p = 0.01 | N/A |

ACS – acute coronary syndrome; DCM – dilated cardiomyopathy; MACE – major adverse cardiac event; TMAO – trimethylamine oxide; a – age; m – male; Q – quartile; T – tertile; HR – hazard ratio; OR – odds ratio; 95% CI – 95% confidence interval; IQR – interquartile range; AUROC – area under the receiver operating characteristic curve; ASCVD – atherosclerotic cardiovascular disease; CAD – coronary artery disease; MI – myocardial infarction; HF – heart failure; HFrEF – heart failure with reduced ejection fraction; HFpEF – heart failure with preserved ejection fraction; BNP – brain natriuretic peptide; HTx – heart transplantation; LURIC – Ludwigshafen Risk and Cardiovascular Health; PCI – percutaneous coronary intervention; SYNTAX – synergy between percutaneous coronary intervention with taxus and cardiac surgery score; STEMI – ST-segment elevation myocardial infarction; NYHA – New York Heart Association; eGFR – estimated glomerular filtration rate; N/A – not available/not applicable; AUC – area under the curve; AF – atrial fibrillation; N/A – not applicable; ns – nonsignificant.

higher TMAO levels are associated with the risk of CAD in previously healthy individuals.²⁶

The prognostic value of TMAO was also assessed in patients with acute coronary syndrome (ACS). Increased TMAO levels showed an association with the risk of death or recurrent myocardial infarction (MI) during a 2-year follow-up,²⁷ as well as with future cardiovascular events during a 5-year follow-up.²⁸ Importantly, the risk persisted despite the improvement regarding traditional cardiovascular risk factors such as hypertension, dyslipidemia or diabetes.²⁸ In another interesting study, Li et al. showed that increased TMAO levels were a risk factor for MACEs at 30 days and 6 months in patients presenting with chest pain of suspected cardiac origin.²⁹ The strong prognostic significance of TMAO was observed irrespective of baseline troponin levels and the final diagnosis of ACS. In the same study, in an independent cohort of patients with ACS who underwent coronary angiography due to ACS, higher TMAO levels were associated with an increased risk of MACEs at 1 year, independent of traditional risk factors.

In addition to predicting future MACEs, plasma TMAO levels were shown to correlate with the extent of CAD and atherosclerotic plaque stability. Studies conducted to date have revealed an association between TMAO levels and the SYNTAX Score, multivessel CAD^{30,31} and the risk of atherosclerotic plaque rupture.^{32,33} Finally, it was reported that TMAO could act as a mediator of clopidogrel resistance and inhibit clopidogrel effects, which has significant implications for the medical treatment of CAD.³⁴

In the context of atherosclerosis, TMAO has also been investigated in patients with chronic kidney disease (CKD).^{35,36} As renal function deteriorates, TMAO level increases and correlates with coronary atherosclerosis burden,³⁵ gut microbiota alterations, increased intestinal permeability, chronic inflammation, and endothelial dysfunction.³⁶ Chronic kidney disease has complex pathogenesis and dynamics. The higher risk of death and

the extent of atherosclerosis are therefore the cumulative effect of many processes. Accordingly, TMAO is one of the bystanders rather than the single and direct causative agent of vascular complications of CKD.

Heart failure

There is a considerable body of evidence on the role of TMAO as a prognostic marker in patients with HF. These associations were studied in the chronic and acute settings as well as depending on the preserved or reduced ejection fraction and the burden of symptoms.

A significant association between increased TMAO levels and mortality risk in patients with chronic HF (CHF) was first described in 2014.³⁷ Subsequent studies reported associations with the New York Heart Association (NYHA) functional class and CHF after MI.^{38,39} Schuett et al. demonstrated that increased TMAO levels were a strong predictor of mortality in patients with HF with reduced ejection fraction, but not in those with preserved ejection fraction, over a mean follow-up of 9.7 years.⁴⁰

Several studies reported data on the effect of increased TMAO levels on disease course and prognosis in patients with acute HF. Suzuki et al. showed that elevated TMAO levels were a strong predictor of mortality or rehospitalization at 1 year.⁴¹ However, after adjustment for renal confounders, the correlation was no longer significant,⁴¹ which is in line with the results of a more recent study by Israr et al.⁴² In a multicenter study including patients with new-onset or progressive HF, higher TMAO levels were strongly associated with an increased risk of mortality and/or rehospitalization during 1-, 2- and 3-year follow-up. In line with previous studies, TMAO levels were not reduced by optimal treatment.⁴³

The association between elevated TMAO levels and poor prognosis in patients with HF has not been fully elucidated

so far. Apart from gut microbiota, the role of FMO3 polymorphism has been postulated.⁴⁴ Moreover, Li et al. suggested a potential inhibitory effect of loop diuretics on renal excretion of TMAO, resulting in its retention in tissues.⁴⁵

Atrial fibrillation

The role of TMAO as a risk factor or mediator of atrial fibrillation (AF) has not been determined so far.⁴⁶ A study on 2 Norwegian cohorts indicated that high TMAO levels were associated with a risk of incident AF, independent of traditional risk factors.⁴⁷ In the AF-RISK study, higher TMAO levels were associated with progression to permanent AF.⁴⁸ Finally, the proarrhythmic and prothrombotic effects of TMAO can result in increased risk of thrombus formation in patients with AF.⁴⁹

Results from meta-analyses

There are several meta-analyses assessing TMAO levels as a predictor of mortality or other adverse events in patients with CVD.^{50–55} The results strongly indicate that elevated TMAO levels are a significant risk factor for death and MACEs. Selected meta-analyses are summarized in Table 2.

Interventions aimed at reducing TMAO levels and toxicity

The knowledge of TMAO synthesis, metabolism and excretion pathways allows investigators to study interventions aimed at reducing TMAO toxicity. Some of the conclusions were formulated on the basis of random findings derived from other studies. Examples include

the association between statin use and reduced TMAO levels⁵⁶ or between aspirin use and reduced TMA synthesis.⁵⁷ In both cases, the lowering effect was probably due to drug-induced alterations in gut microbiota.

A standard targeted approach is to reduce the dietary intake of TMA precursors and TMAO. The elimination of red meat from diet results in reduced TMAO levels after 4 weeks,⁵ while vegetarians and vegans have lower circulating TMAO levels and a lower capacity to synthesize TMA, probably due to changes in gut microbiota.¹⁷ The beneficial effect of Mediterranean diet on reducing TMAO levels is primarily due to the high intake of plant foods,⁵⁸ although the results of studies are equivocal.⁵⁹

The use of broad-spectrum antibiotics was shown to suppress gut microbiota and reduce TMAO levels. However, antibiotic therapy does not offer satisfactory long-term outcomes and is associated with a high risk of side effects.¹¹ Rifaximin has been reported to be a safer alternative, but the results of the recent GUTHEART study are insufficient to confirm this suggestion.⁶⁰ Other interventions include supplementation with probiotics,⁶¹ gut bacteria transplant from healthy donors,⁶² bariatric surgery,⁶³ resveratrol,⁶⁴ and meldonium.⁶⁵ Current interventions are summarized in Table 3 and Fig. 3.

Review limitations and gaps in knowledge

The possibility of discussing all ongoing studies in microbiota biomarkers is beyond the scope of this review. For now, to the best of our knowledge, despite the extensive literature supporting its usefulness, TMAO has not been identified as an established biomarker in CAD or HF guidelines. Perhaps, the ongoing research will consolidate the use of TMAO and other gut microbiota metabolites such as bile acids and short chain fatty acids in everyday practice. Linking the metabolism of the gut

Table 2. Results of meta-analyses on the association of TMAO with cardiovascular risk

| Author | Population (number of studies included) | Endpoints | Results RR/HR (95% CI) |
|------------------------------------|---|------------------------------|---|
| Heianza et al. ⁵⁰ | n = 19,256 (19) | MACCE, death | MACE: RR 1.62 [1.45; 1.80]; p < 0.001, I ² = 23.5% death: RR 1.63 [1.36; 1.95]; I ² = 45.9% |
| Schiattarella et al. ⁵¹ | n = 26,167 (26) | MACCE, death | MACCE: RR 1.67 [1.33; 2.11]; p < 0.00001, I ² = 46% death: RR 1.91 [1.40; 2.61]; p < 0.0001, I ² = 94% |
| Qi et al. ⁵² | n = 7716 (11) | cardiovascular events, death | cardiovascular events: RR 1.23 [1.07; 1.42]; I ² = 31.4% death: RR 1.55 [1.19; 2.02]; I ² = 80.8% |
| Farhang ⁵³ | n = 31,230 (20) | death | death: RR 1.466 [1.291; 1.665]; p < 0.001, I ² = 81.9% |
| Li et al. ⁵⁴ | n = 6879 (7) | MACE, death | MACE: T3 compared to T1: HR 1.68 [1.44; 1.96] death: T3 compared to T1: HR 1.67 [1.17; 2.38] |
| Guasti et al. ⁵⁵ | n = 923 (3) | MACE, death | MACE: RR 2.05 [1.61; 2.61]; I ² = 50% death: RR 3.42 [2.27; 5.15]; I ² = 0% |

TMAO – trimethylamine oxide; MACE – major adverse cardiac events; MACCE – major adverse cardiac and cerebrovascular events; CVE – cardiovascular events; HR – hazard ratio; RR – risk ratio; T – tertile; CI – confidence interval.

Table 3. Results of studies assessing therapeutic strategies aimed at reducing TMAO levels

| Author | Type of study | Population/ model | Intervention | Endpoint | Results | Comment |
|------------------------------|---|---|--|---|---|---|
| Li et al. ⁵⁶ | retrospective study; 3-year follow-up | n = 4007; sequential patients undergoing elective diagnostic coronary angiography | statin use | MACE, defined as death, myocardial infarction, or stroke; reduction of TMAO concentration | n = 322 MACE by 3 years statin use associated with decreased MACE: HR 0.74, 95% CI: [0.60; 0.93]; p = 0.0089 plasma TMAO associated with increased MACE: HR 1.57, 95% CI: [1.40; 1.76]; p = 2.4e-14 statin use associated with decreased TMAO (3.9 compared to 4.3) p = 0.002 | suspected mechanism: alteration in gut microbiome activity |
| Zhu et al. ⁵⁷ | prospective study | healthy vegans/vegetarians (n = 8); healthy omnivores (n = 10) orally supplemented with choline | aspirin 81 mg/day for 3 months | reduction of TMAO concentration | aspirin attenuated TMAO elevation TMAO: choline compared to choline + ASA 36.9 ± 9.4 compared to 21.2 ± 3.0; p = 0.009 | suspected mechanism: alteration in gut microbiome activity |
| Wang et al. ⁵ | prospective study | n = 113; healthy adult participants all omnivores | discontinuation of red meat intake to non-meat or white meat | reduction of TMAO concentration | no meat – TMAO reduction; p < 0.0001 white meat – TMAO reduction; p < 0.0001 | N/A |
| Awoyemi et al. ⁶⁰ | prospective randomized, double-blind study | n = 151; patients with LVEF < 40%; NYHA class II–III despite optimal medical therapy | 3 months: rifaximin, 550 mg twice daily, 250 mg 3 months: probiotic <i>Saccharomyces boulardii</i> NCM I-745 500 mg twice daily standard of care only | LVEF after 3 months of intervention baseline-adjusted NT-proBNP baseline-adjusted TMAO | LVEF: rifaximin compared to standard of care mean difference: –1.2 pp (3.2–0.7); p = 0.22 <i>Saccharomyces boulardii</i> –0.2 pp (2.2–1.9); p = 0.87 NT-proBNP: no significant effects rifaximin p = 0.28 <i>S. boulardii</i> : increase; p = 0.03 TMAO: no significant effects rifaximin; p = 0.8 <i>Saccharomyces boulardii</i> p = 0.16 | patients low in baseline dysbiosis low dose of rifaximin |
| Boutagy et al. ⁶¹ | randomized double-blind, placebo-controlled | n = 19; healthy, non-obese males (18–30 years) | 4-week hypercaloric (+1000 kcal day ⁻¹), high-fat diet (55% fat) + VSL#3 (900 billion live bacteria) orally placebo | reduction of TMAO concentration | plasma TMAO level increased significantly VSL#3 (89 ± 66%); p < 0.05 placebo (115 ± 61%); p < 0.05 VSL#3 compared to placebo: p > 0.05 | VSL#3 does not influence plasma TMAO following a high-fat diet |
| Smits et al. ⁶² | double-blind randomized pilot study | n = 20; male patients with metabolic syndrome | vegan-donor FMT | conversion of choline and carnitine to TMA and TMAO fasting plasma TMAO level TMA/TMAO urinary excretion | no significant effect; p > 0.05 | significant changes in intestinal microbiota composition did not affect TMAO metabolism; residual capacity to convert precursors to TMAO in vegans? short follow-up (2 weeks) |
| Trøseid et al. ⁶³ | observational study | n = 34; obese patients (17 with and 17 without type 2 diabetes) undergoing bariatric surgery | bariatric surgery laparoscopic Roux-en-Y gastric bypass duodenal switch | abseline plasma TMAO level preoperatively (after 3 months of lifestyle intervention) 1 year after bariatric surgery | no significant effect of 3-month lifestyle intervention preoperatively; 1 year after bariatric surgery TMAO plasma levels more than doubled (HR 10.5, 95% CI: [7.5; 13.5]) compared to preoperative (HR 4.4, 95% CI: [2.8; 6.0]; p < 0.001) compared to baseline (HR 4.7, 95% CI: [3.7; 5.8]; p < 0.001), regardless of surgical method | mechanism: changes in gut microbiota profile |

Table 3. Results of studies assessing therapeutic strategies aimed at reducing TMAO levels – cont.

| Author | Type of study | Population/model | Intervention | Endpoint | Results | Comment |
|---------------------------------|--|------------------------------|---|--|--|---------|
| Annunziata et al. ⁶⁴ | double-blind, randomized, placebo-controlled study | n = 380; healthy individuals | grape pomace polyphenol nutraceutical (rich in resveratrol) 400 mg twice daily 4 weeks, 8 weeks | reduction of TMAO concentration | plasma TMAO reduction (–49.78%, p < 0.0001) 8 weeks – 75.85%; p < 0.0001 | N/A |
| Dambrova et al. ⁶⁵ | open label, interventional study | n = 8; healthy volunteers | meldonium orally, 500 mg twice daily, 7 days during TMAO-rich diet | reduction of TMAO concentration urine TMAO excretion | diet compared to diet + meldonium plasma: 81.5 ± 8.6 mM compared to 43.0 ± 3.8 mM; p < 0.05 excretion: 18.2 ± 2.2 mmol/mg creatinine × 7 days compared to 24.3 ± 1.5 mmol/mg creatinine × 7 days; p < 0.05 | N/A |

LVEF – left ventricular ejection fraction; MACE – major adverse cardiac event; N/A – not available/not applicable; NYHA – New York Heart Association functional classification; TMAO – trimethylamine oxide; NT-proBNP – N-terminal pro-B-type natriuretic peptide; FMT – fecal microbiota transplant; TMA – trimethylamine; ASA – acetylsalicylic acid (aspirin); HR – hazard ratio; 95% CI – 95% confidence interval.

microbiota to CVD is an attractive topic of ongoing research. It is worth mentioning the studies NCT04962763⁶⁶ and NCT02728154,⁶⁷ which will deepen the knowledge on the correlation of the intestinal microbiota with HF. The study NCT05014880 is going to assess the effectiveness of a dietary intervention reducing dietary TMAO levels during the rehabilitation of CAD patients.⁶⁸

Conclusions

The TMAO is a biomarker that has been proven useful in a population of patients at higher cardiovascular risk. The use of TMAO in clinical practice requires confirmation in subsequent prospective interventional studies.

ORCID iDs

Radosław Andrzej Konieczny  <https://orcid.org/0000-0002-0949-4364>
Wiktoria Kuliczowski  <https://orcid.org/0000-0001-6284-0820>

References

1. Finegold JA, Asaria P, Francis DP. Mortality from ischaemic heart disease by country, region, and age: Statistics from World Health Organization and United Nations. *Int J Cardiol.* 2013;168(2):934–945. doi:10.1016/j.ijcard.2012.10.046
2. Gambardella J, Castellanos V, Santulli G. Standardizing translational microbiome studies and metagenomic analyses. *Cardiovasc Res.* 2021; 117(3):640–642. doi:10.1093/cvr/cvaa175
3. Velasquez MT, Ramezani A, Manal A, Raj DS. Trimethylamine N-oxide: The good, the bad and the unknown. *Toxins (Basel).* 2016;8(11):326. doi:10.3390/toxins8110326
4. Lombardo M, Aulisa G, Marcon D, et al. Association of urinary and plasma levels of trimethylamine N-oxide (TMAO) with foods. *Nutrients.* 2021;13(5):1426. doi:10.3390/nu13051426
5. Wang Z, Bergeron N, Levison BS, et al. Impact of chronic dietary red meat, white meat, or non-meat protein on trimethylamine N-oxide metabolism and renal excretion in healthy men and women. *Eur Heart J.* 2019;40(7):583–594. doi:10.1093/eurheartj/ehy799
6. Hamaya R, Ivey KL, Lee DH, et al. Association of diet with circulating trimethylamine-N-oxide concentration. *Am J Clin Nutr.* 2020;112(6): 1448–1455. doi:10.1093/ajcn/nqaa225
7. Cho CE, Aardema NDJ, Bunnell ML, et al. Effect of choline forms and gut microbiota composition on trimethylamine-N-oxide response in healthy men. *Nutrients.* 2020;12(8):2220. doi:10.3390/nu12082220
8. Janeiro MH, Ramírez MJ, Milagro FI, et al. Implication of trimethylamine N-oxide (TMAO) in disease: Potential biomarker or new therapeutic target. *Nutrients.* 2018;10(10):1398. doi:10.3390/nu10101398
9. Stremmel W, Schmidt KV, Schuhmann V, et al. Blood trimethylamine-N-oxide originates from microbiota mediated breakdown of phosphatidylcholine and absorption from small intestine. *PLoS One.* 2017; 12(1):e0170742. doi:10.1371/journal.pone.0170742
10. Taesuwan S, Cho CE, Malysheva OV, et al. The metabolic fate of isotopically labeled trimethylamine-N-oxide (TMAO) in humans. *J Nutr Biochem.* 2017;45:77–82. doi:10.1016/j.jnutbio.2017.02.010
11. Wang Z, Klipfell E, Bennett BJ, et al. Gut flora metabolism of phosphatidylcholine promotes cardiovascular disease. *Nature.* 2011;472(7341): 57–63. doi:10.1038/nature09922
12. Geng J, Yang C, Wang B, et al. Trimethylamine N-oxide promotes atherosclerosis via CD36-dependent MAPK/JNK pathway. *Biomed Pharmacother.* 2018;97:941–947. doi:10.1016/j.biopha.2017.11.016
13. Ma G, Pan B, Chen Y, et al. Trimethylamine N-oxide in atherogenesis: Impairing endothelial self-repair capacity and enhancing monocyte adhesion. *Biosci Rep.* 2017;37(2):BSR20160244. doi:10.1042/BSR20160244
14. Seldin MM, Meng Y, Qi H, et al. Trimethylamine N-oxide promotes vascular inflammation through signaling of mitogen-activated protein kinase and nuclear factor-κB. *J Am Heart Assoc.* 2016;5(2):e002767. doi:10.1161/JAHA.115.002767
15. Chou RH, Chen CY, Chen IC, et al. Trimethylamine N-oxide, circulating endothelial progenitor cells, and endothelial function in patients with stable angina. *Sci Rep.* 2019;9(1):4249. doi:10.1038/s41598-019-40638-y
16. Brunt VE, Gioscia-Ryan RA, Casso AG, et al. Trimethylamine-N-oxide promotes age-related vascular oxidative stress and endothelial dysfunction in mice and healthy humans. *Hypertension.* 2020;76(1): 101–112. doi:10.1161/HYPERTENSIONAHA.120.14759
17. Koeth RA, Wang Z, Levison BS, et al. Intestinal microbiota metabolism of L-carnitine, a nutrient in red meat, promotes atherosclerosis. *Nat Med.* 2013;19(5):576–585. doi:10.1038/nm.3145
18. Zhu W, Gregory JC, Org E, et al. Gut microbial metabolite TMAO enhances platelet hyperreactivity and thrombosis risk. *Cell.* 2016; 165(1):111–124. doi:10.1016/j.cell.2016.02.011
19. Subramaniam S, Boukhlof S, Fletcher C. A bacterial metabolite, trimethylamine N-oxide, disrupts the hemostasis balance in human primary endothelial cells but no coagulopathy in mice. *Blood Coagul Fibrinolysis.* 2019;30:324–330. doi:10.1097/MBC.0000000000000838
20. Li Z, Wu Z, Yan J, et al. Gut microbe-derived metabolite trimethylamine N-oxide induces cardiac hypertrophy and fibrosis. *Lab Invest.* 2019;99(3):346–357. doi:10.1038/s41374-018-0091-y

21. Jin B, Ji F, Zuo A, et al. Destructive role of TMAO in T-tubule and excitation-contraction coupling in the adult cardiomyocytes. *Int Heart J*. 2020;61(2):355–363. doi:10.1536/ihj.19-372
22. Oakley CI, Vallejo JA, Wang D, et al. Trimethylamine-N-oxide acutely increases cardiac muscle contractility. *Am J Physiol Heart Circ Physiol*. 2020;318(5):H1272–H1282. doi:10.1152/ajpheart.00507.2019
23. Tang WH, Wang Z, Levison BS, et al. Intestinal microbial metabolism of phosphatidylcholine and cardiovascular risk. *N Engl J Med*. 2013;368(17):1575–1584. doi:10.1056/NEJMoa1109400
24. Senthong V, Wang Z, Li XS, et al. Intestinal microbiota-generated metabolite trimethylamine-N-oxide and 5-year mortality risk in stable coronary artery disease: The contributory role of intestinal microbiota in a COURAGE-like patient cohort. *J Am Heart Assoc*. 2016;5(6):e002816. doi:10.1161/JAHA.115.002816
25. Lee Y, Nemet I, Wang Z, et al. Longitudinal plasma measures of trimethylamine N-oxide and risk of atherosclerotic cardiovascular disease events in community-based older adults. *J Am Heart Assoc*. 2021;10(17):e020646. doi:10.1161/JAHA.120.020646
26. Tang WHW, Li XS, Wu Y, et al. Plasma trimethylamine N-oxide (TMAO) levels predict future risk of coronary artery disease in apparently healthy individuals in the EPIC-Norfolk prospective population study. *Am Heart J*. 2021;236:80–86. doi:10.1016/j.ahj.2021.01.020
27. Suzuki T, Heaney LM, Jones DJ, Ng LL. Trimethylamine N-oxide and risk stratification after acute myocardial infarction. *Clin Chem*. 2017;63(1):420–428. doi:10.1373/clinchem.2016.264853
28. Matsuzawa Y, Nakahashi H, Konishi M, et al. Microbiota-derived trimethylamine N-oxide predicts cardiovascular risk after STEMI. *Sci Rep*. 2019;9(1):11647. doi:10.1038/s41598-019-48246-6
29. Li XS, Obeid S, Kligenberg R, et al. Gut microbiota-dependent trimethylamine N-oxide in acute coronary syndromes: A prognostic marker for incident cardiovascular events beyond traditional risk factors. *Eur Heart J*. 2017;38(11):814–824. doi:10.1093/eurheartj/ehw582
30. Sheng Z, Tan Y, Liu C, et al. Relation of circulating trimethylamine N-oxide with coronary atherosclerotic burden in patients with ST-segment elevation myocardial infarction. *Am J Cardiol*. 2019;123(6):894–898. doi:10.1016/j.amjcard.2018.12.018
31. Senthong V, Li XS, Hudec T, et al. Plasma trimethylamine N-oxide, a gut microbe-generated phosphatidylcholine metabolite, is associated with atherosclerotic burden. *J Am Coll Cardiol*. 2016;67(22):2620–2628. doi:10.1016/j.jacc.2016.03.546
32. Fu Q, Zhao M, Wang D, et al. Coronary plaque characterization assessed by optical coherence tomography and plasma trimethylamine-N-oxide levels in patients with coronary artery disease. *Am J Cardiol*. 2016;118(9):1311–1315. doi:10.1016/j.amjcard.2016.07.071
33. Tan Y, Sheng Z, Zhou P, et al. Plasma trimethylamine N-oxide as a novel biomarker for plaque rupture in patients with ST-segment-elevation myocardial infarction. *Circ Cardiovasc Interv*. 2019;12(1):e007281. doi:10.1161/CIRCINTERVENTIONS.118.007281
34. Ma R, Fu W, Zhang J, et al. TMAO: A potential mediator of clopidogrel resistance. *Sci Rep*. 2021;11(1):6580. doi:10.1038/s41598-021-85950-8
35. Stubbs JR, House JA, Ocque AJ, et al. Serum trimethylamine-N-oxide is elevated in CKD and correlates with coronary atherosclerosis burden. *J Am Soc Nephrol*. 2016;27(1):305–313. doi:10.1681/ASN.2014111063
36. Al-Obaide MAI, Singh R, Datta P, et al. Gut microbiota-dependent trimethylamine-N-oxide and serum biomarkers in patients with T2DM and advanced CKD. *J Clin Med*. 2017;6(9):86. doi:10.3390/jcm6090086
37. Tang WH, Wang Z, Fan Y, et al. Prognostic value of elevated levels of intestinal microbe-generated metabolite trimethylamine-N-oxide in patients with heart failure: Refining the gut hypothesis. *J Am Coll Cardiol*. 2014;64(18):1908–1914. doi:10.1016/j.jacc.2014.02.617
38. Trøseid M, Ueland T, Hov JR, et al. Microbiota-dependent metabolite trimethylamine-N-oxide is associated with disease severity and survival of patients with chronic heart failure. *J Intern Med*. 2015;277(6):717–726. doi:10.1111/joim.12328
39. Zhou X, Jin M, Liu L, et al. Trimethylamine N-oxide and cardiovascular outcomes in patients with chronic heart failure after myocardial infarction. *ESC Heart Fail*. 2020;7(1):188–193. doi:10.1002/ehf2.12552
40. Schuett K, Kleber ME, Scharnagl H, et al. Trimethylamine-N-oxide and heart failure with reduced versus preserved ejection fraction. *J Am Coll Cardiol*. 2017;70(25):3202–3204. doi:10.1016/j.jacc.2017.10.064
41. Suzuki T, Heaney LM, Bhandari SS, et al. Trimethylamine N-oxide and prognosis in acute heart failure. *Heart*. 2016;102(11):841–848. doi:10.1136/heartjnl-2015-308826
42. Israr MZ, Bernieh D, Salzano A, et al. Association of gut-related metabolites with outcome in acute heart failure. *Am Heart J*. 2021;234:71–80. doi:10.1016/j.ahj.2021.01.006
43. Suzuki T, Yazaki Y, Voors AA, et al. Association with outcomes and response to treatment of trimethylamine N-oxide in heart failure: Results from BIOSTAT-CHF. *Eur J Heart Fail*. 2019;21(7):877–886. doi:10.1002/ehf.1338
44. Wei H, Zhao M, Huang M, et al. FMO3-TMAO axis modulates the clinical outcome in chronic heart-failure patients with reduced ejection fraction: Evidence from an Asian population [published online ahead of print on June 22, 2021]. *Front Med*. 2021. doi:10.1007/s11684-021-0857-2
45. Li DY, Wang Z, Jia X, et al. Loop diuretics inhibit renal excretion of trimethylamine N-oxide. *JACC Basic Transl Sci*. 2021;6(2):103–115. doi:10.1016/j.jacbs.2020.11.010
46. Gawaiko M, Linz D, Dobrev D. Gut-microbiota derived TMAO: A risk factor, a mediator or a bystander in the pathogenesis of atrial fibrillation? *Int J Cardiol Heart Vasc*. 2021;34:100818. doi:10.1016/j.ijcha.2021.100818
47. Svingen GFT, Zuo H, Ueland PM, et al. Increased plasma trimethylamine-N-oxide is associated with incident atrial fibrillation. *Int J Cardiol*. 2018;267:100–106. doi:10.1016/j.ijcard.2018.04.128
48. Nguyen BO, Meems LMG, van Faassen M, et al. Gut-microbe derived TMAO and its association with more progressed forms of AF: Results from the AF-RISK study. *Int J Cardiol Heart Vasc*. 2021;34:100798. doi:10.1016/j.ijcha.2021.100798
49. Gong D, Zhang L, Zhang Y, et al. Gut microbial metabolite trimethylamine N-oxide is related to thrombus formation in atrial fibrillation patients. *Am J Med Sci*. 2019;358(6):422–428. doi:10.1016/j.amjms.2019.09.002
50. Heianza Y, Ma W, Manson JE, et al. Gut microbiota metabolites and risk of major adverse cardiovascular disease events and death: A systematic review and meta-analysis of prospective studies. *J Am Heart Assoc*. 2017;6(7):e004947. doi:10.1161/JAHA.116.004947
51. Schiattarella GG, Sannino A, Toscano E, et al. Gut microbe-generated metabolite trimethylamine-N-oxide as cardiovascular risk biomarker: A systematic review and dose-response meta-analysis. *Eur Heart J*. 2017;38(39):2948–2956. doi:10.1093/eurheartj/ehx342
52. Qi J, You T, Li J, et al. Circulating trimethylamine N-oxide and the risk of cardiovascular diseases: A systematic review and meta-analysis of 11 prospective cohort studies. *J Cell Mol Med*. 2018;22(1):185–194. doi:10.1111/jcmm.13307
53. Farhangi MA. Gut microbiota-dependent trimethylamine N-oxide and all-cause mortality: Findings from an updated systematic review and meta-analysis. *Nutrition*. 2020;78:110856. doi:10.1016/j.nut.2020.110856
54. Li W, Huang A, Zhu H, et al. Gut microbiota-derived trimethylamine N-oxide is associated with poor prognosis in patients with heart failure. *Med J Aust*. 2020;213(8):374–379. doi:10.5694/mja2.50781
55. Guasti L, Galliazzo S, Molaro M, et al. TMAO as a biomarker of cardiovascular events: A systematic review and meta-analysis. *Intern Emerg Med*. 2021;16(1):201–207. doi:10.1007/s11739-020-02470-5
56. Li DY, Wang Z, Li XS, et al. Relationship between statin use and trimethylamine n-oxide in cardiovascular risk assessment. *J Am Coll Cardiol*. 2018;71(11):A115. doi:10.1016/s0735-1097(18)30656-9
57. Zhu W, Wang Z, Tang WHW, Hazen SL. Gut microbe-generated trimethylamine N-oxide from dietary choline is prothrombotic in subjects. *Circulation*. 2017;135(17):1671–1673. doi:10.1161/CIRCULATIONAHA.116.025338
58. Guasch-Ferré M, Hu FB, Ruiz-Canela M, et al. Plasma metabolites from choline pathway and risk of cardiovascular disease in the PRE-DIMED (Prevention With Mediterranean Diet) study. *J Am Heart Assoc*. 2017;6(11):e006524. doi:10.1161/JAHA.117.006524
59. Pignanelli M, Just C, Bogiatzi C, et al. Mediterranean diet score: Associations with metabolic products of the intestinal microbiome, carotid plaque burden, and renal function. *Nutrients*. 2018;10(6):779. doi:10.3390/nu10060779
60. Awoyemi A, Mayerhofer C, Felix AS, et al. Rifaximin or *Saccharomyces boulardii* in heart failure with reduced ejection fraction: Results from the randomized GutHeart trial. *EBioMedicine*. 2021;70:103511. doi:10.1016/j.ebiom.2021.103511

61. Boutagy NE, Neilson AP, Osterberg KL, et al. Probiotic supplementation and trimethylamine-N-oxide production following a high-fat diet. *Obesity (Silver Spring)*. 2015;23(12):2357–2363. doi:10.1002/oby.21212
62. Smits LP, Kootte RS, Levin E, et al. Effect of vegan fecal microbiota transplantation on carnitine- and choline-derived trimethylamine-N-oxide production and vascular inflammation in patients with metabolic syndrome. *J Am Heart Assoc*. 2018;7(7):e008342. doi:10.1161/JAHA.117.008342
63. Trøseid M, Hov JR, Nestvold TK, et al. Major increase in microbiota-dependent proatherogenic metabolite TMAO one year after bariatric surgery. *Metab Syndr Relat Disord*. 2016;14(4):197–201. doi:10.1089/met.2015.0120
64. Annunziata G, Maisto M, Schisano C, et al. Effects of grape pomace polyphenolic extract (Taurisolo®) in reducing TMAO serum levels in humans: Preliminary results from a randomized, placebo-controlled, cross-over study. *Nutrients*. 2019;11(1):139. doi:10.3390/nu11010139
65. Dambrova M, Skapare-Makarova E, Konrade I, et al. Meldonium decreases the diet-increased plasma levels of trimethylamine N-oxide, a metabolite associated with atherosclerosis. *J Clin Pharmacol*. 2013;53(10):1095–1098. doi:10.1002/jcph.135
66. Correlation of Intestinal Flora and Metabolomics in Patients With Ischemic Heart Failure. ClinicalTrials.gov. <https://clinicaltrials.gov/ct2/show/NCT04962763?term=gut&recrs=adf&cond=CVD&draw=2&rank=28>. Accessed February 10, 2022.
67. The Role of Gut Microbiota in Heart Failure and Pre-Heart Failure With Preserved Ejection Fraction. ClinicalTrials.gov. <https://clinicaltrials.gov/ct2/show/NCT02728154>. Accessed February 10, 2022.
68. Impact of Time Restricted Eating on Patients With Coronary Artery Disease (CAD) Undergoing Cardiac Rehabilitation. ClinicalTrials.gov. <https://clinicaltrials.gov/ct2/show/NCT05014880>. Accessed February 10, 2022.

